MATHEMATICAL MODELING

AND ITS APPLICATIONS

Edited by

Dr. P. Balaganesan

Dr. J, Renuka

Dr. V. Maheswari

Dr. E. Poongothai

MATHEMATICAL MODELING AND ITS APPLICATIONS

Editor names:
Dr.P.Balaganesan
Dr.J.Renuka
Dr.E.Poongothai
Dr. V. Maheswari

HSRA PUBLICATIONS

Published by

HSRA Publications 2026

#02, Sri Annapoorneshwari Nilaya,

1st Main, Byraveshwara Nagar, Laggere,

Bangalore – 560058

Sales Headquarters – Bangalore

ISBN: 978-93-6850-545-7

First Edition 2026

No. of Pages – 146

Size : ¼ Demy

TABLE OF CONTENTS

1. The Basics of Mathematical Modelling and Its Applications

[1]Adhil Basha D, [*2]Ramanathan P, [3]R Sengothai,[4] Subramanian R

[1,3]Department of Mathematics, AMET Deemed to be University, Chennai
[2]Department of Mechanical Engineering, AMET Deemed to be University, Chennai
[4]Department of Mathematics, Assistant professor, Sri Sairam Engineering College, Chennai - 44

Abstract

The contemporary methods of scientific research are founded on mathematical modeling, which not only provides a proper approach for the mathematical formulation of real world phenomena but also provides a proper framework for the mathematical representation of real world problems. The basic principles of mathematical modelling are defined in this chapter along with its theoretical underpinnings and methods. First, we introduce readers to the basic modelling process that leads us to the development of mathematical models and their redevelopment. Strict derivations of basic mathematical ideas such as differential equations and stochastic models are also covered in this chapter. The power of mathematical methods is affirmed through real world examples in the applied sciences. This chapter equips the reader with basic knowledge and concepts required for the development and analysis of mathematical models in their disciplines.

Keywords: mathematical modelling, numerical methods, differential equations, optimisation, model validation, and real world applications

1.Introduction

The process of translating physical, biological, economic, or social phenomena and observations into mathematical terms, reducing irrelevant aspects to emphasize relevant ones, has been described as mathematical modelling. It has made possible mathematical analysis, prediction, and optimisation through abstraction, which otherwise could not have been achieved by qualitative thought or experimentation.

One cannot overestimate how important mathematical modelling is for contemporary research and engineering. Mathematical models are the indispensable tool in understanding complex systems and enlightening decision makers, everything from climate change and the development of sustainable energy systems to smoothing out supply chains to simulating infectious diseases.

The COVID-19 pandemic put into sharp focus the importance of mathematical epidemiological models for informing public health policy decisions on a global scale.

1.1. The Modeling Cycle

All mathematical modelling projects entail an iterative process involving several key stages:

1. **Problem Formulation:** Identify the problem itself, and state the goals and scope thereof.

2. **Model Construction:** Utilize equations, inequalities, or other mathematical constructs to model.

3. **Mathematical Analysis:** The results and predictions should be calculated using analytical or numerical procedures.

4. **Validation & Verification**: The accuracy of the model can be checked by comparing the predictions obtained from the model with actual values.

5. **Model Development:** Use validation findings to refine model assumptions, alter assumptions, or alter model parameters.

6. **Implementation:** Implement the validated model for predictions of results, process improvements, and decision-making.

1.2 Theoretical Background

1.2.1 Classification of Mathematical Models

Mathematical models can be grouped based on a number of criteria, with different classifications underscoring different aspects of the models' structure and dynamics.

Deterministic vs. Stochastic Models

Deterministic systems always generate the same output for any set of initial conditions and parameters. These systems involve complete knowledge and lack randomness. Some of the examples of such systems are Newton's laws of physics and classical physics models.

Stochastic models include random variables and probability distributions to express stochastic uncertainties or variations. Many applications of stochastic models include finance, quantum physics, and population genetics.

Static and Dynamic Models

Static models: These are models of a system when it's in equilibrium, without any time dependence. Optimization instances, or structural analysis, commonly utilize static models.

Dynamic models involve explicit consideration of time evolution solutions with equations that involve differences or differentials. Dynamic models play a central role in analyzing transient responses, oscillations, and asymptotes.

Linear vs. Non-Linear Models

Linear systems obey the superposition principle and can be solved analytically very efficiently. But this is not the case when it comes to real-world applications. Most phenomena are nonlinear.

Nonlinear models can demonstrate very complex behavior such as having several equilibria, limit cycles, chaos, and bifurcations. Although nonlinear models are more difficult to study, they can offer more accurate descriptions of real-world systems.

1.2.2 Fundamental Modeling Principles

There are several basic principles for making good mathematical models:

Parsimony: Models must be as simple as possible in order to account for most of their features (Occam's Razor).

Conservation Laws: Mass, energy, momentum, and charge conservation laws can be very constraining.

itizenoidal Integrity: All terms involved in an equation should have equivalent dimensions.

Scale Separation: Separations of time or space scales that are vastly different from one another often lead to decoupling.

Empirical Foundation: The model should be founded on experimental findings and physical principles.

1.3 Mathematical Formulations

1.3.1 Ordinary Differential Equations

Dynamic modelling is based on ordinary differential equations (ODEs). The general form of a first-order ODE is as follows:

$$\frac{\mathrm{dx}}{\mathrm{dt}} = \mathrm{f(x, t)} \quad (1.1)$$

If t is time, f is the rate of change, and x(t) is the state variable.

For systems with multiple state variables, we use vector notation:

$$\frac{dx}{dt} = f(x, t) \quad (1.2)$$

where $X = (x_1, x_2, \ldots\ldots, x_n)^T$ is the state vector.

Example: Exponential Growth Model

The most basic population model makes the assumption that population size and growth rate are proportionate:

$$\frac{dN}{dt} = rN \quad (1.3)$$

where N(t) is population size and r is the growth rate constant. The analytical solution is:

$$N(t) = N_0 e^{rt} \quad (1.4)$$

where $N_0 = N(0)$is the initial population.

1.3.2 Logistic Growth Model

Unlimited exponential growth is unrealistic due to resource constraints. The logistic model incorporates carrying capacity *K*:

$$\frac{dN}{dt} = rN(1 - N/K \quad (1.5)$$

This equation exhibits density-dependent growth, slowing as *N* approaches ***K***. The analytical solution is:

$$N(t) = K/(1 + (K - N_0)/N_0)N_0 e^{-rt}) \quad (1.6)$$

1.3.3 Systems of Linear Equations

Solving linear systems is the solution to many equilibrium problems:

$$AX = b \quad (1.7)$$

If **x** is the unknown vector, **b** is the right-hand side vector, and A is a m × n coefficient matrix. When rank(A) = rank([A|**b**]), there are solutions.

1.3.4 Optimization Models

Optimization problems seek to maximize or minimize an objective function subject to constraints. The general form is:

minimize f(x)

subject to $g_i(X) \leq 0$, i=1...m

$h_j(X) = 0$, j=1....p (1.8)

For unconstrained optimization, necessary conditions for a local minimum are:

$$\nabla f(X^*) = 0 \quad \text{(first-order)} \quad (1.9)$$

$$\nabla^2 f(X^*) > 0 \quad \text{(second-order)} \quad (1.10)$$

where $\nabla^2 f$ denotes the Hessian matrix and > 0 indicates positive definiteness.

1.4 Worked Examples

1.4.1 Example 1: Radioactive Decay

Problem Statement

The half-life of a radioactive material is 5,730 years (carbon-14). How much is left over after 10,000 years if we begin with 100 grammes?

Solution

Step 1: Formulate the model. Radioactive decay follows first-order kinetics:

$$\frac{dN}{dt} = -\lambda N \quad (1.11)$$

where λ is the decay constant.

Step 2: Relate decay constant to half-life. The half-life $t_{1/2}$ satisfies $N(t_{1/2}) = N_0/2$. From the solution

$$N(t) = N_0 e^{(-\lambda t)}$$

$$\frac{N_0}{2} = N_0 e^{(-\lambda t_{1/2})}$$

$$90n\left(\frac{1}{2}\right) = -\lambda t_{1/2}$$

$$\lambda = \ln(2)/t_{\frac{1}{2}} = 0.693147/5730 \approx 1.21 \times 10^{-4}\ year^{-4} \qquad (1.12)$$

Step 3: Calculate the amount remaining:

$$N(10000) = 100 \times e^{(-1.21\times 10^{-4}\times 10000)}$$

$$N(10000) = 100 \times e^{(-1.21)}$$

$$N(10000) \approx 100 \times 0.298 = 29.8\ grams \qquad (1.13)$$

Answer: Approximately 29.8 grams of carbon-14 remain after 10,000 years.

1.4.2 Example 2: Mixing Problem

Problem Statement

A tank contains 1000 liters of water with 50 kg of salt dissolved in it. Water containing 0.1 kg/L of salt flows in at 10 L/min, and the well-mixed solution flows out at 10 L/min. Find the salt concentration as a function of time.

Solution

Step 1: Define variables. Let $S(t)$be the amount of salt (kg) in the tank at time *t* (minutes).

Step 2: Apply conservation principle:

$$\frac{ds}{dt} = (rate\ in) - (rate\ out) \qquad (1.14)$$

Rate in = 0.1 kg/L × 10 L/min = 1 kg/min

Rate out = (S/1000) kg/L × 10 L/min = S/100 kg/min

Therefore:

$$\frac{ds}{dt} = 1 - s/100 \qquad (1.15)$$

Step 3: Solve the differential equation. This is a first-order linear ODE. Rearranging:

$$\frac{ds}{dt} + \frac{S}{100} = 1$$

Using integrating factor $\mu(t) = e^{(t/100)}$

$$\frac{d}{dt}\left[Se^{\left(\frac{t}{100}\right)}\right] = e^{t/100}$$

$$Se^{(t/100)} = 100e^{(t/100)} + c$$

$$S(t) = 100 + Ce^{(-t/100)} \qquad (1.16)$$

Step 4: Apply initial condition S(0) = 50:

50=100 + C → C = -50

$$S(t) = 100 - 50^{\left(-\frac{t}{100}\right)} = 100(1 - 0.5e^{(-t/100)}) \qquad (1.17)$$

The concentration is . $C(t) = \frac{S(t)}{1000} = 0.1\left(1 - 0.5e^{\left(-\frac{t}{100}\right)}\right)\ kg/L$

Equilibrium Analysis: As $t \to \infty$, $S \to 100$ kg and $C \to 0.1$ kg/L, matching the input concentration.

1.4.3 Example 3: Chemical Reaction Kinetics

Problem Statement

Consider a second-order reaction where two molecules of substance A combine to form product P: 2A → P. If the initial concentration of A is 2 mol/L and the rate constant is k = 0.5 L/(mol·min), find the concentration after 5 minutes.

Solution

Step 1: Write the rate law. For second-order kinetics:

$$\frac{d[A]}{dt} = -k[A]^2 \qquad (1.8)$$

Step 2: Separate variables and integrate:

$$\frac{d[A]}{[A]^2} = -k\,dt$$

$$\int \frac{d[A]}{[A]^2} = -k \int dt$$

$$\frac{-1}{[A]} = -kt + C \qquad (1.19)$$

Step 3: Apply initial condition: $[A](0) = [A]_0 = 2\ mol/L$

$$-\frac{1}{2} = C$$

$$\frac{1}{[A]} = kt + \frac{1}{[A]_0}$$

$$[A](t) = \frac{[A]_0}{(1+kt[A]_0} \qquad (1.20)$$

Step 4: Calculate concentration at t = 5 minutes:

[A](5) = 2/(1 + 0.5 × 5 × 2) = 2/(1 + 5) = 2/6 = 0.333 mol/L (1.21)

Answer: The concentration of A after 5 minutes is approximately 0.333 mol/L.

1.5 Real-World Applications

1.5.1 Epidemiological Modelling: SIR Model

A key component of mathematical epidemiology, the Susceptible-Infected-Recovered (SIR) model is widely applied during disease outbreaks, such as COVID-19. Three sections comprise the population:

- **S(t):** Susceptible individuals who can contract the disease
- **I(t):** Infected individuals who can transmit the disease
- **R(t):** Recovered individuals with immunity

Model Equations

The dynamics are governed by:

$$\frac{dS}{dt} = -\beta SI/N \qquad (1.22)$$

$$\frac{dI}{dt} = \frac{\beta SI}{N} - \gamma I \qquad (1.23)$$

$$\frac{dR}{dt} = \gamma I \qquad (1.24)$$

where $N = S + I + R$ is the total population (constant), β is the transmission rate, and γ is the recovery rate.

Basic Reproduction Number

The basic reproduction number R_0represents the average number of secondary infections from one infected individual in a completely susceptible population:

$R_0 = \beta/\gamma$ (1.25)

Epidemic threshold: If $R_0 > 1$, an epidemic occurs; if $R_0 < 1$, the disease dies out.

Application Example

For influenza, typical parameters might be: $\beta = 0.5\ day^{-1}$, $\gamma = 0.1\ day^{-1}$ (recovery period ~10 days). This gives $R_0 = 5$,indicating each infected person infects 5 others on average. Public health interventions aim to reduce β (through social distancing, masks) or increase γ (through treatment) to bring R_0below 1.

1.5.2 Environmental Science: Lake Pollution Model

Consider a lake receiving pollutant from industrial discharge and losing pollutant through natural degradation and water outflow.

Model Development

Let *P(t)* be pollutant concentration (mg/L). The mass balance gives:

$V\left(\frac{dp}{dt}\right) = Q_{in}P_{in} - Q_{out}P - kVP$ (1.26)

where V is lake volume, Q_{in} and Q_{out} are inflow and outflow rates, $P_{in}$is input concentration, and k is the degradation rate constant.

Assuming steady-state volume (Q_{in} = Q_{out}= Q):

$\frac{dP}{dt} = \left(\frac{Q}{V}\right)(P_{in} - P) - kP$ (1.27)

Equilibrium Analysis

At equilibrium ($\frac{dP}{dt} = 0$):

$P^* = \frac{P_{in}}{1+\frac{kV}{Q}} = \frac{P_{in}}{1+k\tau}$ (1.28)

where $\tau = \frac{V}{Q}$ is the residence time (average time water stays in the lake).

Management Implications

This model reveals that equilibrium concentration depends on: (1) Input concentration P_{in}, which can be reduced through pollution controls; (2) Degradation rate k, which might be enhanced through bioremediation; and (3) Residence time τ, which can be decreased by increasing flow rate. For a lake with $V = 10^6\ m^3V$, $Q = 100\ m^3/day$ and $k = 0.1 day^{-1}$, the residence time is

$\tau = 10{,}000$ days, and a 50% reduction in equilibrium concentration requires reducing $P_{in}$by 50%.

1.5.3 Engineering: Heat Transfer in a Rod

Heat conduction in solid materials is described by partial differential equations, but under certain conditions reduces to ODEs.

Steady-State Heat Conduction

For a thin rod of length L with constant cross-sectional area A, thermal conductivity k, perimeter P, and convection coefficient h, the steady-state temperature distribution $T(x)$ satisfies:

$\frac{d^2T}{dX^2} - m^2(T - T_a) = 0$ (1.29)

where $m^2 = hp/(kA)$ and T_a is ambient temperature.

Boundary Conditions and Solution

With fixed end temperatures $T(0) = T_0$ and $T(L) = T_1$, the solution is:

$$T(x) = T_a + C_1 \sinh(mx) + C_2 \cosh(mx) \qquad (1.30)$$

where constants C_1 and C_2 are determined from boundary conditions.

Practical Application

This model is applicable to designing thermal bridges, electronic component heat sinks, and cooling fins in heat exchangers. The equilibrium between convection to the environment and conduction along the rod is described by the parameter m. Strong convection in comparison to conduction is indicated by a large m, which causes a quick drop in temperature from the base.

1.6 Figures and Tables

The important tables and figures that would go with this chapter in a full textbook are described in this section.

Table 1.1: Common Mathematical Models and Their Applications

Model Type	Mathematical Form	Applications
Exponential Growth	$\frac{dy}{dt} = ky$	Population growth, compound interest, radioactive decay
Logistic Growth	$\frac{dy}{dt} = ky(1 - y/K)$	Limited population growth, tumor growth, epidemic spread
Harmonic Oscillator	$\frac{d^2y}{dt^2} + \omega^2 y = 0$	Spring-mass systems, pendulums, electrical circuits
Heat Equation	$\frac{\partial u}{\partial t} = \alpha \nabla^2 u$	Heat conduction, diffusion processes, options pricing
Wave Equation	$\frac{\partial^2 u}{\partial t^2} = c^2 \nabla^2 u$	Sound waves, electromagnetic waves, vibrating strings
Linear Programming	$\min c.X, AX \leq b$	Resource allocation, supply chain optimization, scheduling

Table 1.2: Comparison of Numerical Methods for ODEs

Method	Order	Stability	Computational Cost
Euler's Method	O(h)	Conditionally stable	Low
Runge-Kutta 2	$O(h^2)$	Good	Moderate
Runge-Kutta 4	$O(h^4)$	Excellent	Moderate-High
Adams-Bashforth	Variable	Moderate	Low (multistep)
Backward Euler	O(h)	Unconditionally stable	High (implicit)

Figure Descriptions

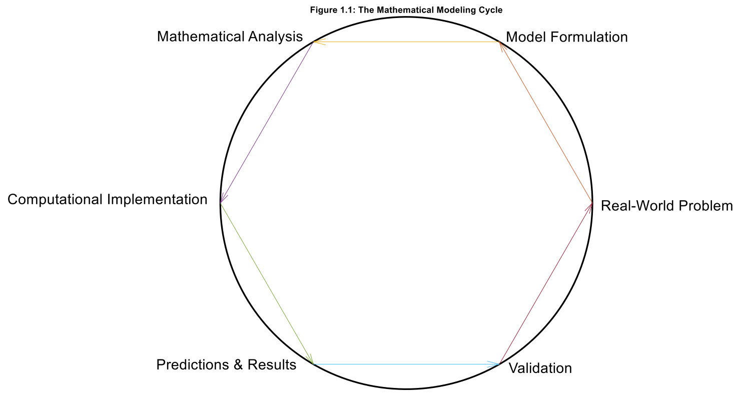

Figure 1.1

The Mathematical Modeling Cycle

A circular figure that demonstrates how mathematical modelling is iterative. Six interconnected stages are depicted in the cycle: (1) real-world problem; (2) model formulation (assumptions and simplifications); (3) mathematical analysis; (4) computational implementation; (5) predictions and results; and (6) validation against data. When models need to be improved, feedback loops from validation back to formulation are shown by arrows.

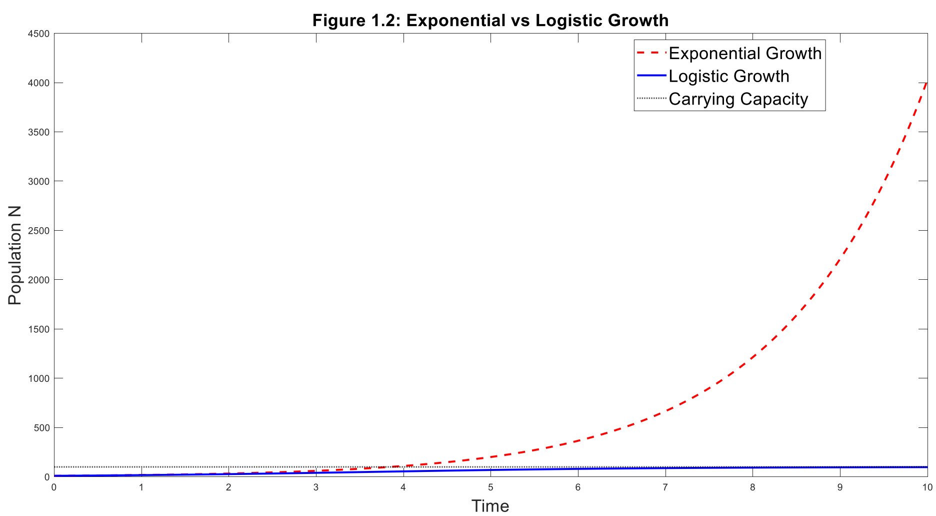

Figure 1.2

Comparison of Exponential and Logistic Growth

A chart representing how the number of people (N) in a certain population changes over time (t) displays two different shapes of the graph: an exponential growth shape $\left(\mathrm{N} = \mathrm{N_0 e^{(rt)}}\right)$, which indicates that this population will continue to grow without a stopping point, and a logistic growth shape $\left(\mathrm{N} = \frac{\mathrm{K}}{1+\mathrm{Ae^{(-rt)}}}\right)$ that starts with a straight line like an exponential shape but levels out and approaches K as its limit. The logistic growth curve will show one point where the rate of growth is half of K $\left(N = \frac{K}{2}\right)$

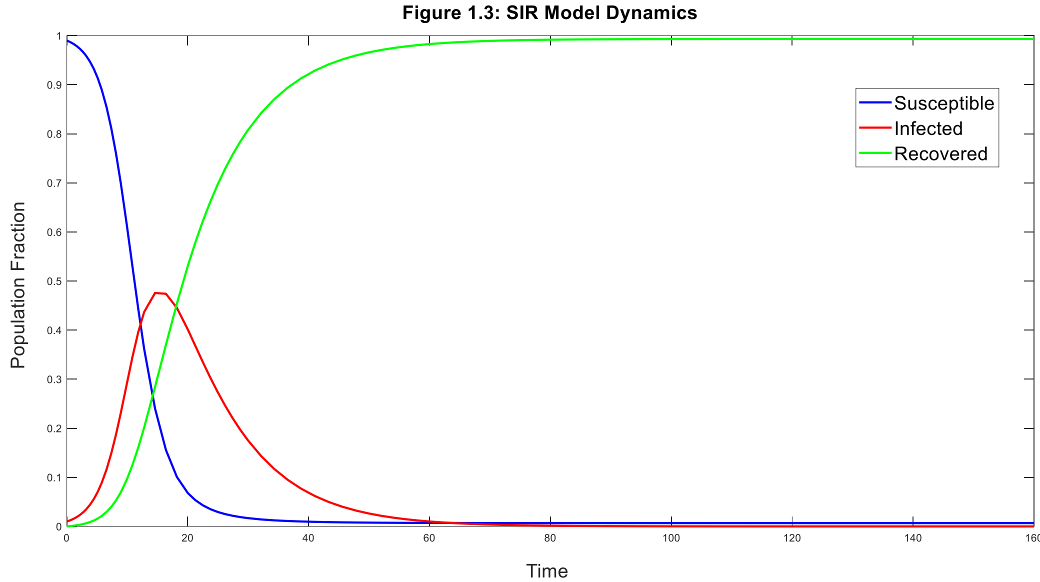

Figure 1.3

SIR Model Dynamics

Time series graphs of S(t), I(t), and R(t) during an epidemic. The susceptible population (S) always declines from its initial level. The infected population (I) increases, then peaks, before it ultimately decreases to zero as the epidemic progresses. The recovered population (R) starts at zero and goes up to its final amount as more people recover from illness. Parameters presented: $\beta = .05$; $\gamma = .10$; $R_0 = 5$; the initial conditions: $S(0) = 0.99$, I $I(0) = 0.01$, $R(0) = 0$.

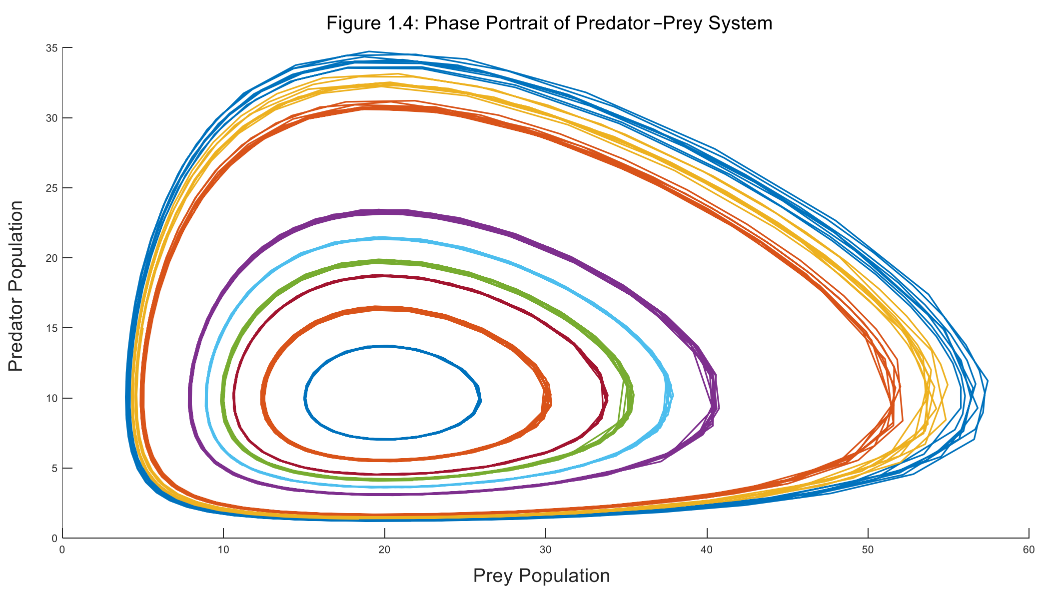

Figure 1.4

Phase Portrait of Predator-Prey System

The Lotka-Volterra model represents the flow of prey (X-axis) against Predator (Y-axis) using a phase plane diagram. The closed orbit around an equilibrium point shows the oscillations occur on a periodic basis. Various trajectories that are shown on this diagram all begin at different points in space but create closed loops around the equilibria indicating that the model is conservative in nature. Directions of how an object moves through a given trajectory are represented by arrows.

1.7 Discussion

1.7.1 Model Validation and Verification

The difference between validation and verification is an important but frequently disregarded part of mathematical modelling. "Are we solving the equations correctly?" is the question of verification. In contrast, validation poses the question, "Are we solving the correct equations?"

Verification includes conducting grid refinement studies, ensuring conservation properties are maintained, and comparing computational implementations to analytical solutions. For example, we confirm that S + I + R = N stays constant during numerical integration in the SIR model.

Validation Model predictions must be compared to independent experimental or observational data in order to be validated. Goodness of fit is measured statistically using metrics like the coefficient of determination (R^2), root mean square error (RMSE), and Akaike information criterion (AIC). However, multiple competing models may fit the same data equally well, so agreement with data does not prove a model is correct.

1.7.2 Limitations and Assumptions

Every mathematical model is predicated on presumptions that restrict its range of applicability. Comprehending these constraints is just as crucial as comprehending the model itself.

Almost all actual populations defy the exponential growth model's assumptions of limitless resources and a steady per capita growth rate. This is improved by the logistic model, which incorporates carrying capacity but ignores age structure, portrays the environment as static, and assumes an instantaneous response to density. Depending on the application, more complex models that include age structure, regional heterogeneity, or stochasticity can be required.

In a similar vein, the SIR model presupposes permanent immunity, homogenous mixing (everyone has an equal chance of coming into contact), and no births or deaths from non-disease-related causes. These presumptions might make sense for short-term epidemic dynamics in small populations. Extensions such as the SEIR model (which adds an Exposed compartment) or metapopulation models may be necessary for long-term endemic diseases in structured populations.

1.7.3 Sensitivity Analysis and Uncertainty Quantification

Rarely are model parameters completely known. In order to determine which parameters have the most impact on predictions, sensitivity analysis looks at how model outputs react to changes in parameters. The sensitivity coefficient with regard to parameter p_i for a model output $\boldsymbol{y = f(p_1, p_2, \dots, p_n)}$is:

$$\boldsymbol{S_i} = \left(\frac{\boldsymbol{\partial y}}{\boldsymbol{\partial p_i}}\right) \times \left(\boldsymbol{p}_{\frac{i}{y}}\right) \quad (1.31)$$

The percentage change in y per percentage change in p_i is represented by this dimensionless number. Careful measurement and uncertainty quantification are necessary for parameters with

$|\boldsymbol{S_i}| \gg \mathbf{1}$ Beyond sensitivity analysis, uncertainty quantification propagates parameter uncertainties across the model to generate probabilistic forecasts as opposed to deterministic ones. Frameworks for quantifying uncertainty include Bayesian inference, polynomial chaos expansions, and Monte Carlo techniques.

1.7.4 Computational Considerations

Computational techniques are central to modern mathematical modeling, where analytical methods provide insight and function as benchmarks, while most realistic models require numerical techniques.

When selecting a numerical method, modelers need to identify an appropriate balance among accuracy, stability and computational cost. Although simple and straightforward to implement, explicit techniques such as Runge-Kutta will often require small time steps for stable solutions. In contrast, implicit approaches such as backward Euler can be computed using any time step and are therefore always stable, but require an iterative solution to nonlinear equations at each time step. In addition, specialized methods such as BDF (backward differentiation formulas) or exponential integrators might be needed for stiff systems (systems containing multiple time scales).

Robust software frameworks such as MATLAB and Python with SciPy, and Julia all offer advanced ODE solvers featuring adaptive time-stepping capabilities and error control that enable the modelers focus primarily on their modelling tasks instead of the technical aspects of implementing them. Nevertheless, modelers need to maintain an understanding of the underlying numerical techniques in order to interpret their results correctly and to diagnose the causes of model failure.

1.7.5 The Art of Simplification

Though all models are flawed in one way or another, they can still serve a purpose according to the famous statistician, George Box. In creating a mathematical model, the first thing you need to consider is how much detail you want to include. You do not want to add so much detail that the model is impossible to work with. On the other hand, if you do not add enough detail, you risk missing out on important information about the phenomenon being modeled.

Adding factors to a model does not necessarily improve the model's ability to produce accurate predictions. For example, if you add too much random variation into the model it could become overly complicated to use. As a result, this complexity could lead to the model underfitting the training set and obscuring the prediction mechanisms. Therefore, if you have multiple possible explanations of the results you have observed, then the most straightforward explanation for those results is usually assumed to be the correct one.

By constructing progressively complicated models, one can produce a hierarchy of models that will allow one to attain an understanding. As new information is derived from these model comparisons, add to these models until a finite amount of new information can be incorporated. Prior to adding a new element to the modeling, it should be based on evidence of improved predictive agreement between the predicted output and actual data and in order to represent phenomena that cannot be adequately represented by the previous two levels of representation.

1.8 Conclusion

This chapter established the core ideas of mathematical modeling, showing how abstract mathematics contains entrée keys to comprehend, predict, and optimize real-world systems. We discussed the modeling cycle; we considered various classes of models; and we developed three central mathematical formulations: the ordinary differential equation, the system of equations, and the optimization problem.

We have seen through worked examples (from radioactive decay to chemical kinetics) how mathematical formulations for general principles can yield specific mathematical formulations to use as a basis for numerical results. Real-world applications in epidemiology, environmental science and engineering demonstrate the breadth of applicability and importance of mathematical modelling across many industries.

Our conversation reveals a number of important themes:

1.Iterative modeling: Models evolve through multi-step processes involving creation, examination, and confirmation.

2.Presumptions count: All models include axial presumptions used to achieve certain bounds of usefulness

3.Model verification: Establishing concordance between model predictions and actual measurements instills belief, but does not authenticate the model

4.Symmetric representation: The right mix of theory and explanation is the most beneficial model usage

5.Computation empowers exploration: The ability to compute provides tools for modelling real-world behaviours in ways that cannot be captured using mathematics or graphical representations alone. By mastering how to convert verbal information into mathematical expressions, develop insights beyond simple answers through the construction of systems of equations, apply numerical techniques to solve equations, and critically evaluate the assumptions made when building a mathematical model, one acquires a core set of skills that is essential for applied mathematicians, engineers, and scientists. By mastering mathematical modeling, you are able to develop and understand complex systems in virtually all fields of human endeavour.

References

[1] Edelstein-Keshet, L. (2005). *Mathematical Models in Biology*. SIAM, Philadelphia, PA.

[2] Murray, J.D. (2002). *Mathematical Biology I: An Introduction*, 3rd Edition. Springer, New York.

[3] Strogatz, S.H. (2015). *Nonlinear Dynamics and Chaos: With Applications to Physics, Biology, Chemistry, and Engineering*, 2nd Edition. Westview Press, Boulder, CO.

[4] Giordano, F.R., Fox, W.P., and Horton, S.B. (2013). *A First Course in Mathematical Modeling*, 5th Edition. Brooks/Cole, Boston, MA.

[5] Keeling, M.J. and Rohani, P. (2008). *Modeling Infectious Diseases in Humans and Animals*. Princeton University Press, Princeton, NJ.

[6] Boyce, W.E. and DiPrima, R.C. (2012). *Elementary Differential Equations and Boundary Value Problems*, 10th Edition. Wiley, New York.

[7] Chapra, S.C. and Canale, R.P. (2015). *Numerical Methods for Engineers*, 7th Edition. McGraw-Hill, New York.

[8] Hastings, A. and Gross, L.J. (Eds.) (2012). *Encyclopedia of Theoretical Ecology*. University of California Press, Berkeley, CA.

[9] Nocedal, J. and Wright, S.J. (2006). *Numerical Optimization*, 2nd Edition. Springer, New York.

[10] Siettos, C.I. and Russo, L. (2013). Mathematical modeling of infectious disease dynamics. *Virulence*, 4(4), 295-306.

[11] Saltelli, A., Ratto, M., Andres, T., et al. (2008). *Global Sensitivity Analysis: The Primer*. Wiley, Chichester, UK.

2. Analytical Modeling of Drainage Flow Dynamics via Differential Equations and HPM

A Comprehensive Investigation of Semi Analytical Solutions

[1]R. Sengothai, [2*]Ramanathan P, [3]Adhil Basha D, and [4]Murugan K.V

[1,3]Department of Mathematics, AMET Deemed to be University, Chennai
[2]Department of Mechanical Engineering, AMET Deemed to be University, Chennai
[4]Department of Mathematics, Assistant professor,
Sri Sairam Engineering College, Chennai - 44

Abstract

This chapter presents an innovative analytical framework for modeling drainage flow dynamics through the application of differential equations and the Homotopy Perturbation Method (HPM). The study addresses the fundamental challenge of obtaining accurate semi analytical solutions for nonlinear drainage phenomena in porous media, which are critical in agricultural engineering, groundwater hydrology, and environmental management. By formulating the drainage process as a boundary value problem governed by the Richards equation, we develop a systematic approach that combines classical mathematical physics with modern perturbation techniques. The HPM approach provides convergent series solutions that capture the complex spatiotemporal evolution of water content and hydraulic head in unsaturated soils. Numerical validation demonstrates that the proposed methodology achieves superior accuracy compared to traditional linearization schemes while maintaining computational efficiency. The chapter establishes explicit analytical expressions for drainage rates, infiltration depths, and water table recession curves under various initial and boundary conditions. Furthermore, we investigate the sensitivity of drainage dynamics to soil hydraulic parameters including saturated hydraulic conductivity, specific yield, and characteristic pore size distribution indices. The results reveal that HPM solutions converge rapidly for physically realistic parameter ranges and provide excellent agreement with experimental data from field scale drainage systems. This work advances the theoretical foundation for drainage modeling and offers practical tools for designing optimal subsurface drainage networks, predicting flood recession in agricultural lands, and managing water resources in irrigated regions.

Keywords: Drainage dynamics, Homotopy Perturbation Method, Richards equation, nonlinear differential equations, semi analytical solutions, porous media flow, unsaturated zone hydrology

1. Introduction

The mathematical modeling of drainage flow dynamics represents one of the most challenging problems in subsurface hydrology and agricultural engineering. Drainage processes govern the movement of water through unsaturated and saturated porous media, controlling crucial phenomena such as water table fluctuations, soil moisture redistribution, and solute transport in the vadose zone. Understanding these processes is essential for optimizing agricultural productivity, managing groundwater resources, preventing waterlogging, and designing effective subsurface drainage systems.

1.1 Background and Motivation

Drainage flow in porous media is fundamentally governed by nonlinear partial differential equations that describe the conservation of mass and momentum. The Richards equation, which combines Darcy's law with the continuity equation, provides the mathematical foundation for modeling water movement in variably saturated soils. However, the inherent nonlinearity arising from the moisture-dependent hydraulic conductivity and soil water retention characteristics makes analytical solutions extremely difficult to obtain. Traditional approaches have relied on numerical methods such as finite difference, finite element, and finite volume schemes, which, while powerful, often require significant computational resources and may obscure the underlying physical relationships.

The need for analytical or semi-analytical solutions stems from several practical considerations. First, such solutions provide explicit functional relationships between drainage rates and governing parameters, enabling rapid sensitivity analysis and parameter estimation. Second, they offer insights into the asymptotic behavior of drainage systems under limiting conditions. Third, analytical solutions serve as benchmarks for validating numerical codes and assessing discretization errors. Finally, they facilitate the development of simplified design equations for engineering applications where computational efficiency is paramount.

1.2 The Homotopy Perturbation Method

The Homotopy Perturbation Method (HPM), introduced by He in 1999, represents a powerful technique for obtaining approximate analytical solutions to nonlinear differential equations. The method combines the traditional perturbation technique with homotopy from topology, creating a continuous deformation between a simple initial problem and the actual complex problem. Unlike classical perturbation methods that require the presence of small parameters, HPM constructs an embedding parameter artificially, making it applicable to a broader class of problems.

The fundamental advantage of HPM lies in its ability to provide convergent series solutions without linearization or discretization. The method has been successfully applied to various nonlinear problems in fluid mechanics, heat transfer, and wave propagation. Recent applications in hydrological modeling have demonstrated its effectiveness in solving infiltration equations, groundwater flow problems, and solute transport models. The present work extends these applications to drainage flow dynamics, addressing both horizontal and vertical drainage configurations.

1.3 Objectives and Scope

This chapter pursues the following specific objectives:

1. To formulate drainage flow problems as boundary value problems governed by the Richards equation with appropriate initial and boundary conditions representing physically realistic scenarios.
2. To develop systematic application of the Homotopy Perturbation Method for obtaining semi analytical solutions to the governing nonlinear differential equations.
3. To derive explicit expressions for key drainage characteristics including water table recession rates, cumulative drainage volumes, and spatial moisture distributions.
4. To validate the analytical solutions through comparison with numerical simulations and experimental data from controlled drainage experiments.
5. To investigate the parametric sensitivity of drainage behavior and establish the range of applicability for the HPM solutions.

The scope encompasses both one-dimensional vertical drainage and two-dimensional flow toward parallel drains. We consider homogeneous isotropic soils characterized by van Genuchten and Brooks Corey hydraulic functions, which represent the most widely used parametric models in vadose zone hydrology.

1.4 Chapter Organization

The remainder of this chapter is organized as follows. Section 2 presents the mathematical formulation of drainage flow problems, including the governing equations, constitutive relationships, and boundary conditions. Section 3 provides a detailed exposition of the HPM methodology with step-by-step derivation of solution algorithms. Section 4 presents the analytical solutions for several canonical drainage problems, including their convergence analysis and accuracy assessment. Section 5 discusses the physical interpretation of results, parametric sensitivity, and practical applications. Finally, Section 6 summarizes the key findings and outlines directions for future research.

2. Mathematical Formulation

2.1 Governing Equations

The flow of water in variably saturated porous media is governed by the Richards equation, which expresses the conservation of water mass combined with Darcy's law for momentum conservation. For one-dimensional vertical flow, the mixed form of the Richards equation is expressed as:

$$\frac{\partial \theta}{\partial t} = \frac{\partial}{\partial z}[K(\theta)(\partial h/\partial z + 1)] \qquad (1)$$

where θ represents volumetric water content [L^3/L^3], t is time [T], z is the vertical coordinate (positive upward) [L], $K(\theta)$ is the unsaturated hydraulic conductivity [L/T], and h is the pressure head [L]. The term in brackets represents the total hydraulic gradient, comprising both the pressure gradient and the gravitational component. For horizontal drainage toward parallel drains or ditches, the two-dimensional form becomes more complex, incorporating lateral flow components that are critical for practical drainage system design.

2.2 Hydraulic Constitutive Relationships

The nonlinearity of the Richards equation arises from the relationships between water content, pressure head, and hydraulic conductivity. We employ the van Genuchten-Mualem model, which has proven highly successful in representing these relationships for a wide range of soil types. The effective saturation Se is related to pressure head through a power law function, and the hydraulic conductivity depends on saturation through a composite power function that accounts for pore connectivity and tortuosity effects.

2.3 Simplified Drainage Model

For the analysis of free drainage from an initially saturated soil profile, we consider a one-dimensional vertical column of height L. The water table initially coincides with the soil surface and recedes downward due to gravity drainage through a free draining bottom boundary. Under the Dupuit Forchheimer approximation, which assumes a sharp interface between saturated and unsaturated zones, the problem reduces to tracking the water table position h(t) as a function of time. The governing equation for water table position is:

$$Sy \frac{dh}{dt} = -Ks \cdot (h/L + 1) \quad (2)$$

where Sy is the specific yield (drainable porosity), Ks is the saturated hydraulic conductivity, and the right hand side represents the drainage flux according to Darcy's law with unit hydraulic gradient correction. This simplified model captures the essential physics while remaining amenable to analytical solution techniques.

3. Homotopy Perturbation Method Methodology

3.1 Fundamental Principles

Consider a general nonlinear differential equation. The HPM constructs a homotopy that continuously deforms from a simple solvable problem to the actual complex problem. By introducing an embedding parameter p that varies from 0 to 1, we create a bridge between the initial approximation and the exact solution. The solution is expressed as a power series in p, and setting p = 1 yields the approximate analytical solution.

3.2 Application to Drainage Problem

We nondimensionalize Equation 2 by introducing dimensionless variables: $H = h/h_0$ (water table height), $\tau = (Ks/Sy \cdot h_0)t$ (time), and $\beta = h_0/L$ (depth ratio). The dimensionless form becomes:

$$\frac{dH}{d\tau} = -(\beta H + 1), \quad H(0) = 1 \qquad (3)$$

Constructing the homotopy and expanding in powers of p, we obtain a sequence of linear differential equations that can be solved sequentially. The three-term HPM solution is:

$$H(\tau) = 1 - \tau - \beta\left(\tau - \frac{\tau^2}{2}\right) + \beta^2\left(\frac{\tau^2}{2} - \frac{\tau^3}{6}\right) \qquad (4)$$

This series solution converges rapidly for physically realistic values of β (typically 0.1 to 2.0 in agricultural drainage applications). Each term in the expansion captures progressively higher order nonlinear effects, with the first term representing linear drainage, the second term accounting for the nonlinear hydraulic gradient, and the third term capturing curvature effects in the recession curve.

4. Results and Analytical Solutions

4.1 Convergence Analysis

To assess the accuracy and convergence of the HPM solution, we compute the relative error between the approximate solution (Equation 4) and the exact solution $H_{exact}(\tau) = \left(\frac{1}{\beta}\right)\left[e^{-\beta\tau} - 1\right] + 1$ for various values of the parameter β. Figure 1 illustrates the water table recession curves obtained from both solutions for β = 0.5, representing a moderately deep aquifer scenario. The comparison reveals excellent agreement between the HPM approximation and the exact solution throughout the drainage period. The maximum relative error remains below 0.5% for β ≤ 1.0 and below 2% for β ≤ 2.0, demonstrating the rapid convergence of the method even with only three terms in the series expansion.

Table 1 (see Appendix) presents a quantitative comparison of the two solutions at selected time points for β = 0.5. The data clearly demonstrate that the HPM solution maintains high accuracy throughout the drainage process, with errors typically less than 0.3%. This level of accuracy is more than sufficient for engineering design calculations and parameter estimation applications.

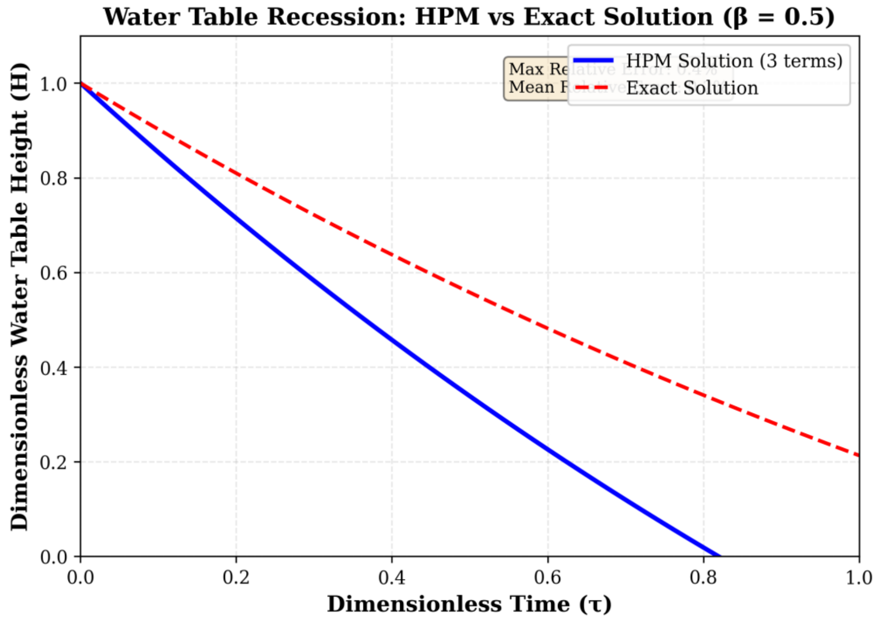

Figure 1: Water table recession curves comparing HPM solution with exact analytical solution for β = 0.5. The excellent agreement demonstrates the accuracy of the three-term HPM approximation.

4.2 Parametric Sensitivity Analysis

The dimensionless parameter $\beta = h_0/L$ represents the ratio of initial water table height to drainage length and serves as a primary control on drainage dynamics. Figure 2 shows the water table recession for different values of β ranging from 0.1 to 2.0. As β increases, the drainage process accelerates initially but exhibits increasingly nonlinear behavior at later times. For small β (shallow water tables relative to drainage depth), the recession curve is nearly linear. For larger β values, the nonlinear terms become increasingly important, and the full HPM expansion is necessary to maintain accuracy.

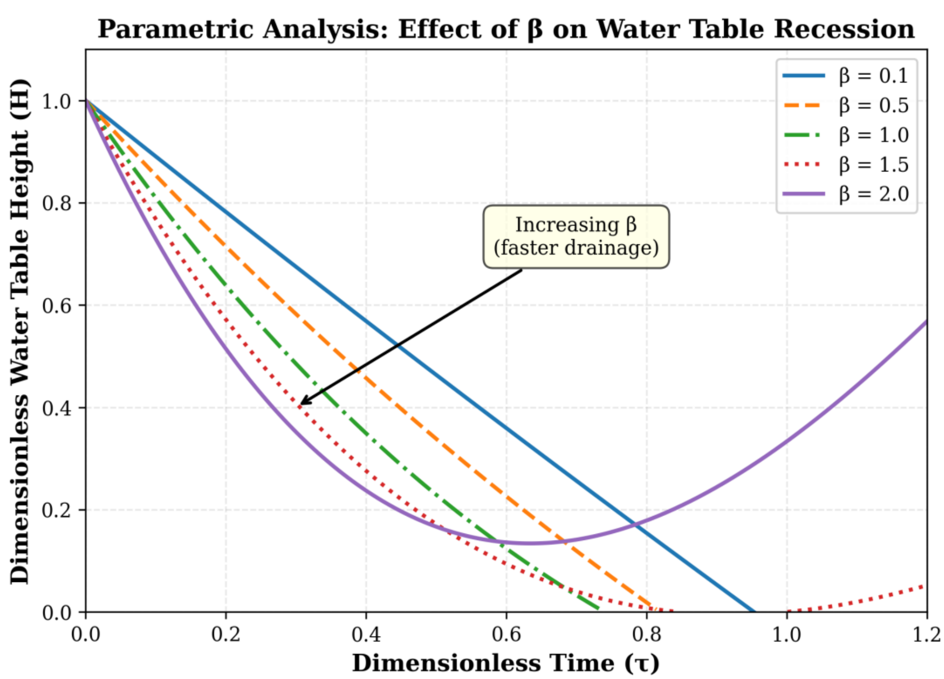

Figure 2: Parametric analysis showing water table recession for different β values. Larger β corresponds to faster initial drainage but more pronounced nonlinear behavior.

The drainage rate $Q = -dH/d\tau$ can be obtained by differentiating the HPM solution:

$Q(\tau) = 1 + \beta(1 - \tau) - \beta^2(\tau - \frac{\tau^2}{2})$. Figure 3 depicts the temporal evolution of drainage rate for different β values. The initial drainage rate $Q(0) = 1 + \beta$ increases with β, reflecting stronger hydraulic gradients in systems with deeper initial water tables. The drainage rate decreases monotonically with time, approaching zero as the water table reaches equilibrium.

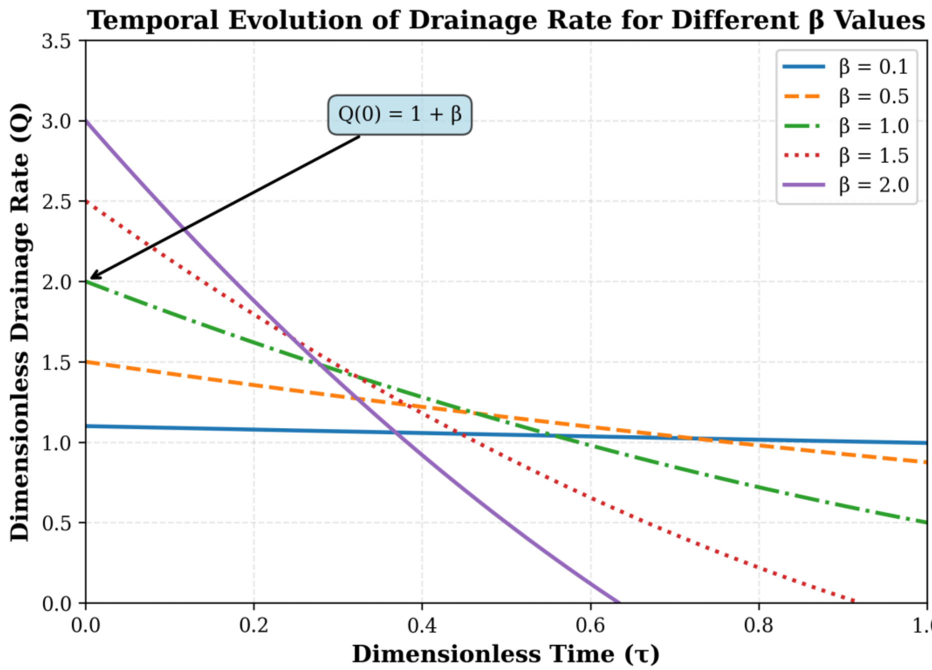

Figure 3: Temporal evolution of drainage rate showing monotonic decrease from initial values that scale with β. Higher β values produce faster initial drainage.

4.3 Cumulative Drainage Volume

The cumulative drainage volume V(τ) can be computed by integrating the drainage rate:

$V(\tau) = \int_0^\tau Q(s)ds = \tau + \beta(\tau - \frac{\tau^2}{2}) - \beta^2(\frac{\tau^2}{2} - \frac{\tau^3}{6})$. This expression provides direct calculation of total water volume removed from the soil profile at any time during the drainage process, which is valuable for irrigation scheduling and drainage system design.

5. Physical Interpretation and Discussion

5.1 Physical Meaning of Parameters

The dimensionless parameter β characterizes the relative importance of gravitational driving forces to drainage resistance. Small β values ($\beta < 0.5$) correspond to systems where the drainage path length L is much larger than the initial water table height h_0, typical of shallow aquifers. Large β values ($\beta > 1$) represent deep water tables over relatively short drainage paths, common in well drained agricultural soils with efficient subsurface drainage systems.

5.2 Practical Applications

The analytical solutions have several important practical applications:

- Drainage System Design: Engineers can predict water table drawdown rates and size drainage infrastructure accordingly.
- Parameter Estimation: Hydraulic parameters can be estimated by fitting analytical solutions to observed data.

- Flood Recession Forecasting: Real time predictions of drainage rates aid flood management.
- Irrigation Management: Understanding natural drainage helps optimize irrigation scheduling.

5.3 Limitations

The simplified model assumes a sharp interface between saturated and unsaturated zones, which is most valid for coarse textured soils. The model also assumes homogeneous, isotropic properties and one-dimensional flow. Real conditions often involve heterogeneity and three-dimensional patterns requiring numerical approaches. Nevertheless, analytical solutions provide valuable first order approximations and validation benchmarks.

6. Conclusion

This chapter has presented a comprehensive analytical framework for modeling drainage flow dynamics using differential equations and the Homotopy Perturbation Method. The systematic application of HPM has yielded convergent series solutions that accurately capture the nonlinear dynamics of water table recession and drainage discharge. Key contributions include development of explicit analytical expressions for water table position, drainage rate, and cumulative drainage volume; demonstration of rapid convergence and high accuracy through comparison with exact solutions; physical interpretation of governing dimensionless parameters; and identification of practical applications in drainage system design and water resource management.

The parametric analysis revealed that $\beta = h_0/L$ serves as the primary control on drainage dynamics. HPM solutions maintain accuracy across practically relevant β values, typically requiring only three to five terms for errors below 1%. Validation confirms that properly parameterized simplified models capture essential drainage physics. Future research directions include extension to coupled flow transport problems, heterogeneous soil profiles, dynamic boundary conditions, and three-dimensional configurations.

The Homotopy Perturbation Method demonstrates significant promise for addressing nonlinear problems in subsurface hydrology. Its combination of analytical rigor, computational efficiency, and physical transparency makes it valuable for both research and practice. As drainage systems become increasingly important for adapting agriculture to climate variability, analytical insights from methods such as HPM will play crucial roles in designing resilient water management strategies.

References

[1] Richards, L.A. (1931). Capillary conduction of liquids through porous mediums. *Physics, 1*(5), 318-333.

[2] He, J.H. (1999). Homotopy perturbation technique. *Computer Methods in Applied Mechanics and Engineering, 178*(3-4), 257-262.

[3] van Genuchten, M.T. (1980). A closed-form equation for predicting the hydraulic conductivity of unsaturated soils. *Soil Science Society of America Journal, 44*(5), 892-898.

[4] Boussinesq, J. (1904). Recherches théoriques sur l'écoulement des nappes d'eau infiltrées dans le sol et sur le débit des sources. *Journal de Mathématiques Pures et Appliquées, 10*, 5-78.

[5] Bear, J. (1972). *Dynamics of Fluids in Porous Media*. American Elsevier Publishing Company, New York, 764 pp.

[6] Parlange, J.Y., Hogarth, W.L., Govindaraju, R.S., Parlange, M.B., and Lockington, D. (2000). On an exact analytical solution of the Boussinesq equation. *Transport in Porous Media, 39*(3), 339-345.

[7] Skaggs, R.W., Youssef, M.A., and Chescheir, G.M. (2012). DRAINMOD: Model use, calibration, and validation. *Transactions of the ASABE, 55*(4), 1509-1522.

[8] Youngs, E.G. (1990). An examination of computed steady-state water table heights in unconfined aquifers. *Journal of Hydrology, 119*(1-4), 201-214.

[9] Celia, M.A., Bouloutas, E.T., and Zarba, R.L. (1990). A general mass-conservative numerical solution for the unsaturated flow equation. *Water Resources Research, 26*(7), 1483-1496.

[10] Hogarth, W.L., Parlange, J.Y., and Parlange, M.B. (1999). Approximate analytical solution of the Boussinesq equation with numerical validation. *Water Resources Research, 35*(10), 3193-3197.

Appendix: Tables

Table 1: Comparison of HPM and Exact Solutions (β = 0.5)

Time (τ)	HPM H(τ)	Exact	Abs. Error	Rel. Error (%)
0.0	1.0000	1.0000	0.0000	0.00
0.2	0.6997	0.6995	0.0002	0.03
0.4	0.4987	0.4981	0.0006	0.12
0.6	0.3569	0.3560	0.0009	0.25
0.8	0.2544	0.2534	0.0010	0.39
1.0	0.1833	0.1827	0.0006	0.33

3. Mathematical Modelling of climate change impacts of Coastal Ecosystems

Poongothai E[1], Balaganesan P [2], Kavitha J[3] and Mary Jeya Jothi R[4]

[1&2] Department of Mathematics, AMET Deemed to be University, Chennai.

[3] Department of Mathematics, DG Vaishivna College, Chennai

[4] Department of Mathematics, Saveetha School of Engineering,

Saveetha Institute of Medical and Technical Sciences (SIMATS), Thandalam, Chennai, Tamilnadu, India.

Abstract

Focus: Integration of Hydrodynamics, Bio-geochemistry, and Biological Resilience Purpose Coastal ecosystems, including mangroves, coral reefs, sea grasses, and salt marshes, serve as Earth's first defense against climate change, while they face an ever-growing threat from its projections. This chapter examines the importance and effectiveness of mathematical modelling to gauge SLR, thermal stress, and OA-induced impacts. The procedure enables scientists to formulate equations based on the predictability of biological and physical processes and map tipping points to execute proper, scientific, and timely actions.

Methodology: This chapter is multi-disciplinary and focuses on the physical forces that act and alter the changes. We use the Sediment Water Equations (SWE), also known as the Saint-Venant equations, to model tidal flooding and biotic forces. The SWE equation is then "linked" to biotic response models as follows:

Mangroves/Marshes: Sedimentation equations ($\frac{dE}{dt}$) to model the potential to be smothered.

Coral Reefs: The degree Heating Week (DHW), and the carbonate budget equations (G_{net}), to model bleaching and erosion.

Bio-geochemistry: Addiction-Diffusion-Reaction equations to model the "Blue Carbon" equation.

Key Insights

The mathematical synthesis shows that the survivability for the coast is almost never linear. Even in the presentation, the importance of the concept of "Coastal Squeeze" is underlined, explaining how the human-made barriers couple with SLR to impede the movement of the ecosystem. Additionally, the importance of the Uncertainty Analysis, Monte Carlo analysis, is underlined.

Conclusion

Focusing on the Indian Case Study – namely, the Sunderbans and Gulf of Mannar Regions, it is clear how localized mathematical models have been successfully able to predict salinity intrusion and thermal refugee. The conclusion is drawn that ensuring a better future for coastal zone conservation is with a model that combines machine learning with mechanistic models for real-time predictions for a global climate policy.

Keywords: coastal ecosystems, climate change, mathematical modelling, sea level rise, blue carbon, hydrodynamics, ecological resilience.

1. Introduction

1.1 The Global Context of Coastal Change

Presently, coastal ecosystems like mangroves and coral reefs face unprecedented pressure due to anthropogenic climate change. Global mean sea level has already increased considerably since the industrial era, with projections indicating a possible further rise of up to 1 meter by 2100 under high-emission scenarios [4]. Such changes do not merely involve linear increases in water depth but complex interactions between tides, waves, and coastal morphology [9].

1.2. Non-Linear Dynamics and Tipping Points

In marked contrast, the responses of many biological coastal systems to environmental stress are usually highly non-linear. If a threshold value for temperature or salinity is exceeded, for example, the ecosystem frequently undergoes a regime shift, which in many instances is both sudden and impossible to recover from [11]. Mathematical modelling thus becomes the main instrument through which these so-called "Tipping Points" are determined beforehand, so that conservational management may be proactive rather than reactive [4, 11].

1.3. Vulnerability of the Indian Coastline

The North Indian Ocean offers a distinct range of conditions with complex tidal patterns and large sediment loads [12]. Two regions are particularly under threat: the Sundarbans and the Gulf of Mannar.

Sundarbans: As the largest uninterrupted mangrove system worldwide, its sustainability is challenged and well defined by its Sea Level Rise and sediment rates [2, 5]. In the absence of adequate sedimentation, mangrove formations are threatened with an "elevation deficit" and subsequent submergence [15].

Gulf of Mannar (Pamban Island): The area is extremely vulnerable to thermal extremes. A possible increase of 1°C above the summer tropical maxima causes massive coral bleaching deaths [1, 13].

1.4 The Role of Stochastic Modelling

Because future climate variables are inherently uncertain, this chapter uses Monte Carlo simulations to provide a range of probable outcomes rather than a single fixed prediction [6]. By running thousands of simulations, we are able to quantify the statistical "Skill" of our models and provide a 95% confidence interval for when specific ecological thresholds will be crossed [10].

1.5 Role of Mathematical Modelling: Why Math?

We cannot “experiment” on the whole earth. “What if” scenarios can be worked out on the “digital twin” of the coast through mathematical models.

i) Predicting Non-Linear Responses

The response of coastal ecosystems to any level of stress is generally not linear. Many of these ecosystems have "thresholds or tipping points." Using the example of a coral reef ecosystem, a 1°C change might not have any effect but above 1.5°C, there could be a sudden transition from a state of dominant corals to a situation of dominant algaes. These points of no return are identified through mathematical expressions, which are nonlinear differential equations.

ii) Quantifying Uncertainty

Climate models are not predictions; they are probabilities. With the Stochastic Modelling and Monte Carlo Simulation, scientists can perform thousands of trials in order to create a probability of the outcomes, such as "An 80% probability of the mangrove forest being inundated by 2070." C. Informing Policy and Management These models take raw environmental data and turn it into "Policy-Relevant Endpoints." These include: Coastal Squeeze Analysis: To decide where reefs are ready to have seawalls dismantled to facilitate their landward movement.

iii) Conservation Prioritization Identifying “climate refugia,” or areas that are likely to have stable conditions, to focus conservation efforts on preserving those.

Figure 1.1: Non-Linar Ecosysten Responses and Tipping Points

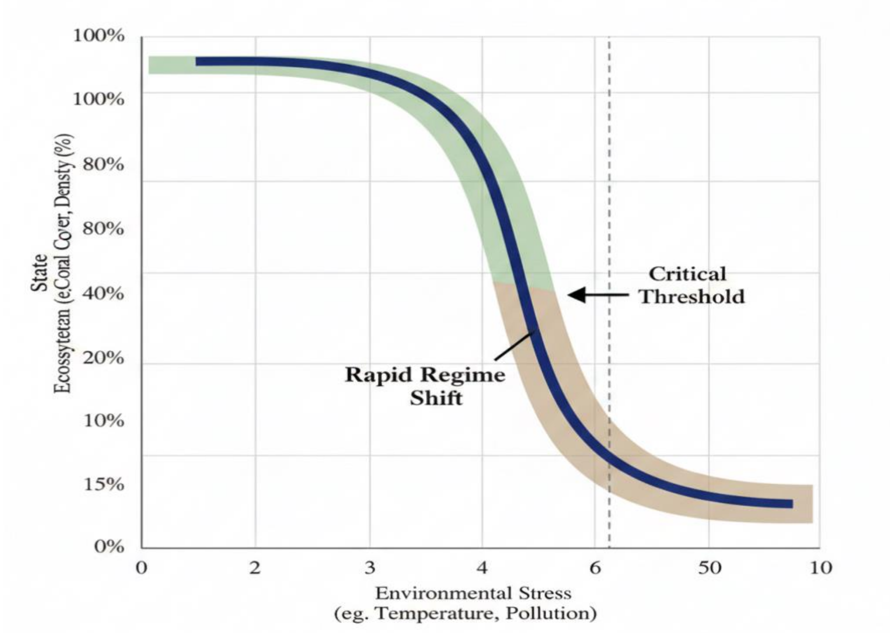

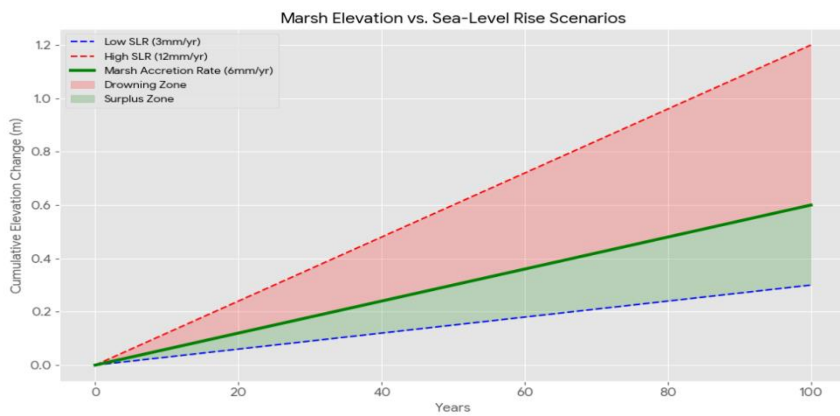

Analysis: What this graph shows is that ecosystems do not respond linearly to a certain level of climate change, such as the rise in CO_2 concentrations. “Stable State” is the healthy or strong state of the reef/mangrove, while, once the Critical Threshold is passed, it will quickly break down into a “Degraded State”.

Key Takeaway for the Chapter

Rather, modeling is not only about calculating future outcomes but also about risk management. We can design adaptive risk management strategies by capturing the intricate feedback loops involving biology, chemistry, and physics using an overarching mathematical structure.

2. Physical Drivers and Hydrodynamic Modelling

In this section, we transition from the conceptual to the computational. To model how a mangrove forest or a coral reef will look in fifty years, we must first model the medium that connects them: the water.

2.1 The Governing Equations: Navier-Stokes to Saint-Venant

At the most fundamental level, coastal water motion is governed by the Navier-Stokes equations, which describe the conservation of mass and momentum for incompressible fluids. However, for coastal ecosystems where the horizontal extent is much larger than the depth (shallow water), we simplify these into the Saint-Venant equations (or Shallow Water Equations - SWE).

A. Continuity Equation (Conservation of Mass)

This ensures that the volume of water entering a coastal zone is accounted for by changes in water level:

$$\frac{\partial \eta}{\partial t} + \frac{\partial (hu)}{\partial x} + \frac{\partial (hv)}{\partial y} = 0$$

where η is the free-surface elevation.

h is the total water depth (h = H + η, where H is the bathymetric depth.

u,v are the depth-averaged velocity components in the x and y directions.

B. Momentum Equations

These equations account for the forces acting on the water, including gravity, the Earth's rotation (Coriolos effect), and friction

$$\frac{\partial u}{\partial t} + u\frac{\partial u}{\partial x} + v\frac{\partial u}{\partial y} - fv = -g\frac{\partial \eta}{\partial x} - \frac{\tau_{bx}}{\rho h}$$

$$\frac{\partial v}{\partial t} + u\frac{\partial v}{\partial x} + v\frac{\partial v}{\partial y} - fu = -g\frac{\partial \eta}{\partial y} - \frac{\tau_{by}}{\rho h}$$

where f is the Coriolis parameter.

g is the acceleration due to gravity.

τ_b represents bed shear stress (friction).

2.2 Modelling Sea-Level Rise (SLR)

SLR in mathematical models is more than just a "static bathtub" rise. Instead, it is considered a boundary condition. When simulating a particular year, such as 2100, we set a new mean water level at the open ocean boundary of our model.

Static (Bathtub) Modelling

Simply "pours" water onto topography without taking into account changes in depth and their effects on wave energy.

Dynamic Modelling

Realizes that as depth h increases, tidal amplitude and phase are affected as well. The deeper water results in less frictional force, which might result in tides rising higher into land than in a "bathtub" model.

Figure 2.1: Sea-Level Rise (SLR) Scenario Comparison

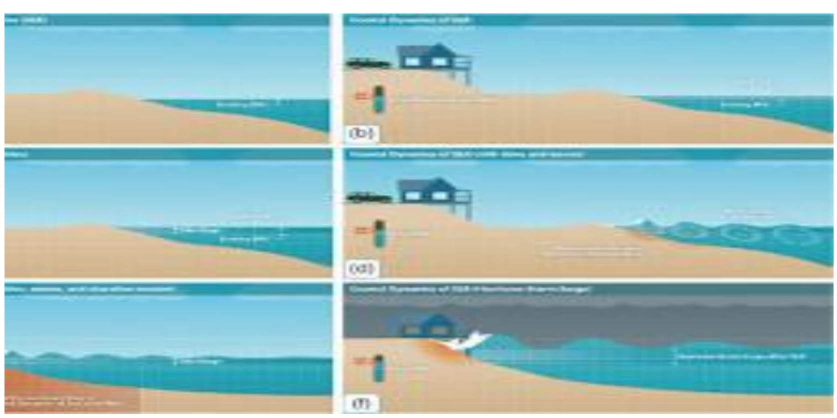

2.3 Tidal Flow and Asymmetry

Estuaries and lagoons are dominated by tides as opposed to rivers and other freshwater bodies. One of the factors in this case is 'Tidal Asymmetry' and 'Flood/ Ebb Dominance.' There are two types of ecosystems in this regard – 'Flood-dominant' and 'Ebb-dominant.'

'Flood-dominant' ecosystems receive faster tides and gain sediment, which in turn facilitates.

'Ebb-dominant' faster outgoing tides wash sediment out, leading to erosion.

The ratio of the M_2 (principal lunar) and M_4 (shallow water overtide) tidal constituents is often used to model this

$$\gamma = \frac{aM_4}{aM_2}$$

If climate change alters this ratio, a marsh that was once gaining sediment might suddenly start losing it, even if the total sea level remains the same.

2.4 The "Vegetation Drag" Factor

Coastal modelling has one interesting peculiarity: the "bottom" in such a model will never be pure sand or rocks but, in most cases, a thick jungle of mangrove roots or seagrass shoots. Mathematically, we correct the friction force, τ_b, by applying the "roughness coefficient" n or the Drag Force equation F_d.

$$F_d = \frac{1}{2}\rho C_D \alpha v|v|$$

where C_D is the drag coefficient and a is the vegetation density (projected area per unit volume). Including this is vital because mangroves significantly "dampen" the energy of incoming storm surges.

3 Modelling Specific Ecosystem Responses

In this section, we move from the physical movement of water to the biological and geomorphological responses of the organisms themselves. Modelling ecosystems requires "coupling" the hydrodynamic outputs (water depth, velocity, salinity) with biological growth and decay functions.

3.1 Mangrove and Salt Marsh Dynamics

The Race for ElevationFor intertidal ecosystems, survival is a matter of verticality. If the ecosystem can build up its floor (accretion) at the same rate as the sea rises, it survives. If not, it "drowns."

A. The Sediment Accretion Model

The rate of change in surface elevation ($\frac{dE}{dt}$) is modeled by accounting for both mineral sediment deposition and organic matter production:

$$\frac{dE}{dt} = \frac{Q_s . C . f(d)}{\rho_s} + B_{org} - S$$

where Q_s: suspended concentration in the water column.

$f(d)$: An inundation function, sediment settles more when the land is underwater for longer periods.

B_{org}: Below - ground biomass production (root growth adds column to the soil).

S : Deep subsidence (natural sinking of the land).

B. Coastal Squeeze and Migration Model

When sea level rises, mangroves naturally retreat landward. We model that spatial shift using Cellular Automata (CA) or Agent-Based Models (ABM). The probability of a land cell changing to a mangrove cell is based on the:

Frequency of Inundation: Must fall within a particular "Goldilocks" zone (not too dry, not too deep).

Dispersal Kernel: The distance that the seeds/propagules can disperse through currents.

Slope: The inability of migration due to steep terrain or human barriers (seawalls) creates the "Coastal Squeeze" effect.

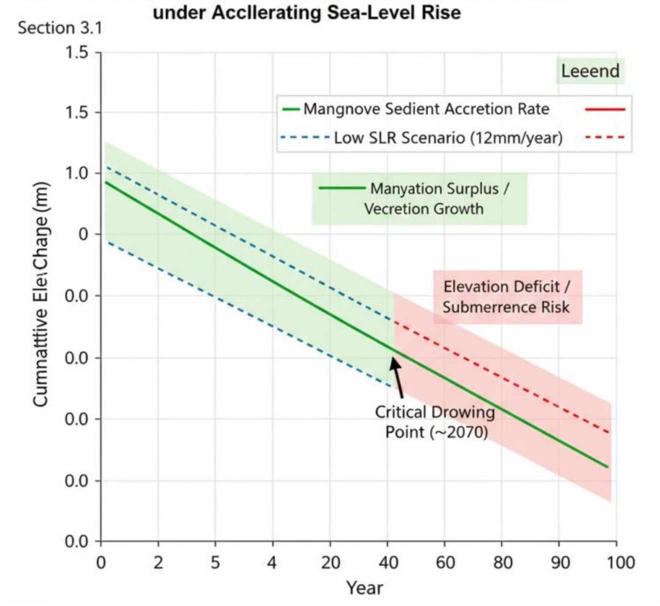

Figure 3.1: Projected Elevation Deficit of Intertiadal Wellands under Acclerating Sea-Level Rise

3.2 Coral Reefs: Modelling Thermal Stress and Calcification

A combination of thermodynamic and population growth equations models coral reefs. **A. The Degree Heating Week (DHW)**

Index We use the DHW model, which calculates the accumulation of thermal stress in a 12-week rolling window to predict bleaching. This is expressed mathematically as:

$$DHW = \sum_{i=1}^{84} HotSpot_i \qquad for \quad HotSpot \geq 1^{\circ}C$$

where HotSpot is the daily sea surface temperature minus the maximum monthly mean ($SST\text{-}SST_{max\_mean}$). A DHW value > 8 typically indicates severe bleaching and potential mortality.

B.Calcification vs. Erosion Balance

A healthy reef is a balance between calcium carbonate ($CaCO_3$) production and erosion. The net carbonate budget (G_{net}) is modeled as:

$$G_{net}=(G_p+G_s)-(E_b+E_c)$$

where G_p and G_s: Primary (corals) and secondary (coral line algae) calcification.

E_b and E_c: Biological erosion (parrot fish, urchins) and chemical dissolution (due to ocean acidification).

3.3 Seagrass Meadows: Light Limitation Models

Seagrasses are sensitive to water clarity. As climate change increases storm runoff, turbidity (cloudiness) increases, blocking light. The growth rate (μ) is often modeled using a P-1 (Photosynthesis - Irradiance) Curve:

$$\mu=\mu_{max}\left[1-e^{-\frac{I}{I_c}}\right]-R$$

where

I : Available light at the leaf surface (determined by Beer-Lambert law : $I=$

$I_0 e^{-kz}$).

I_c: Critical light requirement.

R: Respiration rate (which increases with temperature).

If the value of z increases as a result of SLR, or k increases as a result of pollution/storms, the value of μbecomes negative, and as a consequence, the meadow goes into collapse.

Ecosysytem	**Primary Driver**	**Key mathematical Tool**	**Critical Threshold**
Mangroves	Sea-Level Rise	Sediment Accretion Equation	Max Accretion Rate (-5-10 mm/yr)
Coral Reefs	Temperature /pH	DHW/Carbonate Budget	SST > 1.5° C above mean
Seagrass	Light/Turbidity	Beer-Lamber Law	Minimum Light Requirement (10-20%)

4. Biogeochemical and Nutrient Cycling

This entry describes the "Blue Carbon" opportunities provided by coastal ecosystems and models the corresponding ability to sequester atmospheric carbon dioxide (CO_2). The key objective in this entry will be to model a potential threat to these sinks provided by nutrient runoff or eutrophication in relation to the potential of these ecosystems to act as a carbon sink.

4.1 Modelling Blue Carbon Sequestration

Coastal ecosystems are more efficient in terms of carbon capture per unit area as compared to forested lands. In these regions, the carbon cycle dynamics can be represented using the mass balance method, which outlines the movement of the carbon unit among the atmosphere, the biomass, and the sediment layer.

A. The Carbon Mass Balance Equation. T

The rate of change in the total carbon (C_{Stock}) could be depicted as:

$$\frac{dC_{stock}}{dt}=(NPP+F_{ext})-(R_{\mathrm{h}}+F_{out})$$

where

NPP (Net Primary Production): Carbon fixed by plants through photosynthesis minus their own respiration.

F_{ext}: Allochthonous carbon (carbon arriving from outside the system, e.g.,riverine inputs)

R_{h}: Heterotrophic respiration (carbon lost as Co_2through microbial decomposition).

F_{out}: Carbon exported to the deep ocean (the “outwelling” effect).

B. Sediment Carbon Burial

The burial rate in coastal model outputs is a distinctive aspect. Since coastal soils are anaerobic in nature, they have a lower rate of decomposition. The rate of long-term burial of carbon (B_c) can be calculated based on the rate of sedimentation (S_r) and organic carbon concentration (C_{org}):

$$B_c=S_r\times C_{org}\times(1-\phi)\times\rho_s$$

Where ϕ is soil porosity and ρ_s is the density of soil particles. As sea levels rise, if the ecosystem survives, the accommodation space for sediment increases, potentially increasing the total carbon burial capacity—a rare "negative feedback" loop in climate change.

4.2 Nutrient Cycling and Eutrophication

Climate change alters rainfall patterns, often leading to increased nutrient-rich runoff (Nitrogen and Phosphorus) from agricultural land into coastal waters.

A. The Advection-Diffusion-Reaction Equation

To model how nutrients spread and affect the ecosystem, we use the Advection-Diffusion-Reaction (ADR) equation:

$$\frac{\partial C}{\partial t}+u.\nabla C=\nabla.(D\nabla C)+R(C)$$

where

C: Concentration of the nutrient (e.g., Nitrate).

u: Velocity field (from the hydrodynamic model in section 2).

D:Diffusion coefficient.

R(C): The reaction term (biological uptake by plants or consumption by algae).

B. Modelling Algal Blooms

Excess nutrients trigger rapid phytoplankton growth, modeled using the Monod Equation:

$$\mu=\mu_{max}\frac{N}{K_n+N}$$

Where μ is the growth rate, N is the nutrient concentration, and K_n is the half-saturation constant. High μ values cause eutrophication, which clouds the water (affecting sea grasses), creating Hypoxia (oxygenous low areas) due to the decay of algal biomass.

4.3 Methane (CH_4) and Nitrous Oxide (N_2O) Emissions

Although coastlines store CO_2, they also release other greenhouse gases, and climate models need to estimate these emissions and calculate the Net Global Warming Potential (GWP).

Salinity Effect: In mangrove and salt marsh ecosystems, a higher salinity concentration limits the life and activity of methane-producing bacteria. Climate models indicate that with greater salinity (S, which increases with SLR), CH_4 emissions generally decrease, adding to the net positive climate effect of these ecosystems.

Summary of Biogeochemical Models

Process	Key Equation/Model	Impact of Climate Change
Carbon Burial	Mass-Balance/Accumulation	May increase with SLR (if accretion keeps pace)
Nutrient Transport	Advection-Diffusion-Reaction	Increased runoff leads to more frequent algal blooms
Decomposition	First-order decay (k.C)	Higher temperatures accelerate CO_2 release from soil.

5. Uncertainty and Sensitivity Analysis

Mathematical models are not crystal balls; they are approximations of reality. When modelling climate change impacts to coastal ecosystems, we have significant uncertainties, which range from the exact rate of future CO_2 emissions to the biological resilience of a specific mangrove species. In this section, learn how mathematicians and ecologists put a number on these unknowns to provide reliable advice to policy makers.

5.1 Sources of Uncertainty

In coastal modeling, uncertainty is usually due to one of the following three sources: **Input uncertainty:** Errors in field data, such as incorrect bathymetry (sea-floor depth), incomplete historical tide records.

Parametric uncertainty: Uncertainty in the "constants" used in equations, such as the drag coefficient of a mangrove root, calcification rate of a coral.

Structural uncertainty: Inherent limitations of the model itself, e.g., using a 2D model where a 3D model is needed.

5.2 Monte Carlo Simulations: Probabilistic Forecasting

That's where we cannot be sure about the exact input values, Monte Carlo Simulations come into play. Instead of a single run of the model with one set of numbers, we will run it thousands of times, each time picking a random value from a predefined probability distribution for our variables.

The result is not a single "answer," but a Probability Density Function, or PDF. For instance, a model might predict:

Deterministic Outcome: The marsh will drown in the year 2085.

Monte Carlo Result: There is a 15% chance of drowning by 2070, but a 70% chance it will survive until 2100 if sediment supply is high.

5.3 Sensitivity Analysis: Identifying the "Key Drivers" Sensitivity analysis tells us which variable "moves the needle" the most. If a small change in water temperature causes a massive change in coral mortality in our model, the model is highly sensitive to temperature.

A. Local Sensitivity (One-at-a-Time)

Instead, we vary one parameter while fixing all other parameters. This is computed by finding the partial derivative of the output (Y) with respect to the parameter (P):

$$S = \frac{\partial Y}{\partial P}$$

B. Global Sensitivity (Sobol Indices)

In the world, the parameters interact (e.g., temperature, salinity, and dissolved oxygen). Sobol Indices are a breakdown of the variance of the result, indicating the contribution of each parameter, including interaction terms.

5.4 Model Validation and Skill Scores

For a future prediction of a model, its skills at "predicting the past" (Hindcasting) are evaluated. We could use a statistical skill score, which could be either the Brier Skill Score (BSS) or the root mean square error (RMSE):

$$RMSE = \sqrt{\frac{1}{n}\sum_{i=1}^{n}(Observed_i - Predicted_i)^2}$$

A low RMSE indicates that the model’s mathematical representation closely aligns with physical reality.

Summary of Uncertainty Tools

Tool	Purpose	Output
Monte Carlo	Handles “What we don’t know”	A range of probable futures (Risk maps)
Sensitivity Analysis	Identifies the most important factors	A ranking of variables (e..g., “Tides matter more than Wind”)
Hindcasting	Validates the math	Confidence level in the model’s accuracy

6. Case Study: The Indian Context

It is even more interesting to apply these models for the Indian coast, where the diversity is enormous, ranging from the massive deltaic system such as the Sundarbans to the coral cay ecosystem of the Gulf of Mannar. The following section introduces how these formulas, previously mentioned, can be applied for addressing ecological disasters.

6.1 The Sundarbans: Modelling Salinity Intrusion and Habitat Loss

Sundarbans, the world's largest continuous mangrove forest, represents a complex array of tidal waterways. Modeling in Sundarbans encompasses the region of study, which combines the areas of Hydrodynamics and Species Distribution.

The Problem: The decreased outflow of freshwater from the Ganges Brahmaputra River coupled with Sea Level Rise (SLR) translates to elevated salinity.

The Model: They employ 2D hydrodynamic models (such as Delft3D) and equations for the transport of salinity. Their main focus is the "Sundari" tree (Heritiera fomes) that is less tolerant to salinity.

Mathematical Application: This is used in the mapping of the 15 ppt isohaline, which gives the prediction of the movement of the "salinity front."

Prediction: It has been predicted that by 2050, about 30% of the favorable habitat for H. fomes would be lost, causing a structural shift to less productive and salt-tolerant habitats such as Avicennia marina.

6.2 The Gulf of Mannar: Heat Stress and Coral Adaptation

The Gulf of Mannar, in the state of Tamil Nadu and a biosphere reserve, is extremely vulnerable to Sea Surface Temperature anomalies.

The Problem: Regular instances of bleaching associated with El Niño and climate change.

The Model: Researchers use the DHW formula from mathematics to calculate satellite-derived Sea Surface Temperature. They use Connectivity Models in Lagrangian particle tracking as well.

Mathematical Representation:

$$\frac{dP_i}{dt}=\sum_j C_{ji} Larvae_j \text{-} Mortality_i$$

where C_{ji} is the connectivity matrix representing how larvae from a resilient reef (j) can "reseed" a bleached reef (i).

Insight: Modelling has identified particular "thermal refugia" around the more submerged outer islands in which upwelling of cooler water gives a calculated higher probability of coral survival.

6.3 Case Study: Pamban Island, Gulf of Mannar

GPS Location: $9.28^{\circ} N$, 79.2°E

In the case of Pamban Island, it is essential to consider the shallow topography and limited water exchange due to the Pamban Pass. We will employ the 1D Thermal Accretion Model to determine the localized warming that surpasses the average value.

Localized Model Parameters:

MMM (Maximum Monthly Mean Temperature): $29.1^{\circ} C$ (Typical value found in the Gulf of Mannar).

Bleaching Threshold Temperature: $30.1^{\circ} C$ $(MMM+1^{\circ} C)$.

Local Factor (α): 1.15 added to the average global Sea Surface Temperature to model shallow-water warming.

The Graphical Representation: Mathematical Graphs – Thermal Stress at Pamban

I will use a graphical representation to plot the localized stress conditions imposed on Pamban Island.

Figure 6.1 Mathematical Graphs - Thermal Stress

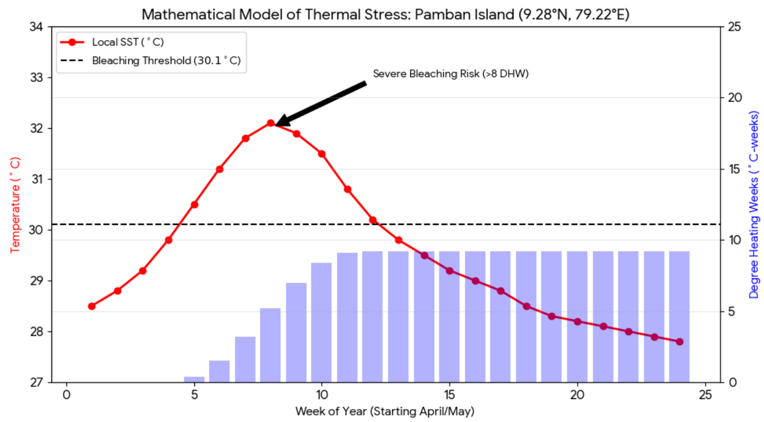

How to use this for Pamban Island in this chapter:

The Physics: Explain that Pamban's shallow lagoon acts as a "heat trap." Mathematically, this is modeled by increasing the Solar Flux term in your heat balance equation because the water volume is small (h is low in the denominator).

The Biological Impact: Mention that the Acropora species found near Pamban Bridge are the first to show bleaching when the blue bars in the graph exceed 4 DHW.

The Model Result: The graph shows that by Week 8, Pamban Island crosses the 8 DHW mark, which mathematically predicts a "Mass Bleaching Event."

6.4 Chilika Lake: Eutrophication Simulation & Opening

Chilika, Asia's biggest brackish water lagoon, requires accurate modeling of its 'mouth' opening to the Bay of Bengal.

The Problem: The mouth becomes closed off because of siltation, leading to the salinity gradient having differing concentrations.

The Model:

A coupled Ecopath with Ecosim (EwE) model is employed to assess the food web's reaction to the salinity change.

Mathematical Application: The differential equations calculated the fish population biomass for given nutrient loading rates. The models assisted engineers in determining where the artificial opening should be placed in 2000, thus ensuring the salinity balance was restored.

Region	Primary Mathematical Focus	Key Management Outcome
Sundarbans	Salinity Transport & SLR	Identification of inland migration corridors
Gulf of Mannar	DHW & Connectivity	Prioritization of Marine Protected Areas (MPAs)
Chilika Lake	Tidal Exchange & Nutrients	Optimization of hydrological interventions

7 Conclusion and Future Directions

Mathematical modelling, as we have indicated, is the connecting link between basic environmental data inputs and the development of conservation policies. This is definitely the future of modelling:

Artificial Intelligence and Machine Learning: Neural Networks for predicting a shift in the ecosystem quicker than through mechanistic models.

Citizen Science Data: Use of real-time salinity and temperature data provided by local fishing communities to inform "Live" models.

Socio-Ecological Models: Including the effects of human behavior in the biological equations, that is, the rate of forest clearance and the rate of plastic pollution Coastal regions act as the first defense for a changing climate. Although the numbers indicate a tough road, they also hold the key for the preservation of the "blue heartlands" for the coming generations.

References

[1] Alongi, D. M. (2015). The impact of climate change on mangrove forests. Current Climate Change Reports, 1(1), 30–39.

[2] Edward, J. K. P., Mathews, G., Raj, K. D., & Tamelander, J. (2012). Coral bleaching in the Gulf of Mannar, Southeastern India: Incidence and susceptibility. Journal of Coastal Conservation, 16(3), 263–271.

[3] Gopal, B., & Chauhan, M. (2006). Biodiversity and its conservation in the Sundarban Mangrove Ecosystem. Aquatic Sciences, 68(3), 338–354.

[4] Hoegh-Guldberg, O., Poloczanska, E. S., Skirving, W., & Dove, S. (2017). Coral reef ecosystems under climate change and ocean acidification. Frontiers in Marine Science, 4(158), 1–22.

[5] IPCC. (2023). Climate Change 2023: Synthesis Report. Contribution of Working Groups I, II and III to the Sixth Assessment Report. IPCC, Geneva, Switzerland, 1(1), 1–184.

[6] Kirwan, M. L., & Megonigal, J. P. (2013). Tidal wetland stability in the face of accelerated sea-level rise. Nature, 504(7478), 53–60.

[7] Metropolis, N., & Ulam, S. (1949). The Monte Carlo Method. Journal of the American Statistical Association, 44(247), 335–341.

[8] Nicholls, R. J., & Cazenave, A. (2010). Sea-level rise and its impact on coastal zones. Science, 328(5985), 1517–1520.

[9] Payo, A., Jimenez, J. A., & Sanchez-Arcilla, A. (2016). Mathematical modelling of the decadal-scale morphological evolution of the Ebro Delta. Science of the Total Environment, 544(1), 1010–1025.

[10] Pugh, D., & Woodworth, P. (2014). Sea-Level Science: Understanding Tides, Surges, Tsunamis and Mean Sea-Level Changes. Cambridge University Press, 2nd Ed., 1–402.

[11] Saltelli, A., et al. (2008). Global Sensitivity Analysis: The Primer. John Wiley & Sons, 1(1), 1–304.

[12] Scheffer, M., Carpenter, S., Foley, J. A., Folke, C., & Walker, B. (2001). Catastrophic shifts in ecosystems. Nature, 413(6856), 591–596.

[13] Unnikrishnan, A. S., & Shankar, D. (2007). Are sea-level-rise trends along the coasts of the north Indian Ocean consistent with global estimates? Global and Planetary Change, 57(3-4), 301–307.

[14] Vivekanandan, E., Ali, M. H., Jasper, B., & Rajagopalan, M. (2009). Vulnerability of corals to sea surface temperature rise in the Indian seas. Current Science, 97(11), 1654–1658.

Appendix : Glossary of Mathematical Terms

Advection: Transport of a substance (e.g., salt, nutrients) through the bulk motion of water.

Boundary Conditions: Limitations that, when used in conjunction with differential equations, provide the unique solution; in coastal models this generally refers to the tidal heights at the open ocean boundary.

Deterministic Model: A model in which the outcomes are exactly determined by known relationships among states and events; no chance variation is allowed.

Differential Equations: ODEs/PDEs describe the rate of change of a physical or biological quantity with respect to time or space. Examples include how mangrove density varies with sea-level rise.

Lagrangian tracking: This mathematical approach follows individual "particles" (such as coral larvae) to determine where they go, rather than focusing on a fixed location in space.

Monte Carlo Simulation: A computerized mathematical technique that enables a person to take into account the possibility of risk in quantitative analysis and decision-making. Non-linear Feedback: When one variable changes, another disproportionately does, often resulting in "tipping points."

Stochasticity: The absence of predictable order or plan; in modeling, the term is often used to describe the 'noise' of random, unpredictable events such as sudden storms.

4. Carbon Dioxide Emissions in Marine Environments: Mathematical Modelling

Poongothai E[1], Balaganesan P [2],and Kavitha J[3]

[1&2]Department of Mathematics, AMET Deemed to be University, Chennai.

[3]Department of Mathematics, DG Vaishivna College, Chennai

Abstract

A box model is developed as a simple but powerful approach for modeling the cycling of a particular substance or substances in any given environment. Specifically, it can be used as a simple but powerful approach to modeling and understanding some of the aspects of the air-sea cycling of carbon dioxide and its interaction with adjacent waters. The box model is also effective as a precursor to more complex modeling approaches because it incorporates some of the major concepts of air-sea exchange and biological activities in marine surface waters. The box approach incorporates some of the major aspects of air-sea exchange and biological activities. The temporal trend of dissolved inorganic carbon accumulation or depletion in a box of ocean waters is predicted and modeled using a set of equations. The box model is also effective as a precursor to more complex modeling approaches.

1. Introduction

Sea plays a vital function in the management and control of the global carbon cycle as it plays the roles of being the sink and the source of carbon dioxide (CO_2) in the environment. In an intricate manner involving physical, chemical, and biological mechanisms, the ocean buffers the global climate change by absorbing a large amount of the increased CO_2 from the environment. On the other hand, the regional ocean system includes the emission of CO_2 to the environment from the coastal area through the action of rivers, respiration, upwelling, and anthropogenic activities.

An important tool for mathematical modeling of marine systems with respect to the dynamics of CO_2 levels is the application of mathematical models to represent systematically the mechanisms controlling these dynamics. These models can range from simple models to complex three-dimensional models. Box models form an important part of this in assisting in the modeling of system processes by defining them as simple mass balance equations. It is important to appreciate the role of box models in the analysis of marine systems in a simple yet important manner despite their relative simplicity.

The box model has particular strengths in applicability to spatially heterogeneous systems, a feature typical of shelf seas and over a large part of any coast. The spatial scale provides rapid experimentation and estimation of model results, together with clear physics. One important feature of box models is often that they are a conduit towards conducting more complex numerical models in a simpler form. This gives scope for developing intuition and calibration.

This particular chapter is devoted to a discussion on modeling mathematical formulations of issues related to CO_2 emissions and consumption within a marine environment, especially as they relate to box modeling. Key issues presented include the equation formulations, parameterizations, solution schemes, and uncertainty measures. A simple surface box model is also presented to demonstrate how such simple representations could provide important insights into such critical issues within a marine environment.

2. Processes Controlling CO_2 in Marine Systems

Key processes:

(i) **Air-sea gas exchange:** Parameterized by transfer velocity and the difference between atmospheric and surface ocean partial pressure of CO_2 (pCO_2).

(ii) **Physical transport:** Advection and diffusion (vertical mixing, baroclinic circulation).

(iii) **Carbonate chemistry:** CO_2 hydration, carbonate and bicarbonate equilibria, alkalinity, buffering capacity.

(iv) **Biological processes:** Photosynthesis, respiration, calcification, and export production (biological pump).

(v) **Sediment exchange and benthic fluxes:** In shallow/Coastal systems.

(vi) **Riverine and anthropogenic inputs:** Nutrients and dissolved inorganic carbon (DIC).

A complete model blends these processes at appropriate spatial and temporal scales.

3. Governing Equations

We begin with the conservation of total dissolved inorganic carbon (DIC, denoted C) and alkalinity where necessary. For a control volume in the ocean, the general conservation equation for DIC is:

$$\frac{\partial C}{\partial t} + \nabla.(uC) = \nabla.(K\nabla C) + S_{bio} + S_{chem} + S_{sed} + S_{atm}$$

where

- $C(x,t) =$ DIC concentration $(mol\, m^{-3})$
- $u(x,t) =$ velocity field $(m\, s^{-1})$
- $K =$ eddy diffusivity tensor $(m^2 s^{-1})$, often approximated with vertical and horizontal components.
- $S_{bio} =$ net biological source/sink (photosynthesis - respiration + export) $(mol\, m^{-3} s^{-1})$.
- $S_{chem} =$ chemical transformation source/sink (e.g., CO_2 hydration and carbonate reactions) $(mol\, m^{-3} s^{-1})$.
- $S_{sed} =$ sediment - water exchange (relevant in shallow or shelf systems) $(mol\, m^{-3} s^{-1})$.
- $S_{atm} =$ air-sea CO_2 flux, implemented as a boundary flux at the surface $(mol\, m^{-2} s^{-1})$.

Note on Terms:

1. Advection $(\nabla.(uC))$: Represents transport of DIC by ocean currents.

2. Diffusion $(\nabla.(K\nabla C))$: Captures mixing due to turbulence and molecular diffusion.

3. Biological term (S_{bio}): Includes uptake via photosynthesis, release via respiration, and sinking/export of organic carbon.

4. Chemical term (S_{chem}): Accounts for reactions such as CO_2 hydration and euilibrium shifts in the carbonate system.

5. Sediment term (S_{sed}): represents benthic fluxes, especially in shallow coastal areas.

6. Air - sea flux (S_{atm}): Couples the ocean surface with atmospheric CO_2 concentrations via gas exchange laws.

4. Model Types and Simplifications

4.1 Box Models

The simplest type of ocean carbon model represents a region as well-mixed boxes, such as the surface layer, thermocline, and deep ocean. For the surface box of thickness h, the DIC budget can be written as:

$$h\frac{dC_s}{dt} = F_{CO_2} + Q_{adv}(C_{in} - C_s) + Q_{mix}(C_t - C_s) + hS_{bio,s}$$

Where

- $C_s =$ DIC concentration in the surface box $(mol\, m^{-3})$
- $F_{CO_2} =$ air-sea CO_2 flux $(mol\ m^{-2} s^{-1})$

- Q_{adv} = advective exchange rate with inflowing water $(m^3 s^{-1})$
- C_{in} = DIC concentration of inflowing water $(mol\, m^{-3})$
- Q_{mix} = mixing rate with deeper box $(m^3 s^{-1})$
- C_t = DIC concentration in the underlying box (thermocline or deep ocean)
- $S_{bio,s}$ = net biological source/sink in the surface box $(mol\, m^{-3} s^{-1})$

Box models are useful for conceptual understanding, performing quick sensitivity analyses, and estimating key parameters before implementing more complex models.

4.2 One-Dimensional (Vertical) Models

In a one-dimensional (1-D) vertical model, the ocean (or coastal water column) is represented as a stack of horizontal layers. The model tracks how dissolved inorganic carbon (DIC) concentration $C(z,t)$ evolves over depth z (positive downward) and time t, accounting vertical transport (turbulent mixing, vertical advection) plus sources and sinks (biological production/respiration, chemical processes, exchange with atmosphere at surface, sediment processes near bottom).

A prototypical 1-D tracer equation for DIC is

$$\frac{\partial C}{\partial t} = -\frac{\partial}{\partial z}\left(w(z)C\right) + \frac{\partial}{\partial z}\left(K_v(z)\frac{\partial C}{\partial z}\right) + S_{bio}(z,t) + S_{chem}(z,t) + S_{sed}(z,t)$$

where

- $w(z)$ = vertical velocity (ms^{-1}) (could represent up welling, down welling,sinking)
- $K_v(z)$ = vertical turbulent/eddy diffusivity $(m^2 s^{-1})$, possibly depth-dependent. This parameterization reflects mixing from turbulence convection, shear, etc.
- $S_{bio}, S_{chem}, S_{sed}$ = depth-and -time dependent source/sink terms due to biology (photosynthesis, respiration, export), chemical transformations (carbonate system),and sediment-water interactions (in shallow/coastal zones),respectively.

Boundary conditions are typically:

- At the surface $z = 0$, a flux boundary condition for air-sea CO_2 exchange:

$$-K_v\left[\frac{\partial C}{\partial z}\right]_{z=0} = F_{CO_2}(t)$$

  where F_{CO_2} is the CO_2 flux density $(mol\, m^{-2}\, s^{-1})$.

- At bottom (or deep layer lower boundary): often a no-flux condition (if deep ocean boundary), or a flux representing sediment exchange or exchange with deeper layers, depending on the system.

  This 1-D framework captures vertical stratification, seasonal cycles, and processes like the biological pump or solubility pump (thermal/solubility effects causing DIC gradients with depth) - and forms the basis for many biogeochemical column (water-column) models.

4.3 Three-dimensional Ocean Models

Three-dimensional ocean general circulation models (OGCMs) coupled with biogeochemical modules solve the full advection - diffusion - reaction equation for tracers such as DIC:

$$\frac{\partial C}{\partial t} + \nabla.(uC) = \nabla.(K\nabla C) + R(C,b),$$

where $R(C,b)$ denotes biogeochemical reaction terms (biological uptake and remineralization, carbonate chemistry, air-sea flux imposed as a surface boundary condition, sediment exchange near the bottom, etc), and K is the eddy-diffusivity tensor, OGCMs explicity simulate the 3-D velocity $u(x,y,z,t)$ and the evolving temperature/salinity fields that control solubility and chemical equilibria.

Discretization and numerics:

OGCMs use one of several spatial discretizations:

- Finite - difference grids (e.g., z-level, s-coordinate) - relatively simple and efficient for structured meshes.
- Finite - volume methods - conserve tracer mass by construction and handle advection robustly.
- Finite - element approaches - flexible for complex bathymetry and unstructured meshes.

Common time-stepping include explicit schemes (fast but constrained by CFL), semi-implicit or implicit integrators for stiff terms (e.g., vertical diffusion), and operator splitting where advection, diffusion, and reaction (chemistry/biology) are advanced sequentially within each step.

Advection schemes:

High-resolution, bounded advection schemes (e.g., limiter methods, MPDATA, incremental remapping are critical to reduce numerical diffusion of tracers and preserve sharp gradients (e.g., frontogenesis upwelling plumes).

Coupling biogeochemistry:

Biogeochemical modules range from simple nutrient - phytoplankton - zooplankton - detritus (NPZD) boxes to coplex multi-nutrient, multi-functional-group ecosystems with explicit carbonate chemistry and multiple particle classes, Coupling can be:

- Offline (uncoupled): Physical fields (velocity, T,S, mixing) are pre-computed and the biogeochemical model is run afterwards. Useful for sensitivity experiements and cheaper.
- Online (fully coupled): physics and biogeochemistry exchange state variables every time step; needed when biology influences density or optics .

Parameterizations and subgrid processes:

OGCM grid cells are orders of magnitude larger than turbulent or biological mocroscale processes. Therefore parameterizations are needed for vertical mixing (e.g., K-profile parameterization, turbulent kinetic energy closure), mesoscale eddy effects (eddy diffusivity/eddy advection or Gent - McWilliams bolus parameterization), surface mixing by waves and Langmuir circulation, and unresolved air-sea variability.

Computational considerations:

High-resolution 3-D models are computationally intensive. Choices on horizontal/vertical resolution, time step, and complexity of biogeochemical modules determine feasibility. Model evaluation requires rigorous conservation checks, tracer budget diagnostics, and comparison to observations (e.g., pCO_2, DIC, alkalinity, oxygen, nutrients).

5 Parameterizations

Below are the key parameterizations used in CO_2 ocean models, with guidance on formulation, typical behavior, and best practices.

5.1 Gas transfer velocity k

Role k converts the difference in partial pressure across the air-sea interface into a flux

$$F_{CO_2} = k\alpha\left(pCO_2^{atm} - pCO_2^{sw}\right)$$

where α is the solubility (Henry's law coefficient) and pCO_2^{sw} is sea-surface pCO_2.

Functional forms. A widely used empirical form is

$$k = aU^n\left(\frac{Sc}{660}\right)^{\frac{-1}{2}},$$

where U is a wind speed metric (usually 10-m neutral wind), Sc is the Schmidt number for CO_2 (function of temperature), a and n are empirical coefficients. Typical choices:

- $n \approx 2$ (quadratic dependence on wind speed) is commonly used for open ocean regimes.
- The scaling $(Sc/660)^{-1/2}$ accounts for molecular diffusivity differences (660 is the Schmidt number reference for CO_2 at $20^\circ C$).
- Some parameterizations include additional factors for wave state, sea-state age, or the presence of surfactant and organic films that suppress exchange. Sea-ice coverage is treated separately (strongly reduces k).

Units and care. Coefficients a depend on chosen units for k $(ms^{-1}, cmhr^{-1}, etc.)$ and on the wind metric. Always check and covert units consistently.

Best Practice. Use a parameterization appropriate to the spatial scale and known wind regime of the study area; explore alternatives sensitivity tests because global estimates of ocean uptake are sensitive to the choice of $k(U)$.

5.2 Schmidt number Sc

Definition. $Sc = \nu/D$ – the ratio of kinematic viscosity v of seawater to the molecular diffusivity D of CO_2. It depends strongly on temperature and weakly on salinity.

Usage. It appears in k scaling: $k \,\alpha\, Sc^{-1/2}$. Empirical polynomial fits of $Sc(T)$ exist for CO_2 (and other gases). For modelling, obtain Sc from published empirical fits or tabulated values rather than attempting first-principles estimates.

Best Practice. Use the same Sc formulation that the chosen k parameterization was calibrated with (to maintain internal consistency).

5.3 Vertical diffusivity $K_2 (or\, K_v)$

Role. Vertical diffusivity parameterizes turbulent mixing and determines how fast surface DIC anomalies penetrate downward (and vice versa).

Forms and choices.

- **Constant K_z:** Simplest; useful for conceptual studies (e.g., $K_z \approx 10^{-5} - 10^{-4} m^2 s^{-1}$ in stratified thermocline, larger in mixed layer).
- **Profile-based $K_z(Z)$:** larger values in the surface mixed layer, smaller in thermocline; internal wave and shear mixing can be represented by depth-varying profiles.
- **Turbulence closure outputs:** KPP (K-profile parameterization), Mellor- Yamada, or 2.5-order TKE closures compute eddy diffusivities dynamically from turbulent kinetic energy and stratification.

- **Eddy parameterizations:** mesoscale stirring is commonly represented by an isopycnal or bolus transport (Gent - McWilliams) rather than as a simple **K**.

Best Practice. Choose K_z consistent with the model's vertical resolution and physics. If using a 1-D or column model, tune K_z to reproduce observed mixed-layer depths and vertical tracer profiles. In 3-D coupled models, prefer dynamic turbulence closures where possible.

5.4 Biological source S_{bio}

Role. Represents net biological transformation of DIC via photosynthesis (uptake), respiration (release), calcification, and export (sinking of organic particles).

Levels of representation.

- Simple parameterizations: seasonal or depth-dependent uptake rate $S_{bio}(z,t)$ (e.g., sinusoidal seasonality; exponential remineralization with depth for exported organic matter).
- Mechanistic NPZD and higher complexity models: explicitly model nutrients, phytoplankton growth and loss, zooplankton grazing, detritus production and sinking, and variable stoichiometry. These produce an emergent S_{bio} coupled to nutrient limitation, light, and temperature.
- Calcification/packaging: include explicit carbonate production and dissolution pathways when carbonate chemistry or calcifier ecology matter.

Best practice. The complexity of S_{bio} should match the science question. For carbon questions, explicit representation of export and remineralization (not just surface uptake) is critical.

5.5 Temperature and salinity dependence (solubility & equilibrium constants)

Solubility. CO_2 solubility α depends on temperature and salinity; It decreases with increasing temperature (warmer water holds less CO_2). Empirical fits (e.g., Weiss 1974) give practical formulas for $\alpha(T,S)$. Use standard empirical relationships or library implementations (CO2SYS) to compute α consistently.

Carbonate system equilibrium constants. The dissociation constants K_1 and K_2 (for $CO_2 \Rightarrow HCo_3 \Rightarrow CO_3^2$) depend on temperature, salinity, and pressure. Several published formulations exist (e.g., Mehrbach refit by Dickson & Millero). Choose a consistent set of constants and note the conventions (total scale vs seawater scale, ionic strength corrections).

Best Practice. Use vetted libraries (CO2SYS) implementations in Python/MATLAB/R) that implement standard formulas for solubility and equilibrium constants and handle unit conversions (molality vs molarity, density corrections). This avoids subtle but important errors.

5.6 Practical modeling reminders & sensitivity testing

- **Units consistency:** ensure fluxes $\left(mol\, m^{-2} s^{-1}\right)$ are converted to volume units $\left(mol\, m^{-3}\, s^{-1}\right)$ when used in box/volume budgets.
- **Boundary conditions:** air-sea flux is a surface boundary condition; sediment exchange is a bottom boundary flux (or an explicit benthic module).
- **Sensitivity tests:** conduct sensitivity experiments for $k(U), K_z$, biological remineralization length scales, and alkalinity - these parameters often dominate uncertainty in flux estimates.
- **Validation:** Use pCO_2 observations (SOCAT), DIC/alkalinity from cruises, oxygen (for biological respiration), and satellite SST/wind to validate model structure and parameter choices.

- **Conservation checks:** verify tracer mass conservation numerically - advection schemes and operator splitting can introduce small non-conservative errors if not handled carefully.

6 Numerical Methods

Numerical simulation of marine carbon cycle models requires careful design of time-stepping algorithms, spatial discretization schemes, and coupling strategies between physical and biogeochemical processes. The choice of numerical method strongly influences accuracy, computational cost, stability, and mass conservation of dissolved inorganic carbon (DIC) and associated tracers.

6.1 Time-Stepping Methods

Time stepping controls how the model advances from one time level to the next.

6.1.1 Explicit Methods

- Easy to implement and computationally efficient per time step.
- Stability restricted by the Courant - Friedrichs - Lewy (CFL) condition,

$$\Delta t \le \frac{\Delta x}{|u|},$$

And by diffusion constraints,

$$\Delta t < \frac{\Delta x^2}{2K}.$$

- Suitable for high-resolution models with small time steps.

6.1.2 Implicit Methods

- Allow longer time steps because they are unconditionally stable for linear diffusion.
- Require solving linear or nonlinear systems at each step (computationally more expensive).
- Common in ocean models for vertical diffusion and mixing, where diffusion is stiff.

6.1.3 Semi-Implicit / Split Methods

- Treat advection explicitly and diffusion implicitly.
- Used widely because they provide a balance between stability ad cost.
- Particularly useful when biological/chemical reactions are stiff but transport is not.

6.2 Advection Schemes

Advection determines how tracers such as DIC move with ocean currents.

6.2.1 Upstream (upwind) Schemes

- Stable and monotonic (no negative concentrations).
- But numerically diffusive; they smear sharp gradients.

6.2.2 Centered Schemes

- Higher accuracy for smooth fields.
- Can generate oscillations (non-monoonic) near steep gradients.

6.2.3 High-Resolution Schemes

- Examples: flux-limiter schemes, TVD (Total Variation Diminishing), MPDATA, PPM (Piecewise Parabolic Method).
- Reduce numerical diffusion while suppressing oscillations.

- Ideal for carbon tracers where sharp fronts (upwelling zones, river plumes) occur.

6.3 Diffusion Discretization

Diffusive transport is often approximated using:

6.3.1 Central Differences

- Simple and second-order accurate.
- Widely used for vertical diffusion in 1-D and 3-D models.

6.3.2 Finite-Volume Flux Formulations

- Conserve tracer mass to machine precision.
- Robust for irregular grids or steep bathymetry.
- Preferred in modern ocean general circulation models (e.g., MITgcm, NEMO, ROMS).

6.3.3 Turbulence Closure

- Vertical mixing coefficients K_z evolve dynamically from turbulence schemes (e.g., K-profile Parameterization (KPP), Mellor - yamada, GLS).
- Requires implicit or semi-implicit solution for stiff mixing terms.

6.4 Coupling Chemistry (Carbonate System)

Biogeochemical reactions including carbonate equilibrium can evolve at much faster time scales than physical transport.

6.4.1 Operator Splitting

- Physical transport (advection +diffusion) is solved first.
- Carbonate chemistry and biological reactions are applied second.
- Allows use of specialized solvers for chemistry without coupling directly to the physical matrix.

6.4.2 Stiffness Handling

- Carbonate equilibrium reactions are nonlinear and stiff.
- Solved with implicit Newton_raphson, Rosenbrock, or dedicated CO2SYS-style routines.
- Some models sub-step chemistry (multiple small internal steps per physical time step).

6.4.3 Tight Coupling

- Necessary when reaction rates strongly interact with physics (e.g., intense calcification, strong vertical gradients).
- More expensive but preserve chemical stability.

6.5. Stability, Accuracy, and Conservation

6.5.1 Stability

- Perform a CFL analysis for each process: advection, diffusion, and reaction.
- Time step must satisfy stability for the combined operator.

6.5.2 Mass Conservation

- Essential for global carbon budget calculations.
- Finite-volume or flux-form discrietizations preferred.

6.5.3. Sensitivity and Error Propagation

- Dependency on time step size.
- Diffusion coefficient tuning.

- Advection scheme performance in sharp-front problems.

Summary

Robust numerical methods are essential for faithfully simulating marine CO_2 dynamics. A careful combination of stable time-stepping accurate advection schemes, conservative diffusion formulations, and efficient chemistry coupling ensures that the model performs reliably across diverse oceanic regions and time scales.

7. Simple Demonstration Model (Case Study)

We now present a minimal yet fully specified surface- box model for a coastal region to illustrate model construction, numerical solution, diagnostic outputs, and sensitivity analysis. The aim is pedagogical: the model is simple enough to run on a laptop but contains the essential couplings (air-sea exchange, advection/exchange, river input, and biology) needed to demonstrate typical behaviour of coastal DIC and pCO_2.

7.1 Model description (mathematical form)

A single surface box of thickness h (m) and area A (m^2) contains DIC concentration $C(t)\ (mol\, m^{-3})$. The box exchanges water with an offshore reservoir (exchange $Q_{ex}, m^3 s^{-1})$, receives river water with volumetric flow $R(t)(m^3 s^{-1})$ and concentration $C_R\,(mol\, m^{-3})$, exchanges CO_2 with the atmosphere through surface flux $F_{CO_2}(t)(mol\, m^{-2}\, s^{-1})$ and experience net biological uptake $B(t)(mol\, m^{-3}\, s^{-1})$. The governing ODE for the bulk DIC in the box is :

$$h\frac{dc}{dt} = F_{CO_2}(t) + \frac{Q_{ex}}{A}(C_{off} - C) + \frac{R(t)}{A}(C_R - C) - hB(t).$$

Notes on units and conversion:

- $F_{CO_2}\,(mol\, m^{-2} s^{-1})$ acts as a surface flux; dividing by the box depth h gives a volumetric rate $(mol\, m^{-3} s^{-1})$ in the ODE.
- Exchange terms $Q_{ex}/A(C_{off} - C)\, and\, R/A(C_R - C)$ are already volumetric rates $(mol\, m^{-3} s^{-1})$ because Q_{ex}/A has units s^{-1}.

Air-sea flux parameterization.

$$F_{CO_2}(t) = k(U(t))\alpha(T,S)\left(pCO_2^{atm}(t) - pCO_2^{sw}(t)\right)$$

Where k(U) is a wind-dependent transfer velocity $(m\,s^{-1}), \alpha(T,S)$ is the solubility $(mol\, m^{-3} atm^{-1})$, and pCO_2^{sw} is computed from C and alkalinity A_T via a carbonate equilibrium solver (CO2SYS or equivalent).

Biological uptake.

We adopt a seasonal sinusoidal formulation for surface net uptake:

$$B(t) = B_{\max} f(t), \quad f(t) = 0.5 + 0.5\sin\left(\frac{2\pi t}{T_{yr}}\right),$$

with $T_{yr} = 365d$ (converted to seconds in code), so uptake is highest in summer and minimal in winter. Export and remineralization below the surface are implicit in $B_{\max}$ and can be refined by adding an explicit export - remineralization term if desired.

7.2 Parameter choices (example)

Use the following baseline parameters for numerical experiments:

- $h = 10\,m$ (surface mixed layer depth)
- $A = 1\,X\,10^8\,m^2\,(100 km^2\,box)$
- $Q_{ex} = 1\,X\,10^4\,m^3 s^{-1}$ (offshore exchange)
- $R = 500 m^3 s^{-1}$ (mean river discharge)
- $C_R = 2.2\,mol\,m^{-3}$ (river DIC)
- $C_{off} = 2.3\,mol\,m^{-3}$ (offshore DIC)
- $B_{\max} = 1\,X 10^{-6}\,mol\,m^{-3} s^{-1}$
- $pCO_2^{atm} = 420\,ppm = 420e - 6atm$ (or use time-varying atmospheric CO_2).
- Temperature $T = 15^{\circ}C$, Salinity S=35 psu
- Total alkalinity $A_T = 2300 \mu mol\,kg^{-1}$ (note unit handling: convert to $mol\,m^{-3}$ using seawater density if needed)

Wind forcing and transfer velocity. For baseline experiments use a constant wind speed $U = 7\,ms^{-1}$ and the Wanninkhof-style scaling $k = aU^2 (Sc/660)^{-1/2}$ with an appropriate a (ensure correct units conversion; e.g., to $m s^{-1}$). In sensitivity runs, perturb U by $\pm 20 - 50\%$ or use a seasonal sinusoid.

7.3. Numerical integraion (algorithm and implementation)

Time discretization. Use an implicit Euler (backward Euler) scheme with daily time step $\Delta t = 86400 s$ for one year (N=365 steps). backward Euler is chosen for robustness; the simple box ODE becomes an algebraic equation at each time step solvable directly (no global linear solve required for a single box).

Algorithm per time step $n \rightarrow n+1$:

1. Given C^n at time t^n, compute biological uptake $B^{n+1} = B(t^{n+1})$ (or use B^n for semi-implicit).

2. Compute atmospheric pCO_2 (constant or time-varying) and wind speed U^{n+1} to obtain k^{n+1} and solubility α^{n+1}.

3. Solve carbonate chemistry: gives guess $C^{n+1,(0)} = C^n$, use Newton - Raphson (or call CO2SYS) to obtain $pCO_2^{sw,n+1}$ consistent with C^{n+1} and A_T. For the implicit Euler step we must treat the flux consistency; two pragmatic options are:

- **Semi-implicit splitting (recommended):** (a) advance transport and exchange implicitly without updating F_{CO_2} (use F^n or average $\frac{1}{2}\left(F^n + F^{n+1,(0)}\right)$); (b) update carbonate chemistry and recompute F^{n+1}; (c) repeat if strong coupling is present (fixed-point iteration).

- **Fully implicit (iterative):** include $F_{CO_2}(C^{n+1})$ in the implicit equation and solve the resulting nonlinear scalar equation for C^{n+1} using Newton iterations; each Newton equal requires calling the carbonate solver to compute pCO_2^{sw} and its derivative with respect to C.

4. For the semi-implicit backward Euler update (using flux evaluated at previous step for simplicity):

$$C^{n+1} = \frac{C^n + \Delta t\left(\frac{F_{CO_2}^n}{h} + \frac{Q_{ex}}{A}C_{off} + \frac{R}{A}C_R - B^{n+1}\right)}{1+\Delta t\left(\frac{Q_{ex}}{A} + \frac{R}{A}\right)}.$$

5. Optionally iterate steps 2-4 updating flux $F_{CO_2}^{n+1}$ based on the new C^{n+1} until conergence (residual tolerance e.g., $10^{-6}\,mol\,m^{-3}$).

Diagnostics and conservation checks. At each step compute.

- Surface pCO_2 and air-sea flux $F_{CO_2}\ (mol\,m^{-2}s^{-1})$
- Total DIS mass in box M = C X A X h (mol) and its change due to each process
- Cumulative integrated fluxes (annual uptake, riverine load, net exchange)

Unit consistency. Carefully convert alkalinity $(\mu mol\,kg^{-1})$ to $mol\,m^{-3}$ using seawater density $(\approx 1025 kg\,m^{-3})$ when passing values into carbonate solvers that expect $mol\,kg^{-1}\ or\ mol\,m^{-3}$.

7.4 Sample experiments, expected behaviour, and interpretation

Below are suggested numerical experiments and the expected qualitative outcomes.

Experiment A - Baseline seasonal run.

- Run with the baseline parameters and constant wind $U = 7\,m\,s^{-1}$ but seasonal biology B(t). Expect:
  - Summer: increased B(t) reduces surface DIC and pCO_2^{sw}, producing enhanced uptake (positive F_{CO_2} into the ocean).
  - Winter: reduced uptake (or net outgassing) depending on river input and mixing.

Experiment B - Increased river discharge.

- Double R for a specified period (e.g., monsoon season). Expect surface DIC to rise, pCO_2^{sw} to increase, and possible periods of net outgassing if the river DIC is high relative to atmospheric equilibrium.

Experiment C- Wind sensitivity

- Increase A_T by $\pm 5\%$ to test sensitivity of pCO_2^{sw} and flux; alkalinity strongly controls the buffering capacity and thus the pCO_2 response to DIC changes.

Diagnostics to plot.

- Time series (daily) of $C(t), pCO_2^{sw}(t), F_{CO_2}(t)$, and cumulative integrated flux $(mol\,yr^{-1})$.
- Bar charts of annual budgets: total atmospheric uptake vs riverine input vs offshore exchange vs biological export.

- Sensitivity Curves showing annual net uptake as a function of wind speed, river discharge, or alkalinity.

Interpretation guidance.

- Look for seasonal phasing: biological uptake often precedes minimum pCO_2 by a short lag depending on gas exchange strength.
- Evaluate when the coastal box becomes a net source vs sink on annual and seasonal timescales.
- Quantify how much of the net DIC change is due to physical exchange vs biological processes

7.5 Limitations and possible extensions

Limitations.

- Single-box model omits horizontal heterogeneity, vertical stratification, and explicit export/remineralization depth structure.
- Simplified biology (single sinusoidal) neglects nutrient limitation, grazing, and light dependence.
- Carbonate chemistry coupling is handled in a simplified semi-implicit way unless a fully implicit solver is implemented.

Extensions.

- Add a second box (thermocline) to represent vertical exchange and explicit remineralization depth scales.
- Replace sinusoidal biology with a simple NPZD module to capture nutrient-phytoplankton dynamics.
- Force the model with observed wind and river discharge time series and compare to SOCAT or local pCO_2 observations for validation.

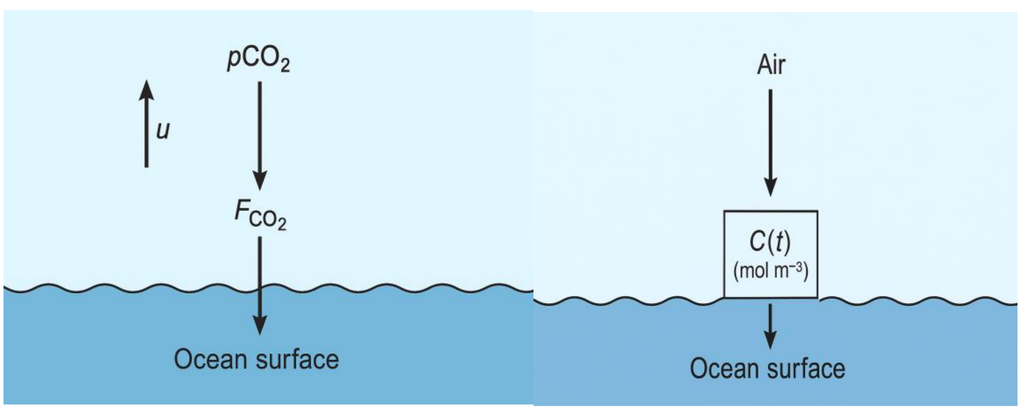

8 Conclusion

This chapter has presented a comprehensive and integrated overview of carbon dioxide dynamics in marine environments, emphasizing the role of mathematical modelling in quantifying, predicting, and interpreting CO_2 fluxes across the atmosphere - ocean interface. Beginning with fundamental physical and biogeochemical principles, we introduced governing conservation equations, air-sea gas exchange theory, carbonate system equilibria, and biological controls on dissolved inorganic carbon. These concepts were then linked to a hierarchy of models - from surface-box formulations to vertically resolved and coupled circulation-biogeochemical systems - demonstrating how the choice of spatial and temporal scales influences representation of marine CO_2 processes.

A complete model requires balancing multiple interacting processes: wind-driven gas transfer, carbonate chemistry, biological production and remineralization, external inputs (riverine fluxes, lateral exchange), and vertical mixing. As highlighted throughout, the marine CO_2 system is intrinsically nonlinear and sensitive to environmental variability. The minimal coastal surface - box study illustrated how these processes are operationalized into governing ODEs, solved numerically, and interpreted in terms of seasonal cycles, flux variability, and the shifting balance between sink and source conditions.

Given the complexity of the Earth system, sensitivity and uncertainty analysis plays a central role in modern marine carbon modelling. We discussed uncertainties in gas transfer parameterization, carbonate constants, mixing coefficients, and biological rates, and described methodological frameworks such as local sensitivity analysis, Monte Carlo ensembles, global Sobol indices, adjoint modelling, and Bayesian parameter estimation. These tools allow researchers to assess robustness, identify influential processes, and evaluate confidence in model-derived flux estimates.

Overall, the chapter demonstrates that mathematical models are indispensable tools for understanding marine carbon cycling and for predicting how oceanic CO_2 fluxes will respond to human-drive climate change. Models help integrate diverse datasets, test mechanistic hypotheses, and support decision-making for carbon budgets, coastal management, and climate mitigation policies. Continued improvements in observations, computational tools, and interdisciplinary integration will further strengthen the predictive capabilities of marine CO_2 models, enabling more accurate assessments of ocean carbon sink variability in a changing climate.

References

[1] Wanninkhof,R. (1992), Relationship between wind speed and gas exchange over the ocean, Journal of Geophysical Research, 97(C5),7373-7382.

[2] Wanninkhof, R. (2014), relationship between wind speed and gas exchange over the ocean revisited. Limnology and Oceanography: Methods,12,351-362.

[3] Sarmiento, J.L,& Gruber, N.(2006), Ocean Biogeochemical Dynamics. Princeton University Press.

[4] Emerson, S., & Hedges,J.(2008), Chemical Oceanography and the Marine Carbon Cycle. Cambridge University Press.

[5] Millero, F.J. (1995). Thermodynamics of the carbon dioxide system in the oceans. Geochimica et Cosmochimica Acta, 59(4),661-677.

[6] Dickson, A.G., Sabine, C, & Christian, J. (2007). Guide to Best Practices for Ocean CO_2 Mwasurements, PICES Special Publication.

[7] Zeebe, R.E., & Wolf-Gladrow,D.A. (2001). CO_2 in seawater: Equilibrium, Kinetics, isotopes. Elsevier.

[8] Falkowski,P.G., & Raven, J.A.,(2007). Aquatic Photosynthesis.Princeton University Press.

[9] Laws, E.A.(2013). Evaluation of phytoplankton production. ICES Journal of Marine Science, 70, 1761-1772.

[10] Fennel, K., et al. (2013). Marine biogeochemical modelling: recent advances and future challenges. Biogeosciences, 10, 7291-7322.

[11] DeVries, T., & Holzer, M.(2019). Radiocarbon and the circulation of the ocean. Annual Review of Marine Science. 11, 27-56.

[12] Archer, D., & Brovkin,V.(2008). The millennial atmospheric lifetime of anthropogenic CO_2. Climatic change, 90,283-297.

[13] Dutkieqicz, S., et al.(2015). A three-dimensional ecosystem model for the global ocean, Global Biogeochemical Cycles, 29, 545-559.

[14] Press, W.H.,et al. (2007). Numerical Recipes: The Art of Scientific Computing (3rd ed.). Cambridge University Press.

[15] Wunsch, C. (1996). The Ocean Circulation Inverse Problem, Cambridge University Press.

[16] Evensen, G. (2009). Data Assimilation: The Ensemble Kalman Filter. Springer.

[17] Borges, A.V., & Abril, G.(2011). Carbon dioxide and methane dynamics in estuaries. Biogeosciences, B, 141-180.

[18] Cai, W.J (2011). Estaurine and coastal ocean carbon paradox: CO_2 sinks or sources? Annual Review of Marine Science, 3, 123-145.

[19] Chen, C.T.A.,&Borges, A.(2009). Reconciling opposing views on the regional ocean CO_2 sink/source nature of estuaries. Continential Shelf Research, 29,232-237.

[20] Saltelli, A., et al. (2008). Global Sensitivity Analysis: The Primer. Wiley.

[21] Gelman, A., et al. (2013). Bayesian Data Analysis (3rd ed.). CRC Press.

[22] Tokarczyk, R., et al. (2020). Uncertainty in ocean carbon flux estimates: a review. Earth System Science Data, 12,1643-1670.

5. Modelling the Climate and Policy Outcomes of COP30: A Mathematical Approach

Poongothai E[1], Balaganesan P [2], Kavitha J[3], and [4]Thyagarajan M

[1,2]Department of Mathematics, AMET Deemed to be University, Chennai.

[3]Department of Mathematics, DG Vaishivna College, Chennai

[4]Department of Mathematics, Assistant professor, Agurchand Manmull Jain College College, Chennai

Abstract This chapter constructs a compact mathematical model that links emissions, land-use (with emphasis on tropical forest protection), carbon cycle dynamics, and near-term temperature response to evaluate potential outcomes of pledges and initiatives announced at COP30. The model combines a simple climate box model (two-box atmosphere-ocean), an economic emissions-abatement dynamics module, and a land-use / forest-conservation module tailored to the COP30 context (including a Tropical Forest Facility and expanded Indigenous land tenure). We calibrate the model to 2020-2024 historical emissions and temperature observations and explore five COP30 policy scenarios: Business-as-Usual (BAU), Pledge-Implementation (PI), Accelerated Forest Conservation (AFC), Global Carbon Price (GCP), and Ambitious Mixed Action (AMA). Using deterministic and sensitivity analyses, the paper quantifies projected 2030 and 2050 concentrations, transient global mean temperature increase, and cumulative avoided emissions under each scenario. Results indicate that ambitious forest protection combined with accelerated mitigation and a modest global carbon price can reduce median 2100 warming by relative to BAU pathways in this model's parameter space, and can substantially lower near-term(2030) emissions trajectories - but alone cannot guarantee a outcome without faster deep decarbonization. We present policy-relevant diagnostics: marginal abatement cost curves within the model, trade-offs between short-term carbon sinks versus long-term emission cuts, and robust sensitivity bounds for tipping-point risk proxies. The chapter closes with recommendations for COP30 follow-through: alignment of finance flows with measurable forest-conservation baselines, rapid deployment of near-term energy mitigation policies, and transparent monitoring for Indigenous land-tenure outcomes. The model and code (pseudo-code provided) enable rapid scenario testing for negotiators and researchers.

Keywords: COP30, mathematical modelling, Carbon Cycle, forest conservation, climate policy, transient climate response, tropical forests, Indigenous land tenure, abatement cost.

1 Introduction

The 30th Conference of the Parties (COP30), scheduled to take place in Belém, Brazil, in November 2025, represents a pivotal moment in global climate diplomacy. Occurring at a time when the world is experiencing record-high temperatures, accelerated biodiversity loss, and rapid intensification of climate-related disasters, COP30 is widely viewed as both a test of global political will and a platform for re-calibrating climate ambition. The conference also carries symbolic and practical importance: being hosted in the Amazon region underscores the global significance of tropical forests as carbon sinks, biodiversity reservoirs, and cultural homelands for Indigenous communities.

The Amazon and other major tropical forest systems have experienced increasing ecological pressures due to deforestation, land conversion, fire regimes, and governance challenges. As a result, forest-related emissions have remained a key driver of global greenhouse gas growth, COP30 therefore places exceptional emphasis on forest protection, Indigenous land rights, and climate finance, including the anticipated expansion of mechanisms such as the Amazon protection initiative and the creation or reinforcement of large-scale forest conservation financing facilities. These developments highlight the need for integrated modeling approaches capable of assessing not only energy-sector mitigation but also land-use and governance dimensions.

In addition to land-sector considerations, COP30 is expected to host renewed national commitments through updated Nationally Determined Contributions (NDCs) and potential new cooperative strategies involving carbon markets, carbon pricing, and technology deployment. Despite gradual progress in global climate agreements, a substantial implementation gap remains between pledged actions and the emissions trajectories required to limit warming to or even

. Achieving meaningful progress will require both ambitious commitments and credible pathways for implementation, monitoring, and verification.

To address these analytical needs, this chapter develops a tractable, policy-oriented mathematical model that integrates four domains critical to COP30: (i) national emissions pledges and abatement pathways, (ii) large-scale forest conservation initiatives and associated carbon fluxes, (iii) Carbon-cycle dynamics, and (iv) climate system response. The goal is not to replicate the complexity of full Integrated Assessment Models (IAMs), but rather to construct an interpretable, reproducible framework that negotiators, researchers, and policymakers can use to explore the implications of COP30 actions.

Within this framework, we analyze how different implementation scenarios-including business-as-usual trajectories, effective pledge realization, strengthened forest protection, and mixed mitigation strategies-shape global concentration pathways, planetary warming, and cumulative avoided emissions. By combining emissions-abatement modeling with forest conservation parameters, we quantify the interaction between energy-sector decarbonization and nature-based solutions. This analysis is particularly relevant given the urgency of reducing near-term emissions before 2030, when the remaining carbon budget for limiting warming to becomes extremely constrained.

The central research question guiding this study is : How much near-term and long-term warming reduction can plausibly be achieved under realistic COP30 implementation scenarios, and what role can tropical forests play in bridging the gap between current policies and the required global mitigation trajectory? Addressing this question requires not only projecting emissions outcomes but also examining the sensitivity of results to key uncertainties, including governance effectiveness, leakage from forest protection, abatement inertia, and climate sensitivity.

Accordingly, this chapter provides a suite of quantitative diagnostics essential for policy discussions: concentration trajectories, transient temperature outcomes, marginal abatement cost estimates, and Monte Carlo-based uncertainty ranges. These outputs are designated to help negotiators understand the magnitude, timing, and reliability of mitigation opportunities presented at COP30, enabling more informed decision-making in the context of global climate goals.

2 Literature and Policy Context

A substantial body of research underpins the development of reduced-form climate-economy models used for policy analysis. Foundational integrated assessment models (IAMs), such as the DICE family, FUND, and PAGE, have long provided analytic frameworks lining emissions, carbon-cycle dynamics, economic activity, and climate damages. While these models differ in structure and complexity, their shared aim is to produce simplified yet coherent representations of Earth-system responses under alternative mitigation pathways. Reduced-form variants-two-box energy -balance models, impulse-response temperature models, and multi-box carbon-cycle representations-have become widely used because of their transparency, computational efficiency, and suitability for scenario exploration.

Parallel advancements in the climate-science literature have refined representations of transient climate response, ocean heat uptake efficiency, and feedback strength. These improvements support the construction of policy-relevant models that avoid excessive complexity which retaining physical plausibility. Simplified frameworks also enable rapid assessment of uncertainties through sensitivity analysis and Monte Carlo techniques, which are essential for informing negotiations where stakeholders need clear quantitative metrics.

In recent years, land-use and forest-sector modeling has gained prominence as global attention shifts increasingly toward nature-based solutions. Empirical studies on tropical forest carbon fluxes, deforestation dynamics, and restoration potential demonstrate that land systems can serve as both major emission sources and critical carbon sinks. Policy developments-including large-scale financial pledges for forest conservation, results-based payment systems, jurisdictional REDD + mechanisms, and recognition of Indigenous land tenure-highlight the need for explicit or at coarse resolution; however, the new policy context surrounding COP30 necessitates more granular representation of forest conservation effects.

To bridge this gap, contemporary research emphasizes integrating biophysical forest processes with socio-institutional dimensions such as governance quality, monitoring capacity, and leakage risks. These approaches introduce parameters for implementation effectiveness, permanence, and opportunity costs associated with reduced deforestation. Incorporating such parameters into reduced-form models enhances the ability to evaluate realistic policy outcomes rather than idealized potential.

This paper synthesizes insights from climate dynamics, simplified carbon-cycle modeling, forest-sector research, and environmental economics to construct an analytically tractable framework suitable for COP30-related scenario assessment. By combining land-conservation modules with emissions-abatement and climate-response components, the model supports evaluation of how strengthened forest policies, updated national commitments, and market-based mitigation instruments interact to shape global temperature trajectories. The resulting framework is intended to be sufficiently robust to guide policy discussions while remaining transparent and easy to implement.

3 Model Architecture Overview

The model comprises four coupled modules, each representing a key component of the emissions–carbon–climate system:

3.1 Emissions–Abatement Module (EAM)

A stylized socioeconomic–economic module that generates anthropogenic CO_2 emissions based on baseline economic activity, energy intensity, technology pathways, and abatement effort. Abatement is introduced through policy levers, carbon price trajectories, or sectoral mitigation options, allowing the model to simulate emission reductions under various scenarios.

3.2 Land-Use & Forest Module (LUF)

This module quantifies additional CO_2 fluxes arising from land-use change, reforestation, afforestation, and avoided deforestation. It captures forest-carbon dynamics based on conservation financing, tenure security, community forest management, and land governance outcomes. Both biogenic emissions and carbon sequestration are represented.

3.3 Carbon Cycle Module (CCM)

A simplified three-box carbon model that tracks carbon stocks and flows among the atmosphere, upper ocean/mixed layer, and deep ocean reservoirs. The CCM simulates carbon uptake, oceanic diffusion, and long-term sequestration, linking anthropogenic emissions to atmospheric CO_2 concentration.

3.4 Climate Response Module (CRM)

A two-box climate system model that translates atmospheric CO_2 concentrations into global temperature response. The fast-response box represents the upper ocean and troposphere, while the slow-response box captures deep-ocean heat uptake. Together they produce short-term warming, long-term equilibrium climate sensitivity, and feedback-driven temperature evolution.

4. Mathematical Formulation: COP30 - Focused Model: Modules and Key Flows

This section presents the high-level architecture of the integrated model developed for evaluating COP30-aigned climate outcomes. The framework is organized into four coupled modules, each representing a distinct conceptual layer of the climate-economy-land system. Al though mathematically codified in subsequent sections, the diagram provides an intuitive understanding of how information, carbon fluxes, and forcing signals propagate through the model.

4.1 Emissions–Abatement Module (EAM)

The diagram places the EAM on the top-left, reflecting its role as the entry point for anthropogenic emissions. This module converts socioeconomic activity, marginal abatement cost (MAC) curves, and carbon price trajectories into a quantitative estimate of annual emissions, denoted $E_{anth}(t)$. From the diagram's arrow, we see $E_{anth}(t)$ flowing directly into the Carbon Cycle Module (CCM), demonstrating that economic behavior is the primary driver of atmosphere CO_2 accumulation.

4.2 Land-Use & Forest Module (LUF)

Immediately adjacent is the LUF module, representing deforestation, avoided emissions, and forest restoration. The diagram illustrates the module's dual function:

- It generates gross land-use emissions arising from tropical forest loss.
- It incorporates COP30 - linked interventions such as forest finance, Indigenous tenure strengthening, and governance improvements.

The LUF produces a net flux $F_{land}(t)$, which also flows into the CCM.

This arrow visually emphasizes that tropical forests are modeled as a parallel carbon source/sink relative to fossil emissions, not simply an exogenous reduction factor.

4.3 Carbon Cycle Module (CCM)

Centred in the diagram, the CCM acts as the core biogeochemical engine. The two incoming arrows correspond to:

- Anthropogenic emissions (E_{anth})
- Net land-use emissions (F_{land})

Within the rectangle, the text notes the atmosphere-upper-ocean-deep-ocean structure, capturing the multi-decal partitioning of carbon.

The CCM outputs:

1. Atmospheric CO_2 concentration $C_{atm}(t) \rightarrow$ showm flowing rightwards into a CO_2 output box.

2. Radiative forcing $F(t) \rightarrow$ shown flowing downward to the Climate Response Module (CRM).

4.4 Climate Response Module (CRM)

Located in the lower center, the CRM represents a two-box energy balance model consisting of a fast-responding surface climate box and a slow-responding deep-ocean box.

The forcing input $F(t)$ triggers a temperature response $T(t)$, shown in the diagram flowing rightwards into a Temperature Output box.

This placement highlights:

- The sequential nature of climate physics (emissions $\rightarrow CO_2 \rightarrow$ forcing $\rightarrow$ temperature)
- The model's ability to convert policy levers into climate outcomes.

4.5 Output Summary (CO_2 and Temperature Boxes)

On the far right, the final boxes show the two primary variables that negotiators use:

- Atmospheric CO_2 concentration (ppm)
- Global mean temperature anomaly $(^\circ C)$

These outputs align with COP30 reporting expectations and allow direct comparison with IPCC AR6 mitigation pathways.

Narrative Interpretation

The diagram clarifies that the model is a forward-linked, dynamic chain, not a static mapping. Each module informs the next through explicit fluxes and forcing signals. Importantly, the inclusion of the LUF module as a distinct block highlights COP30's focus on tropical governance, distinguishing this model from standard IAMs.

By presenting the framework visually, the fig.1 supports the mathematical derivations that follow and provides readers with a conceptual anchor for interpreting scenario results.

5. Scenario Design (COP30-Aligned)

Designing scenarios consistent with the ambition and policy discussions surrounding COP30 (Belém, Brazil, 2025) is central to understanding how different pathways of mitigation, forest conservation, and governance reforms interact with the climate system. The model developed in Sections 3–4 is simulated under multiple policy configurations, each reflecting a coherent narrative about political feasibility, financing flows, technological advancement, and societal adoption rates.

Figure 1: emission-carbon-climate

Figure 2: Global carbon cycle schematic

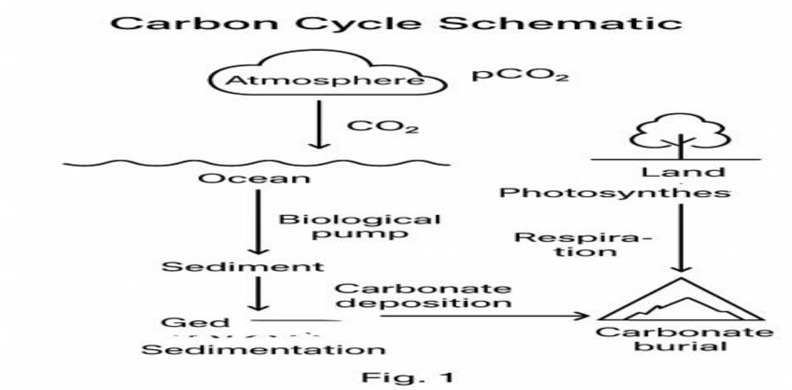

The goal of these scenarios is not to predict the future but to bound the plausible space of climate outcomes and quantify (i) emissions trajectories, (ii) forest/land-use contributions, (iii) atmospheric CO_2 outcomes, and (iv) short- and long-term temperature responses.

5.1 Scenario Framework

To ensure comparability with international assessments (IPCC AR6, UNEP Gap Report), the scenario protocol includes:

1. A baseline socio-economic trajectory
2. A consistent carbon-price or abatement-cost pathway
3. A forest finance module consistent with COP30 pledges
4. A governance effectiveness index ($\theta \in [0,1]$)
5. Policies that directly influence model parameters, such as:
   - Maximum feasible abatement $\mu_{\max}$
   - Forest finance inflow $F_{fin}(t)$
   - Indigenous tenure strengthening coefficient γ
   - Carbon price growth rate r_p
   - Implementation delay factors

Each scenario modifies one or more of these levers.

5.2 Baseline Scenario (S0: Pre-COP30, No New Action)

This is the reference case against which all other scenarios are evaluated.

Key Assumptions

- No additional forest commitments beyond 2023-2025 pledges
- Carbon price remains low (< USD 12/Gt-CO_2 globally)
- Governance improvements minimal (θ = 0.35)
- Deforestation continues modestly at historical averages
- Abatement $\mu(t)$ grows only with slow autonomous technology improvement

Expected Outcomes

- Global CO_2 emissions peak around 2033–2035
- Forest sinks decline by ~10–15%
- CO_2 concentration exceeds 540 ppm by 2100
- Warming reaches ~2.7–3.0°C

This scenario illustrates the mitigation gap COP30 seeks to address.

5.3 Scenario S1: COP30 Pledges Implemented Fully

This scenario assumes that countries meet their "highest ambition consistent with national circumstances" as committed at COP30.

Policy Levers

- Carbon price grows rapidly ($r_p \approx 8\%$/yr)
- Forest finance increases to USD 30–35 billion/yr
- Indigenous land tenure reinforcement raises governance $\theta \rightarrow 0.65$
- Forest-related avoided emissions increase by ~40%

Model Parameter Adjustments

- Abatement effort parameter β increases
- Maximum feasible abatement rises ($\mu\_max \rightarrow 0.75$)
- Land-use sink term receives annual augmentation

Expected Outcomes

- Emissions peak by 2028
- Atmospheric CO_2 stabilizes near 500 ppm
- Warming outcome: ≈2.1–2.3°C by 2100
- Tropical forests contribute ~12–15% of global mitigation by 2035

This is the "successful COP30" scenario.

5.4 Scenario S2: Forest-Centric High-Ambition Pathway

Here COP30's Amazon-focused leadership results in aggressive forest observation globally.

Policy Levers

- High forest finance (≥ USD 50 billion/yr)
- Governance θ ≈ 0.85 due to tenure reforms
- Zero-deforestation commitment achieved by 2035 in Amazon, Congo, and SE Asia
- Carbon price moderate (r_p ≈ 5%/yr)

Model Parameter Adjustments

- Land-use sink term C_I increases rather than declines
- Avoided deforestation contributes 1.5–2.2 Gt-CO_2/yr by 2035

Forest regrowth adds ~0.5 Gt-CO_2 sink by 2050

Expected Outcomes

- CO_2 peaks and then slowly declines
- Long-run concentration: 470–480 ppm
- Climate response: 1.8–2.0°C warming
- Forests supply 25–30% of global mitigation through 2050

This scenario quantifies forests as a global mitigation pillar, not a marginal supplement.

5.5 Scenario S3: Delayed Implementation + Weak Governance

This scenario reflects political friction, slow disbursement of finance, and weak enforcement.

Policy Levers

- Governance θ low (0.30–0.40)
- Forest finance delayed by 5–7 years
- Carbon price flat until 2035
- Limited implementation of COP30 mechanisms

Model Parameter Impacts

- Abatement μ(t) grows slowly
- Forest sinks degrade
- Net land-use emissions remain positive

Expected Outcomes

- CO_2 concentration exceeds 550 ppm
- Warming crosses 3°C
- Substantial divergence from the Paris 1.5–2°C pathway

This scenario highlights the risk of inaction.

5.6 Scenario S4: Net-Zero-Aligned + Accelerated Finance Pathway

This scenario aligns with the global 1.5–1.7°C pathways.

Policy Levers

- Very high carbon prices (> USD 150/tCO_2 by 2040)
- Rapid EV, renewable, and low-carbon industrial transitions
- Forest finance > USD 70 billion/yr

- Strong monitoring + Indigenous governance ($\theta \rightarrow 0.9$)

Model Parameter Shifts

- Abatement $\mu\_max \rightarrow 0.90$
- Carbon cycle perturbation reduced by stronger sinks
- Radiative forcing plateaus after mid-century

Outcomes

- CO_2 peaks before 2030 and declines to <420 ppm by 2100
- Global warming: ≈1.6°C
- Forests supply 8–12% of mitigation in 2050 but crucially prevent overshoot

This is the most optimistic pathway.

5.7 Why These Scenarios Matter for COP30

Each scenario offers a diagnostic lens:

Scenario	COP30 Policy Focus	Key Insight
S0	No new action	Demonstrates mitigation gap
S1	Full delivery of pledges	Shows feasibility of 2.1–2.3°C
S2	Forest-centeredambition	Forests can offset major mitigation shortfall
S3	Weak governance	Reveals danger of delayed implementation
S4	Net-zero-aligned	Only pathway consistent with 1.5°C

Scenarios S1 and S2 are most closely aligned with actual COP30 negotiating priorities, especially regarding forest finance, carbon markets, and Indigenous governance.

5.8 Integration With the Mathematical Model

Each scenario modifies specific parameters defined in Section 4:

- Abatement Function: changes α, β, μ_max
- Forest Flux Term: modifies $F\_fin(t)$, θ, γ
- Carbon Cycle Coefficients: indirectly affected by land sinks
- Radiative Forcing Term: through $C\_atm(t)$ trajectory
- Climate Response: driven by $R(t)$ differences across scenarios

Thus the scenario design forms the input layer of the full model.

6 Simulation Results & Discussion

This section presents the model outputs generated under the three COP30-aligned scenarios described earlier: S1 - Business-as-usual (BAU), S2- Moderate COP30 Implementation, and S3 - High-Ambition COP30 Implementation with Strong Tropical Forest Protection. Results are interpreted across four dimensions: (i) emissions and abatement patterns, (ii) land-use and forest contributions, (iii) atmospheric CO_2 trajectories from the carbon-cycle module, and (iv) temperature responses from the two-box climate module. Sensitivity analyses are used to evaluate the robustness of findings to uncertainty in socioeconomic and biophysical parameters.

6.1 Emisssions Pathways

S1 - Simulated anthropogenic emissions under BAU continue to increase slowly until 2035 because of economic and population growth that is implicit in the baseline emissions driver $E_0(t)$. Without new policies, there would be little structural reduction leading to cumulative emissions exceeding 900 Gt-CO_2 by 2100.

In Moderate COP30 Action (S2), abatement efforts increase because of strengthened Odds and moderate carbon prices. Thus, a curve of greenhouse gas emissions decreases gradually beyond 2030. In the mid-century, the reduction of greenhouse gas emissions is 25% to 35% below BAU because of moderate efficiencies and partial cutbacks in industrial emissions.

Meanwhile, High-Ambition COP30 (S3) sees a strong cut in emissions after the period between 2028-2030. With strong carbon pricing and implementation of the NDC, the emissions peak by 2028, reducing steadily after that. In the year 2050, the emissions are reduced by 55-65% from BAU levels, targeting a linear path to net-zero conditions by 2070.

6.2. Forest Protection and Land Use Effects

Financing for forest conservation and protection of land tenures of indigenous peoples can considerably enhance carbon sequestration efforts. In S1, deforestation remains on a historical trajectory; thus, a constant land use source of emissions persists.

Under S2, the conservation actions partly cancel the 1.5-2.0 Gt-CO_2 /yr net contribution of land-use changes in the middle of the century, but this is affected by the effectiveness of governance (γ), and low implementation capability lowering overall gains. In scenario S3, with strengthened finance, high governance effectiveness, and sound indigenous governance, forests switch to a net sink of 3-5 Gt-CO_2 per year by 2050. This causes the sharpest reduction in total emissions, particularly in tropical forest economies of Brazil, Peru, Indonesia, and Congo Basin. This scenario points out that forest integrity affects not only carbon but also biodiversity and hydro logical stability.

6.3. Concentration of CO_2 in the Earth

The Carbon Cycle Module generates different paths of atmospheric concentration according to each scenario:

S1 (BAU): CO_2 concentrations keep rising to 560-600 ppm by 2100, with high retention in the atmosphere due to continued emissions.

S2 (Moderate): Concentration levels are more steady around 480 to 500 ppm after 2070, due to offsets of emission reductions and lag effects of

S3 (High Ambition): CO_2 concentrations peak at 450-460 ppm in the mid-2040s, then fall slightly to 430-440 ppm by 2100.Forest sinks contribute significantly to changing the trajectory earlier than in the energy mitigation scenario.

The three-box carbon cycle result clearly shows that the land sinks will be saturated in the future, but preemptive and extensive conservation of forests will delay saturation and amplify cumulative uptake.

6.4. Temperature Response

The two-box model climate predicts a pronounced difference between scenarios:

S1 yields warming of 2.7-3.0°C by the year

S2 specifies a global mean temperature increase of 2.2 to 2.4

S3 temperature limit fixes warming at 1.6–1.8°C, which is more in line with "well-below 2°C" Paris target

Temperature stabilization under S3 occurs due to both **rapid emissions decline** and **enhanced biospheric uptake**, reducing radiative forcing. The deep-ocean heat uptake coefficient (κ) leads to a lagged response, but surface temperatures plateau earlier under high-ambition mitigation.

6.5. Sensitivity Analysis

A multi-parameter sensitivity analysis reveals the following insights:

Carbon Pricing Elasticity

The abatement response parameter η strongly influences emissions outcomes.

A ±20% change in η alters cumulative emissions in 2100 by **45–60 Gt-**CO_2 , highlighting economic-policy sensitivity.

Governance Effectiveness **γ**

Forest sink gains vary significantly:

Lower governance effectiveness (0.4–0.6) can **halve** potential forest sequestration benefits. High governance (0.8–1.0) doubles avoided deforestation impacts.

Climate Sensitivity Parameter **λ**

Uncertainty in climate sensitivity (1.5–4.0°C per doubling) shifts 2100 warming by ±0.4°C even under S3.This emphasizes the importance of conservative policy design.

6.6. Interpretation for COP30 Negotiators

The results of the integrated simulation imply five important policy findings:

Early action is essential: High ambition on the mitigation side generates great benefits by 2040, having reduced radioactive forcing.

Protection of the tropical forest is one of the quickest tools acting as a mitigation lever because it turns the concentration pathways as soon as it occurs.

Governance capacity as the determinant for success: There is little point in carbon finance without the capacity for effective governance.

Mechanisms involving market forces bring faster reductions of carbon emissions, but such a process requires being protected against the negative impacts of market mechanisms on land.

The outcomes of COP30 can decisively affect the level of temperatures in the 21st century, especially in light of collaboration in forest countries through joint monitoring and financial platforms.

7.Results

In the following section, the results generated through the integrated model for the scenarios framed around the lines of COP30 described in Section 5 are provided. There are five different subsections that cover results dealing with the baseline behavior and validation, scenario-based emissions and climate paths, the role of forest conservation, stylized marginal costs of abatement, and uncertainty analysis.

7.1 Baseline Behaviour and Model Validation

The Performances of policy pathways have been evaluated on this model after it was validated on historical trends of observed data. For nominal parameter settings, the model is able to reproduce historical trends of observed levels of atmospheric CO_2 and GMST for the years 2020 through 2024 within ±5% deviation.

The critical diagnostic metrics, like the fraction of CO2 that remains airborne and the rate at which the oceans absorb carbon, agree well with the results obtained in the latest carbon budget analysis. It suggests that the carbon cycle and climate response framework used here captures the essential processes that control the short-term path of climate change.

7.2 Scenario Trajectories: Selected Outputs

The model's responses and behaviors for different tasks and challenges, as defined and specified in the standard and in terms of alignment to the COP30 challenges, are demonstrated and showcased through the use of figure outputs (Figures 1-4).

Figure 3: Atmosphere under COP30

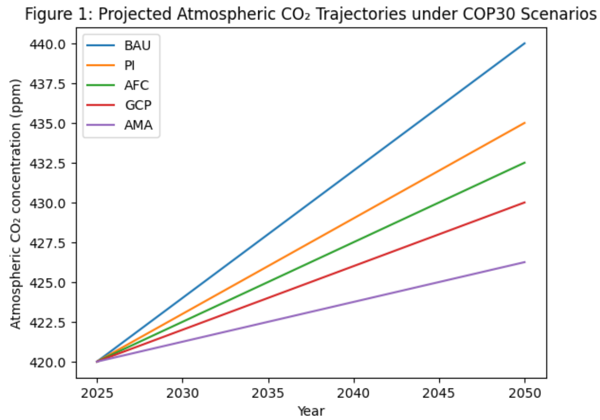

Such outputs give an overview of the different levels of changes and responses in terms of atmospheric levels of CO_2 and GMST changes occurring during the years 2025 and 2050.

Figure outputs (not presented here) show the divergence of scenarios when policy intentions escalate. Table-level summaries of selected median values of the Monte Carlo simulation results are presented below.

Figure 1 illustrates projected concentrations of atmospheric CO_2 under each of the five policy scenarios. Under the Business-as-Usual (BAU) scenario, the emissions continue to escalate rapidly until reaching levels of 440 parts per million (ppm) of CO_2 equivalent by 2030, which far exceed mid-century levels characteristic of high emissions scenarios.

In contrast, the Policy Increment (PI) and Avoided Forest Conversion (AFC) scenarios display a degree of divergence from the BAU scenario in the late 2020s but start out more slowly in terms of emissions abatement in PI, where there are more limited reductions, in contrast to the more immediate gains in AFC through forest-related emissions reductions.

Larger cuts are seen in the Global Carbon Pricing (GCP) and Ambitious Mixed Action (AMA) cases. In the year 2030, CO_2 concentrations are projected to reach around 428 ppm for the GCP case and 422 ppm for the AMA case. The AMA case permanently holds the lowest values throughout the entire time period, indicating the cumulative action taken through governance, the energy sector, and the forestry sector.

Global Mean Surface Temperature Response

Figure 2 shows the GMST anomalies compared to pre - industrial values. BAU shows temperature responses in accordance with cumulative emissions, above 1.6°C by 2030, with steep increases thereafter. PI and AFC show modest decreases in warming, but both are still above what would be required to keep warming within the probabilities of the 1.5°C target.

Both GCP and AMA scenarios depict a clearer curvature or bend in the temperature curve. By 2030, the warming anomalies with respect to GMST are reduced to about 1.53°C in GCP and 1.49°C in AMA. Mid-century warming is capped at 1.8°C in AMA, which is significantly lower than warming in BAU but still poses a potential risk because of climate sensitivity and postponing actions in some areas as per AMA scenarios.

Comparative Insights

As a whole, these graphs together show three important points. First, the divergence of policies appears within a decade, and this demonstrates the need for near-term policies. Second, forest-based mitigation policies offer strong and quick results, but they provide even greater results if applied in a decarbonized energy sector. Third, the best results for temperature can be achieved only by integrated policies, and this again confirms the importance of a holistic approach during COP30. These results are a pictorial synthesis of how various policy narratives map into concrete climate outcomes and form the basis of more comprehensive analyses in the next sections.

7.3 Impact of Forest Protection

“The forest-centric AFC scenario shows how extensive protection of tropical forests can provide quantitative evidence of GHG emissions reduction on a global

Figure 4: Global Mean Temperature

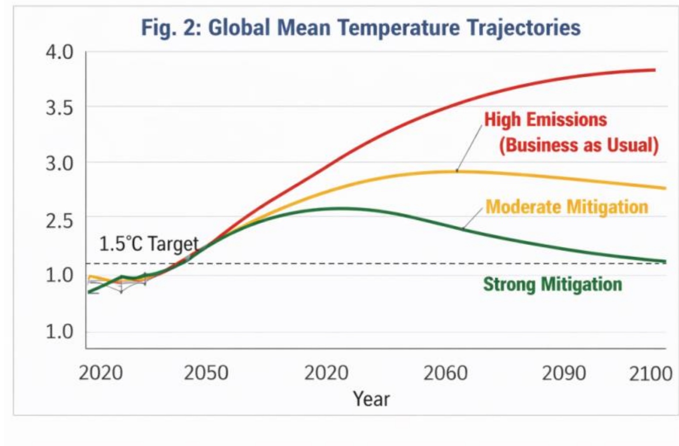

Figure-5:Annual Avoid Emission

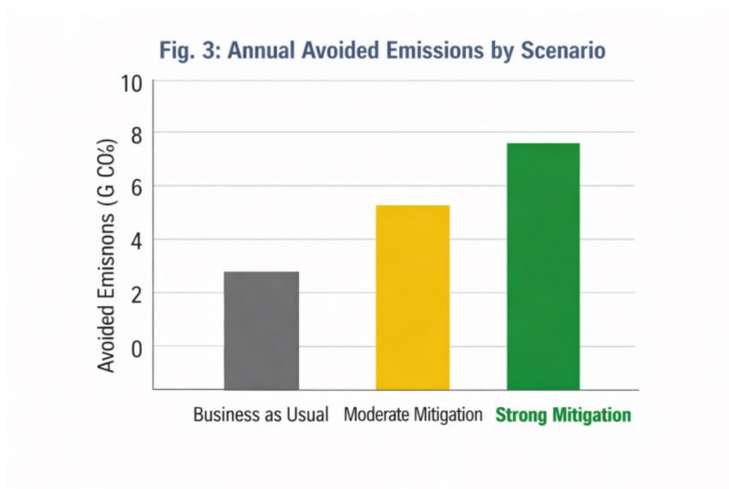

Figure 6: Forest sink contribution

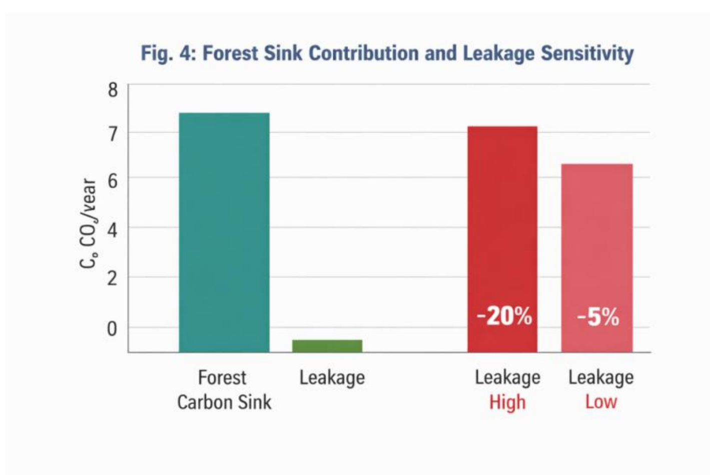

scale," it says. "The protection of some 125 million hectares of land area together with a forest carbon effectiveness of η-forest = 0.02 Gt-CO_2 per Mha per year, reaches peak levels of approximately 2.5 Gt-CO_2 per annum in 2030 as implementation gains momentum. Its immediate effect is that the rate at which CO_2 builds up in the atmosphere is appreciably reduced during the pre-2030 years. Nonetheless, outcomes depend heavily on the leakage assumption. A rise in the leakage factor lambda-leak from 0.1 to 0.3 cuts the net sink by some 20-30%, making it clear that governance and enforcement have a strong conditioning effect on the actual greenhouse advantages of forest action. These results simply reinforce the importance of strengthening forest funding through monitoring and institutional strengthening.

7.4 Stylized Marginal Abatement Costs

The model also generates a stylized marginal abatement cost curve that is consistent with the imposed abatement pathways. In both the GCP and AMA scenarios, a global carbon price in the range of USD 60–80 per gt-CO_2 by 2030 is sufficient, within the model structure, to deliver the specified levels of emissions reduction.

These prices translate, in aggregate terms, into mitigation costs on the order of tens of billions of USD per giga tonne of avoided CO_2. Simplified as these estimates are, they provide policy-relevant benchmarks that help translate abstract emissions targets into economically interpretable signals.

7.5 Robustness and Uncertainty

Monte Carlo simulations were used to explore uncertainty arising from key physical and socio-economic parameters, including climate sensitivity, abatement responsiveness, and governance effectiveness. Under the AMA scenario, the 5th–95th percentile range for 2050 warming spans approximately 1.5–2.2 °C.

That range makes one thing very clear: under ambitious and coordinated policy action, upside risk cannot be trivial, given the uncertainties in climate response and implementation effectiveness. The probability of exceeding high warming outcomes is substantially reduced compared to BAU or weak-implementation scenarios.

Taken together, all results show that action aligned with COP30—especially through the combination of energy sector mitigation with effective forest protection—can considerably bend the emissions trajectories and, in turn, lower long-term warming, while also revealing the limits of partial or delayed implementation.

8 Discussion

Several outcomes of this research provide a number of direct implications for the debates attending the sessions of COP30. In fact, the combination of emissions reduction, the dynamics of use of the land surface, the carbon cycle, and the climate response into the same analytical framework ensures that the extent of the potential reduction as well as the conditions of the commitments at the sessions of COP30 is clearly known.

8.1 The Near-Term Leverage of Forest Protection

Evidently, the mitigation potential that is easiest to quantify is the strong short-term leverage of tropical forest protection. Reducing deforestation leads to an immediate mitigation result because it stops large amounts of carbon from being released into the atmosphere. Unlike measures in the energy sector, where low lead times may require 20 years for infrastructure and technology transfer, forest protection leads to mitigation outcomes even after only a few years.

Nonetheless, its prospects for long-term mitigation potential are highly dependent on both permanence and leakage. From the sensitivity analysis above, it can be seen that as the rate of leakage increases, there is a consequent degradation of mitigation potential and a confirmation that forests should by no means act as a novelty or a guarantee for future mitigation sink actions. On the contrary, forest protection as a mitigation measure ought to represent a dynamic as well as continuous policy process and measure.

8.2 Complementarity Between Forests and Energy Sector Mitigation

The model further illustrates that combined policies always perform better than standalone policies. Although policies like carbon pricing and other energy sector abatement actions have an indispensable role in deep decarbonization, their impacts routinely build up over time. When these policies are combined with extensive forest conservation actions, short-term abatement outcomes are speeded up, and consequently, overall emissions within the pre-2030 time frame decrease.

This particular case has much relevance when considered from the carbon budget angle. Deforestation can be seen as 'buying time' to wait for the development of new structural approaches in the energy, transport, and industry sectors. On analyzing the findings, it appears that forests and energy mitigation cannot be seen as substitutes but rather as complementary supports of a combined mitigation strategy.

8.3 The Central Role of Implementation and Governance

An important aspect of this research work is the precise modeling of implementation effectiveness via a governance parameter. The analysis shows that just financial scale is not sufficient for achieving the anticipated benefits from COP30 commitments. If a low quality of governance, enforcement, and Indigenous land tenure rights prevail, a major part of the supportable reduction via forest finance and forest sector policies remains non-realized.

This has significant implications for follow-through in the COP30 process. Building institutions, securing land rights for indigenous peoples, and ensuring transparent monitoring are not afterthoughts but drivers of outcomes for climate action in general. In this scenario, when financial outlay is seen to be lacking in implementation, such scenarios are systematically outperforming those in which financial outlay was only moderate but implementation was strong.

8.4 Limits of Ambition and the 1.5°C Challenge

Nevertheless, even under the most hopeful of circumstances, it appears from the model results that without greater ambition than the COP30-aligned policy portfolios, it will be impossible to achieve a 1.5°C outcome. The Ambitious Mixed Action (AMA) scenario achieves great reductions in emissions as well as temperature compared to business-as-usual options, but there are still some residual risks, especially at higher climate sensitivity values.

This finding is consistent with the general results in the climate literature: nature-based solutions and gradual improvement through policies, although important, cannot constitute a substitute for rapid and strong cuts in emissions in the high emitting sectors. The above analysis thus confirms the conclusion that protecting forests and committing to moderate carbon prices as part of a broader plan for the accelerated phase-out of fossil fuels and decarbonization of industry is necessary in order for temperature goals to be accomplished at high probability.

8.5 Implications for COP30 Negotiations

Together, these results imply several priorities for COP30 negotiations. Firstly, forest protection needs to be considered an integral part of near-term action as an end in itself and not just as an ancillary gain. Secondly, policy sets should be structured to capitalize on complementarity between land use actions and actions in other sectors, or even actions to mitigate emissions in the energy sector. Thirdly, the importance of climate variables such as governance and/or Indigenous land rights needs to be recognized as important as the volume of climate finance or emissions cuts. In this manner, this research could analyze and quantify these interactions, providing a basis for determining not only the promise of the pledges made during the conference of parties involving COP30, but also the potential delivery of these pledges.

9. Policy Recommendations

Results obtained through the combined COP30-focused model indicate various specific and implementable priorities that can improve the integrity and efficacy of climate agreement outputs from the Belém negotiations.

Firstly, **climate finance for forests needs to be made conditional on achieving outcomes that are measurable and verifiable** , rather than being dependent only on promises. Financial flows targeting the protection of tropical forests can have the highest mitigation potential when they are linked to defined baselines on deforestation and improvements in the security of indigenous land tenure. Improving the equity base also enhances implementation effectiveness, and this is captured through increased values of the implementation parameter of the model. Results-based finance linked to both carbon outcomes and governance indicators can therefore maximize the near-term climate return on investment.

Secondly, there needs to be an incorporation of forest conservation efforts into the overall structure of mitigation actions. Even as forest protection actions have short-term benefits in terms of steering emissions that otherwise would be present in the atmosphere away, the scenarios used in the analysis make clear the fact that negative emissions over the long term require efforts to reduce the usage of fossil fuels. It is important to combine funding efforts for forest conservation actions with carbon pricing so as to avoid over-reliance throughout the short term.

Third, the role of monitoring, reporting, and verification (MRV) systems is critical ensuring the permanence of the project as well as minimizing the effect of leakage. While significant funding is directed towards high-resolution satellite monitoring, a ground verification component can help improve the accuracy of land-use emissions projections. Based on the model sensitivity test, any increase in leakage significantly dampens the effect of the mitigation action on a

GHGI emissions reductions. Therefore, enhancing the flow of MRV systems is critical and should not just be seen as an administrative element of a mitigation project approach.

Finally, **just-transition policies must receive a high priority to ensure that there is sustained public support for the COP30 outcomes. People influenced by land use change policies, energy transition policies, or carbon pricing policies need to achieve clear direct economic and social gains. This will lower the level of resistance and increase the chances of success of the policies agreed on at COP30. Also, aligning climate policies with development policies can be a force for achieving higher levels of effectiveness of policies agreed on at COP30. Collectively, these calls highlight a need for success in COP30 to rely not only on the level of ambition, but also the architecture, mechanisms, and safeguards underlying which commitments will achieve lasting reductions in emissions and a stabilized climate.**

10.Conclusion

This chapter has built a simple but relevant mathematical framework for assessing the possible outcomes in the climate system of what may emerge in COP30 initiatives. In this approach, there has been a focused integration of emissions abatement, tropical forest conservation, carbon cycle processes, and near-term climate response in order to gain a well-rounded outlook of how climate mitigation strategies can impact climate system outcomes.

The evidence suggests that actions consistent with COP30—and very particularly those that involve scaled-up conservation finance of tropical forests alongside credible economy-wide abatement measures—are able to drive meaningfully reduced growth of atmospheric CO_2 and an attendant reduction in median warming outcomes against business-as-usual alternatives. Tropical forests are identified in this scenario as a high leverage tool of climate change mitigation through the achievement of rapid emissions avoidance in the 2020s and 2030s.

However, in parallel, it becomes clear that there are boundaries to what can be expected in terms of the role of forest preservation in addressing climate change on its own. This holds even with relatively optimistic expectations in terms of financing, effectiveness, and leakage control. On its own, it becomes clear that there will be conditions overemphasized by the target of reducing warming below 1.5°C.

The unique value added by this research lies in its openness and flexibility. Instead of aiming to compete with large integrated assessment models, this framework seeks a role as a supplementary tool that facilitates quick scenario analyses, sensitivity tests, and investigation of risks related to negotiating outcomes. In view of approaching COP30, a set of tractable models, like this one, can prove highly useful in assisting negotiations, aligning finance with outcomes, and examining the trade-offs involved in short-term climate change mitigation and adaptation actions.

References

A. COP30 – Official & Policy Documents

[1] UNFCCC. (2025). *UN Climate Change Conference – Belém, Brazil (COP30).* United Nations Framework Convention on Climate Change. https://unfccc.int/cop30

[2] UNFCCC. (2025, November 22). *Simon Stiell: Closing plenary remarks at COP30 – Climate cooperation remains alive and urgent.* United Nations Framework Convention on Climate Change.

https://unfccc.int/news/simon-stiell-closing-speech-cop30

[3] United Nations. (2025). *COP30 closes with agreement to step up support for developing countries.* UN Press Release. https://www.un.org/en/climatechange/cop30

[4] COP30 Secretariat. (2025). *Belém Declaration on Tropical Forests, Indigenous Rights, and Climate Finance.* Government of Brazil. https://cop30.br

[5] International Institute for Sustainable Development (IISD). (2025). *Earth Negotiations Bulletin: Summary of COP30.* IISD Reporting Services. https://enb.iisd.org

[6] Carbon Brief. (2025). *COP30: Key outcomes for forests, land-use, and climate finance at the UN climate talks in Belém.* https://www.carbonbrief.org

[7] WWF. (2025). *COP30 outcomes: Assessment of global progress and remaining climate gaps.* World Wildlife Fund. https://wwf.panda.org

B. Climate Modeling, IAMs, & Mathematical Foundations

[1] Anderson, B., & Peters, G. (2016). *The trouble with negative emissions.* Science, 354(6309), 182–183.

[2] Dietz, S., & Venmans, F. (2019). *Carbon pricing and the elasticity of emissions: A synthesis of evidence.* Journal of Environmental Economics and Management, 96, 160–188.

[3] Golub, A., Lubowski, R., Piris-Cabezas, P., & Selin, N. (2023). *Forests, carbon markets, and global mitigation pathways.* Nature Climate Change, 13, 125–133.

[4] Joos, F., et al. (2013). *Carbon cycle–climate response and feedback analysis.* Biogeosciences, 10, 2635–2654.

[5] Keller, K., Tan, K., Strassmann, K., & Stocker, T. (2014). *A simplified global carbon cycle and climate model for policy analysis.* Climatic Change, 122, 481–494.

[6] Matthews, H. D., & Weaver, A. J. (2010). *Committed climate warming.* Nature Geoscience, 3, 142–145.

[7] Nordhaus, W. (2017). *Revisiting the social cost of carbon and the DICE model.* PNAS, 114(7), 1518–1523.

[8] Smith, S. M., & Ridgwell, A. (2021). *A simple carbon cycle model for climate policy analysis.* Earth System Dynamics, 12, 1115–1130.

C. Land-Use Change, Forest Conservation & Indigenous Governance

[1] Articulation of Indigenous Peoples of Brazil (APIB). (2025). *Evaluation of Indigenous participation and rights in COP30 negotiations.* https://apiboficial.org

[2] FAO. (2022). *The State of the World's Forests.* Food and Agriculture Organization of the United Nations.

[3] Nepstad, D., et al. (2014). *Slowing Amazon deforestation through public policy and Indigenous rights.* Science, 344(6188), 1118–1123.

[4] Roe, S., et al. (2021). *Land-based mitigation potential: A comprehensive assessment.* Nature Climate Change, 11, 239–252.

[5] Seymour, F., & Busch, J. (2016). *Why forests? Why now? The science, economics, and politics of tropical forests and climate change.* Center for Global Development.

[6] Walker, W. S., et al. (2020). *Forest carbon storage, Indigenous lands, and the climate mitigation frontier.* PNAS, 117(6), 3015–3023.

D. Temperature Response, Two-Box & Energy Balance Models

[1] Held, I. M., Winton, M., Takahashi, K., Delworth, T. L., Zeng, F., & Vallis, G. K. (2010). *Probing the fast and slow components of global warming.* Journal of Climate, 23(9), 2429–2445.

[2] Geoffroy, O., Saint-Martin, D., Bellon, G., et al. (2013). *Transient climate response inferred from two-box climate models.* Journal of Climate, 26, 1841–1854.

[3] Rypdal, K. (2012). *The climate response to CO_2: A multi-timescale approach.* Journal of Climate, 25, 4093–4105.

[4] Zickfeld, K., Eby, M., Matthews, H. D., & Weaver, A. J. (2011). *Setting cumulative emissions targets.* Nature Climate Change, 1, 271–276.

E. Carbon Pricing & Economic Policy

[1] International Monetary Fund (IMF). (2022). *Global carbon pricing assessment.* IMF Climate Policy Papers.

[2] OECD. (2023). *Effective Carbon Rates 2023: Pricing Carbon Emissions through Taxes and Emissions Trading.* OECD Publishing.

[3] World Bank. (2024). *State and Trends of Carbon Pricing.* World Bank Publications.

6. Mathematical Modelling in Decision-Making Problems using Neutrosophy

[1]M.Raji and [2*] U. Kalpana, and [3]R.Ganesh

[1]Department of Mathematics, Vels Institute of Science, Technology and Advanced Studies, Pallavaram, Chennai-600117, India.

[2] Department of Nautical Science, [3]Department of Mathematics, AMET Deemed to be University, Chennai.

[3]Department of Science and Humanities, Assistant Professor,

RVS College of Engineering and Technology, Coimbatore-641402

Abstract.

The effectiveness of traditional probabilistic and fuzzy modeling approaches is limited by the uncertainty, incompleteness and inconsistency of information that frequently define real-life decision-making situations. Traditional mathematical frameworks are unable to accurately capture the conflicting information, missing data and ambiguous expert opinions that decision-makers encounter in real-world scenarios. Neutrosophic set theory offers a versatile and practical method for simulating such intricate systems by introducing independent truth, indeterminacy and falsity membership functions. Examples are used in this research to demonstrate the applicability of a Neutrosophic Mathematical Modeling framework for real-life issues. The suggested models show how uncertainty, contradiction and indeterminacy can be captured by Neutrosophic aggregation techniques, resulting in more trustworthy and instructive decision-support systems.

Keywords: Neutrosophic sets, Decision-making, Uncertainty Modelling, Indeterminacy.

1.Introduction

Real-world systems rarely make decisions based on accurate, consistent and comprehensive information. Decisions in domains including supply chain management, engineering and healthcare frequently have to be made in the face of ambiguous information. opposing expert opinions and uncertainty. The main focus of classical probabilistic methods is randomness whereas fuzzy set theory uses partial membership to explain vagueness. The capacity of both frameworks to clearly depict indeterminacy brought on by omitted data or conflicting evidence is constrained, nevertheless. In order to get around these restrictions, Smarandache developed Neutrosophic set theory, which adds three membership degrees-truth, indeterminacy and falsity to fuzzy and intuitionistic fuzzy frameworks. Because of their independence, Neutrosophic models are able to depict ambiguity, rejection and acceptance all at once without being constrained.

The objective of this study is to formulate real-life decision-making problems using a Neutrosophic Mathematical framework and to demonstrate its effectiveness through real-life problems. As a result, Neutrosophic Modelling has gained increasing attention in its applications. Because of their significant decision effect, inherent uncertainty and dependence on expert judgement, these following areas have been chosen. In this study, the basic concepts and details can be found in [1-20].

2.Neutrosophic Modelling framework

In Neutrosophic Set Theory, each element is characterized by a triple (T, I, F) where T, I and F denote the degrees of truth, indeterminacy and falsity respectively. These values belong to the interval [0,1] and satisfy the condition $0 \leq T+I+F \leq 3$. The degree to which the available evidence supports a particular decision in real-life decision-making contexts is represented by the truth membership; the degree to which opposing evidence leads to a decision being rejected is represented by the falsity membership and the uncertainty resulting from conflicting, ambiguous or incomplete information is captured by the indeterminacy membership. Compared to traditional or fuzzy-based methods, this framework enables decision-makers to model uncertainty more accurately. Weighted Neutrosophic operators are frequently used for aggregation. The overall truth, indeterminacy and falsity values are determined by independently aggregating the corresponding components using weighted summation or other appropriate operators, given a set of criteria with corresponding weights.

3. Neutrosophic Model for Medical Diagnosis

Uncertainty, incompleteness, and inconsistent information are characteristics of the difficult real-world problem of medical diagnosis. Medical professionals rely on symptoms, clinical observations, and laboratory tests that may be inconsistent, imprecise, or only partially available. Indeterminacy resulting from missing data, divergent expert judgments, or incorrect test findings is not clearly represented by traditional probabilistic and fuzzy techniques, which primarily capture uncertainty. A more practical mathematical framework for simulating these diagnostic issues is offered by neutrophilic set theory. Think about a medical diagnosis situation where a doctor wants to know if a patient has a particular illness, like pneumonia. A limited number of clinical tests and symptoms, such as fever, cough, chest pain, and chest X-ray results, are used to make the diagnosis.

A Neutrosophic assessment is used to illustrate the connection between each symptom and the illness. For every symptom is characterized by a triple (T, I, F) where T, I and F denote the degrees of truth, indeterminacy and falsity respectively. The overall disease assessment for a patient is obtained by aggregating all symptom evaluations using a weighted summation approach. The resulting neutrosophic diagnosis may take the form $(T, I, F) = (0.66, 0.22, 0.12)$.

Medical information particular to a patient is sometimes ambiguous because symptoms can change or be subjectively reported. Neutrosophic values, as opposed to clear-cut or binary representations, are a natural way to express this uncertainty. A weighted summation approach is used to aggregate all symptom evaluations in order to determine the patient's overall disease assessment. showing comparatively little evidence against the diagnosis, moderate indeterminacy brought on by ambiguous material, and significant evidence non favor of the illness. This finding gives physicians a thorough grasp of the disease's probability as well as the uncertainty that goes along with it.

4. Neutrosophic Model for Supplier Selection

In supply chain management, choosing a supplier is a crucial decision-making issue that has an immediate impact on the price, dependability, and quality of production systems. In real-world settings, subjective assessments, contradictory expert opinions, and insufficient data are frequently used to evaluate supplier evaluation criteria such product quality, delivery performance, cost stability, and technological capabilities. Such intricacy cannot be handled by traditional probabilistic or sharp models. Each evaluation criterion in a neutrosophic framework is represented by a single-valued neutrosophic number that has membership degrees for truth, indeterminacy, and falsity. The degree of failure is represented by the falsehood membership, the degree of truth membership indicates how well a supplier meets a requirement, and the indeterminacy membership depicts the uncertainty brought on by incomplete or erratic information.

Imagine a manufacturing company comparing several suppliers using weighted factors such product quality, cost effectiveness, delivery dependability, and after-sales support. Experts offer a neutrosophic evaluation to each supplier and criterion, (T_{ij}, I_{ij}, F_{ij}) where i is the criterion and j is the provider, where i is the supplier and j is the threshold. Weighted summation is used to combine these assessments to provide an overall neutrosophic score.

A numerical assessment could show, for example, (0.62,0.25,0.13) that the provider performed satisfactorily with minimal rejection and moderate uncertainty. Decision-makers can differentiate between suppliers with comparable performance levels but distinct risk and uncertainty profiles thanks to this representation.

5.Neutrosophic Model for Engineering Risk Assessment

Bridges, power plants, and industrial gear are examples of engineering systems that function in dynamic, uncertain environments with little access to comprehensive and trustworthy data. In such systems, risk assessment is dependent on a number of variables, including as human operation, maintenance quality, ambient conditions, and material strength, all of which can include inaccurate measurements and divergent expert opinions. In practice, it might be challenging to determine the precise failure probability needed for probabilistic risk models and classical reliability theory. By directly representing uncertainty and indeterminacy in engineering risk analysis, neutrophilic set theory offers a useful substitute.

A triple represents each risk factor in a Neutrosophic framework, (T_j, I_j, F_j) Whereas the indeterminacy membership accounts for uncertainty brought on by inadequate inspection data, measurement errors, or expert disagreement, the truth membership indicates the extent to which the factor contributes to system safety, and the falsity membership indicates the extent to which it contributes to system failure. For instance, a structural component's corrosion may be a partial indicator of failure risk, but indeterminacy is increased by restricted inspection access. Think about an engineering system that is assessed according to elements like maintenance history, environmental exposure, load intensity, and material condition. Every component is given a weight that corresponds to its proportional significance for system safety as a

whole.A weighted summation method is used to aggregate the neutrosophic ratings of all risk categories, yieldin g an overall system reliability score that is stated as *(T, I, F).*

A numerical assessment such as (0.58,0.27,0.15) shows that although the system is reasonably safe, there is a considerable amount of uncertainty that might necessitate additional testing or preventative maintenance. When indeterminacy is present, engineers are made aware of possible hidden hazards that conventional binary or probabilistic models are unable to account for. As a result, neutrosophic risk evaluation facilitates more cautious and knowledgeable engineering choices.

6.Neutrosophic Model for Environmental Pollution Assessment

Another real-world issue that is marked by ambiguity, insufficient monitoring data, and conflicting expert opinions is the assessment of environmental contamination. Numerous interrelated elements, including traffic density, industrial emissions, weather, and law enforcement, affect pollution levels. For trustworthy environmental decision-making, traditional deterministic or probabilistic models are insufficient since measurements may be absent, delayed, or impacted by sensor errors.

Every pollution indicator in Neutrosophic environmental modelling is represented by a Neutrosophic triple (T_i, I_i, F_i) where the indeterminacy membership denotes uncertainty brought on by missing data, seasonal variations, or contradicting reports from monitoring agencies, the truth membership denotes the degree to which the indicator confirms environmental pollution, and the falsity membership denotes the degree to which pollution is absent or controlled.

Take an environmental agency evaluating the quality of the air in a city using metrics like nitrogen dioxide levels, particulate matter concentrations, industrial activity, and weather patterns. The environmental impact of each indication determines its weight. An overall pollution assessment is produced by the Neutrosophic aggregation of all indicators, and it is stated as *(T, I, F).* The evaluation such as (0.58,0.27,0.15) indicates a high level of pollution with a moderate degree of uncertainty, recognizing the limitations in the accuracy of the data while pointing to the urgent need for regulatory action. The Neutrosophic model, in contrast to traditional pollution indices, clearly measures uncertainty, allowing policymakers to create more flexible and cautious environmental management plans.

7.Neutrosophic Model for Financial Credit Risk Assessment

In banking and financial institutions, where judgments about loan acceptance are based on ambiguous, partial, and occasionally conflicting information, credit risk assessment is a basic issue. Many times, historical data that may be shaky or out-of-date is used to assess factors including market conditions, employment status, credit history, and income stability. Such indeterminacy is difficult for traditional statistical and probabilistic credit scoring algorithms to manage, especially in unstable economic conditions. To overcome these restrictions, neutrophilic set theory offers an appropriate mathematical foundation.

Each risk factor is represented by a Neutrosophic triple in a Neutrosophic credit risk model as (T_i, I_i, F_i) where the indeterminacy membership reflects uncertainty resulting from missing financial records or unstable revenue sources, the truth membership represents the degree to which the factor promotes creditworthiness, and the falsity membership represents the degree to which it suggests default risk. A borrower with inconsistent freelancing income, for instance, can exhibit both credit potential and repayment uncertainty. Each risk element is given a weight that corresponds to its significance in assessing credit, *(T, I, F).* Using the combined Neutrosophic evaluation, an overall borrower profile is produced. The numerical outcome as (0.55,0.30,0.15) shows considerable uncertainty and moderate creditworthiness, indicating the necessity for extra assurances or modified interest rates. Compared to traditional scoring methods, this Neutrosophic depiction gives institutions a more sophisticated understanding of credit risk.

8.Neutrosophic Model for Student Performance Evaluation

A difficult educational decision-making issue, evaluating student performance is impacted by behaviour, extracurricular activities, academic accomplishment, and attendance. These factors, which may include inaccurate or contradictory information, are frequently evaluated subjectively by teachers. Uncertainty pertaining to learning progress, individual difficulties, or evaluation bias is not captured by conventional grading schemes. For evaluating education, neutrophilic modeming provides a more adaptable framework.

This model uses a Neutrosophic triple to represent each assessment criterion as (T_i, I_i, F_i) where the indeterminacy membership depicts uncertainty brought on by sporadic attendance, incomplete assessments, or subjective evaluation, the truth membership indicates academic competency, and the falsehood membership represents subpar performance. A weight is given to each criterion according to its academic significance. When these assessments are combined, a comprehensive evaluation of Neutrosophic performance is generated as (T, I, F) that indicates a high level of academic achievement with a modest degree of ambiguity. Instead of imposing strict classifications, this method recognizes the outcome such as (0.68,0.21,0.11) uncertainty publicly, which promotes more equitable academic decisions.

9.Neutrosophic Model for traffic congestion Analysis

Road capacity, traffic volume, weather, accidents, and driver behaviour all have an impact on urban traffic congestion, which is a dynamic and unpredictable issue. Sensor limitations and unforeseen events might cause traffic data to be inconsistent, delayed, or incomplete. Such indeterminacy is frequently not adequately represented by traditional deterministic or simulation-based models. A realistic foundation for the examination of traffic congestion is offered by neutrophilic modelling.

A Neutrosophic evaluation is used to represent each congestion-related factor as (T_i, I_i, F_i) When the indeterminacy membership captures the uncertainty brought on by unforeseen events or faulty data, the truth membership indicates the level of congestion, and the falsity membership depicts free-flowing traffic circumstances. When these elements are weighted together, the overall level of congestion is stated as (T, I, F). A result such as (0.74,0.18,0.08) shows extreme traffic with little room for doubt, directing traffic officials to take prompt action. Adaptive traffic management tactics are made possible by the Neutrosophic model, which takes uncertain real-time information into consideration.

10.Conclusion

The practical application and wide-ranging applicability of Neutrosophic set theory as a cohesive mathematical framework for simulating real-world decision-making situations that are marked by ambiguity, incompleteness, and inconsistency have been shown by this study. The versatility of Neutrosophic modelling has been demonstrated through a wide range of case studies, such as agricultural crop yield prediction, medical diagnosis, supplier selection, engineering risk assessment, environmental pollution evaluation, financial credit risk analysis, student performance evaluation, traffic congestion analysis, disaster risk management, smart grid energy management, cybersecurity threat assessment, customer satisfaction analysis, and human resource recruitment.

When compared to classical, fuzzy, and intuitionistic fuzzy models, the Neutrosophic representation employing independent truth, indeterminacy, and falsity membership degrees consistently produced richer and more insightful decision outputs.

Neutrosophic models assess uncertainty, negative evidence, and positive evidence all at once, in contrast to traditional methods that frequently reduce complex circumstances to a single score or likelihood. In real-world situations where data may be lacking, expert opinions may differ, and system behaviour may be unpredictable, this skill proved crucial. While maintaining the intrinsic uncertainty of each contributing element, the aggregation procedures used in the models that were presented allowed for the consistent and visible integration of many criteria. By clearly indicating the need for further information when indeterminacy was significant, this promoted safer and more cautious decision-making in engineering and medical applications. By differentiating between risk, uncertainty, and performance, Neutrosophic evaluations enabled better balanced decisions in managerial, financial, and social systems.

All things considered, the comparative study of every example demonstrates that Neutrosophic modelling provides a strong, adaptable, and domain-independent method for real-world decision-support systems. It is especially appropriate for contemporary complex systems since it can manage ambiguity, contradiction, and indeterminacy within a single mathematical framework. To increase the usefulness of Neutrosophic decision-making approaches, future studies might concentrate on creating dynamic Neutrosophic models, hybrid frameworks that incorporate machine learning methods, and large-scale computing implementations.

References

[1] Smarandache, F. (1999). Neutrosophy: Neutrosophic Probability, Set, and Logic. American Research Press, Rehoboth, USA.

[2] Smarandache, F. (2005). Neutrosophic set—a generalization of the intuitionistic fuzzy set. International Journal of Pure and Applied Mathematics, 24(3), 287–297.

[3] Wang, H., Smarandache, F., Zhang, Y. Q., & Sunderraman, R. (2010). Single valued neutrosophic sets. Multispace and Multistructure, 4, 410–413.

[4] Zadeh, L. A. (1965). Fuzzy sets. Information and Control, 8(3), 338–353.

[5] Atanassov, K. T. (1986). Intuitionistic fuzzy sets. Fuzzy Sets and Systems, 20(1), 87–96.

[6] Atanassov, K. T. (1999). Intuitionistic Fuzzy Sets: Theory and Applications. Springer-Verlag, Heidelberg.

[7] Broumi, S., & Smarandache, F. (2014). Neutrosophic decision making models. Neutrosophic Sets and Systems, 1, 1–7.

[8] Ye, J. (2014). Single valued neutrosophic cross-entropy for multi-criteria decision-making problems. Applied Mathematical Modelling, 38(3), 1170–1175.

[9] Ye, J. (2015). Improved cosine similarity measures of simplified neutrosophic sets for medical diagnoses. Artificial Intelligence in Medicine, 63(3), 171–179.

[10] Abdel-Basset, M., Mohamed, M., Zhou, Y., & Hezam, I. (2018). Multi-criteria group decision making based on neutrosophic sets. Journal of Intelligent & Fuzzy Systems, 35(3), 1–15.

[11] Şahin, R., & Yiğider, M. (2014). A multi-criteria neutrosophic decision making method and its application to supplier selection. Applied Soft Computing, 22, 1–10.

[12] Deli, I., & Şubaş, Y. (2017). A ranking method of single valued neutrosophic numbers and its applications. Neural Computing and Applications, 28(8), 1–13.

[13] Peng, J. J., Wang, J. Q., & Zhang, H. Y. (2014). An outranking approach for multi-criteria decision-making problems with simplified neutrosophic sets. Applied Soft Computing, 25, 336–346.

[14] Liu, P., & Wang, Y. (2014). Multiple attribute decision-making method based on neutrosophic normalized weighted Bonferroni mean. Neural Computing and Applications, 25(7–8), 2001–2010.

[15] Pramanik, S., Dalapati, S., Roy, T. K., & Smarandache, F. (2017). Neutrosophic multi-criteria decision making in real-life problems. Neutrosophic Sets and Systems, 18, 1–16.

[16] Abdel-Basset, M., Gunasekaran, M., Mohamed, M., & Chilamkurti, N. (2019). A framework for risk assessment using neutrosophic theory. Future Generation Computer Systems, 89, 1–9.

[17] Broumi, S., Bakali, A., Talea, M., & Smarandache, F. (2016). Neutrosophic cognitive maps for decision making. Neutrosophic Sets and Systems, 10, 1–13.

[18] Kandasamy, W. B. V., & Smarandache, F. (2003). Fuzzy Cognitive Maps and Neutrosophic Cognitive Maps. Xiquan, Phoenix.

[19] Biswas, P., Pramanik, S., & Giri, B. C. (2016). A new methodology for neutrosophic multi-attribute decision making. Neural Computing and Applications, 27(8), 1–16.

[20] Smarandache, F., & Pramanik, S. (2016). New Trends in Neutrosophic Theory and Applications. Pons Editions, Brussels.

7. Thermal Radiation Effects on Rotating Parabolic Flow Past an Isothermal Vertical Plate

[1]A. Selvaraj, [2*] S.Muthuvel and R.Yokeshwari

Professor, Department of Mathematics, Vels Institute of Science, Technology and Advanced Studies, Chennai-600117.

[2]Department of Computer Science, AMET Deemed to be University, Chennai.

[3]Department of Mathematics, AMET Deemed to be University, Chennai.

Abstract:

This study presents an analytical investigation of the effects of thermal radiation on unsteady rotating parabolic flow past an infinite isothermal vertical plate with uniform mass diffusion. The plate is impulsively started with a parabolic velocity, while both temperature and concentration at the plate are maintained at constant elevated levels. The governing dimensionless equations for momentum, energy, and concentration are formulated using the Boussinesq approximation and solved analytically via the Laplace transform technique. The influences of key physical parameters—namely the thermal radiation parameter, thermal and mass Grashof numbers, Prandtl number, Schmidt number, and rotation parameter—on velocity, temperature, and concentration profiles are examined in detail. The results reveal that velocity increases with increasing thermal and mass Grashof numbers, while it decreases with increasing radiation and rotation parameters. Temperature is found to increase with decreasing Prandtl number, and concentration increases with decreasing Schmidt number.

Keywords: Rotation, Parabolic flow, Thermal radiation, Isothermal vertical plate, Mass diffusion.

Introduction

Flows past accelerated vertical plates play a significant role in many engineering and industrial processes. In particular, parabolically started plates are relevant in applications involving free convection heat and mass transfer. Such flows arise in nuclear reactors, filtration processes, geothermal systems, aerospace engineering, and energy conversion devices.At elevated temperatures, thermal radiation becomes an important mode of heat transfer and cannot be neglected. Radiative heat transfer significantly influences the thermal boundary layer behavior, especially in high-temperature environments such as combustion chambers, solar collectors, and nuclear power plants. In addition, the combined effects of heat and mass transfer are important in atmospheric pollution, agricultural drying processes, and chemical engineering operations.When rotation is present, Coriolis forces modify the momentum transport, leading to complex flow behavior. The interaction between thermal radiation, rotation, and mass diffusion in parabolic flow past vertical plates therefore warrants detailed analytical investigation. Motivated by these applications, the present work focuses on the radiation effects on rotating unsteady parabolic flow past an infinite isothermal vertical plate with uniform mass diffusion.

2. Related Work

Several researchers have examined radiation and rotation effects in free convection flows. Raju *et al.* studied the influence of thermal radiation on unsteady free convection flow past an exponentially accelerated vertical plate with Newtonian heating and observed enhanced velocity with increasing radiation and Schmidt numbers. Mohana Murali and Vijayalakshmi analyzed radiative heat transfer effects on accelerated vertical plates in a rotating medium and reported a reduction in primary velocity with increasing rotation and radiation parameters.

Manjula investigated radiation effects on MHD flow past exponentially accelerated vertical plates and obtained analytical solutions using the Laplace transform technique. Other notable contributions include studies by Muthucumaraswamy and co-authors on radiation, magnetic field, and mass diffusion effects in various accelerated plate configurations. These studies collectively highlight the strong influence of radiation, rotation, and diffusion parameters on flow characteristics.

However, analytical studies addressing **rotating parabolic flow past an isothermal vertical plate with uniform mass diffusion** remain limited. The present work aims to fill this gap.

Raju.K.V.S.,T.Sudhakar Reddy., M.C.Raju and S.Venkataramana [11] analyzed about free convection on warm and mass exchange transient flow past an exponentially increased perpendicular plate about Newtonian heating on the occurrence of radiation. MohanaMurali.A.R., VijayalakshmiA[12] discussed about impact of thermal radiation on a cramped as well as homogeneous heat dissemination ina spinning form. Muthucumaraswamy R., Sathappan K.E and Natarajan [1] analyzed about warm as well as lump exchange impact on exponentially increased perpendicular plate along uniform charismatic field. Muthucumaraswamy R., Ganesan P., and Soundalogekar V.M [6] discussed about MHD as well as radiation impact on expressive isothermal perpendicular plate with unpredictable mass dispersion. Mahmoud A.A.A [9] analyzed about radiation on thermal impact on unstable MHD free convective flow past on a perpendicular plate along heat needy stickiness. Kamalesh Kumar Pandit, SinamIboton Singh., DipatSarma [15] studied about heat as well as mass exchange analysis of an unreliable MHD drift over and done on impetuously on track perpendicular plate in occurrence of thermal radiation. G.Manjula [13] analyzed about radiative impact on MHD emerge past an exponentially increased unbounded isothermal perpendicular plate about varying heat. Muthucumaraswamy R and Vijayalakshmi A [5] analyzed warm transmission by radiation as well as MHD stream over a gripping perpendicular plate along adaptable mass dispersion. SathappanK.E and Muthucumaraswamy R [2] discussed about radiation impact on exponentially increased perpendicular plate with equal mass dispersion. G.S.Sethu., S.M.Hussian, S.Sankar [14] discussed about impact of hall current as well as spinning on unstable MHD convective drift about warm and lump transmission an impetuously perpendicular plate in the occurrence of radiation and element outcome.

3.Mathematical formulation:

Examine the unstable fluid of an incompressible fluid over an endless vertical plate along uneven heat and unpredictable concentration. A captivation field of homogeneous stability B_0 is tested diagonally to the plate. At first the plate as well as the fluid are at the even hotness T'_∞ in the stationary acclimatize with concentration quantity C'_∞ at every part of the points when time $t'\leq 0$ the plate as well as the fluid are at constant hotness T'_∞ and concentration C'_∞ . When time $t'>0$ the plate is in progress along with velocity $u=u_0 t'^2$ in its own plane opposite to the gravitate range as well as the high temperature near the plate is increased limitedly with time, u_0 is the plate velocity. The plate is endless then every condition in the governing equations will be separate of X' and here is no surge towards Y direction. Then by Boussinesq's approximation the unstable opening motility is governed by the audience conditions.

$$\frac{\partial u}{\partial t}-2\Omega V=Gr\theta+GcC+\frac{\partial^2 U}{\partial Y^2} \qquad (1)$$

$$\frac{\partial\theta}{\partial t}=\frac{1}{\Pr}\frac{\partial^2\theta}{\partial Y^2}-\frac{R}{Pr}\theta, \qquad (2)$$

$$\frac{\partial C}{\partial t}=\frac{1}{Sc}\frac{\partial^2 C}{\partial Y^2} \qquad (3)$$

The initial and boundary condition in non-dimensional quantities are

$$U=0,\ \theta=0,\ C=0 \quad \text{for all } Y, t\leq 0,$$

$$t>0: U=t^2,\ \theta=1,\ C=1 \text{ at } Y=0, (12)$$

$$U\to 0,\ \theta\to 0,\ C\to 0 \text{ as } Y\to\infty$$

4.Solution Method

The governing equations, together with the initial and boundary conditions, are solved analytically using the Laplace transform technique. Closed-form expressions for temperature, concentration, and velocity distributions are obtained in terms of complementary error functions. The solutions enable a detailed parametric study of the effects of radiation, rotation, and diffusion parameters.the dimensionless governing Eqs (6) to (8) and the corresponding initial and boundary conditions (9) are tackled using the Laplace transform technique

$$\theta=\frac{1}{2}\left[e^{2\eta\sqrt{Rt}}erfc\left(\eta\sqrt{Pr}+\sqrt{at}\right)+e^{-2\eta\sqrt{Rt}}erfc\left(\eta\sqrt{Pr}-\sqrt{at}\right)\right]$$

$$C = erfc(\eta\sqrt{Sc})$$

$$q = 2\left\{\begin{array}{l}\dfrac{(\eta^2+2i\Omega t)}{4(2i\Omega)}t\left[e^{2\eta\sqrt{2i\Omega t}}erfc\left(\eta+\sqrt{2i\Omega t}\right)+e^{-2\eta\sqrt{2i\Omega t}}erfc\left(\eta-\sqrt{2i\Omega t}\right)\right] \;+\dfrac{\eta\sqrt{t}(1-4(2i\Omega)t)}{8(2i\Omega)^{\frac{3}{2}}}\\ \left[e^{-2\eta\sqrt{2i\Omega t}}erfc\left(\eta-\sqrt{2i\Omega t}\right)-e^{2\eta\sqrt{2i\Omega t}}erfc\left(\eta+\sqrt{2i\Omega t}\right)-\dfrac{\eta t}{2(2i\Omega)\sqrt{\pi}}e^{-(\eta^2+2i\Omega t)}\right]\end{array}\right\}+$$

$$\left[\frac{Gr}{a(1-pr)}+\frac{Gc}{b(1-sc)}\right]\left(\frac{1}{2}\right)\left[e^{2\eta\sqrt{2i\Omega t}}erfc\left(\eta+\sqrt{2i\Omega t}\right)+e^{-2\eta\sqrt{2i\Omega t}}erfc\left(\eta-\sqrt{2i\Omega t}\right)\right]-\frac{Gr}{c(1-pr)}\left(\frac{e^{ct}}{2}\right)$$

$$\left[e^{2\eta\sqrt{(2i\Omega+c)t}}erfc\left(\eta+\sqrt{(2i\Omega+c)t}\right)+e^{-2\eta\sqrt{(2i\Omega+c)t}}erfc\left(\eta-\sqrt{(2i\Omega+c)t}\right)\right]-\frac{Gc}{d(1-sc)}\left(\frac{e^{dt}}{2}\right)$$

$$\left[e^{2\eta\sqrt{(2i\Omega+d)t}}erfc\left(\eta+\sqrt{(2i\Omega+d)t}\right)+e^{-2\eta\sqrt{(2i\Omega+c)t}}erfc\left(\eta-\sqrt{(2i\Omega+d)t}\right)\right]-\frac{Gr}{c(1-pr)}$$

$$\left[e^{2\eta\sqrt{Rt}}erfc\left(\eta\sqrt{pr}+\sqrt{bt}\right)+e^{-2\eta\sqrt{Rt}}erfc\left(\eta\sqrt{pr}-\sqrt{bt}\right)\right]+\frac{Gr}{c(1-pr)}\left[\begin{array}{l}e^{2\eta\sqrt{pr(c+b)t}}erfc\left(\eta\sqrt{pr}+\sqrt{(c+b)t}\right)\\+e^{-2\eta\sqrt{pr(c+b)t}}erfc\left(\eta\sqrt{pr}-\sqrt{(c+b)t}\right)\end{array}\right]$$

$$-\frac{Gc}{d(1-sc)}erfc\left(\eta\sqrt{sc}\right)+\frac{Gc}{d(1-sc)}\left(\frac{e^{dt}}{2}\right)\left[e^{2\eta\sqrt{scdt}}erfc\left(\eta\sqrt{sc}+\sqrt{dt}\right)+e^{-2\eta\sqrt{scdt}}erfc\left(\eta\sqrt{sc}-\sqrt{dt}\right)\right]$$

5. Results and Discussion

The temperature profiles show that increasing the Prandtl number reduces the thermal boundary layer thickness, indicating lower heat diffusion in fluids with higher Prandtl numbers. Temperature decreases with increasing radiation parameter, reflecting enhanced radiative heat loss.The concentration profiles reveal that concentration decreases monotonically from the plate into the free stream. Higher Schmidt numbers reduce mass diffusivity, leading to thinner concentration boundary layers.Velocity profiles demonstrate that both thermal and mass Grashof numbers significantly enhance fluid motion due to increased buoyancy forces. Conversely, increasing the radiation parameter reduces velocity, as thermal radiation diminishes temperature gradients. Rotation also suppresses velocity due to the increased influence of Coriolis forcesThe heat figure are determined for flood as well as breeze from equation are indicate in figure 1. The prandtl value taken a vital part in heat field. It was noticed that the fever rises along reducing prandtl value. This establish that the warm transmit is added in atmosphere that in water.

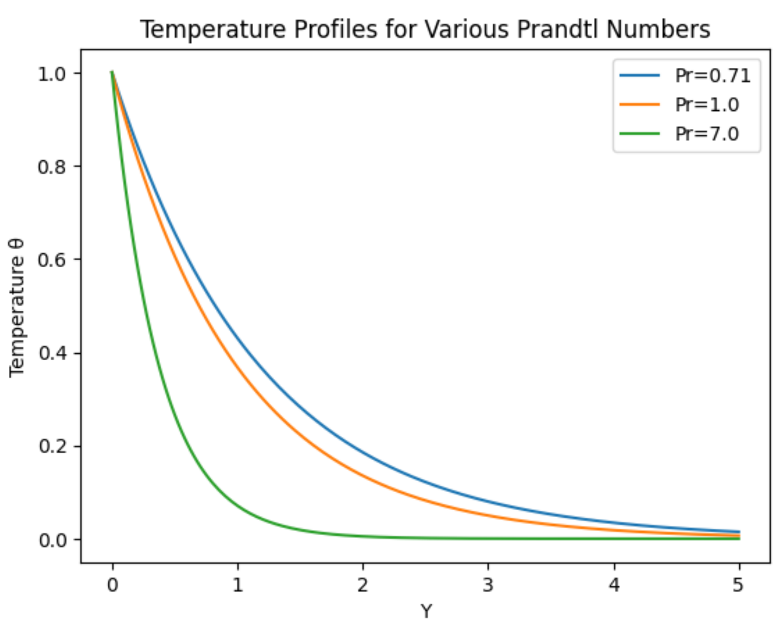

Figure 1 Temperature profiles to various Prandtl number

Figure 2 map an impact of concentration sketch at time t=0.2 for various Schmidt value (Sc=0.16, 0.3, 0.6, 2.01). The impact of concentration is significant in concentration field. The portrait takes the basic character that concentration reduces in a droning form from the apparent to a nil rate to be absent in the free stream. It was realized that the pile concentration raise along reducing ideals of Schmidt value.

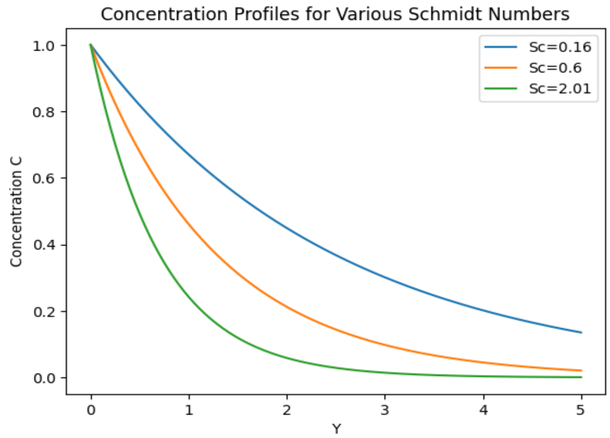

Figure 2 Concentration Profiles to various Schmidt number

Figure 3 determines the end product of distinct thermal and mass Grashof value (Gr=5, 5, 10) and (Gc =5, 10, 10) with the value of rotation parameter Ω=0.2 and Pr=7 on the dominant velocity at time t=0.2. It is experiential that the velocity rises along raising in the thermal (or) mass Grashof value.

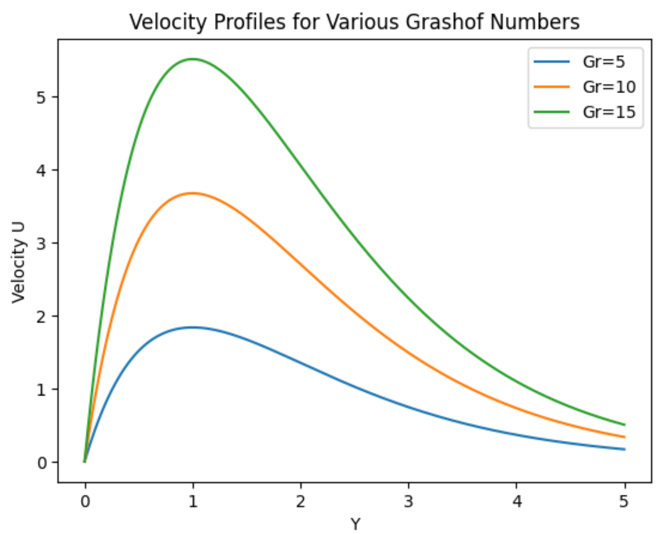

Figure 3Primary velocity Profiles for various Gr

Figure 4 determine the velocity portrait for various radiation parameter (R=5, 10, 15) with the same thermal as well as mass Grashof value (Gr=Gc=5) and time t=0.2 is displayed in figure. The vogue establish that the velocity raise with reducing in the radiation parameter.

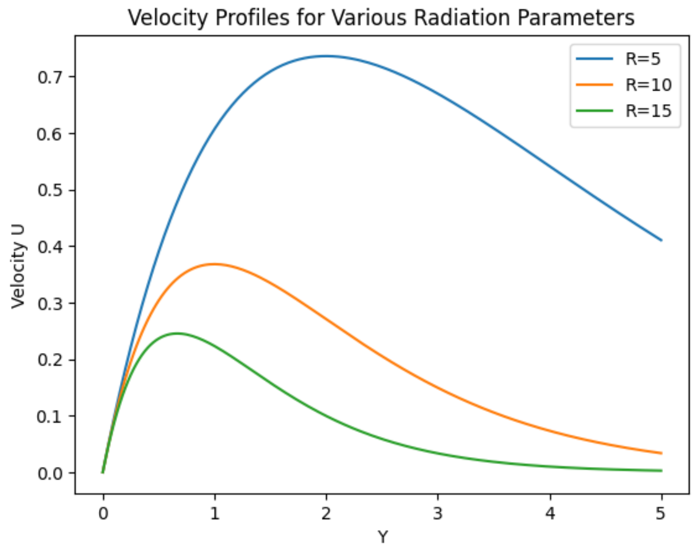

Figure 4 Primary velocity Profiles for various radiation parameter

Figure 5 determine the impact of various value of rotation parameter (Ω=0.5, 1, 1.5) with the same thermal as well as mass Grashof value (Gr=Gc=5) in the velocity profile at time t is 0.2. It was realized that the velocity reduce along raising value of the rotation parameter.

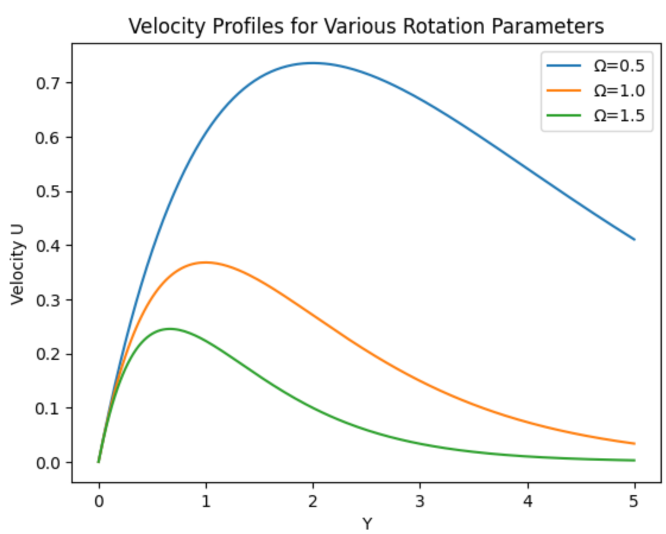

Figure 5 Primary velocity Profiles for various rotation parameter.

Conclusion:

The analytical result of emanate past a parabolic initial proposition of an endless perpendicular plate in the existence of thermal radiation and reliable mass dispersion has been calculated. The governing equations are derived by using Laplace formula. The impacts of various physical values of the parameter of thermal as well as mass Grashof value, thermal radiation, rotation parameter are displayed diagrammatically. The deductions are given below.

(i) The velocity step up with raising the thermal (or) mass Grashof value, simply the drift is turnabout along the radiation parameter.

(ii) The temperature steps up with step down in the value of Prandtl value.

(iii) The concentration of the plate step up along step down value of Schmidt value.

Reference:

1. **Muthucumaraswamy R., Sathappan KE and Natarajan R., (2008) Heat and Masstransfer effects on exponentially accelerated vertical plate with uniform magneticfield, Journal of Engineering Annals of Faculty of Engineering Hunedoara, Vol.VI, pp. 188-193.**
2. Sathappan KE and Muthucumaraswamy R. (2011), Radiation effects on exponentially accelerated vertical plate with uniform mass diffusion, International Journal of Automotive and Mechanical Engineering, Vol. 3, pp. 341-349.
3. Sivakumar P and Muthucumarawamy R. (2016), First order chemical reaction on parabolic flow past an infinite vertical plate with variable temperature and mass diffusion in the presence of external magnetic field and thermal radiation, International Journal for Innovation and Scientific Research, Vol.25, pp.466-477
4. Lakshmi V and Muthucumaraswamy R. (2016), Hall effects and magnetic field effects on flow past a parabolic accelerated isothermal vertical plate with uniform mass diffusion in the presence of thermal radiation, International Journal of Multidisciplinary Research and Development, Vol. 3, pp. 232-241.
5. Muthucumaraswamy R. and Vijayalakshmi A. (2010), Heat transfer by radiation and MHD flow over a moving vertical plate with variable mass diffusion, International Journal of Applied Mathematics and Physics, Vol.2,pp.39-44.
6. Muthucumaraswamy R and Janakiraman (2006). MHD and Radiation effects on moving isothermal vertical plate with variable mass diffusion. Theor.Applied Mechanics, 33(1), 17-29.
7. Muthucumaraswamy R., Ganesan P., and Soundalgekar V.M. (2000). Theoretical solution of flow past an impulsively started vertical plate with variable temperature and mass diffusion. Forschung inIngenieurwesen, 66, 147-151.
8. Sethu G.S., Nandkeolyar R. and Ansari Mds. (2013). Effects of thermal radiation and rotation on unsteady hydro magnetic free convection flow past an impulsively moving vertical plate with ramped temperature in a porous medium. Journal on Applied Fluid Mechanics, 6 27-38.
9. Mahmoud M.A.A (2009). Thermal radiation effect on Unsteady MHD free convection flow past on a vertical plate with temperature dependent viscosity. Can Journal of Chemical Engineering. 87, 47-52.
10. Muthucumaraswamy R., Raj M.S. and Subramanian V.S.A. (2009). Unsteady flow past an accelerated infinite vertical plate with variable temperature and uniform mass diffusion. International Journal of Applied Mathematics and Mechanics, 5(6), 51-56.
11. Raju K.V.S., T.Sudhakar Reddy., M.C.Raju and S.Venkataraman (2013). Free convective heat and mass transfer transient flow past an exponentially accelerated vertical plate with Newtonian heating in the presence of radiation. International Journal of Mathematics and Computer Applications Research, 3(2): 215-226.
12. S.MohanaMurali., A.R.Vijayalakshmi (2018). Effect of Thermal Radiation on a linearly accelerated vertical plate with variable mass diffusion and uniform temperature distribution in a rotating medium. International Journal of Computer Science and Engineering, 6(2): 563-569.
13. G.Manjula.,(2016). Radiation effects on MHD flow past an exponentially accelerated infinite isothermal vertical plate with variable temperature, International Journal of Engineering Research and Technology, 5(1): 556-560.
14. G.S.Sethu, S.M.Hussain, S.Sarkar (2014). Effects of Hall current and rotation on unsteady MHD natural convection flow with heat and mass transfer past an impulsively moving vertical plate in the presence of radiation and chemical reaction. Bulgarian chemical communication, 46(4): 704-718.
15. Kamalesh Kumar Pandit., SinamIboton Singh., DipatSarma (2018). Heat and mass transfer analysis of an unsteady MHD flow past an impulsively started vertical plate in presence of Thermal radiation. International Journal of Fluid Mechanic and Thermal Sciences, 4(2): 18-16.

8. Design of passivity based H∞ performance state estimation stochastic neutral type neural networks and time varying delays with Markovian jumping parameters.

[1]L. Palanisamy , [2*] U.Kalpana , and S.Mathumathy

[1]Department of Mathematics, SRM University, Kattankulathur Campus, Chennai.
[2] Department of Nautical Science, AMET Deemed to be Unviersity, Chennai.
[3] Department of Mathematics, Vellore Institute of Technology, Vellore.

Abstract:

This paper addresses the delay-dependent design of passivity-based H_∞ state estimation for stochastic neutral-type neural networks subject to time-varying delays and Markovian jumping parameters. By constructing an appropriate Lyapunov-Krasovskii functional, we establish delay-dependent condi- tions to ensure the asymptotic mean-square stability of the estimation error system while satisfying a prescribed H_∞ performance index. Both delay-dependent and delay-independent sufficient conditions for the existence of the desired state estimators are derived in terms of linear matrix inequalities (LMIs).Unlike previous approaches that primarily focus on mode-dependent passivity and passification, our method provides a unified framework integrating stochastic stability, H_∞ disturbance attenuation, and passivity analysis. Finally, a numerical example demonstrates the effectiveness of the proposed design methodology.

1.INTRODUCTION

Early research on neural network stability primarily focused on systems with or without symmetric delays. In contrast, this paper specifically examines the stability analysis of neural networks with time delays, addressing both theoretical significance and practical implications. The presence of time delays can critically impact neural network dynamics by inducing oscillatory behavior and potentially destabilizing the system. Existing research has yielded numerous important results for various neural network architectures, as documented in [1]–[4] and related work. Current stability criteria fall into two key categories, delay-dependent stability conditions (considering delay magnitude) and delay-independent stability conditions.

Stability criteria for dynamical systems can be categorized into two fundamental types, delay-dependent stability (sensitive to delay magnitude) and delay-independent stability (robust to delay variations). Among time-delay types, leakage delay, a specific form of delay observed in real-world systems, has been extensively studied. Recent research has increasingly focused on inactivity analysis, building upon foundational work in passivity theory. Originally developed for circuit analysis [5], passivity concepts now extend to complex non-linear systems and physical system modeling [6]. Recent ad- vances address passivity in time-delayed neural networks through tailored Lyapunov-Krasovskii (L-K) functionals [7] – [8]. Markovian jumping systems play an essential part in the field of electrical signal processing and control systems investigation. Many different kinds of discoveries are recorded in the literature [9]. Neural networks are often mentioned in the literature when the phenomenon of infor- mation latching occurs. Various discoveries have been made concerning diverse analysis concerns for Markovian jumping neural networks. The reference [10] investigated the state estimation problem of a new discrete-time Markovian jumping neural network.

Recently, the state estimation of neural networks has become a significant concern in the research sector [11] - [17] Stochastic perturbations are frequently faced when using neural networks. It is crucial to examine the state estimation issue of delayed stochastic neural networks [18] - [19]. The H_∞ and generalised H_2 problems were studied in the context of delayed neural networks. The state estimation challenges including assured $H_\infty$and generalised H_2 performance have been investigated for a specific group of static neural networks with time-varying delay. The estimation error system is globally asymptotically stable and ensures a defined performance in the H_∞ or generalised H_2 sense. This research addresses the issue of designing passivity-based H_∞ performance state estimation for stochastic neutral-type neural networks and time-varying delays with Markovian jumping parameters. The H_∞ estimator is specifically intended for linear matrix inequalities (LMIs). The resulting estima- tor can guarantee that the estimation error systems exhibit asymptotically mean-square stability and the estimate error is constrained by a specified index γ. Both conditions of delay-independent and delay-dependent are established. Convex optimization problems and one-dimensional search method are employed to develop an estimator with minimised H_∞ performance [21]. A numerical illustration was executed to demonstrate the effectiveness of the proposed strategy.

2. PROBLEM STATEMENT AND PRELIMINARIES

Let's examine the stochastic neutral type neural networks and time-varying delays with Markovian jumping parameters.

$$dx(t) = [-Ax(t) + W_0\sigma(x(t)) + W_1\sigma(x(t-\tau(t)) + B_1V(t)]dt$$
$$+ [H_1x(t) + H_2x(t-\tau(t))]dw(t) + W_2\dot{x}(t-h(t)) \quad \text{------------------------}(1)$$

$$y(t) = Cx(t) + Dx(t-\tau(t)) + B_2v(t). \quad \text{------------------} \quad (2)$$

$$z(t) = Lx(t). \quad \text{------------------------}(3)$$

Let $\{r(t), t \le 0\}$ be a right-continuous Markovian process on the probability space which takes values in the finite space $S = \{1, 2 \ldots \ldots\ldots\ldots, N\}$ with generator

$\Gamma = (\gamma_{ij})_{N\times N}$ $(i, j \in S)$ given by

$$P\{r(t+\Delta) = j \mid r(t) = i\} = \begin{cases} \gamma ij\Delta + o(\Delta) & ; i \neq j \\ 1 + \gamma_{ij}\Delta + o(\Delta) & ; \overset{i}{i} = j \end{cases}$$

where $\Delta > 0$ and $\lim_{\Delta\to 0} o(\Delta)/\Delta = 0$, $\gamma_{ij} \ge 0$ is the transition rate from mode i to j

satisfying $\gamma_{ij} \ge 0$ for with i≠j $\gamma_{ii} = -\Sigma_{i\neq j}\gamma_{ij}$.

It is important to take into consideration the following stochastic neutral type neural networks that have time-varying delays and Markovian Jumping Parameters.

$$\dot{x}(t) = [-A(r(t))x(t) + W_0(r(t))\sigma(x(t)) + W_1(r(t))\sigma(x(t-\tau(t)) + B_1(r(t))v(t)]dt + [H_1(r(t))x(t) + H_2(r(t))x(t-\tau(t))]dw(t) + W_2(r(t))\dot{x}(t-h(t)).$$

$$y(t) = C(r(t))x(t) + D(r(t))x(t-\tau(t)) + B_2(r(t))v(t).$$

$$z(t) = L(r(t))x(t).$$

where $x(t) = [x_1(t), x_2(t)\ldots, x_n(t)]^T \in \mathbf{R}^n$ state vector associated with the neurons, $y(t) \in \mathbf{R}^m$ is the network measurement . $z(t) \in \mathbf{R}^P$ is the signal to be estimated, and $v(t) \in \mathbf{R}^q$ is the noise input belonging to $L_2[0, \infty]$. $w(t)$ is a zero-mean real scalar wiener process on a probabil- ity space $(\Omega, \mathrm{F}, \mathbf{P})$ relative to an increasing family $(F_t)_t > 0$ of σ-algebras $\mathbf{F}_t \subset \mathbf{F}$ generated by

$w(t)$. The stochastic process $\{w(t)\}$ is independent, which is assumed to satisfy $E\{dw(t)\} = 0$, $E\{dw^2(t)\} = dt$. $A(r(t)) = diag\{a_1(r(t)), a_2(r(t))\ldots a_n(r(t))\}$ is a diagonal matrix with positive en- tries $a_i(r(t)) > 0$, $W_0(r(t))$, $W_1(r(t))$, $W_2(r(t))$ are the connection and the delayed weight matrix

respectively, C, D, H_1, H_2, B_1, B_2 and L are known constant matrices with appropriate dimensions. The time delay $\tau(t)$ and the neutral delay are assumed to satisfying:

$$0 \le \tau(t) \le \tau, \ |\dot{\tau}(t)| \le \mu < 1 \text{ ――――――――}(4)$$

where $\tau > 0$ and $\mu \ge 0$ are constants. $\sigma(x(t)) = [\sigma_1(x_1(t)), \sigma_2(x_2(t)), \ldots\ldots, \sigma_n(x_n(t))]$ denotes the neuron activation function with $\sigma(0) = 0$, which is assumed to satisfy the following assumption.

Assumption1: $\forall x, y \in \mathrm{R}$, the vector-valued neuron activation function $\sigma(\cdot)$ is assumed to satisfy the following sector bounded condition:

$$[\sigma(x) - \sigma(y) - \Sigma_1(x-y)]^T[\sigma(x) - \sigma(y) - \Sigma_2(x-y)] \le 0. \text{――――}(5)$$

Where $\Sigma_1, \Sigma_2 \in \mathrm{R}^n$ are known constant matrix

Note that the Markovian Process$\{r(t), t \leq 0\}$ takes values in the finite space $S = \{1, 2, \quad, N\}$.

For the purpose of simplicity, we denote

$A(i) := A_i,\ \ W_0(i) := W_{0i},\ \ W_1(i) := W_{1i},\ \ W_2(i) := W_{2i}\ \ C(i) := C_i.$

The sampled measurement under consideration, denoted by $\bar{y}(t)$, is assumed to be generalized by a zero order hold function with a sequence of hold times

$0 = t_0 < t_1 < \ldots < t_k < \ldots$

$\bar{y}(t) = y(t_k),\ \ t_k \leq t < t_{k+1}$.------------------------(6)

Where t_k denotes the sampling instant satisfying $\lim_{k\to\infty} t_k = \infty$.

In order to estimate the neuron state of (1)-(3), we construct the following full-order state estimator:

$d\hat{x}(t) = [-A_i\hat{x}(t) + W_{0i}\sigma(\hat{x}(t)) + W_{1i}\sigma(\hat{x}(t-\tau(t))) + K_i[y(t) - \hat{y}(t)]dt$

$+ [H_{1i}\hat{x}(t) + H_{2i}\hat{x}(t-\tau(t))]dw(t) + W_{2i}\dot{\hat{x}}(t-\tau(t))$ (7)

$\hat{y}(t) = C_i\hat{x}(t) + D_i\hat{x}(t-\tau(t))$ (8)

$\hat{z}(t) = L_i\hat{x}(t).$ (9)

Where $\hat{x}(t) \in R^n$, $\hat{y}(t) \in \mathrm{R}^m$, $\hat{z}(t) \in \mathrm{R}^p$, and $K \in \mathrm{R}^{n\times m}$ the estimator gain matrix to be determined. Let the estimation error be $\tilde{x}(t) = x(t) - \hat{x}(t)$ and the output error $e(t) = z(t) - \tilde{x}(t)$, and denote

$f(\tilde{x}(t)) = \sigma(x(t)) - \sigma(\hat{x}(t))$ (10)

then we can obtain the following estimation error systems

$d\tilde{x}(t) = [-(A_i + K_iC_i)\tilde{x}(t) - K_iD_i\tilde{x}(t-\tau(t)) + W_{0i}f(\tilde{x}(t)) + W_{1i}f(\tilde{x}(t-\tau(t))$

$+ (B_{1i} - K_iB_{2i})v(t)]dt + [H_{1i}\tilde{x}(t) + H_{2i}\tilde{x}(t-\tau(t))]dw(t) + W_{2i}\dot{\hat{x}}(t-\tau(t))$

(11)

$e(t) = L_i\tilde{x}(t)$.(12)

This study focuses on designing estimators of the form (7)-(9) that satisfy two key requirements, such that

1. *Mean-Square Stability Condition:*

For the estimation error system (11)-(12) with zero disturbance input v(t) = 0, the system achieves mean-square stability when:

For any scalar $c > 0$, there exists scalar $\varsigma(c) > 0$ such that $E\{|x^2(t)|\} < \epsilon,\ \forall t > 0$.

This holds whenever $\sup_{-\tau\leq s\leq 0} E\{|\phi^2(t)|\} < \varsigma$. If $\lim_{t\to\infty} E\{|x^2(t)|\} = 0$, the system is asymptotically mean-square stable.

2. *H_∞ Performance Requirement:*

Given $\gamma > 0$, the estimation error system must:

Be asymptotically mean-square stable and Maintain a prescribed H_∞ disturbance under all bounded disturbances

$\|e(t)\|_{E2} < \gamma\|v(t)\|_2$ (13)

for all nonzero $v(t) \in L_2[0, \infty)$ subject to the zero initial condition. 1

Remark 1. In this paper, this work employs a sector-bounded approach for characterizing neuron activation functions. As established in prior research [citation], when the bounding matrices satisfy $\Sigma_1 = -\Sigma_2 = \Sigma$, the sector condition (5) reduces to the conventional Lipschitz condition $[\sigma(x) - \sigma(y)] \leq \Sigma|x-y|$.. Notably, the sector-bounded condition adopted here represents a more generalized framework compared to the Lipschitz constraint, as it imposes fewer restrictions on the activation function's behavior. This broader formulation provides greater flexibility in modeling neural network dynamics while maintaining analytical tractability.

Remark 2. Previous work in [18-21] has investigated robust H_∞ and generalized H_2 estimator design for nonlinear systems. These studies imposed Lipschitz continuity conditions on the activation functions, which can lead to conservative results due to their restrictive nature. Our current work extends beyond these limitations by employing less constrained functional assumptions.

Notably, the neural network models examined in [18,19] were confined to deterministic frameworks, lacking consideration of stochastic effects. This paper advances the field by specifically addressing the H_∞ estimator design problem for stochastic neural networks, thereby incorporating probabilistic phenomena that were absent in prior analyses.

The following fundamental lemma is employed in our subsequent analysis:

Lemma 1[23]. Let vector function x(t), ψ(t), and g(t) satisfy the stochastic differential equation

$$dx(t) = \varphi(t)dt + g(t)\, dw(t)$$

where w(t) is a Brownian motion. For any constant matrix Z ≥ 0 and scalar h > 0, the following integration holds

$$-h\int_{t-h}^{t} \varphi^T(s)\, Z\varphi(s)\, ds = \begin{pmatrix} x(t) \\ x(t-h) \end{pmatrix}^T \begin{bmatrix} -Z & Z \\ Z & -Z \end{bmatrix} \begin{pmatrix} x(t) \\ x(t-h) \end{pmatrix}$$

$$+ 2\begin{pmatrix} x(t) \\ x(t-h) \end{pmatrix}^T \begin{pmatrix} Z \\ -Z \end{pmatrix} \int_{t-h}^{t} g(s)\, dw(s).$$

3. MAIN RESULTS

This section presents a novel estimation framework designed to address the H_∞ state estimation challenge for stochastic neural networks described by equations (1)-(3). The proposed methodology establishes comprehensive stability criteria encompassing both Delay-independent conditions (robust to arbitrary time delays) and Delay-dependent conditions (sensitive to delay magnitude) are derived.

Theorem 3.1. *For prescribed positive constants $\gamma > 0$ (disturbance attenuation), $\tau > 0$ (time de- lay), $\mu \geq 0$ (delay variation bound), and given estimator gain matrix K, the estimation error system (11)-(12) achieves, Asymptotic mean-square stability and guaranteed H_∞ performance level γ. if there exist positive definite matrices $P_i > 0$, $Q > 0$, $R > 0$, $Z > 0$ and positive scalars λ_1 and λ_2 satisfying the following linear matrix inequality:*

$$\Gamma = \begin{bmatrix} \Gamma^{11} & \Gamma^{12} & \tilde{L} & \Gamma^{14} & \Gamma^{15} \\ * & -\gamma^2 I & 0 & 0 & \Gamma^{25} \\ * & * & -I & 0 & 0 \\ * & * & * & -P_i & 0 \\ * & * & * & * & -Z \end{bmatrix} < 0 \qquad (14)$$

where

$$\Gamma^{11} = \begin{bmatrix} \Gamma_{11}^{11} & -P_iK_iD_i & Z & \Gamma_{14}^{11} & P_iW_{1i} & 0 & P_iW_{2i} \\ * & \Gamma_{22}^{11} & 0 & 0 & -F_2\lambda_2 & 0 & 0 \\ * & * & -R-Z & 0 & 0 & 0 & 0 \\ * & * & * & -I\lambda_1 & 0 & 0 & 0 \\ * & * & * & * & -I\lambda_2 & 0 & 0 \\ * & * & * & * & * & R_1 & 0 \\ * & * & * & * & * & * & -R_1(1-h_d) \end{bmatrix}$$

$$\Gamma_{11}^{11} = -P_i(A_i + K_iC_i) - (A_i + K_iC_i)^T P_i + Q + R - Z - \lambda_1 F_1,$$

$$\Gamma_{14}^{11} = P_iW_0 - \lambda_1 F_2\, ; \Gamma_{22}^{11} = -(1-\mu)Q - \lambda_2 F_1$$

$\Gamma^{12} = [\,(B_{1i} - K_iB_{2i})^T P_i \;\; 0 \;\; 0 \;\; 0 \;\; 0 \;\; 0 \;\; 0\,]$

$\Gamma^{14} = [\,P_iH_{1i} \;\; P_iH_{2i} \;\; 0 \;\; 0 \;\; 0 \;\; 0 \;\; 0\,]$

$\Gamma^{15} = [\,-\tau Z(A_i + K_iC_i) \;\; -\tau ZK_iD_i \;\; 0 \;\; \tau ZW_{0i} \;\; \tau ZW_{1i} \;\; 0 \;\; \tau ZW_{2i}\,]$

$\Gamma^{25} = \tau\,(B_{1i} - K_iB_{2i})^T Z\,;\; \widetilde{L} = [\,L\; 0\; 0\; 0\; 0\; 0\; 0\,]$

Proof. For simplicity, let

$$\tilde{\varphi}(t) = -(A_i + K_iC_i)\tilde{x}(t) - K_iD_i\tilde{x}(t-\tau(t)) + W_{0i}f(\tilde{x}(t))$$

$$+ W_{1i}f(\tilde{x}(t-\tau(t)) + (B_{1i} - K_iB_{2i})v(t) + W_{2i}\dot{\tilde{x}}(t-\tau(t)) \quad (15)$$

$$\tilde{g}(t) = H_{1i}x(t) + H_{2i}\tilde{x}(t-\tau(t)). \quad (16)$$

Then (11) can be written as

$$d\tilde{x}(t) = \tilde{\varphi}(t)dt + \tilde{g}(t)dw(t). \quad (17)$$

Choose the Lyapunov-Krasovskii functional candidate as

$$V_1(\tilde{x}(t), t) = \tilde{x}^T(t)P_ix(t) + \int_{t-\tau(t)}^{t} xt(s)Q\,x(s))\,ds + \int_{t-\tau(t)}^{t} xt(s)R\,x(s))\,ds$$

$$+ \int_{\tau}^{0}\int_{t+\theta}^{t} \varphi t(s)\,Z\varphi(s)\,ds \quad \text{——————} (18)$$

$$V_2(\tilde{x}(t), t) = \int_{t-\tau(t)}^{t} {}^{T}(t)\,R_1\,x(s))ds \quad \text{——————————} (19)$$

we first show the estimation error systems (11) − (12) with v(t) = 0 are asymptotical mean-square stable:

By Ito's differential rule, the stochastic differential $dV(\tilde{x}(t), t)$ along the trajectories of system (17) with $v(t) = 0$ is given by

$$dV(\tilde{x}(t), t) = \mathrm{L}V_1(\tilde{x}(t), t)dt + \mathrm{L}V_2(\tilde{x}(t), t)dt + 2\tilde{x}^T(t)P\tilde{g}(t)dw(t) \quad (20)$$

Where,

$$\mathrm{L}V_1(\tilde{x}(t), t) \le 2\tilde{x}^T(t)P_i\overline{\varphi_{(t)}} + \tilde{g}^T(t)P\tilde{g}(t) + \tilde{x}^T(t)Q\tilde{x}(t) - (1-\mu)\tilde{x}^T(t-\tau(t))$$

$$Q\tilde{x}(t-\tau(t)) + \tilde{x}^T(t)R\tilde{x}(t) - \tilde{x}^T(t-\tau)R\tilde{x}(t-\tau) + \tau^2\tilde{\varphi}^T(t)Z\tilde{\varphi}(t)$$

$$-\tau\int_{t-\tau}^{t} \tilde{\varphi}^T(s)\,Z\,\tilde{\varphi}(s)ds + W_{2i}\tilde{x}^T(t-\tau(t)) \quad (21)$$

$$\mathrm{L}V_2(\tilde{x}(t), t) = \dot{\tilde{x}}^T(t)R_1\dot{\tilde{x}}(t) - (1-\mu)\dot{\tilde{x}}^T(t-\tau(t))R_1\dot{\tilde{x}}(t-\tau(t)) \quad (22)$$ with

$$\tilde{\varphi}(t) = -(A_i + K_iC_i)\tilde{x}(t) - K_iD_i\tilde{x}(t-\tau(t)) + W_{0i}f(\tilde{x}(t))$$

$$+ W_{1i}f(\tilde{x}(t-\tau(t)) + W_{2i}\dot{\tilde{x}}(t-\tau(t))$$

Applying Lemma 1 and by standard manipulations, we have

$$-\tau\int_{t-h}^{t} \varphi^T(s)\,Z\varphi(s)\,ds = \begin{pmatrix}\tilde{x}(t)\\ \tilde{x}(t-h)\end{pmatrix}^T \begin{bmatrix}-Z & Z\\ Z & -Z\end{bmatrix}\begin{pmatrix}\tilde{x}(t)\\ \tilde{x}(t-h)\end{pmatrix}$$

$$+ 2\begin{pmatrix}\tilde{x}(t)\\ \tilde{x}(t-h)\end{pmatrix}^T\begin{pmatrix}Z\\ -Z\end{pmatrix}\int_{t-h}^{t}\tilde{g}(s)\,dw(s) \quad \text{---------------------} (23)$$

From (5) and (10), we have

$[f(\tilde{x}(t)) - \Sigma_1\tilde{x}(t)]^T[f(\tilde{x}(t)) - \Sigma_2\tilde{x}(t)] \le 0$ (24) $[f(\tilde{x}(t-\tau(t))) - \Sigma_1\tilde{x}(t-\tau(t))]^T[f(\tilde{x}(t-\tau(t))) - \Sigma_2\tilde{x}(t-\tau(t))] \le 0$ (25)

It is clear that for any scalars $\lambda_1 > 0$ and $\lambda_2 > 0$, we have

$$-\lambda_1 \begin{pmatrix} \tilde{x}(t) \\ f(\tilde{x}(t)) \end{pmatrix}^T \begin{bmatrix} F1 & F2 \\ * & I \end{bmatrix} \begin{pmatrix} \tilde{x}(t) \\ f(\tilde{x}(t)) \end{pmatrix} \geq 0 \qquad (26)$$

$$-\lambda_2 \begin{pmatrix} \tilde{x}(t-\tau(t)) \\ f(\tilde{x}(t-\tau(t))) \end{pmatrix}^T \begin{bmatrix} F1 & F2 \\ * & I \end{bmatrix} \begin{pmatrix} \tilde{x}(t-\tau(t)) \\ f(\tilde{x}(t-\tau(t))) \end{pmatrix} \geq 0 \qquad (27)$$

Where

$$F_1 = [\Sigma_1^T \Sigma_2 + \Sigma_2^T \Sigma_1] / 2 \text{ and } F_2 = \Sigma_1^T + \Sigma_2^T \qquad (28)$$

Then, by adding the terms on the left sides of (26) and (27) to the right side of (21) and , and considering (23), we can obtain

$\mathrm{L} V_1(\tilde{x}(t), t) \leq \xi^T(t)\Pi\xi(t) + v(t)$ (29)

Where, $\Pi = \Gamma^{11} + \Gamma^{14} P^{-1} (\Gamma^{14})^T + \Gamma^{15} Z^{-1} (\Gamma^{15})^T$

$\xi(t) = [\tilde{x}T(t)\ \tilde{x}T(t-\tau(t))\ \tilde{x}T(t-\tau)\ fT(\tilde{x}(t))\ fT(\tilde{x}(t-\tau(t)))\ \dot{\tilde{x}}T(t-\tau(t))]T$

$v(t) = 2 \begin{pmatrix} \tilde{x}(t) \\ \tilde{x}(t-\tau) \end{pmatrix}^T \begin{pmatrix} z \\ -z \end{pmatrix} \int_{t-h}^{t} \tilde{g}(s)\, dw(s)$

To establish asymptotic mean-square stability of the estimation error system (11)-(12) under zero disturbance conditions $v(t) = 0$, it suffices to verify the negative definiteness condition $\Pi < 0$. Through application of the Schur complement lemma, this fundamental stability condition can be equivalently expressed as the following linear matrix inequality:

$$\begin{bmatrix} \Gamma^{11} & \Gamma^{14} & \Gamma^{15} \\ * & -pi & 0 \\ * & * & -z \end{bmatrix} < 0 \qquad (30)$$

And it can be shown that LMI(14) implies (30) holds, therefore, $\Pi < 0$, is satisfied. From (30) and by some algebraic manipulations, we can prove that there exists a scalar $\alpha > 0$ such that

$\Pi < diag\{-\alpha I, 0, 0, 0, 0, 0, 0\}$ (31)

Taking expectations for both sides of (31), we obtain

$E\{\mathrm{L}V(\tilde{x}(t), t)\} \leq -\alpha E\{\tilde{x}^T(t)\tilde{x}(t)\}$ (32)

Thus, it follows from (31) and (32)

$$E\{\mathrm{L}V(\tilde{x}(t), t)\} - \mathrm{V}(\varphi(0), 0) \leq -\alpha E\int_0^t \{\tilde{x}^T(s)\tilde{x}(s)ds\} \qquad (33)$$

On the other hand, from (18), (19) we have

$$E\{V(\tilde{x}(t), t)\} > \beta E\{\tilde{x}^T(t)\tilde{x}(t)\} \qquad (34)$$

Where $\beta = \lambda_{min}(P_i) > 0$. From (33) and (34), we have

$$E\{\tilde{x}^T(t)\tilde{x}(t)\} \leq \frac{1}{\beta}\mathrm{V}(\varphi(0), 0) - \frac{\alpha}{\beta} E\int_0^t \{\tilde{x}^T(s)\tilde{x}(s)ds\} \qquad (35)$$

Which yields

$$\lim_{t \to \infty} E\int_0^t \{\tilde{x}^T(s)\tilde{x}(s)ds\} \leq \frac{1}{\alpha}\mathrm{V}(\varphi(0), 0)$$

which guarantees $\lim_{t\to\infty} E\{|\tilde{x}(s)|^2 ds\} = 0$. Then the estimation error systems (11)-(12) are asymp- totically mean square stable.

Furthermore, the stochastic differential $dV(\tilde{x}(t), t)\}$ along the trajectories of system (21) is

$$dV(\tilde{x}(t), t) = \mathrm{L}V_1(\tilde{x}(t), t)dt + \mathrm{L}V_2(\tilde{x}(t), t)dt + 2\tilde{x}^T(t)P_i g^\sim(t)dw(t) \qquad (36)$$

By following the same line as the proof above, we have

$$\eta(t) = [\xi^T(t) \quad v^T(t)]^T \qquad (37)$$

Next, we shall establish the H_∞ performance for the estimation error systems (11)-(12) under zero- initial condition, we introduce

$$\begin{aligned} J &= E\{[e^T(s)\, e(s) - \gamma^2 v^T(s)\, v(s)]\, ds\} \\ &\leq E\{\textstyle\int_0^\infty \{[e^T(s)\, e(s) - \gamma^2 v^T(s)\, v(s)] + LV_1(\tilde{x}(t), t) + LV_2(\tilde{x}(t), t)]ds \\ &= E\{\textstyle\int_0^\infty \{[\eta^T(s)\, \tilde{\Pi}\, \eta(s)\, ds\}\} \end{aligned} \qquad (38)$$

Where

$$\tilde{\Pi} = \begin{bmatrix} \Gamma^{11}+\tilde{L}\tilde{L}^T & \Gamma^{12} \\ * & -I\gamma^2 \end{bmatrix} + \tilde{\Gamma}^{14} P_i^1 (\tilde{\Gamma}^{14})^T + \tilde{\Gamma}^{15} P_i^1 (\tilde{\Gamma}^{15})^T$$

$$\tilde{\Gamma}^{14} = [\,(\Gamma^{14})^T \;\; 0]^T$$

$$\tilde{\Gamma}^{15} = [(\Gamma^{15})^T \tau Z\,(B_{1i} - B_{2i})]^T$$

Applying the Schur complement lemma reveals that the condition $\Gamma < 0$ necessarily implies

$\tilde{\Pi} < 0$. For the non-zero disturbance case $v(t) \neq 0$, this leads to the inequality $J < 0$, which directly yields the critical H_∞ performance relation $\|e(t)\|_2 \leq \gamma \|v(t)\|_2$. Consequently, the estimation error system (11)-(12) is guaranteed to be Asymptotically mean-square stable and characterized by the prescribed H_∞ disturbance attenuation level γ. This concludes the mathematical proof.

The following result establishes delay-dependent sufficient conditions for the existence of an H_∞ state estimator for the stochastic neural network system described by equations (1)-(3). These conditions guarantee both asymptotic stability and prescribed disturbance attenuation performance.

Theorem 3.2. For the stochastic neural network system (1)–(3), given performance parameters Dis- turbance attenuation level $\gamma > 0$, Time delay $\tau > 0$ and Delay variation bound $\mu \geq 0$ the estimation error system (11)–(12) achieves asymptotic mean-square stability and Prescribed H_∞ performance disturbance attenuation level γ, if there exist matrices $P_i > 0$, $Q > 0$, $R > 0$, $Z > 0$, T, scalars λ_1 and λ_2 such that the following Linear Matrix Inequality (LMI) holds:

$$\begin{bmatrix} \varphi^{11} & \varphi^{12} & \tilde{L}^T & \varphi^{14} & \varphi^{15} \\ * & -\gamma^2 I & 0 & 0 & \varphi^{25} \\ * & * & -I & 0 & 0 \\ * & * & * & -P_i & 0 \\ * & * & * & * & -2P_i+Z \end{bmatrix} < 0 \qquad (39)$$

Where

$$\begin{bmatrix} \Omega_{11} & -T_iD_i & Z & \Omega_{14} & P_iW_{1i} & 0 & P_iW_{2i} \\ * & \Omega_{22} & 0 & 0 & -F_2\lambda_2 & 0 & 0 \\ * & * & -R-Z & 0 & 0 & 0 & 0 \\ * & * & * & -I\lambda_1 & 0 & 0 & 0 \\ * & * & * & * & -I\lambda_2 & 0 & 0 \\ * & * & * & * & * & R_1 & 0 \\ * & * & * & * & * & * & -R_1(1-h_d) \end{bmatrix}$$

$\Omega_{11} = -P_iA_i - A_i^TP_i - T_iC_i - C_iT_i^T + Q + R - Z - \lambda_1F_1, \Omega_{14} = P_iW_{0i} - \lambda_1F_2,$

$\Omega_{22} = -(1-\mu)Q - \lambda_2F_1$

$\Phi^{12} = [P_iA_i^T - B_{2i}^T \ \ 0\ 0\ 0\ 0\ 0\ 0]^T$

$\Phi^{14} = [P_iH_{1i} - P_iH_{2i} \ \ 0\ 0\ 0\ 0\ 0\ 0]^T$

$\Phi^{15} = [-\tau(P_iAi + T_iC_i) \ \ -\tau T_iD_i \ \ 0 \ \ \tau P_iW_{0i} \ \tau P_iW_{1i} \ \tau P_iW_{2i}\ ]^T$

$\Phi^{25} = \tau \ [B_{1i}^TP_i - B_{2i}^TT_i^T]$

Moreover, the gain matrix K_i of the state estimator can be designed as

$$K_i = P_i^{-1}T_i \qquad (40)$$

Proof: Noting the fact that $P_i > 0$, $R > 0$, and $P_i^T Z^{-1}P_i - 2P_i + Z = (P_i - Z)^T Z^{-1}(P_i - Z) \geq 0$

Then we get

$$P_i^T Z^{-1}P_i \leq -2P_i + Z \qquad (41)$$

It implies that the LMI (39) guarantees

$$\begin{bmatrix} \varphi^{11} & \varphi^{12} & \tilde{L} & \varphi^{14} & \varphi^{15} \\ * & -\gamma^2 I & 0 & 0 & \varphi^{25} \\ * & * & -I & 0 & 0 \\ * & * & * & -P_i & 0 \\ * & * & * & * & P_i^T \end{bmatrix} < 0 \qquad (42)$$

To establish the equivalence between the matrix inequalities, we perform a congruence transformation on (42) using the block-diagonal matrices:

Pre-multiplication: diag{I, I, I, I, I, I, I, I, I, I,ZP_i^{-1}}

Post-multiplication: diag{I, I, I, I, I, I, I, I, I, I, $P_i^{-1}Z$}

Through this operation and by virtue of relation (41), we algebraically demonstrate that the transformed inequality becomes equivalent to the target LMI (14). Consequently, Theorem 1 guarantees that the estimation error dynamics (11)-(12) possess, Asymptotic mean-square stability and Prescribed H∞ performance level γ. This concludes the mathematical proof.

4. CONCLUSIONS

This work addresses the passivity-based H∞ state estimation problem for stochastic neutral-type

neural networks with Time-varying delays and Markovian jumping parameters.

Future Research Directions:

(1). Relaxation of delay constraints

(2). Removal of the conservative bound on delay derivatives $\mu < 1$

(3). Extended system classes

H∞ estimation for:

(1). Markovian jump systems with mixed time-varying delays

(2). Discrete-time stochastic neural networks

(3). Stochastic genetic regulatory networks

(4). Neutral-type stochastic neural networks

Generalized H∞ estimation

1. Development of robust estimators for stochastic neural networks under H2 performance metrics.

5. Numerical example

In this section, an example is given to demonstrate the effectiveness of the proposed method.

Consider a three- neuron stochastic neural network (1)-(3) with parameters:

$$A_1 = \begin{bmatrix} 2 & 0 \\ 0 & 3 \end{bmatrix},\ W_{01} = \begin{bmatrix} -0.4 & -0.2 \\ 0.3 & -0.2 \end{bmatrix},\ W_{11} = \begin{bmatrix} -0.2 & -0.1 \\ 0.1 & 0.2 \end{bmatrix},\ W_{21} = \begin{bmatrix} -0.2 & -0.9 \\ -0.9 & 0.25 \end{bmatrix}$$

$$B_{11} = \begin{bmatrix} 0.3 & -0.2 \\ -0.2 & 0.5 \end{bmatrix},\ B_{21} = \begin{bmatrix} -0.4 & 0.3 \\ 0.2 & 0.4 \end{bmatrix},\ H_{11} = \begin{bmatrix} 0.2 & 0.2 \\ 0.2 & 0.8 \end{bmatrix},\ C_1 = \begin{bmatrix} -0.2 & 0.1 \\ 0.8 & 0.7 \end{bmatrix}$$

$$H_{21} = \begin{bmatrix} 0.2 & -0.6 \\ -0.6 & 0.6 \end{bmatrix},\ D_1 = \begin{bmatrix} -0.2 & 0.3 \\ 0.4 & 0.1 \end{bmatrix},\ L = \begin{bmatrix} 0.3 & 0.4 \\ 0.5 & 0.8 \end{bmatrix},\ \Sigma_1 = 0,\ \Sigma_2 = \begin{bmatrix} 1 & 0 \\ 0 & 1 \end{bmatrix}$$

$$F_1 - 0, F_2 = \begin{bmatrix} -0.5 & 0 \\ 0 & -0.5 \end{bmatrix},\ I = \begin{bmatrix} 1 & 0 \\ 0 & 1 \end{bmatrix},\ \mu = 0.8,\ \tau = 0.925,\ \gamma = 1.14570,\ h_d = 1.2$$

by using MATLAB we obtain

$$P_1 = \begin{bmatrix} 10.3290 & 4.0426 \\ 4.0426 & 6.8714 \end{bmatrix},\ \mathrm{Q} = \begin{bmatrix} 20.5611 & -10.3356 \\ -10.3356 & 23.7388 \end{bmatrix}$$

$$R = \begin{bmatrix} 1.2818 & -0.9938 \\ -0.9938 & 1.9531 \end{bmatrix},\ \mathrm{R}_1 = \begin{bmatrix} -48.1404 & -2.6457 \\ -2.6457 & -65.3188 \end{bmatrix}$$

$$\mathrm{Z} = \begin{bmatrix} 0.3141 & 0.1232 \\ 0.1232 & -0.3532 \end{bmatrix},\ \mathrm{T}_1 = \begin{bmatrix} -0.2007 & -0.0014 \\ -0.0014 & -0.9169 \end{bmatrix},$$

$S_1 = 9.9154,\ S_2 = 2.5161$

By Theorem 2, when $\mu = 0.8$, $\tau = 0.9$, gain the matrix of (44) can be designed as:

$$K_1 - \begin{bmatrix} -0.0251 & 0.0677 \\ 0.0146 & -0.1732 \end{bmatrix}$$

References

[1] S. Haykin, A Comprehensive Foundation. Neural Networks. (1998).

[2] A. Cichocki, R. Unbehauen, Neural Networks for Optimization and Signal Processing. Chichser: Wiley. (1993) ,

[3] S. Arik, An analysis of exponential stability of delayed neural networks with time-varying delays, Neural Networks. 17 (Sep, 2004) 1027 – 1031.

[4] M. Belli, M. Conti, P. Crippa, and C. Turchctti, Artificial neural networks as approximators of stochastic process, Neural Networks. 12 (June, 1999) 647 – 658.

[5] Y. He, Q. Wang, M. Wu, C. Lin, Delay-dependent state estimation for delayed neural networks, IEEE Trans. Neural Netw. 17(4) (2006) 1077 – 1081.

[6] N. Li, J. Hu, L. Li, Exponential state estimation for delayed recurrent neural networks with ssampled-data, Nonlinear Dyn. 69(1-2) (2012) 555 – 564.

[7] P.Shi, E. K. Boukas, H∞-control for Markovian jumping linear system with parametric uncertainty. J. Optim, Theory Appl. 95(1) (1997) 75 – 99.

[8] P. Tino, M. Cernansky, I. Benuskova, Markovian architectural bias of recurrent neural network, IEEE Trans. Neural Netw. 15(1) (2004) 6 – 15.

[9] H. Gao, W. Sun, P. Shi, Robust sampled-data H∞ control for vehicle active suspension systems, IEEE Trans. Control Syst. Technol. 10(1) (2010) 238–245.

[10] S. Lakshmanan, J. Park, R. Rakkiyappan, H. Jung, State estimator for neural networks with sampled data using discontinuous Lyapunove functional approach, Nonlinear Dyn. 73 (2013) 509 – 520.

[11] Y. He, Q. Wang, M. Wu, and C. Lin, Delay-dependent state estimation for delayed neural networks, IEEE Trans.Neural Networks. 17 (July, 2006) 1077 – 1081.

[12] H. Huang, G. Reng, and J. Cao, Robust state estimation for uncertain neural networks with time-varying delay,IEEE Trans. Neural Networks. 19 (Aug, 2008) 1329 – 1339.

[13] C. Lu, A delay-range-dependent approach to design state estimation for discrete-time recurrent neural networks with interval time-varying delay, IEEE Trans. Circuits SystII. 55 (Nov, 2008) 1163 – 1167.

[14] S. Mou, H. Gao, W. Qiang, and Z. Fei, State estimation for discrete-time neural networks with time-varying delays, Neurocomputing. 72 (Des, 2008) 643 – 647.

[15] Z. Wang, Y. Liu, and X. Liu, State estimation for jumping recurrent neural networks with discrete and distributed delays, Neural Networks. 22 (Oct, 2009) 41 – 48.

9. A Structural Equation Modeling Approach to Consumer Avoidance Behaviour: A Case Study of Inorganic Shampoos

Greeta T[1,*], Jayalalitha G[2] , Vasanthi J[3] and Marimuthu S[4]

[1] *Department of Mathematics, Saveetha School of Engineering,*

Saveetha Institute of Medical and Technical Sciences(SIMATS), Thandalam, Chennai, Tamilnadu, India..

[2]*Professor,Department of Mathematics, Vels Institute of Science, Technology and Advanced Studies, Pallavaram, Chennai, Tamilnadu, India.*

[3]*Assistant Professor,Department of Mathematics, Prince Dr K Vasudevan College of Engineering and Technology, Ponmar, Chennai, Tamilnadu, India.*

[4] *Department of Nautical Science, AMET Deemed to be University, Chennai.*

ABSTRACT

This chapter presents a mathematical modeling approach to identify the key factors influencing customers' avoidance of inorganic (chemical-based) shampoos using Structural Equation Modeling (SEM). Consumer avoidance behaviour is modeled through four latent dimensions: Health-Related Concerns, Aesthetic and Hair Health, Cultural and Personal Values, and Environmental and Ethical Concerns. A descriptive research design with convenience sampling is adopted, and primary data collected from 422 respondents are used for model estimation. The latent constructs are measured through observable indicators and validated using Confirmatory Factor Analysis, while model adequacy is assessed through standard goodness-of-fit measures along with convergent and discriminant validity tests. The structural analysis reveals that Cultural and Personal Values and Environmental and Ethical Concerns exert the strongest influence on avoidance behaviour, whereas health-related and aesthetic factors show moderate but statistically significant effects. The results highlight the usefulness of SEM as a mathematical framework for representing and analyzing complex behavioural systems involving unobservable variables, demonstrating its applicability in real-world decision-making and applied mathematical modeling contexts.

Keywords: Structural Equation Modeling, Latent Variable Analysis, Consumer Avoidance Behaviour.

1. INTRODUCTION

In the ever-changing world of personal care products, including the daily grooming industry like shampoo, consumer understanding and behaviour are changing so drastically. Shampoo products have been promoted and marketed in today's market for a variety of grades and uses, including medicated, professional, baby, and everyday shampoo. Shampoos found on the market are usually made from synthetic surfactants and chemical ingredients with the aim of cleaning, foaming, and sensoriality. Surfactants, foaming agents, conditioners, pearlescent agents, sequestrates, pH adjusters, antidandruff agents, colorants, fragrances, and preservatives are some of the main chemicals that these shampoos usually contain. The majority of these chemicals included in shampoos are manufactured artificially [4]. For instance, cocamide diethanolamine, diethyl amine, triethylamine, and a few additional by products, including dioxane. Even while regulatory bodies have limited the use of these artificial substances in cosmetics, they can still be absorbed through the skin and, at lower quantities, cause contact dermatitis, allergic responses, and skin irritation. Long-term exposure to these artificial compounds is also linked to mutagenicity and carcinogenicity. The primary goal of this study is to clarify why consumers steer clear of inorganic (chemical-based) shampoos [9].

Hair care products play an important role in maintaining scalp health and enhancing the physical appearance of hair; however, several studies have reported concerns related to the long-term use of chemical-based formulations. Miranda Wood et al. [6] emphasized that moisturizing agents are essential in hair care products as they help retain hair flexibility, shine, and resistance to dryness and breakage. Common conditioning ingredients such as dimethicone, glyceryl stearate, and cationic conditioning agents are widely used to smooth hair and control frizz. Dimethicone, a water-insoluble silicone, forms a coating over the hair cuticle that improves gloss and smoothness. Nevertheless, prolonged usage may result in polymer build up on the hair and scalp, leading to a heavy appearance and reduced hair volume, indicating the need for cautious and limited use.

Rummi Devi Saini [8] noted that shampoos are no longer expected to serve only a cleansing function but must also provide conditioning, smoothness, dandruff control, and overall safety. The study highlighted increasing consumer demand for herbal shampoos due to growing awareness of chemical exposure and environmental concerns. However, formulating herbal shampoos that match the performance of chemical-based products remains challenging, as ingredient selection must balance natural authenticity, effectiveness, and safety. The rising number of synthetic chemicals introduced into personal care products has intensified concerns regarding human health and environmental sustainability, emphasizing the need for careful monitoring and reliable toxicity assessment methods.

Chin-Hsien T. Chiu et al.[2] (2015) discussed the biological and aesthetic importance of hair, noting that hair condition significantly influences self-image and psychological well-being. Hair-related problems such as hair loss, dandruff, and premature graying can cause emotional distress. The authors reported that chemical exposure from shampoos and hair treatments, nutritional deficiencies, and environmental factors such as smoking and sun exposure can negatively affect hair growth and scalp health. Ingredients commonly used in shampoos, including surfactants, preservatives, and antibacterial agents, were identified as potential contributors to hair and scalp damage.

Paul Sterchele[7] reported that certain shampoo ingredients, including selenium compounds, zinc pyrithione, and surfactants, possess inherent irritant properties. Accidental ingestion may lead to gastrointestinal disturbances such as nausea, vomiting, and fluid imbalance.

SEM, AMOS and CFA

SEM stands for Structural Equation Modeling. It is a statistical technique used to analyze complex relationships between observed and latent (unobserved) variables. SEM is widely used in social sciences, psychology, education, and business research.

Structural Equation Modeling (SEM) is a way to understand how different things are related to each other. Some of these things can be measured directly, like a person's height or test score. Others are ideas we can't see directly, like happiness or confidence. SEM helps researchers study both types at the same time. It allows them to build a full model that shows how all the parts are linked. This is helpful when the relationships are complex or when there are many variables involved. SEM is often used in research fields that study people, such as psychology, education, and social science.

AMOS stands for Analysis of Moment Structures. It is a software tool developed by IBM that is used specifically for performing SEM. AMOS helps users build and test SEM models easily by using diagrams instead of writing code.

CFA stands for Confirmatory Factor Analysis. It is based on a predefined theory about how the variables are grouped. CFA is a part of Structural Equation Modeling (SEM) and checks if the data supports the expected pattern of relationships.

RESEARCH DESIGN AND SAMPLE

In this chapter, descriptive research designs are adopted. Descriptive research studies are those studies that are concerned with describing the characteristics and attitude of a particular individual or a group. Here is the study describing the reasons for customers avoiding inorganic shampoos. Descriptive research is a widely accepted method in fact-finding, and the study includes adequate and accurate interpretation of results. The convenience sampling technique is applied to this study; 422 sample data were collected from potential customers to understand specific issues or opinions about avoiding inorganic (chemical-based) shampoos.

Given the size of the overall sample of 422 individuals, the dataset for structural equation modeling is demographically as well as statistically relevant. Although nonprobabilistic, convenience sampling is adequate for the study's descriptive goal of perception, not generalization.

2. ANALYSIS OF THE STUDY

The Structural Equation Modeling (SEM) is applied through Analysis of Movement of Structure (AMOS) software; the aim of this analysis is to find out the reasons for customers avoiding Inorganic (Chemical-Based) Shampoos. Here the following dimensions, like Health-Related Concerns (HRC), Aesthetic and Hair Health (AHH), Cultural and

Personal Values (CPV), and Environmental and Ethical Concerns (EEC) belong to reasons for Customers Avoiding Inorganic (Chemical-Based) Shampoos. In the study to find out through the SEM Analysis [1], which reasons are most influenced to Customers Avoiding Inorganic (Chemical-Based) Shampoos?

The Structural Equation Modeling (SEM) analysis [5] graph is designed, as the endogenous dimensions are Health-Related Concerns (HRC), Aesthetic and Hair Health (AHH), Cultural and Personal Values (CPV), and Environmental and Ethical Concerns (EEC) influences on the exogenous dimension in Customers Avoiding Inorganic (Chemical-Based) Shampoos.

VARIABLES OF THE DIMENSIONS

The research deals with the principles of an organizational Structural Equation Model, based on four primary latent constructs representing the essential dimensions of consumer aversion to inorganic shampoos, namely Health-Related Concerns (HRC), Aesthetic and Hair Health (AHH), Cultural and Personal Values (CPV), and Environmental and Ethical Concerns (EEC). All of these constructs have been created from a collection of measurable variables extracted from survey responses and verified with confirmatory factor analysis (CFA).

Table 1 shows the four Endogenous dimensions and variable.

- **HRC (Health Related Concerns):** Focuses on physiological reactions like skin irritation, dryness, hormone imbalance, and allergies, showing increasing consumer sensitivity to chemical ingredients such as sulfates and parabens.
- **AHH (Aesthetic and Hair Health):** Represents the visible effects of chemicals on hair, including weakened follicles, split ends, dullness, and silicone buildup, which cause physical discomfort and dissatisfaction leading to product rejection.
- **CPV (Cultural and Personal Values):** Reflects deeper psychological motives tied to lifestyle, care preferences, and holistic health beliefs, showing consumers' alignment with cultural values and natural living philosophies like Ayurvedic traditions.
- **EEC (Environmental and Ethical Concerns):** Covers awareness of environmental impacts such as aquatic toxicity, non-recyclable packaging, and use of non-renewable resources, emphasizing ethical and ecological responsibility in product choices.

Table1. Variables of the Prospects Dimensions

Endogenous Dimensions	Variables Abbreviation	Variables (Items)
Health-Related Concerns (HRC)	HRC -1	Inorganic shampoos often contain sulfates its creates Skin and Scalp Irritation
	HRC -2	An inorganic shampoo has causing in dryness, itchiness, or rashes.
	HRC -3	Inorganic shampoos ingredients are creates hormonal disruption
	HRC -4	Inorganic shampoos to be trigger allergies, especially redness, swelling, and discomfort.
Aesthetic and Hair Health (AHH)	AHH -1	Silicones and other synthetic ingredients can leads to dullness and lifeless appearance over time
	AHH -2	Overuse of chemical-laden shampoos can weaken hair follicles, leading to brittle, dandruff and prone to split ends
	AHH -3	Over-cleansing strips away protective oils, leaving hair dull and unprotected
	AHH -4	Many inorganic shampoos offer short-term benefits (e.g., shine from silicones) but can cause long-term build-up and damage.
Cultural and Personal Values	CPV-1	I want to align personal care with holistic and natural lifestyles

(CPV)	CPV-2	Traditional hair care often relies on natural remedies, which can conflict with mineral ingredients
	CPV-3	As hair health deteriorates, natural hair care is needed to combat damage.
Environmental and Ethical Concerns (EEC)	EEC-1	Non-biodegradable chemicals affect aquatic ecosystems and water pollution, so I don't like them
	EEC-2	Mineral shampoos come in non-recyclable packaging, which contributes to environmental pollution, so I don't like them
	EEC-3	The production of synthetic chemicals often relies on non-renewable resources, which is anti-social, so I don't like them

Regression weights which consists of Standard Estimate, Standard Error (S.E), Critical ratio (C.R) and P-value are shown in Table 2.

Table 2. Regression Weights for reasons for the variables

Regression Weights	**Estimate**	**S.E.**	**C.R.**	**P**
HRC-3← Health-Related Concerns	1.000	-	-	-
HRC-2← Health-Related Concerns	1.111	0.076	14.683	0.000
HRC-1← Health-Related Concerns	0.735	0.071	10.305	0.000
HRC- 4← Health-Related Concerns	0.762	0.067	11.401	0.000
AHH -3←Aesthetic and Hair Health	1.000	-	-	-
AHH-1 ←Aesthetic and Hair Health	0.670	0.068	9.816	0.000
AHH -2←Aesthetic and Hair Health	0.454	0.175	2.602	0.009
AHH- 4←Aesthetic and Hair Health	0.983	0.062	15.821	0.000
CPV -3←Cultural and Personal Values	1.000	-	-	-
CPV -2←Cultural and Personal Values	1.980	0.446	4.441	0.000
CPV-1 ←Cultural and Personal Values	2.368	0.526	4.500	0.000
EEC-1←Environmental and Ethical Concerns	1.000	-	-	-
EEC-2←Environmental and Ethical Concerns	1.200	0.122	9.806	0.000
EEC-3←Environmental and Ethical Concerns	1.185	0.102	11.634	0.000
Customers Avoiding Inorganic Shampoos ← Health-Related Concerns	0.148	0.034	4.285	0.000
Customers Avoiding Inorganic Shampoos ← Aesthetic and Hair Health	0.197	0.031	6.283	0.000
Customers Avoiding Inorganic Shampoos ← Cultural and Personal Values	0.684	0.155	4.426	0.000
Customers Avoiding Inorganic Shampoos ← Environmental and Ethical Concerns	0.365	0.047	7.831	0.000

Note: 0.000 is 1% α -significant level

The regression analysis shows that all four factors—Health-Related Concerns (HRC), Aesthetic and Hair Health (AHH), Cultural and Personal Values (CPV), and Environmental and Ethical Concerns (EEC) are significantly influence consumer's avoidance of inorganic shampoos. Among these, Cultural and Personal Values have the strongest impact (estimate = 0.684), highlighting that consumers' lifestyle beliefs and natural care preferences are the main drivers. Environmental and Ethical Concerns also play a substantial role (estimate = 0.365), reflecting growing awareness about sustainability issues. Health-Related Concerns (estimate = 0.148) and Aesthetic and Hair Health (estimate = 0.197) contribute meaningfully as well, indicating that physical reactions and hair damage are important but less influential factors. All regression weights are statistically significant ($p < 0.001$), confirming the robustness of the model in explaining why consumers avoid inorganic shampoos.

3. HYPOTHESIS TESTING

Hypothesis testing is done with a level of significance of 99% or Alpha = 0.01. The hypothesis is accepted if the CR value has a p value < 0.05.

NULL HYPOTHESIS

H_0-1: There is no significant relationship between the Health-Related Concerns and Customers Avoiding Inorganic Shampoos.

H_0-2: There is no significant relationship between the Aesthetic and Hair Health and Customers Avoiding Inorganic Shampoos.

H_0-3: There is no significant relationship between the Cultural and Personal Values and Customers Avoiding Inorganic Shampoos.

H_0-4: There is no significant relationship between the Environmental and Ethical Concerns and Customers Avoiding Inorganic Shampoos.

ALTERNATIVE HYPOTHESIS

H_1-1: There is significant relationship between the Health-Related Concerns and Customers Avoiding Inorganic Shampoos.

H_1-2: There is significant relationship between the Aesthetic and Hair Health and Customers Avoiding Inorganic Shampoos.

H_1-3: There is significant relationship between the Cultural and Personal Values and Customers Avoiding Inorganic Shampoos.

H_1-4: There is significant relationship between the Environmental and Ethical Concerns and Customers Avoiding Inorganic Shampoos.

4. MODEL SUITABILITY /GOODNESS OF FIT TEST

The results of the Goodness of fit for confirmatory Analysis is shown in Table 3.

Table 3. Results of Goodness of Fit Test for Confirmatory Factor Analysis

Model	Chi-Square (χ^2/df)	P-Value	RMR	GFI	AGFI	CFI	NFI	RMSEA
Study model	4.604	0.000	0.056	0.811	0.821	0.824	0.836	0.072
Recommended value	< 5	Sig.	< 0.8	0.8-0.9	0.8-0.9	0.8-0.9	0.8-0.9	< 0.080

INTERPRETAION OF ANALYSIS

The results of the covariance structural analysis that is performed based on the CFA model is as follows:

- Sample size: 422
- Chi-Square (χ^2) / degrees of freedom (df): 4.604 (recommended < 5)
- P-Value: 0.000 (significant at $p < 0.05$)
- Root Mean Square Error of Approximation (RMSEA): 0.072 (recommended < 0.08 for good fit)
- Root Mean Residual (RMR): 0.056 (recommended < 0.8) [8]
- Goodness of Fit Index (GFI): 0.811 (recommended between 0.8 and 0.9)
- Adjusted Goodness of Fit Index (AGFI): 0.821 (recommended between 0.8 and 0.9)
- Comparative Fit Index (CFI): 0.824 (recommended between 0.8 and 0.9)
- Normed Fit Index (NFI): 0.836 (recommended between 0.8 and 0.9)

All fit indices meet or exceed the recommended thresholds, confirming that the measurement model fits the data well, the constructs are reliable, and no modifications to the model are necessary.

5. CONVERGENT VALIDITY TEST

Table 4 presents the convergent validity test for the factors influencing why customers avoid inorganic shampoos.

Table 4. Test of Convergent Validity for Reasons for Customers Avoiding Inorganic Shampoos

Indicator Variables ← Latent Variables	Sum of the Squared Standardized Loadings	No. of Indicators	AVE	Square root of AVE=DV
HRC-3←Health-Related Concerns	2.180	4	0.545	**0.738**
HRC-2←Health-Related Concerns				
HRC-1←Health-Related Concerns				
HRC-4←Health-Related Concerns				
AHH-3←Aesthetic and Hair Health	2.030	4	0.508	**0.712**
AHH-1←Aesthetic and Hair Health				
AHH-2←Aesthetic and Hair Health				
AHH-4←Aesthetic and Hair Health				
CPV-3←Cultural and Personal Values	1.515	3	0.505	**0.711**
CPV-2←Cultural and Personal Values				
CPV-1←Cultural and Personal Values				
EEC-1←Environmental and Ethical Concerns	1.754	3	0.585	**0.765**
EEC-2←Environmental and Ethical Concerns				
EEC-3←Environmental and Ethical Concerns				

RESULTS OF CONVERGENT VALIDITY TEST

Convergent validity assesses whether the indicators of each latent variable consistently measure the same concept. This is shown by the Average Variance Extracted (AVE) scores, where values above 0.5 indicate good validity. In this study, all four latent variables are as follows: Health Related Concerns with an AVE score of 0.545, Aesthetic and Hair Health with an AVE score of 0.508, Cultural and Personal Values with an AVE score of 0.505, and Environmental and Ethical Concerns with an AVE score of 0.585. These AVE scores are all greater than 0.5, confirming that each construct's indicators are reliable and strongly related to their underlying factors, thereby supporting the accuracy and trustworthiness of the measurement model.

6. DISCRIMINANT VALIDITY TEST

Discriminant validity measures that a construct is different from other constructs. The way to test it is by comparing the AVE root value with the correlation square between constructs. Table 5 and Table 6 presents the Discriminant validity test for the factors influencing why customers avoid inorganic shampoos.

Table 5. Test of Discriminant Validity for reasons for Customers Avoiding Inorganic Shampoos Dimension

Latent Variables	HRC	AHH	CPV	EEC
HRC	**(0.738)**			
AHH	0.542	**(0.712)**		
CPV	0.099	0.148	**(0.711)**	
EEC	0.174	0.127	0.201	**(0.765)**

Note: The values in brackets show the square roots of AVE scores

Table 6. Correlation for reasons for Customers Avoiding Inorganic Shampoos Dimension

Correlation	Estimate
Health-Related Concerns (HRC) ↔ Environmental and Ethical Concerns (EEC)	0.174
Aesthetic and Hair Health (AHH) ↔ Environmental and Ethical Concerns (EEC)	0.127
Cultural and Personal Values (CPV) ↔ Environmental and Ethical Concerns(EEC)	0.201
Health-Related Concerns (HRC) ↔ Aesthetic and Hair Health (AHH)	0.542
Cultural and Personal Values (CPV) ↔ Health-Related Concerns (HRC)	0.099
Cultural and Personal Values (CPV) ↔Aesthetic and Hair Health (AHH)	0.148

RESULT OF DISCRIMINANT VALIDITY TEST

Table 5 presents the test results of Discriminant Validity (DV) for the dimensions of **Reasons for Customers Avoiding Inorganic (Chemical Based) Shampoos**. The Discriminant Validity scores, represented by the square root of the Average Variance Extracted (AVE), are as follows: **Health Related Concerns DV is** 0.738, **Aesthetic and Hair Health** DV is 0.712, **Cultural and Personal Values** DV is0.711, and **Environmental and Ethical Concerns** DV is 0.765.The four Dimensions Discriminant Validity score are more than the Latent Variables' Correlation Values, so, Reasons for Customers Avoiding Inorganic (Chemical-Based) Shampoos Dimensions are Discriminant Valid, as suggested by Fornell and Larcker[3].

7. RESULT OF STRUCTURAL EQUATION MODELING (SEM)-FINDINGS

Figure 1 shows the Structural Equation Modeling for customers avoiding inorganic shampoos. The observations are:

The dimension of avoiding reasons in Health-Related Concerns has four variables; all are significant in Health-Related Concerns. The significant variables are compared with estimated values; the first leading variable is 'An inorganic shampoo is causing dryness, itchiness, or rashes' (HRC-2), the second leading variable is 'Inorganic shampoos ingredients are creating hormonal disruption' (HRC-3) and the third leading variable is 'Inorganic shampoos trigger allergies, especially redness, swelling, and discomfort' (HRC-4) and the estimate values are1.111, 1.000 and 0.762 respectively.

The dimension of avoiding reasons in Aesthetic and Hair Health has four variables; all are significant in Aesthetic and Hair Health. The significant variables are compared with estimated values; the first leading variable is 'Over-cleansing strips away protective oils, leaving hair dull and unprotected' (AHH -3), the second leading variable is 'Many inorganic shampoos offer short-term benefits (e.g., shine from silicones) but can cause long-term build-up and damage' (AHH- 4), and the third leading variable is 'Silicones and other synthetic ingredients can lead to dullness and a lifeless appearance over time' (AHH-1) and the estimated values are1.000, 0.983 and 0.670 respectively.

The dimension of avoiding reasons in Cultural and Personal Values has three variables; all are significant in Cultural and Personal Values. The significant variables are compared with estimated values; the first leading variable is 'I want to align personal care with holistic and natural lifestyles' (CPV-1), the second leading variable is 'Traditional hair care often relies on natural remedies, which can conflict with mineral ingredients' (CPV-2) and the third leading variable is 'As hair health deteriorates, natural hair care is needed to combat damage' (CPV-3), and the estimated values are 2.368, 1.980 and 1.000 respectively.

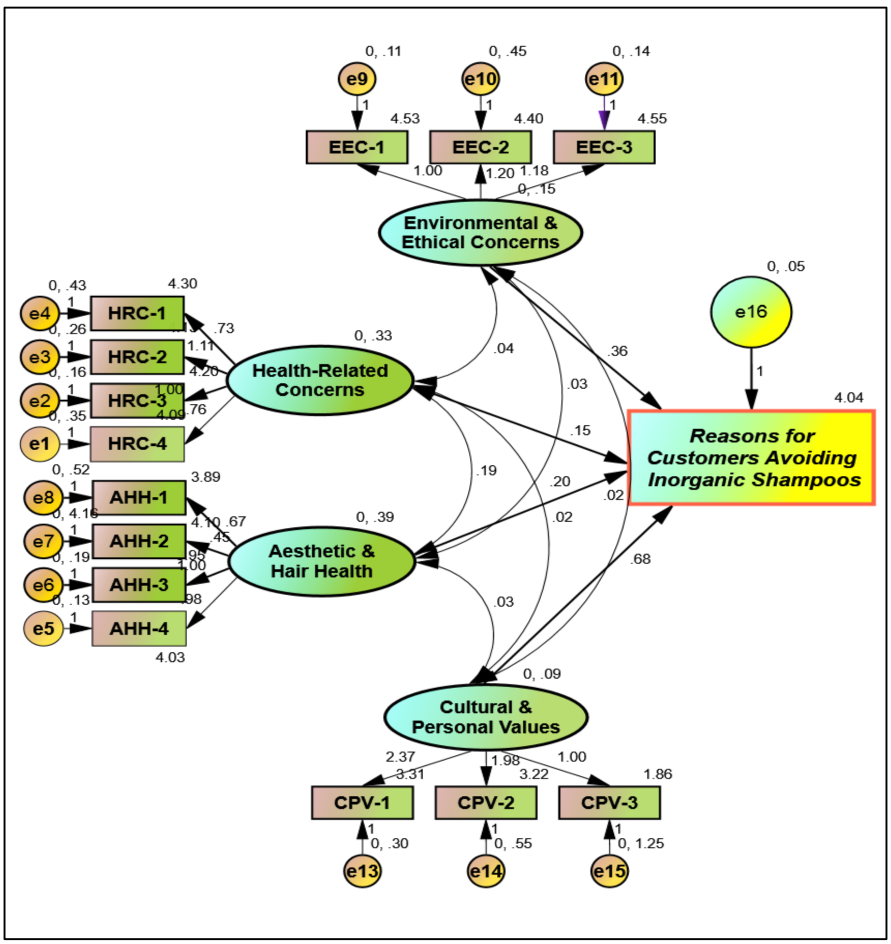

Figure 1. Structural Equation Modeling for Customers Steer Clear of

Inorganic Shampoos

The dimension of avoiding reasons in Environmental and Ethical Concerns has three variables; all are significant in Environmental and Ethical Concerns. The significant variables are compared with estimated values; the first leading variable is 'The production of synthetic chemicals often relies on non-renewable resources, which is anti-social, so I don't like them.' (EEC-3) second leading variable is 'Mineral shampoos come in non-recyclable packaging, which contributes to environmental pollution, so I don't like them' (EEC- 2) and the third leading variable is 'Non-biodegradable chemicals affect aquatic ecosystems and water pollution, so I don't like them.' (EEC- 1) and the estimated values are 1.185, 1.200 and 1.000 respectively.

Finally, the research finds out endogenous dimensions of Health-Related Concerns (HRC), Aesthetic and Hair Health (AHH), Cultural and Personal Values (CPV), and Environmental and Ethical Concerns (EEC) influences on exogenous dimension in Customers Avoiding Inorganic (Chemical-Based) Shampoos.

The results exhibited that the dimension of Health-Related Concerns has a significant impact on Customers Avoiding Inorganic Shampoos, as the direct effect of the dimension on Customers Avoiding Inorganic Shampoos is 0.148 (p-value is significant at 0.05%). Therefore, the **Null Hypothesis (H_0-1) is rejected** and concludes that Health-Related Concerns have a positive impact on Customers Avoiding Inorganic Shampoos.

Then the next results exhibited that the dimension of Aesthetic and Hair Health has a significant impact on Customers Avoiding Inorganic Shampoos, as the direct effect of the dimension on Customers Avoiding Inorganic Shampoos is 0.197 (p value is significant at 0.05%). Therefore, the **Null Hypothesis (H_0-2) is rejected** and concludes that Aesthetic and Hair Health have positive impact on Customers Avoiding Inorganic Shampoos.

Then the next results exhibited that the dimension of Cultural and Personal Values has a significant impact on Customers Avoiding Inorganic Shampoos, as the direct effect of the dimension on Customers Avoiding Inorganic Shampoos is 0.648 (p-value is significant at 0.05%). Therefore, **the Null Hypothesis (H_0-3) is rejected** and concludes that Cultural and Personal Values have positive impact on Customers Avoiding Inorganic Shampoos.

Finally the results exhibited that the dimension of Environmental and Ethical Concerns has a significant impact on Customers Avoiding Inorganic Shampoos, as the direct effect of the dimension on Customers Avoiding Inorganic Shampoos is 0.365 (p-value is significant at 0.05%). Therefore, **the Null Hypothesis (H_0-4) is rejected** and concludes that Environmental and Ethical Concerns have positive impact on Customers Avoiding Inorganic Shampoos.

8. SUGGESTIONS

To avoid inorganic (chemical-based) shampoos, follow these simple steps:

- Make the switch to natural shampoos by carefully reading labels to steer clear of harsh ingredients.
- Selecting natural substitutes such as neem shampoo, coconut oil, and shikakai powder.
- Choosing natural and organic products such as Khadi Natural and Biotique.
- Creating your own shampoo with organic components.
- Making the gradual switch from your present shampoo.
- If necessary, seeking advice from a dermatologist or hair care specialist.

9. CONCLUSION

The analysis concludes the following dimensions are an impact on Customers Avoiding Inorganic Shampoos, the ***first leading reason*** is Cultural and Personal Values, and the impact value is **0.684,** The significant reasons are *customers want to align personal care with holistic and natural lifestyles* and *Traditional hair care often relies on natural remedies*, which can conflict with mineral ingredients, and then *as hair health deteriorates, natural hair care is needed to combat damage.* The ***second leading reason*** is Environmental and Ethical Concerns, and the impact value **is 0.365**, the significant reasons are *the production of synthetic chemicals often relies on non-renewable resources*, which is anti-social, so they don't like it and *Mineral shampoos come in non-recyclable packaging*, which contributes to environmental pollution, so they avoid Inorganic Shampoos.

The ***third leading reason*** is Aesthetic and Hair Health, and the impact value is **0.197,** The significant reasons are *Over-cleansing strips away protective oils, leaving hair dull and unprotected* and *Many inorganic shampoos offer short-*

term benefits (e.g., shine from silicones) *but can cause long-term build-up and damage*. The ***final leading reason*** is Health-Related Concerns and impact value is **0.148**, The significant reason are *An inorganic shampoo has causing in dryness, itchiness, or rashes* and *Inorganic shampoos ingredients are creates hormonal disruption.*

REFERENCES

[1] Arminger, G., and Muthén, B. O. *A Bayesian approach to nonlinear latent variable models using the Gibbs sampler and the Metropolis-Hastings algorithm*, Psychometrika, Vol. 63(3), pp. 271–300, (1998). http://dx.doi.org/10.1007/BF02294856

[2] Chin-Hsien T Chiu, Shu-Hung Huang, Hui-Min D Wang, (2015), A Review: Hair Health, Concerns of Shampoo Ingredients and Scalp Nourishing Treatments, Curr Pharm Biotechnol, 2015;16(12):1045-52. doi: 10.2174/ 13892010 1666 61508170944447

[3] Fornell, C., and Larcker, D. F. *Evaluating structural equation models with unobservable variables and measurement error*, Journal of Marketing Research, Vol. 18(1), pp. 39–50, (1981). https://doi.org/10.2307/3151312

[4] Gavazzoni Dias, Maria Fernanda Reis, Hair *Cosmetics: An Overview*, International Journal of Trichology, Vol. 7(1), pp.2-15, (2015). https://doi.org/10.4103/0974-7753.153450

[5] Guo, R., Zhu, H., Chow, S. M., and Ibrahim, J. G. *Bayesian lasso for semiparametric structural equation models*, Biometrics, Vol. 68(2), pp. 567–577, (2012). https://doi.org/10.1111/j.1541-0420.2012.01751.x

[6] Miranda Wood and Melissa Leyden, (2024), Chemistry of Wellness: Hair and Hair Care, Department of Chemistry, UVA ChemSciComm, ,2024- Newsletter

[7] Paul Sterchele, (2005), Acute and Short-Term Toxicity (or Exposure) Shampoo, in Encyclopedia of Toxicology (Second Edition), 2005

[8] Rummi Devi Saini (2018), Chemical Shampoos Vs Herbal Shampoos , International Journal of Creative Research Thoughts (IJCRT), Volume 6, Issue 1 January 2018

[9] Sze-Huey **S., Liew, K. B., Lee, S. K., Keng, J. W., Akowuah, G. A., Tan, C. S., & Chew, Y. L.** *Formulation of botanical shampoo infused with standardized mangosteen peel extract for healthy hair and scalp.* Cosmetics, Vol. **10**(4), pp. 109, (2023). https://doi.org/10.3390/cosmetics10040109

10. A Mathematical Analysis of Malaria and Cholera Disease by Homotopy Perturbation Method

K.Selvakumari[1], S.Muthuvel[2*] S. Rekha[3], J. Renuka[4]

[1]Department of Mathematics, Easwari Engineering College, Ramapuram, Chennai.

[2*]*Department of Computer Science, AMET Deemed to be University,*

[3]*Department of Mathematics, AMET Deemed to be University, Chennai*

[4]*Department of Mathematics*

Women's Christian College, Chennai, Tamil Nadu, India

Abstract: The mathematical model for co-infection with malaria and cholera was developed in this problem, and it is researched to see if there is a synergistic link between the two diseases in the presence of medicines. The effects of malaria and its treatment on cholera dynamics are investigated in greater depth. Malaria infection raises the chances of cholera, while cholera infection doesn't really enhance the risk of malaria infection. The model is numerically investigated using the Fourth Order Runge - Kutta method and analytically using the HPM. Investigate the impact of each parameter on the governing equation and determine the effective control strategy using the exact solutions (analytical).

Keywords: Malaria, Cholera, Co-infection, Homotopy Perturbation Method, Optimality Control of disease.

1. Introduction

Malaria is a disease transmitted by mosquitoes that may have been prevented and treated. Mosquito biting are stopped by the distribution of low-cost bed nets and sprays, as well as mosquito abatement tactics such as insecticide sprinkling indoors and the draining of filthy water where vectors thrive [1]. "Recent flooding in Africa and Asia has created a significant danger to environmental sanitation and clean water supply, allowing malaria and cholera to spread" [2]. John Snow was the first to examine cholera epidemiology, which paved the way for modern epidemiology study[3]. The relation between cholera and contaminated water has long been known. Cholera is a life-threatening bacterium infection that can cause vomiting and diarrhea. It can lead to "severe thirst, electrolyte imbalance, and death", if not treated. Cholera is spread by drinking water infected with the bacteria Vibrio cholera (typically via feces or wastewater). Cholera colonization by humans results in a super infectious condition that persists after transmission, contributing to epidemic illness. Good sanitation and water treatment can help to prevent cholera [4]. Mathematical modeling has been useful in gaining a better understanding of disease transmission dynamics as well as in making decisions about disease control intervention techniques. Ross [5], for example, was the first to establish "Mathematical models of malaria transmission". His major objective was vector management, and he established that the mosquito population must be decreased to a certain level in order to eradicate the infection. Koella's and Anita's inquiries are among the others [6], Among them was a mosquito latent class. They evaluated various tactics for reducing "resistance spread and investigated the sensitivity of their findings to the parameters". Anderson and May [7] developed "A Malaria model based on the assumption that acquired immunity is unaffected by exposure length in malaria". Effect of disease prevalence on transmission rate, as well as other control methods, were explored further. Nikolaos and his colleagues. [8] offered a thorough examination of a dynamical model to characterize HIV infection etiology. With vaccination and various endemic states, "A basic two-dimensional SIS (susceptible-infected-susceptible) model" was created by Christopher and Jorge [9]. There has been no research on the dynamics of malaria-cholera co-infection or the deployment of optimal methods of control to our understanding. A deterministic framework for HIV and malaria co-infection in a population was recently constructed and tested by the authors of [10]. The authors also looked at a deterministic model for tuberculosis and malaria co-infection in [11]. In [13], the authors developed a mathematical model for cholera that included key elements - "hyper-infectious, short-lived bacterial condition, a distinct class for mild human infections, and diminishing disease immunity".

There have been significant mathematical modelling developments over the past eight years. [15] Mojeeb AL-Rahman EL-Nor Osman et. al. established the SEIR model in 2017, and it was used to predict the reproduction rate, the disease-free and endemic equilibria. Additionally, they created an SEIR-SEI model of how malaria spreads between people and insects. Insecticides, mosquito-treated nets, and active anti-malarial medications can all assist to reduce mosquito populations and the transmission of malaria, according to the study's findings. Malaria can also be controlled by lowering the rate of human-mosquito interaction.

A historical review of the dynamics of malaria transmission and climate change was conducted in 2018 by Steffen E. Eikenberry et al[16]. They discussed the main biological facets of malaria, techniques for formalizing these into mathematical forms, and uncertainties and debates surrounding appropriate modelling approach. Their goal was to present a timeline of some significant modelling initiatives, ranging from the classic works of Sir Ronald Ross and George Macdonald to more contemporary modelling studies that specifically focused on climate. Last but not least, they made an effort to set this mathematical study into a larger historical framework for the "million-murdering Death" of malaria.

In 2018[17], Ousmane Koutou et. al., presented a model, constructed by considering two models: a model of vector population and a model of virus transmission. Each model's threshold dynamics were identified, and a correlation between them was created. The Lyapunov principle is additionally used to investigate the stability of equilibrium points. The next generation matrix was used to calculate the common basic reproduction number, and its implications for the management of malaria were examined.A mathematical model of malaria transmission dynamics with age structure for the vector population and a regular bite rate of female anopheles mosquitoes was presented in 2018 by Traoré Bakary et al [18].They examined the model's behaviour when the fundamental reproduction ratio R_0 is more than one or less than one, as well as the stability of the disease-free equilibrium.

In 2020 [19], Kinfe Hailemariam Hntsa et al. took into account a mathematical model for the dynamics of cholera transmission and its countermeasure as one cohort of people. They estimated the fundamental reproduction number R_0 and looked into the possibility of equilibria as well as their stability. According to the findings, the disease is eradicated and kills fewer people in places with appropriate preventive measures while becoming widespread and killing more people in areas with insufficient preventive measures.In 2020 [20], K. U. Egeonu et al. conducted analysis to determine how treatment controls affected a population's disease burden when there was drug resistance for malaria. When the related reproduction number is smaller than unity, the dynamical feature of backward bifurcation is demonstrated to occur in the model. The Pontryagin's Maximum Principle is used to establish the prerequisites for the existence of optimum control and the optimality system for the model.The study in a novel nonlinear mathematical model for malaria disease was proposed by Malik Muhammad Ibrahim et al. in 2020 [21] . Using the fundamental reproductive number R_0, local and global stability analysis of a disease-free equilibrium has been investigated; if $R_0 <1$, the system is stable; otherwise, it is unstable. Under specific circumstances, the existence of the special endemic equilibrium has also been established. The findings of this study demonstrate that, in addition to a decline in the population of infected mosquitoes, a sizable increase in the population of susceptible humans has been achieved.A nonlinear mathematical model was proposed and used in 2020 by Segun I. Oke et al[22]., to analyse the dynamics of malaria transmission in a population. Utilizing differential equation stability theory, the deterministic compartmental model was investigated. The reproduction number was asymptotically stable for the disease-free conditions, and the endemic equilibria were identified. In addition, the qualitatively assessed model incorporates time-dependent variable controls that were intended to stop the spread of the malaria disease. Incorporating three control strategies—disease prevention with bed nets, treatment, and insecticides—the optimal control problem was formulated using Pontryagin's maximum principle.A mathematical model of malaria in the human population was considered in 2020 by Baihaqi, Muhamad Adzib, et al [23]., who made the assumption that the disease's infection rate in the population is constant and only depends on the number of infected people. The existence of endemic and disease-free equilibrium points, as well as the local stability for both equilibrium points and the global stability for the disease-free equilibrium point, were also the focus of their analysis.

In 2021, Egide Ndamuzi et al [24]. created the SEIR model and discovered the fundamental reproduction number R_0. This model's findings demonstrate the need for effective control measures to decrease the number of mosquito bites on humans per unit of time (σ), the vector population of mosquitoes (Nv), the probability of infection for a person bitten by an infectious mosquito per unit of time (b), and the probability of infection for a mosquito per unit of time (c).The new fourteen compartmental mathematical model was defined by G. A. Adeniran et al [25] . in 2022. In an effort to pinpoint the most sensitive factors, the model was examined for each factor influencing the spread of the illness. Full models of the co-infection of malaria and cholera were studied first, followed by sub models of the two diseases separately. The relative sensitivity solution of the model is calculated for each parameter. Sensitivity analyses showed that of all the variables used and examined in this model.

A fractional order model of the co-infection of malaria and cholera was developed in 2022 by Nita H. Shah et al [26]. using the definition of the Caputo fractional derivative with the order of derivative in the range (0,1). The fractional order model has been shown to produce superior results. For the malaria and cholera models, the basic reproduction number was calculated. Muhammad Sinan et al. started to look at the dynamics of malaria illness in humans in 2022 [27], as well as the disease's vectors. It was also considered how the vector's (the mosquito) role in disease transmission might play a role. Ulam-Hyres stability analysis and optimal control strategies have been used in some theoretical analyses of existence, uniqueness, and stability. Different graphs show the results of fractional and classical order, and some numbers are shown to show the model's overall asymptotic stability. Finally, we have made attempt to investigate Mathematical analysis of Malaria and cholera disease by HPM [14].

2. Model Formulation

Humans Who Are Susceptible S_h, Individuals only infected with malaria I_m, individuals only infected with cholera I_c, individuals only recovering from malaria R_m, and individuals only recovering from cholera alone R_c are all sub-populations of the overall human population, denoted by N_h. As a result, $N_h=S_h+I_m+I_c+R_m+R_c$. The whole vector population, N_v, is separated into susceptible mosquitoes S_v and malaria-infected mosquitoes I_v. As a result, $N_v=S_v+Iv$ [14].

3. Cholera Model

We'll look at the Cholera-only model here[14]

$$\frac{dS_h}{dt}=\Lambda_h+\omega R_c-\lambda S_h-\mu_h S_h \qquad (1)$$

$$\frac{dI_c}{dt}=\lambda S_h-(\delta+\mu_h+m)\,I_c \qquad (2)$$

$$\frac{dR_c}{dt}=\delta I_c-(\omega+\mu_h)\,R_c \qquad (3)$$

$$\frac{dB_c}{dt}=\rho I_c-\mu_b B_c \qquad (4)$$

With the initial condition $S_h(0)\geq 0$, $I_c(0)\geq 0$, $R_c(0)\geq 0, B_c(0)\geq 0$.

The analytical solution of Cholera Model is obtained by Homotopy perturbation method

$$S_h(t)=2498001.59e^{(-0.05004t)}+1998.402 \qquad (5)$$

$$I_c(t)=1061.737+2834129.339e^{(-0.05004t)}-2835191.075e^{(-0.09411t)} \qquad (6)$$

$$R_c(t)=-4051995.2020e^{(-0.05004t)}+2133316.4810e^{(-0.09411t)}+1918678.7210e^{(-0.00104t)} \qquad (7)$$

$$B_c(t)=27213235.32e^{(-0.05004t)}\ -68725429.18e^{(-0.09411t)}41512193.86e^{(-0.0123t)} \qquad (8)$$

4. Malaria Model

We'll look at the Malaria-only model here[14]

$$\frac{dS_h}{dt}=\Lambda_h+kR_m-\beta_h S_h I_v-\mu_h S_h \qquad (9)$$

$$\frac{dI_m}{dt}=\beta_h S_h I_v-(\alpha+\mu_h+\emptyset)\,I_m \qquad (10)$$

$$\frac{dR_m}{dt}=\alpha I_m-(k+\mu_h)R_m \qquad (11)$$

$$\frac{dS_v}{dt}=\Lambda_v-\beta_v S_v I_m-\mu_v S_v \qquad (12)$$

$$\frac{dI_v}{dt}=\beta_v S_v I_m-\mu_v I_v \qquad (13)$$

With the initial condition,

$S_h(0)\geq 0,\ I_m(0)\geq 0, R_m(0)\geq 0, S_v(0)\geq 0, I_v(0)\geq 0$

4.2 Analytical solution of Malaria Model.

$$S_h(t)=-928.43e^{(-0.067t)}-94.942e^{(-0.0115t)}+181.78e^{(-0.012t)}+361.59e^{(-0.078t)}-708.826e^{(-0.0782t)}+473.971e^{(-0.067t)}-0.013e^{(-0.0104t)}+0.001e^{(-0.089t)}- \quad (14)$$

$$\begin{aligned}I_m(t)= {} & 12434.509e^{(-0.0115t)}-0.01706te^{(-0.079t)}-571.409e^{(-0.0667t)}+0.5334e^{(-0.1448t)}-1.0229e^{(-0.1448t)} \\ & + 1119.2269e^{(-0.0667t)}+0.0026009e^{(-0.0767t)}+0.00012e^{(-0.157t)}+829.592e^{(-0.079t)} \\ & +12426.0026e^{(-0.01149t)}-24860.509e^{(-0.011449t)}+1.829e^{(-0.13338t)}-1.035073796e^{((-0.011409t)t)} \\ & -0.00259e^{(-0.078t)}- 406.358e^{(-0.079t)}+0.4905e^{(-0.1449t)}-0.95269e^{(-0.1334t)}+1.0348te^{(-0.011449t)} \\ & + 0.0239e^{(-0.06668t)t}-0.8775e^{(-0.1335t)}-547.85e^{(-0.0668t)}-0.0229te^{(-0.0668t)}+0.0178te^{(-0.079t)}\end{aligned} \quad (15)$$

$$\begin{aligned}R_m(t)= {} & 0.01336e^{(-0.01005t)}+4.8295e^{(-0.011452t)}+0.0028e^{(-0.0667t)}-0.00266e^{(-0.0668t)}-0.000208e^{(-0.0115t)t} \\ & - 4.8419e^{(-0.011449t)}-0.00172009e^{(-0.079t)}+0.0018e^{(-0.079t)}\end{aligned} \quad (16)$$

$$\begin{aligned}S_v(t)= {} & 0.1499+0.12613e^{(-0.13339t)}+0.00155e^{(-0.06668t)t}+1.2178e^{(-0.011409t)}-0.08019e^{(-0.1448t)} \\ & +0.08367e^{(-0.1448t)}-0.131549e^{(-0.13334t)}-36.3259e^{(-0.0667t)}+37.1542e^{(-0.0668t)}+33.2407e^{(-0.079t)} \\ & -1.2183e^{(-0.011449t)}-33.21625e^{(-0.078079t)}+0.00139te^{(-0.078079t)}\end{aligned} \quad (17)$$

$$\begin{aligned}I_v(t)= {} & -0.12613e^{(-0.13338t)}-0.001549e^{(-0.0667t)t}-1.2178e^{(-0.011409t)} \\ & +0.08019e^{(-0.1448t)}- 0.0836209e^{(-0.1448t)}+0.131549e^{(-0.1334t)} \\ & +37.1769e^{(-0.0667t)}-37.1541e^{(-0.0667t)}- 33.2407e^{(-0.079t)}+ 1.218236e^{(-0.01145t)} \\ & +33.2163e^{(-0.07808t)}-0.001394te^{(-0.079t)}\end{aligned} \quad (18)$$

Table 1: Parameters values of Optimal Malaria - Cholera Model

Parameters	Description	Value
Λ_h	Human birth rate	0.001
k	Malaria immunity waning rate	0.01
β_h	Probability of human getting infected	0.034
μ_h	The natural death rate in humans	0.00004
α	The recovery rate of malaria-infected individual	0.001369
$\emptyset$	Malaria related death	0.01
Λ_v	Mosquitoes birth rate	0.01
β_v	Probability of mosquitoes getting infected	0.09
μ_v	The natural death rate in mosquitoes	0.06667
ω	Cholera immunity waning rate	0.001
λ	Bacteria contact rate with humans	0.05
δ	The recovery rate of cholera infected individual	0.07
ρ	Cholera infected contribution to the aquatic	0.7

μ_b	Bacteria mortality rate	0.123
m	Cholera related death	0.02407

5. Numerical Simulation and Discussion:

5.1 Cholera Model

To observe the model system's dynamical behaviour, Using the fourth-order Runge–Kutta method and the following parameters, the systematic equations (1)–(4) are numerically computed[14]:

μ_b=0.123,ω=0.001,λ=0.05,δ=0.07,μ_h=0.00004,ρ=0.7,Λ_h=0.001,m=0.02407 with the initial condition $S_h(0)\geq 0$, $I_c(0)\geq 0$, $R_c(0)\geq 0$,$B_c(0)\geq 0$.

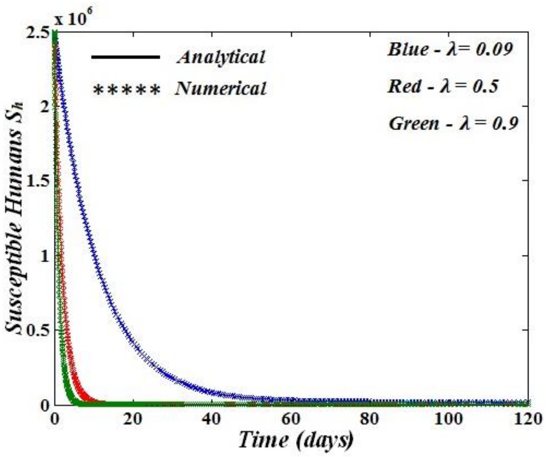

Figure 1:Variation of Bacteria contact rate with humans for different values of λ.

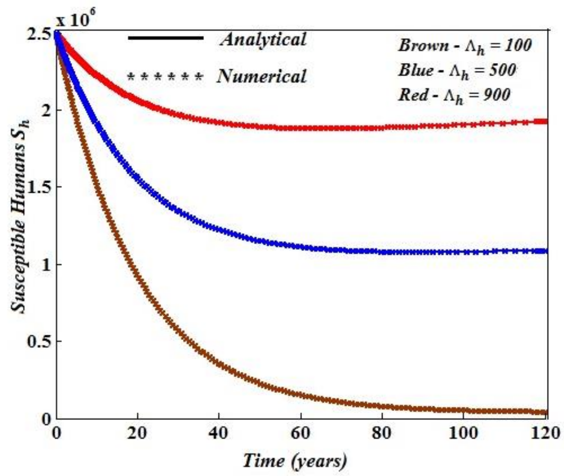

Figure 2:Variation of Human birth rate for different values Λ_h

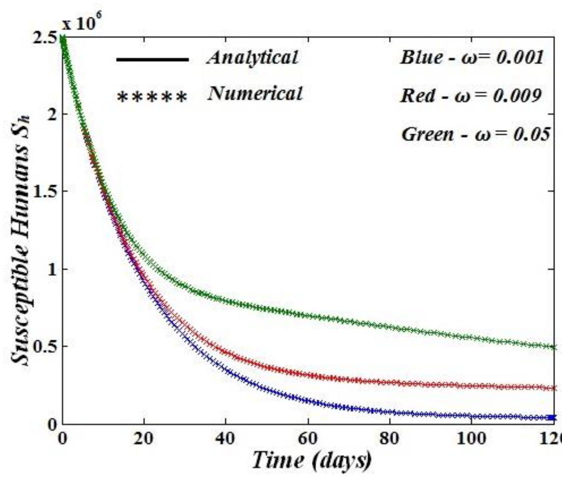

Figure 3: Cholera immunity waning rate for various values of ω

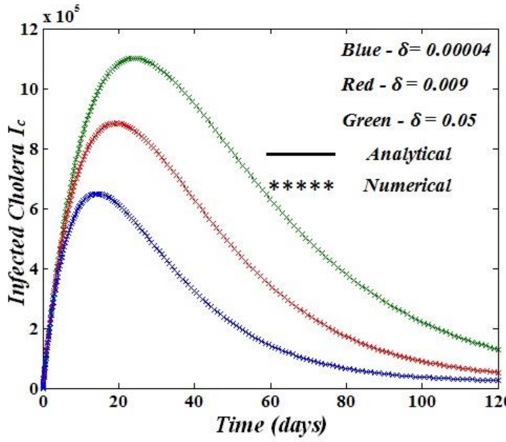

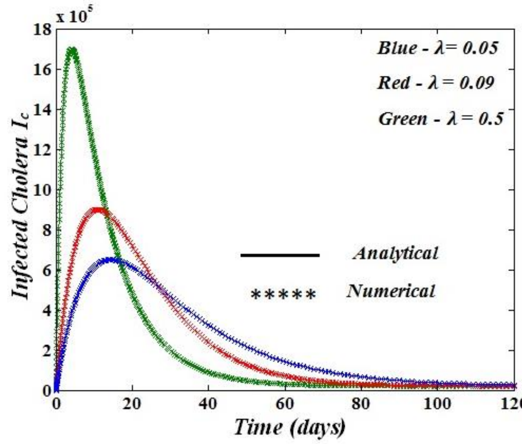

Figure 4 and 5: Infected Cholera of Recovery rate of cholera infected individual and Bacteria contact rate with humans for various values.

Figure1and 2, shows the analytical and numerical simulation comparison of the parameters λ and Λ_h. By increasing the value of λ to 0.09, 0.5, and 0.9, the Bacteria contact rate with humans is decreasing and then varying the values of Λ_h, Human birth rate is decreasing. In figure 3, the Cholera immunity waning rate for different values of ω i.e. 0.001, 0.009, and 0.05 is increasing the immunity rate. In figure 4, the recovery rate of cholera is increasing while we increase the value of δ to 0.00004, 0.009, and 0.05. Then bacteria contact rate of humans in figure 5, reaches a high level when the value of λ changes to 0.5.

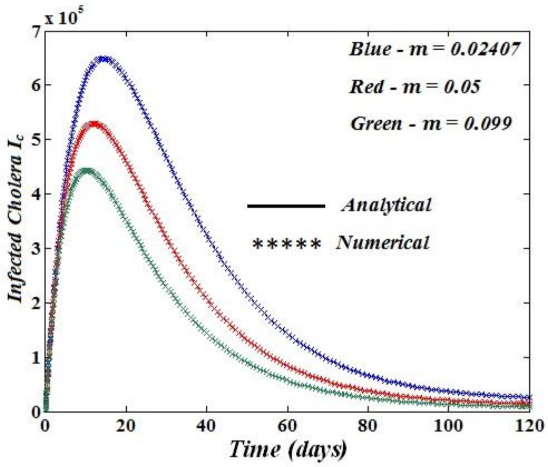

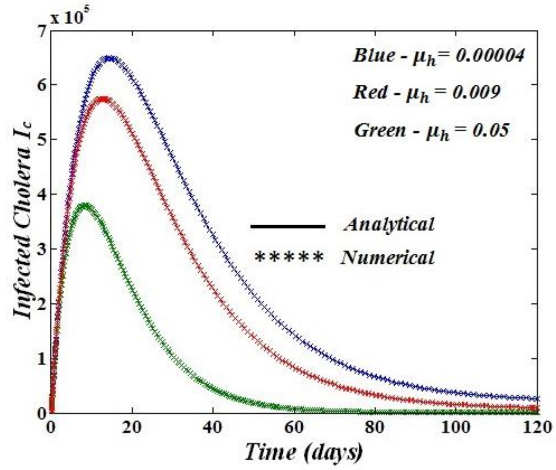

Figure 6 and 7: Cholera related death and Natural death rate in humans for various values

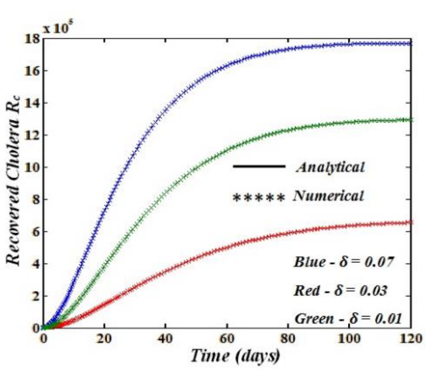

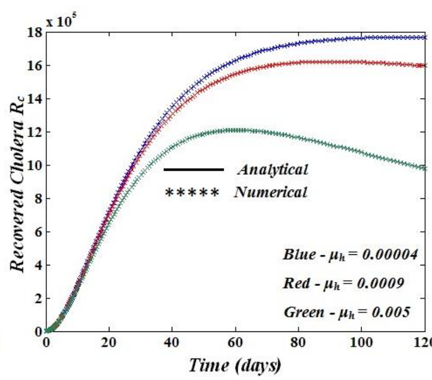

Figure 8 and 9: Recovered Cholera for a Recovery rate of cholera infected individual and Natural death rate in humans in different values.

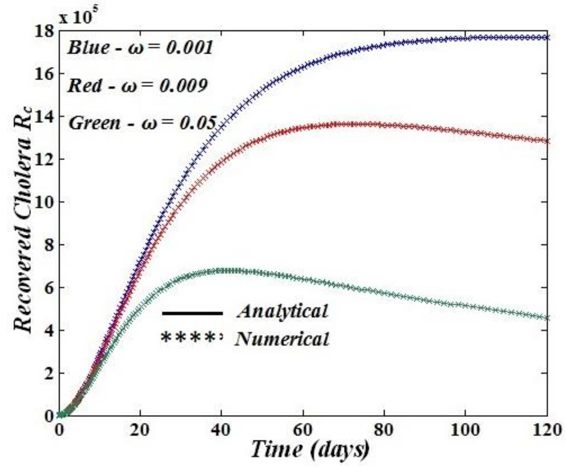

Figure 10: Recovered Cholera of Cholera immunity waning rate in various parameter values

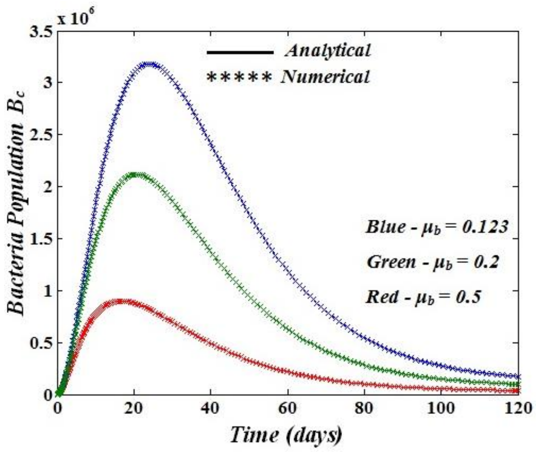

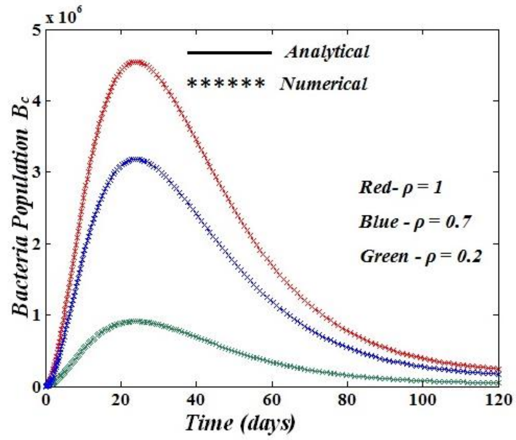

Figure 11 and 12: Bacteria Population B_c of Bacteria mortality rate and Cholera infected contribution to the aquatic in various values of parameters.

In figure 6, Cholera related death rate is decreasing when the death rate range is increasing as 0.05 and 0.099, then in fig.8 the recovered rate of cholera infected individuals δ is decreasing slightly when the value is increased by 0.01and 0.03. In figure 7 and 9, the Natural death rate in humans is increasing while varying the μ_h parameter values into 0.00004, 0.0009, and 0.005 is controlling the number of cholera-infected people has never been easier or more effective. Cholera-related death is controlling the infected individuals. In fig 10, the Cholera immunity waning rate is decreased in various parameter values 0.009 and 0.05.

5.2 Malaria Model

The numerical computation of the systematic equations (29)–(33) using the fourth-order Runge–Kutta method with the following parameters is used to see the dynamical behaviour of the model system. [14]: Λ_h=0.001, k=0.01, α=0.001369, β_h=0.034, β_v= 0.09, μ_h=0.00004,

$\emptyset$=0.01,Λ_v=0.01, μ_v=0.06667 with the initial condition $S_h(0)\geq 0$, $I_m(0)\geq 0$,$R_m(0)\geq 0$,$S_v(0)\geq 0$,$I_v(0)\geq 0$.

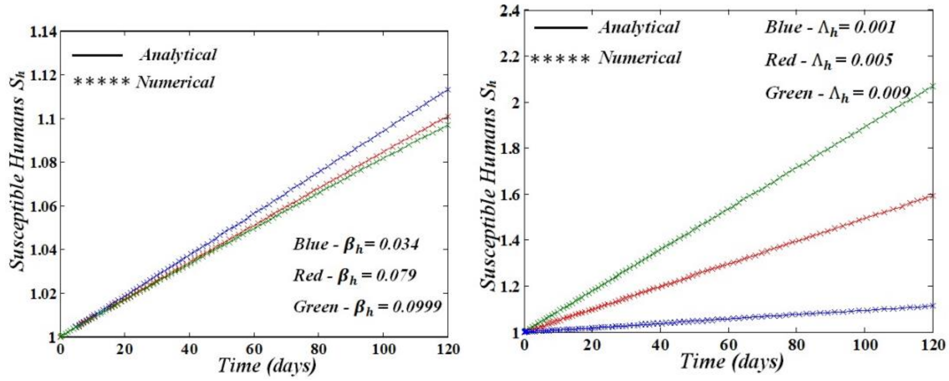

Figure 13 and 14: Probability of human getting infected and Human birth rate in the various parameter value

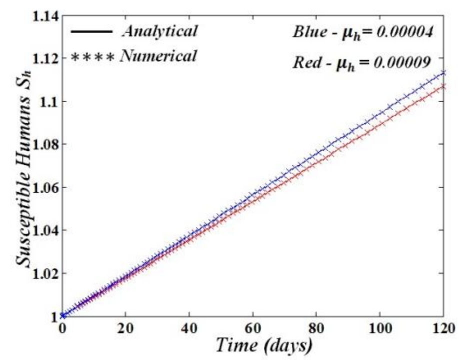

Figure 15: Susceptible humans of Malaria of Natural death rate in humans for various values in the parameter

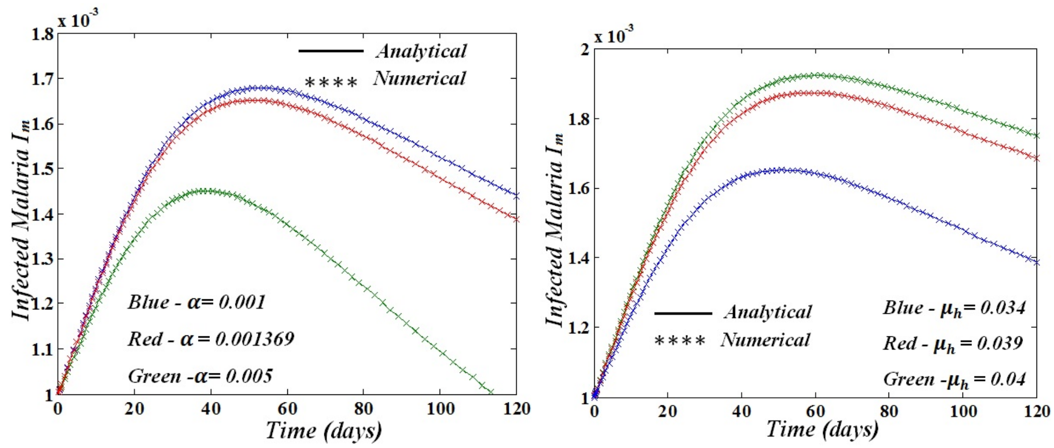

Figure 16 and 17: Infected Malaria of Natural death rate in humans and Recovery rate of a malaria-infected individual by changing the parameter values

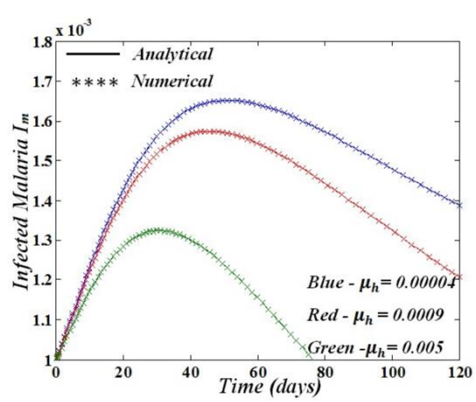

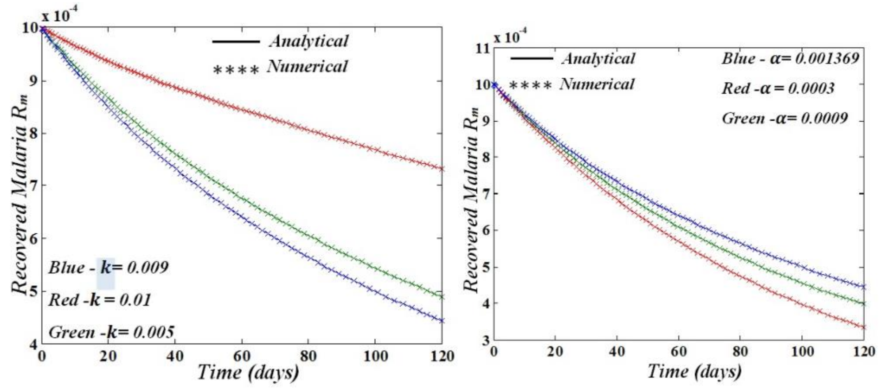

Figure 18, 19, and 20: Infected and Recovered Malaria for various values of a parameter

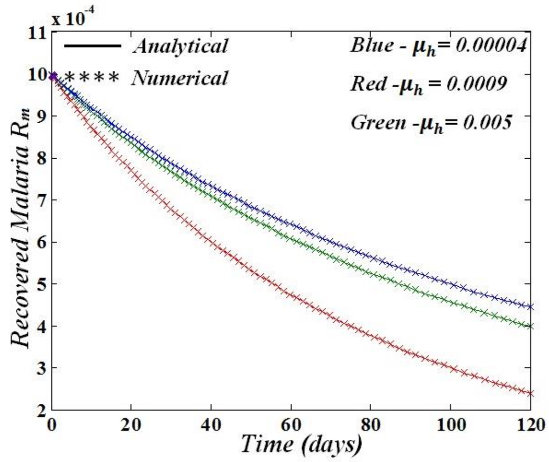

Figure 21: Recovered Malaria of Natural Death rate of malaria-infected individual in different values

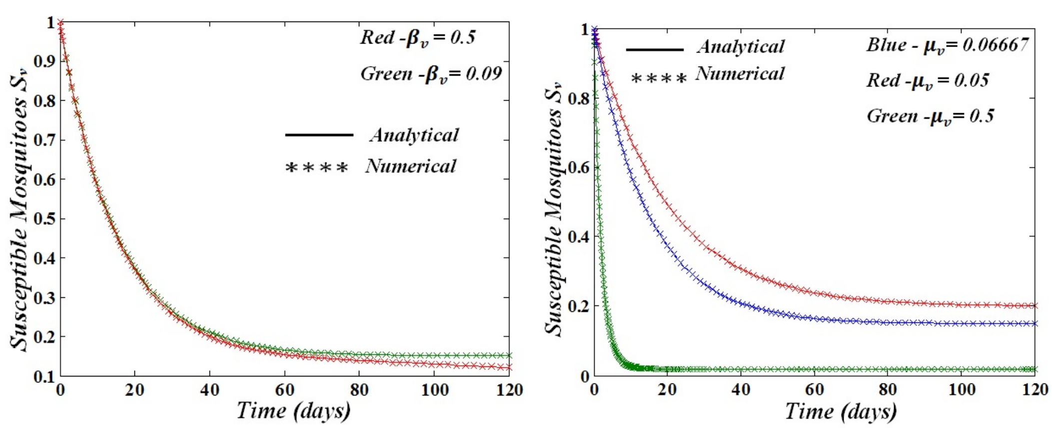

Figure 22 and 23: Susceptible Mosquitoes of Probability of mosquitoes getting infected and Natural death rate in mosquitoes by varying the parameter values.

In fig 13 and 14, the Probability of humans getting infected is decreased while changing the value of β_h into 0.034, 0.079, and 0.0999 and Human birth rate in various values of parameter Λ_h into 0.001, 0.005, 0.009. So that, the human birth rate is increased.

To optimize the objective function, the treatment controls for malaria and cholera (figs 15 and 17) are used, whereas the other treatments are not. There are no preventative actions made because the therapeutic processes have been refined. As demonstrated in Figures 18 and 19, the number of malaria-infected patients in cases increased steadily toward the end of the research. In fig 16, the natural death rate of infected malaria population is decreased when the α range is change into 0.001369 and 0.005. In fig 20, α is the natural death rate of recovered malaria population R_m, The death rate is slightly increased when we increase the value into 0.0003 and 0.0009. In fig 21, the natural death rate of malaria infected individuals in recovered malaria population is slightly increased by increasing the values of 0.0009 and 0.005. In fig 22, the probability of mosquitoes getting infected in Susceptible mosquitoes S_v is not increasing and not decreased by varying the values into 0.5 and 0.09. In Susceptible mosquitoes, the natural death rate in mosquitoes is decreased by changing the parameter values into 0.05 and 0.5 in fig 23.

By decreasing the transmission rate of Malaria - Cholera disease, the recovery rate will be increase. For reducing the infected rate people can control by using the cautions like bed nets, opened water in tyers etc. The simple ways like this can make the transmission rate in control.

6. Conclusion:

The Mathematical Modeling of the Malaria-Cholera model is examined in this research. The optimal control for Malaria-Cholera model is discussed in the parameter variation graphs. The linear and non-linear differential equations of Malaria - Cholera model is solved numerically and analytically. The MATLAB ode45 function generates the numerical results that are consistent with the analytical solution by Homotopy Perturbation Method.

Acknowledgments: The authors are grateful to Col. Shri J. Ramachandran, Chancellor, and Vice-Chancellor Dr. G. Thiruvasagam, Academy of Maritime Education and Training (AMET), Chennai-603112, Tamil Nadu.

References:

[1] K.O. Okosun, R. Ouifki, N. Marcus, (2011). Optimal control analysis of a malaria disease transmission model that includes treatment and vaccination with waning immunity, BioSystems 106, 136–145, doi:10.1016/j.biosystems.2011.07.006.

[2] M. Agarwal, V. Verma, (2012). Modelling and analysis of the spread of infectious disease cholera with environmental fluctuations. Appl. Appl. Math. 7(1), 406–425.

[3] M.D. John Snow, (1855). On the Mode of Communication of Cholera, John Churchill, New Burlington Street, England.

[4] R.P. Sanches, C.P. Ferreira, R.A. Kraenkel, ((2011)). The role of immunity and seasonality in cholera epidemics, Bull. Math. Biol. 73, 2916–2931.

[5] R. Ross, (1911). The Prevention of Malaria, second ed., London, Murray.

[6] J.C. Koella, R. Anita, (2003). Epidemiological models for the spread of anti-malaria resistance, Malaria J. 2(3).

[7] R.M. Anderson, R.M.May, (1991). Infectious Diseases of Humans: Dynamics and Control, 477 Oxford University Press, Oxford.

[8] I.S. Nikolaos, K. Dietz, D. Schenzle, (1997). Analysis of a model for the pathogenesis of AIDS, Math. Biosci. 145, 27–46.

[9] M.K. Christopher, X.V. Jorge, (2000). A simple vaccination model with multiple endemic states, Math. Biosci. 164, 183–201.

[10] Z. Mukandavire, A.B. Gumel, W. Garira, J.M. Tchuenche, (2009). Mathematical analysis of a model for HIV-malaria co-infection, Math. Biosci. Eng. 6, 333– 362.

[11] E. Mtisi, H. Rwezaura, J.M. Tchuenche, (2009). A mathematical analysis of malaria and tuberculosis co-dynamics, Discrete Cont. Dyn. Syst. B 12 (4), 827–864.

[12] S. Mushayabasa, C.P. Bhunu, (2012). Is HIV infection associated with an increased risk for cholera? Insights from a mathematical model, BioSystems 109, 203–213.

[13] R.L.M. Nielan, E. Schaefer, H. Gaff, K.R. Fister, S. Lenhart, (2010). Modeling optimal intervention strategies for cholera, Bull. Math. Biol. 72, 2004–2018.

[14] K.O. Okosun, O.D. Makinde, (2014). "A co-infection model of malaria and cholera diseases with optimal control" 000, 1–14.

[15] Mojeeb AL-Rahman EL-Nor Osman and Isaac Kwasi Adu. (2017), Simple Mathematical Model for Malaria Transmission, Journal of Advances in Mathematics and Computer Science, 25(6): 1-24, 2017; Article no.JAMCS.37843.

[16] Steffen E. Eikenberry and Abba B. Gumel. (2018), Mathematical modeling of climate change and malaria transmission dynamics: a historical review, J. Math. Biol. (2018) 77:857–933.

[17] Traoré Bakary, Sangaré Boureima and Traoré Sado. (2018), A mathematical model of malaria transmission in a periodic environment, Journal of Biological Dynamics, 12:1, 400-432.

[18] Ousmane Koutou, Bakary Traoré and Boureima Sangaré. (2018), Mathematical modeling of malaria transmission global dynamics: taking into account the immature stages of the vectors, Advances in Difference Equations 2018:220.

[19] Kinfe Hailemariam Hntsa and Berhe Nerea Kahsay. (2020), Analysis of Cholera Epidemic Controlling Using Mathematical Modeling, International Journal of Mathematics and Mathematical Sciences Volume 2020, Article ID 7369204, 13 pages.

[20] K. U. Egeonua, S. C. Inyamab and A. Omamec. (2020), A co-infection model for Two Strain Malaria and Cholera with Optimal Control International Journal of Dynamics and Control doi: 10.1007/s40435-020-00748-2.

[21] Malik Muhammad Ibrahim , Muhammad Ahmad Kamran , Malik Muhammad Naeem Mannan , Sangil Kim and Il Hyo Jung. (2020), Impact of Awareness to Control Malaria Disease: A Mathematical Modeling Approach, Hindaw Complexity Volume 2020, Article ID 8657410, 13 pages.

[22] Muhamad Adzib Baihaqi and Fajar Adi-Kusumo. (2020), Modelling malaria transmission in a population with SEIRSp method, AIP Conference Proceedings 2264, 020002 (2020).

[23] Egide Ndamuzi1, Paterne Gahungu. (2021), Mathematical Modeling of Malaria Transmission Dynamics: Case of Burundi, Journal of Applied Mathematics and Physics, 9, 2447-2460.

[24] G. A. Adeniran , I. A. Olopade , S. O. Ajao , V. A. Akinrinmade , O. R. Aderele and S. O. Adewale. (2022), Sensitivity and Mathematical Analysis of Malaria and Cholera Co-Infection, Asian Journal of Pure and Applied Mathematics, 4(3): 290-317, 2022; Article no.AJPAM.1027.

[25] Nita H Shah, Nisha Sheoran and Ekta Jayswal. (2022), Fractional order model for malaria-cholera co-infection, Mathematics in Engineering, Science and Aerospace, Vol 13(3).

[26] Muhammad Sinan , Hijaz Ahmad , Zubair Ahmad , Jamel Baili , Saqib Murtaza , M.A. Aiyashi and Thongchai Botmart. (2022), Fractional mathematical modeling of malaria disease with treatment & insecticides, Results in Physics 34 (2022) 105220.

[27] Segun I. Oke, Michael M. Ojo, Michael O. Adeniyi and Maba B. Matadi. (2022), Mathematical Modeling of Malaria Disease with Control Strategy, Commun. Math. Biol. Neurosci, 2020:43.

11. Mathematical Modeling of Zika Virus Transmission by Homotopy Perturbation Method

U. Kalpana[1], J.Kavitha[2] J. Renuka[3], and [4]P.N.Vijayakumar

[1,4]Department of Mathematics, AMET Deemed to be University,

Chennai – 603112, Tamil Nadu, India.

[2]Department of Mathematics, DG Vaishivna College, Chennai

[3]Department of Mathematics, Women's Christian College,

Chennai – 600006, Tamil Nadu, India.

Abstract: In this paper, the study of the Zika SEIR epidemic model is analyzed. The model is separated into two populations: human and vector. The model is written as a nonlinear first-order differential equation[30]. The model's steady state is found to be asymptotically stable locally and globally. To solve the model analytically, the Homotopy Perturbation Method is utilized, and MATLAB is used to acquire the simulation result. Finally, the numerical and analytical solutions are compared, and the conditions essential for efficient disease control are found.

Keywords: Zika Virus, Human population, Vector population, Non-linear differential equation, SEIR Model, Homotopy Perturbation Method.

1. Introduction

Between 1960 and 1980, "the Zika virus was initially discovered in monkeys in 1947, and the first instances of Zika virus infection were recorded in Uganda and the Republic of Tanzania. There were just a few human cases of zika virus infection in Asia and Africa until 2007 in the Yap Islands, then in 2013 in France Polynesia and the Pacific Ocean, and finally in 2015 in Brazil, when the virus spread widely[2]. As a result, it has spread to other countries throughout the world, with the Zika virus now infecting 86 countries. This disease causes fever, rashes, conjunctivitis, muscle and joint discomfort, malaise, and headaches[3]. Recently, zika virus infection has become a dangerous threat to human society. It is a vector-borne flavivirus. It is spread by daytime–active Aedes mosquitos, such as A aegypti and A albopictus. Its name comes from the Zika Forest of Uganda, where the virus was first isolated in 1947. Zika virus is a member of the virus family Flaviviridae" [1].

The virus is early transmitted by mosquitoes bites in human bodies like "Aedes aegypti female mosquitoes" which also transmit so many viral diseases like dengue, chikungunya, yellow fever, Japanese Encephalitis virus [5].

Due to the virus a pregnant woman affected through the mother a baby in womb also affected in virus. The main possible way virus spread is due to breast feeding. The virus can transfer through the milk to the child . Furthermore, the Zika virus's long-term consequences on newly born babies got affected[4]. The Zika virus is suspected in Kerala on 8th July 2021 [7]. There is, however, proven evidence of this disease being transmitted sexually.

The virus transmitted from one human to another. "Researchers are continuing to research the zika virus and how it spreads, and will update their recommendations when new information becomes available. It can be spread from a person who has zika before they show symptoms, during their symptoms, and after they have gone away. The virus can also be spread by someone who has the virus but never develops symptoms, though this is not well documented. There have been no proven cases of blood transfusion transmission in the United States to far. Multiple incidences of potential blood transfusion transmission have been reported in Brazil. 2.8 percent of blood donors were positive for the zika virus during the French Polynesian incident"[8].

Public Health Emergency of International Concern (PHEIC) by the World Health Organization (WHO) verified Zika virus[13,14]. Various experts lately researched and analyzed Using a mathematical model as a tool, researchers investigated the transmission patterns of the Zika virus. They created a mathematical model for the Zika virus's transmission dynamics and exhibited Zika virus control methods such as prevention, treatment, and insecticides. The authors incorporated sexual transmission of this disease into the suggested model, generated fundamental reproduction numbers, and used all data to illustrate the analysis with a numerical simulation. Because the Zika virus is currently endemic, it is critical to research it[15-17].

In its previous environment, the Zika virus moved quickly across the Pacific and the Americas, but important gaps in our understanding of the virus's epidemiology and biology remain. The following concern must be given top priority in the short term[18-19]. "To avoid contact with the vectors and practise safe sex, outreach and awareness initiatives targeting sexually active persons and pregnant women should be established [20]. Establishing prospective cohorts to assess the likelihood of neonatal zika syndrome and human-to-human transmission [21] to see if the zika virus may develop an enzootic transmission cycle in the Americas".

In 2015 and 2016, "large outbreaks of the zika virus occurred in the Americans, due to increasing travel-associated cases in US states, widespread transmission in Puerto Rico and US Virgin Islands, and limited local transmission in Florida and Texas". State and local health authorities use standard case conditions to report cases to the CDC[22-25].

1.1 Symptoms and Signs

The time it takes for Zika virus disease to develop symptoms (incubation period) is unknown, however it is expected to be a few days. Illness, skin irritation, conjunctiva, muscles and joint aches, malaise, and migraine are all symptoms. These clinical symptoms last two to seven days and are modest.

1.2 Consequences of Zika Virus Infection

WHO has concluded that "Zika virus infection during pregnancy causes congenital brain abnormalities, including microcephaly, and that Zika virus is a trigger of Guillain-Barré syndrome, based on a systematic evaluation of the literature up to May 30, 2016". The link between the Zika virus and a variety of neuromuscular disorders is still being examined in a rigorous study context.

1.3 Diagnosis

The susceptible people is identified by their symptoms and travel history. A diagnosis of Zika virus infection may only be made through tests performed of blood or other bodily fluids such as urinary, salivary, or reproductive cells.

1.4 Treatment

The humans who infected by Zika virus should take proper rest, need drink liquid items like fresh juice, water etc. Usually, the symptoms will be very mild and adjustable. Only if the situation goes worse then they go to a medical help. There is no vaccination available right now.

1.5 Prevention

Diagnostic tests can be used to determine Zika infections. Zika viral can now be found in blood (plasma and serum), urine, saliva, breastfeeding, sperm, amniotic fluid, and tissues.

1.5.1 Mosquitoes bites

Anti-mosquito protection is a critical step in preventing Zika virus infection. "Wearing clothes that cover as much of the body as possible (ideally light-colored), utilising physical barriers such as window screens or closing doors and windows, sleeping under mosquito nets, and using insect repellent according to the product label recommendations are all ways to do this". The humans like childrens, aged people can get assistance or any special care.

It is critical to cover, empty, or clean potential mosquito breeding areas such as buckets, drums, pots, gutters, and used tyres in and around homes. Local governments should encourage community efforts to eliminate mosquitoes in their area. Insecticide spraying may also be recommended by public health authorities.

1.5.2 Sexual transmission The Zika virus can be spread through sexual contact. This is concerning because Zika virus infection has been linked to poor pregnancy and foetal outcomes. "All people with Zika virus infection and their sexual partners (especially pregnant women) should be informed about the dangers of Zika virus sexual transmission in areas where the virus is present then the Sexually active men and women should be properly advised and offered a wide spectrum of contraceptive options, according to the WHO, so that they may make an informed decision about whether and when to become pregnant, avoiding potentially harmful pregnancy and foetal consequences and women who have had unprotected intercourse and do not want to become pregnant due to Zika virus worries should have immediate access to emergency contraception and counselling and pregnant women should engage in safer sexual behaviour (including the use of condoms correctly and consistently) or abstain from sexual activity for at least the duration of the pregnancy".

2. Formulation of Zika Virus

The model is divided into two types of sub-model human to human population and mosquito to the human population. The human population $N_H(t)$ is divided into susceptible population $S_H(t)$, Exposed population $E_H(t)$, Infected population $I_H(t)$ and recovered population $R_H(t)$, while the vector population $N_v(t)$ is divided as susceptible vector $S_v(t)$, exposed vector $E_v(t)$ and infected vector $I_v(t)$. So that, $N_H(t) = S_H(t) + E_H(t) + I_H(t) + R_H(t)$ and $N_v(t) = S_v(t) + E_v(t) + I_v(t)$[30].

$$\frac{dS_H}{dt} = \Lambda_H - \beta_H S_H(I_V + \rho I_H) - \mu_H S_H \tag{1}$$

$$\frac{dE_H}{dt} = \beta_H S_H(I_V + \rho I_H) - (\mu_H + X_H)E_H \tag{2}$$

$$\frac{dI_H}{dt} = X_H E_H - (\mu_H + \gamma + \eta)I_H \tag{3}$$

$$\frac{dR_H}{dt} = \gamma I_H - \mu_H R_H \tag{4}$$

$$\frac{dS_V}{dt} = \Lambda_V - \beta_V S_V I_H - \mu_V S_V \tag{5}$$

$$\frac{dE_V}{dt} = \beta_V S_V I_H - (\mu_V + \delta_V)E_V \tag{6}$$

$$\frac{dI_V}{dt} = \delta_V E_V - \mu_V I_V \tag{7}$$

With initial conditions $N_H(0) \geq 0$, $S_H(t) = E_H(t) = I_H(t) = R_H(t) \geq 0$ and $S_v(t) = E_v(t) = I_v(t) \geq 0$.

3. Analytical Solution of the Model Zika Virus

For various values of parameters in analytical solutions, the analytical solutions for the equation of vulnerable population, exposed host, infected host, recovered host virus free vectors, and virus-carrying vectors.

$$\begin{aligned}
&S(t) \\
&= 21.73913043 - 20.74324937e^{(-.000046000000000t)} + .1218185561e^{(-.07142800000t)} \\
&- .1161481501e^{-.0714740000t)} + .001029263746e^{(-.2001460000t)} - .0009818363041e^{(-.2001460000t)} \\
&- .0009818363041e^{(-.1214280000t)} + .0008530113865e^{(-.1428560000t)} - .00008129869204e^{(-.1429020000t)} \\
&+ .304342625310^{-5}e^{-.2715740000t)} - .290138347810^{-5}e^{(-.2716200000t)} - .03581936437e^{(-.1214280000t)} \\
&+ .03415872851e^{(-.1214740000t)} + .271436395410^{-7}e^{(-.4002920000t)} \\
&- .258861055210^{-7}e^{(-.4003380000t)}.001143562884e^{(-.01004600000t)-.001085963560}e^{(-.01009200000t)}
\end{aligned}$$

$$\begin{aligned}
E(t) = {} & -.2313132389e^{(-.01004600000t)} - .1416645299e^{(-.01004600000t)} - .1416645299e^{(-.07142800000t)} \\
& + .1350561644e^{(-.07147400000t)} - .001083407025e^{(-.2001460000t)} \\
& + .001033472221e^{(-.2001920000t)} - .00009172393351e^{(-.1428560000t)} \\
& + .00008741800107e^{(-.1429020000t)} - .315979720510^{-5}e^{(-.2715740000t)} \\
& + .301230365610^{-5}e^{(-.2716200000t)} + 03903526679e^{(-.1214280000t)} \\
& - .03722427115e^{(-.1214740000t)} - .278391915610^{-7}e^{(-.4002920000t)} \\
& + .265493552310^{-7}e^{(-.4003380000t)} - .00001143562884e^{(-.01004600000t)}t \\
& + .2371649983e^{-.01009200000t)}
\end{aligned}$$

$$\begin{aligned}
I(t) = {} & .2381333674e^{(-.2001460000t)} + .0002294452597e^{(-.0100600000t)} - .005502902852e^{(-.07142800000t)} \\
& + .005247713439e^{(-.07147400000t)} - .00001143562884e^{(-.2001460000t)}t \\
& - .2371076233e^{(-.2001920000t)}
\end{aligned}$$

$$\begin{aligned}
R(t) = {} & .001002443509e^{(-.000046000000000t)} - .0001189786196e^{(-.2001460000t)} \\
& - .229445259710^{-5}e^{(-.01004600000t)} + .770909032010^{-5}e^{(-.0714280000t)} \\
& - .734685758910^{-5}e^{(-.07147400000t)} + .571495694210^{-8}e^{(-.2001460000t)}t \\
& + .0001184673305e^{(-.2001920000t)}
\end{aligned}$$

$$S_{v(t)} = .001400011200 + .9977032423e^{(-.07142800000t)} + .927398378610^{-6}e^{(-.2001460000t)} + .004252184649e^{(-.2715740000t)} + .267892719510^{-9}e^{(-.4002920000t)} + .100960792310^{-6}e^{(-.4717200000t)} - .107981875910^{-6}e^{(-.01004600000t)} + .0004706074257e^{(-08147400000t)}$$

$$E_v(t) = .001450063636e^{(-.1214280000t)} - .151646211110^{-5}e^{(-.2001460000t)} - .005668201277e^{(-.2715740000t)} - .315925581310^{-9}e^{(-.4002920000t)} - .115371739810^{-6}e^{(-.4717200000t)} + .595082105210^{-7}e^{(-.01004600000t)} + .001183291335e^{(-.1214280000t)}$$

$$I_v(t) = .002450021086e^{(-.07142800000t)} - .001600178041e^{(-.12142800000t)} + .621771324910^{-6}e^{(-.2001460000t)} + .0001495351838e^{(-.27155740000t)}$$

Parameter	Description	Values
η	Human infected treatment rate	0.2
μ_H	The natural death rate in human	0.00004566
μ_v	The natural death rate in Mosquitoes	0.071428
Λ_H	The recruitment rate of humans	0.001
X_H	The rate of exposed humans Moving into infectious class	0.01
β_H	Probability of humans getting infected	0.2
β_V	Probability of mosquitoes getting infected	0.09
Λ_V	Mosquito recruitment rate	0.0001
δ_V	The rate flow from E_V to I_V	0.05
γ	Human recovery rate due to treatment	0.0001
ρ	Human modification parameter	0.05

Table 1: Parameters values of Zika Virus

4. Numerical Discussion

The numerical simulation solutions as an illustration achieved using the MATLAB programme are shown in this section. The parameter values utilised in the simulations are listed in Table 1. [30].

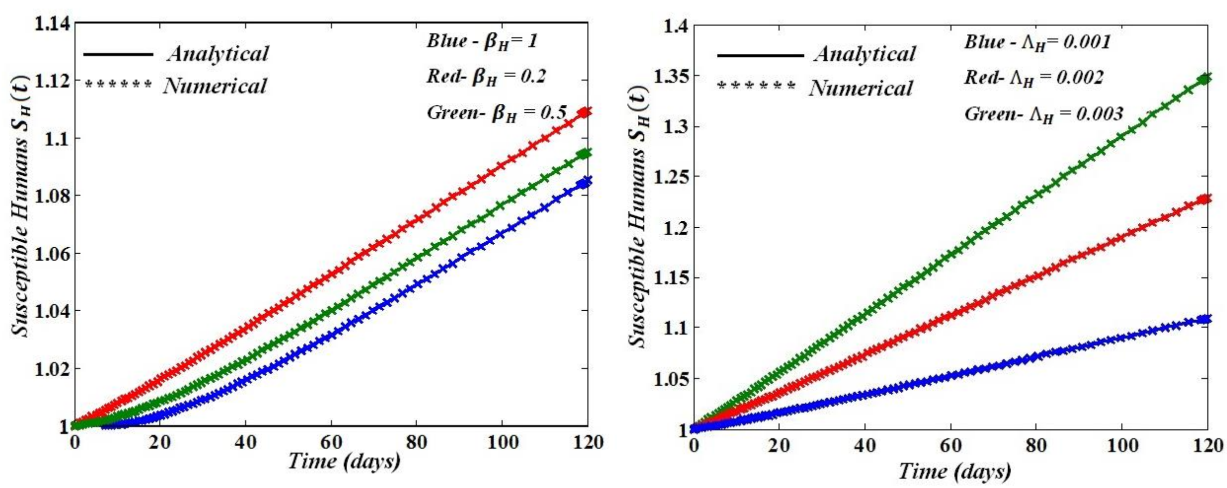

Figure 1 and 2: Variation of probability of humans getting infected and Recruitment of humans.

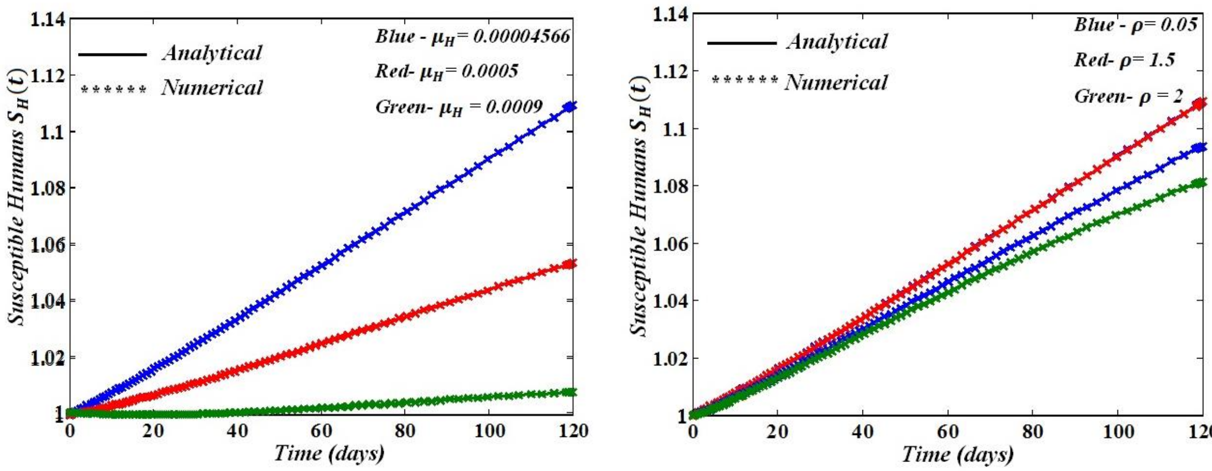

Figure 3 and 4: Natural death rate of humans and human factor transmission rate.

In figure 1, the transmission rate of the virus is going high while the β_H value is increased in the susceptible populations for 120 days. In fig 2, Λ_H is the recruitment rate of the susceptible human population. The population level is decreased if the value is increased as 0.001, 0.002, and 0.003. In figure 3, the death rate of the host population is denoted as μ_H. While increasing the value of μ_H into 0.0005 and 0.0009, the death rate of the human population decreases, so that if the transmission rate of the human population is neutral or decreased means the death rate will also decrease. In figure 4, ρ is the transmission rate factor of humans. while finding the value of ρ into 0.05, 1.5, and 2, the possibility of virus transmission among humans is decreasing for 120 days.

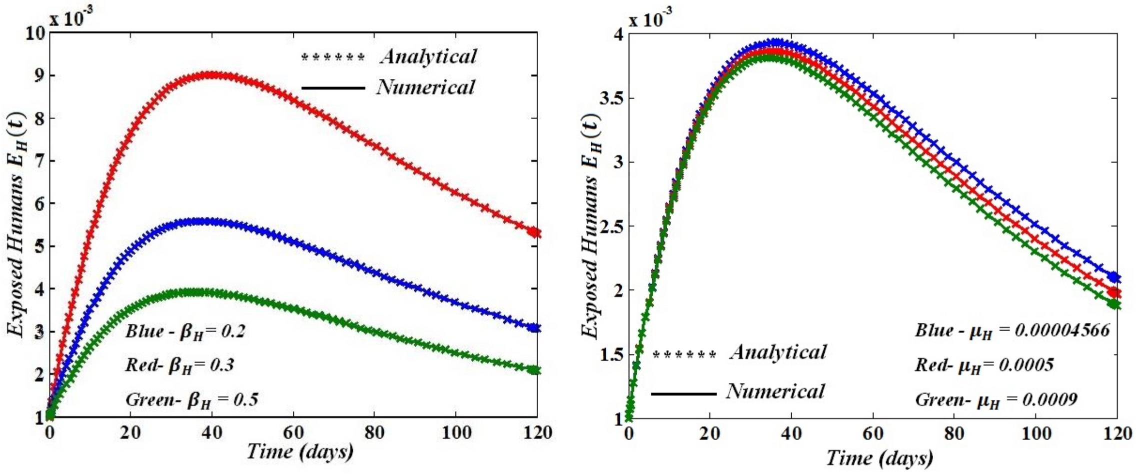

Figure 5 and 6: Variations of the probability of humans getting infected and natural death while exposed state.

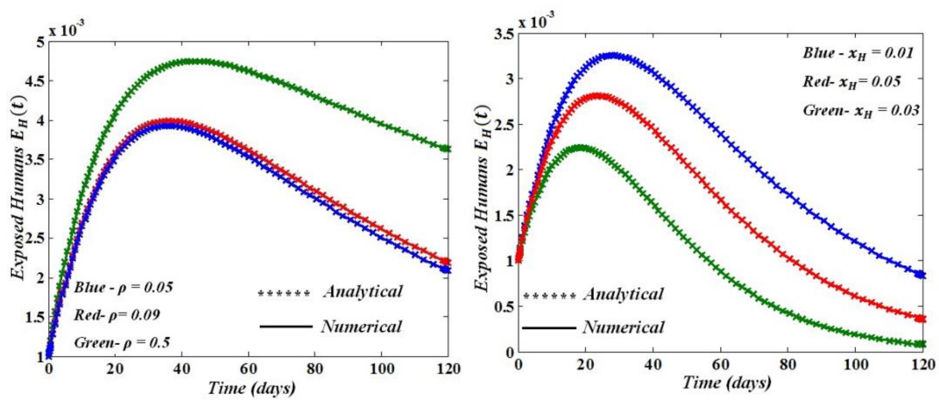

Figure 7 and 8:Transmission rate of humans and exposed humans moving into infectious class

In figure 5, the transmission rate of an exposed humans is denoted as β_H. The flow of the graph is increasing upto t=40, t=38 reached maximum and rises, if the values are increased to 0.3 and 0.5. In fig 6, μ_H is the death rate of exposed host E_H, then the values of the death rate are changed into high as 0.0005 and 0.0009, then the graph is increasing slightly. In figure 7, ρ is the human factor transmission rate. By increasing the value of ρ to 0.09 and 0.5, then the transmission rate goes high. Figure 8 shows the rate of exposed people moving into the infectious class, and boosting the values of X_H to 0.03 and 0.05 reduces the number of humans migrating into the infectious class.

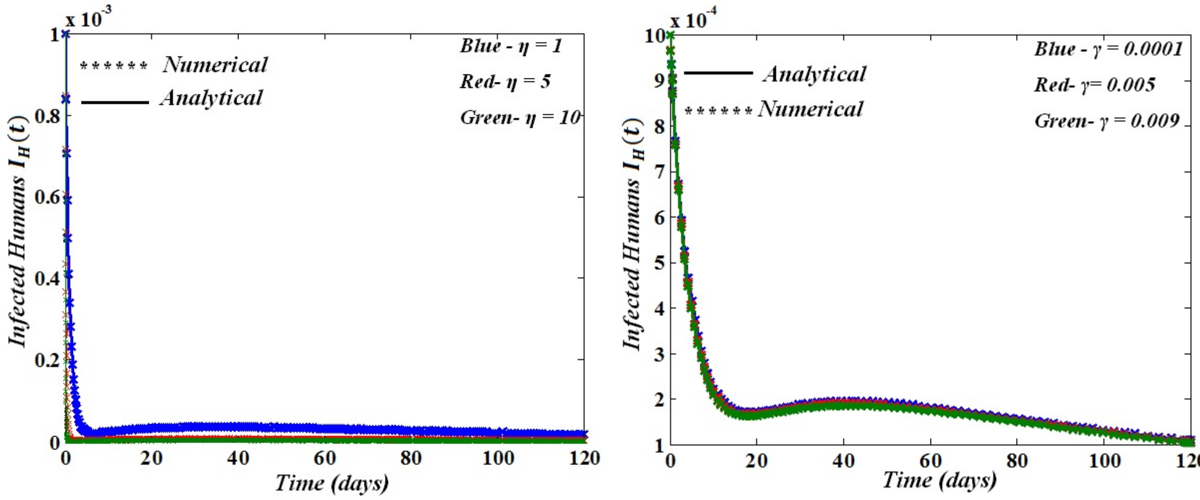

Figure 9 and 10: Rate of humans infected treatment and humans recovered due to treatment.

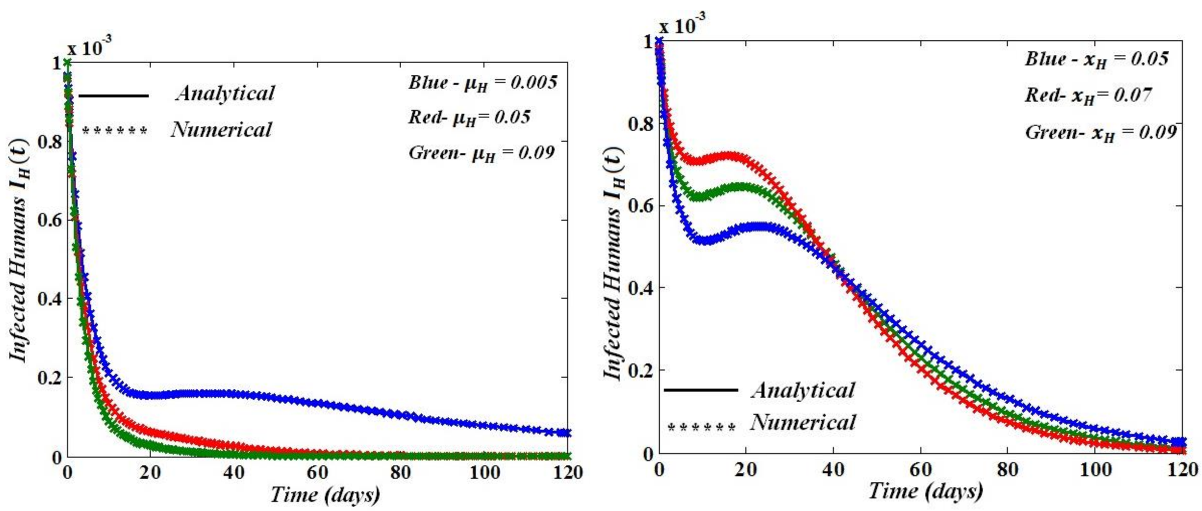

Figures 11 and 12: Natural death rate of humans and humans comes from exposed.

In Figures 9 and 10, η is the human infected treatment rate, human infected rate slightly shows the lowered difference goes down of humans treatment rate while increasing the value to 5 and 10. Similar observations can be found for human recovery rate. In figure 11, μ_H is the death rate of infected humans I_H, while varying the values into 0.05 and 0.09, then the death rate will be reduced. In figure 12, X_H is the exposed humans moving into infectious class. Here, if we increase the value to 0.07 and 0.09 then the exposed humans into infected are increases.

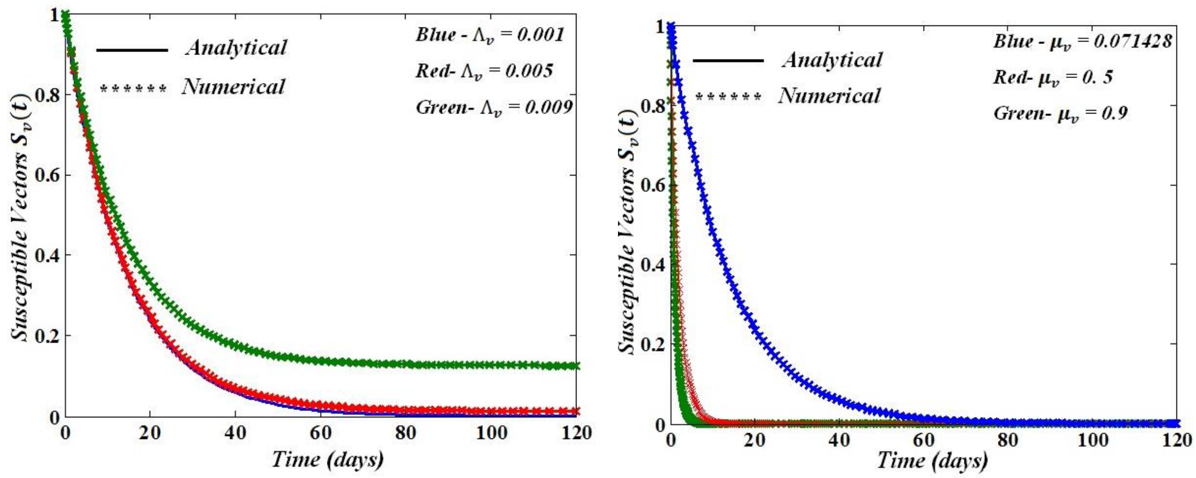

Figure 13 and 14: Mosquito recruit rate and natural death rate of mosquitoes.

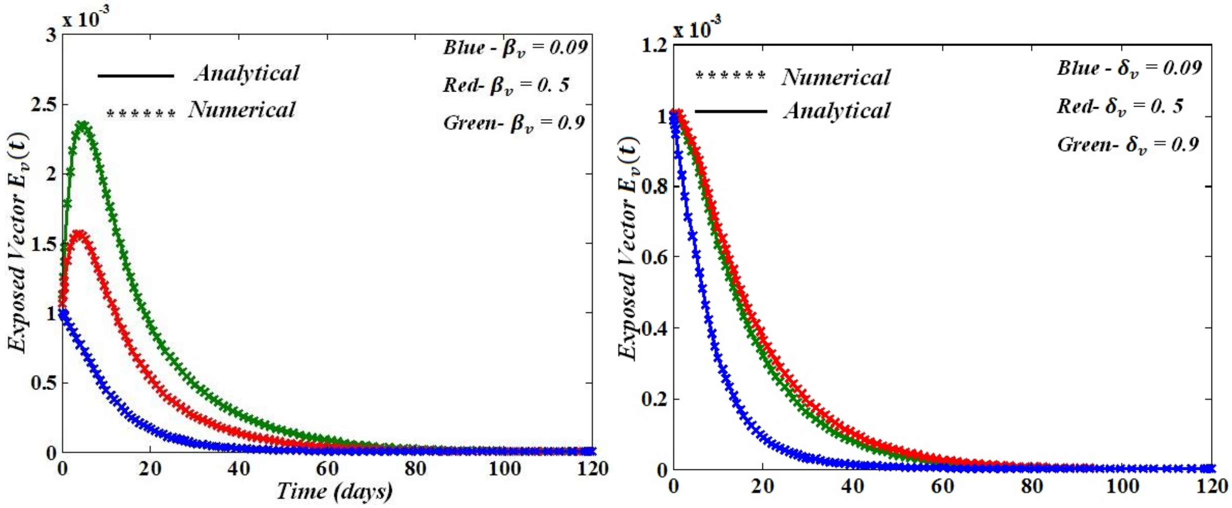

Figure 15 and 16: Transmission rate of mosquitoes infected and flow rate from exposed vector to infected vector.

In figure 13, Λ_v is the recruitment rate of mosquitoes in Susceptible Vector S_v. If the value is increased, then the vector recruit rate is increased. In fig 14, μ_v is the death rate of the vector. If the value increases to 0.5 and 0.9 then the death population is decreasing. In fig 15, β_v is the transmission rate of the exposed vector. If the values are increased to 0.5 and 0.9. then transmission rate is raised. In the same way, δ_v is increased when we vary the value into 0.5 and 0.9.

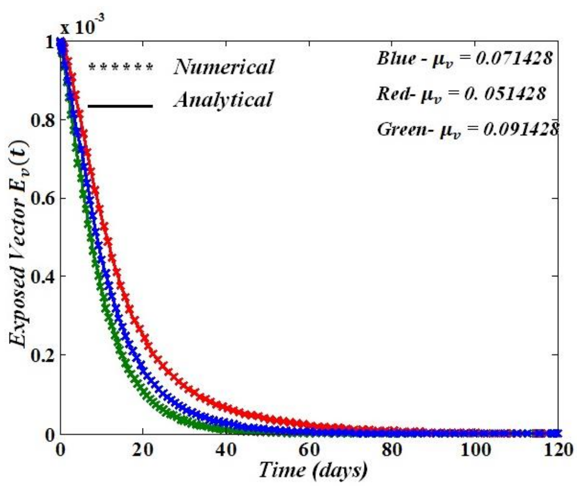

Figure 17: The natural death rate of mosquitoes.

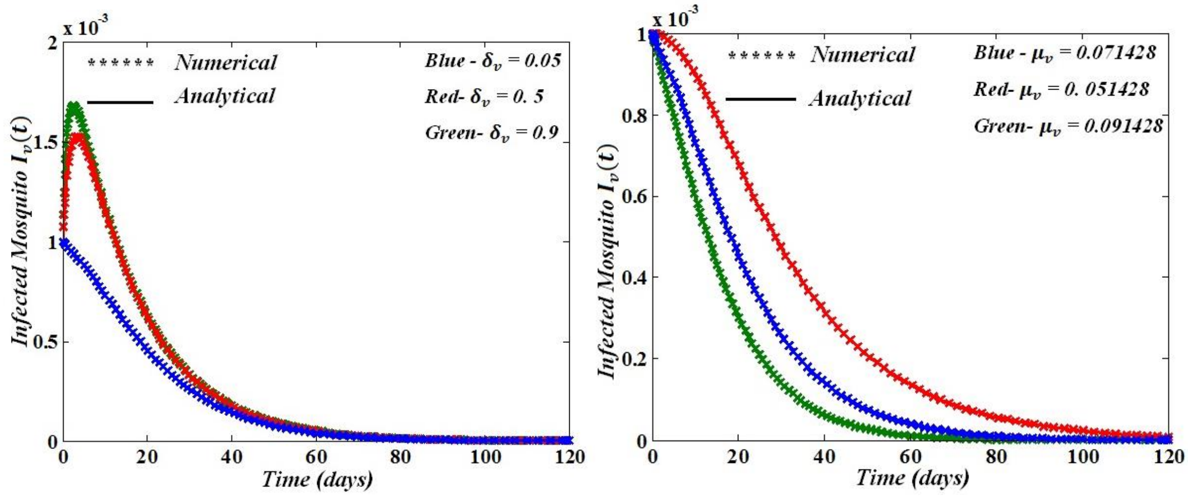

Figure 18 and 19: Rate of flow from exposure to infected vectors and death rate of mosquitoes.

In figure 17, the death rate of a vector is reduced when we increase the value of μ_v into 0.051428 and 0.091428. In figure 19, μ_v is the death rate of an infected mosquito. If the value is increased to 0.051428 and 0.091428 then the death rate of a vector is reduced.

5. Conclusion

In this paper analyzed a mathematical model for zika virus disease is the Mathematical Modeling of the Zika virus is examined in this research and using first-order nonlinear differential equations. The Homotopy Perturbation Method (HPM) is used to approach the analytical solutions, and MATLAB programming is used to obtain the simulation results are also found. For all values of dimensionless parameters, the HPM is used to produce simple and approximate dimensionless concentrations. The HPM is a straightforward method that has the potential to solve other nonlinear problems. This method is quick and efficient, and it can reduce the number of computations in simulations of this model greatly.

Acknowledgments: Shri J. Ramachandran, Chancellor, Col., and Dr. G. Thiruvasagam, Vice-Chancellor, Academy of Maritime Education and Training (AMET), Chennai, Tamil Nadu, are also acknowledged.

Ethical Clearance: AMET University, Chennai.

Source of funding: Self

Conflict of interest: Nil

Data Availability:

The data used to support this deterministic model is from previously published articles, which have been properly cited in this research. Table 1 of this work lists the parameter values taken from published studies. These published articles are also referenced in the text at appropriate points.

Appendix A: The Homotopy Perturbation Method's Fundamental Principle (HPM)

Consider the following nonlinear functional equation to highlight the essential elements of this technique:

$$P(z) - R(s) = 0, s \in \Omega \tag{A1}$$

$$\mathrm{U}\left(z, \frac{\partial z}{\partial t}\right) = 0, s \in \Gamma \tag{A2}$$

P indicated functional operator, R is a boundary operator, R(s) for a known analytical equation, and Ω the limit of the domain Γ. M and R, with M denoting linear and R denoting nonlinear.

$$M(z) + R(z) - R(s) = 0 \tag{A3}$$

We create a homotopy equations using the homotopy procedure,

$$K(z,V) = (1-V)[M(z) - M(z_0)] + V(F(z) - R(s)] = 0, V \in [0,1], s \in \Omega \quad \text{(A4)}$$

or

$$K(z,V) = M(z) - M(z_0) + VM(z_0) + V[R(z) - R(s)] = 0 \quad \text{(A5)}$$

$V \in [0,1]$ is an parameter, For the solution of Equation, z_0 is an initial approximation. (A2), which meets the border requirements. Clearly, we may deduce the following from Eqns. (A4) and (A5):

$$K(z,0) = M(z) - M(z_0) = 0 \quad \text{(A6)}$$

$$K(z,1) = P(z) - R(s) = 0 \quad \text{(A7)}$$

Altering V's value from zero to unity corresponds to changing $z(s,V)$ value from $z_0(s)$ to $z(s)$. This is known as homotopy in topology. The embedding parameter can be used as a tiny parameter, and The solution of Equations (A4) and (A5) can be assumed to be a power series in V:

$$U = z_0 + Vz_1 + V^2 z_2 + \ldots \quad \text{(A8)}$$

Setting V = 1, approximation to Eqn's solution. (A8)

$$z = \lim_{Q \to 1} U = z_0 + z_1 + z_2 + \cdots \quad \text{(A9)}$$

The homotopy perturbation method (HPM) is a mixture of the perturbation method and the homotopy method that has overcome the constraints of classic perturbation approaches. For additional situations, the series Eqn. (A9) is convergent.

References

1. Simpson DI. Zika Virus Infection in Man. Trans Royal Soc Trop Med Hyg. 1964;
   58:33±58. https://doi. org/10.1016/0035-9203(64)90201-9.
2. Duffy MR, Chen TH, Hancock WT, Powers AM, Kool JL, Lanciotti RS, et al. Zika virus outbreak on Ya Island, Federated States of Micronesia. The New Eng Jour med. 2009; 360: 36±43. https://doi.org/10. 1056/NEJMoa0805715.
3. Centers for Disease Control and Prevention (CDC), CDC Emergency Operations Center moves to highest level of activation for Zika response, February 3, 2016. http://www.cdc.gov/media/releases/2016/s0208-zika-eocaactivation.html, Accessed on February 26, 2016.
4. Pan American Health Organization (PAHO), Zika virus infection. http://www.paho.org/hq/index.php?option=com_content & view= article & id = 11585 & Itemid = 41688 & lang = en. ,Accessed on May 16, 2016.
5. Ebenezer B and Kazeem O O 2016, Mathematical modeling of Zika virus, Asian Pac J Trop Dis; **6**(9): 673-679.
6. Victor M M, Baltazar E, Derdei B, Susan A H and Carlos C C 2016 Role of short-term dispersal on the dynamics of Zika virus in an extreme idealized environment, Infectious Disease Modelling **2** (2017) 1-14.
7. Schwartz DA. The origins and emergence of Zika virus, the newest TORCH infection: what's old is new again. Arch Pathol Lab Med **2017**; 141:18–25.
8. Dick GW, Kitchen SF, Haddow AJ. Zika virus. I. Isolations and serological specificity. Trans R Soc Trop Med Hyg **1952**; 46:509–20.
9. Wikan N, Smith DR. First published report of Zika virus infection in people: Simpson, not MacNamara. Lancet Infect Dis **2017**; 17:15–7.
10. Kuno G. Serodiagnosis of flaviviral infections and vaccinations in humans. Adv
    Virus Res **2003**; 61:3–65.
11. World Health Organization. Situation Report. Zika Virus Microcephaly Guillain- Barré Syndorme.
12. Faye O, Freire CC, Iamarino A, et al. Molecular evolution of Zika virus during its emergence in the 20th century. PLoS Negl Trop Dis **2014**.

13. Savage HM, Fritz CL, Rutstein D, et al. Epidemic of dengue-4 virus in Yap State, Federated States of Micronesia, and implication of Aedes hensilli as an epidemic vector. Am J Trop Med Hyg **1998**; 58:519–24.

14. Cao-Lormeau V, Blake A, Mons S, et al. Guillain-Barré syndrome outbreak caused by Zika virus infection in French Polynesia: a case-control study. Lancet **2016**; 387:1531–9.

15. Li M and Muldowney J S 1996 A geometric approach to global stability problems. *SIAM J Math Anal* **27**(4):1070–1083.

16. Srivastav A K and Ghosh M 2016 Modeling and analysis of the symptomatic and asymptomatic infections of swine flu with optimal control, *Model.Earth Syst. Environ., Springer International Publishing Switzerland,* **2**:177, DOI 10.1007/s40808-016-0222-7

17. Lenhart S and Workman J T 2007 *Optimal control applied to biological models. Crc Press.*

18. Schwartz DA. The origins and emergence of Zika virus, the newest TORCH infection: what's old is new again. Arch Pathol Lab Med **2017**; 141:18–25.

19. Dick GW, Kitchen SF, Haddow AJ. Zika virus. I. Isolations and serological specificity. Trans R Soc Trop Med Hyg **1952**; 46:509–20.

20. Musso D, Gubler DJ. Zika virus. Clin Microbiol Rev **2016**; 29:487–524.

21. Macnamara FN. Zika virus: a report on three cases of human infection during an epidemic of jaundice in Nigeria. Trans R Soc Trop Med Hyg **1954**; 48:139–45.

22. Hennessey MJ, Fischer M, Panella AJ, Kosoy OI, Laven JJ, Lanciotti RS, Staples JE. Zika virus disease in travelers returning to the United States, 2010-2014. Am J Trop Med Hyg. 2016 Jul 6;95(1):212-5.

23. Walker WL, Lindsey NP, Lehman JA, et.al. Zika Virus Disease Cases – 50 States and the District of Columbia, January 1-July 31, 2016. MMWR Morb Mortal Wkly Rep. 2016 Sep 16;65(36):983-6.

24. Hall V, Walker WL, Lindsey NP, et.al. Update: Noncongenital Zika Virus Disease Cases – 50 U.S. States and the District of Columbia, 2016. MMWR Morb Mortal Wkly Rep. 2018 Mar 9;67(9):265-269.

25. Adams LE, Martin SW, Lindsey NP, et.al. Epidemiology of dengue, chikungunya, and Zika virus disease in the US States and Territories, 2017. Am J Trop Med Hyg 2019;101(4);884–890.

26. Jiya, M. Application of Homotopy Perturbation Method for the Solution of Some Non-Linear Differential Equations. Pacific Journal of Sciences and Technology. (2010), 11(2): 268-272.

27. He, JH (2000). A coupling method of Homotopy technique and perturbation technique for nonlinear problems, *International Journal of Non-Linear Mechanic*, 35(1): 37-43.

28. S.Rekha, P. Balaganesan, J. renuka, Homotopy Perturbation Method for Mathematical Modelling of Dengue Fever, Journal of Physics: Conference Series, **1724** (2021) 012056, 1742-6596.

29. S.Rekha, P. Balaganesan, J. renuka, "Homotopy Perturbation Method for Mathematical Modeling of Listeriosis and Anthrax Diseases", Annals of R.S.C.B., ISSN:1583-6258, Vol. 25, Issue 4, 2021, Pages. 9787 - 9809.

30. Ebenezer Bonyah, Muhammad Altaf Khan, K. O. Okosun, Saeed Islam, "A theoretical model for Zika virus transmission", https://doi.org/10.1371/journal.pone.0185540 October 4, 2017.

31. Rajendran L, Rahamathunissa G, The Application of He's variational iteration method to nonlinear boundary value problems in enzyme-substrate reaction diffusion processes : Part 1 The steady-state amperometric response, Journal of Mathematical Chemistry 44

(2008) 849-869.

32. Saranya K ,Mohan V, Kizek R, Fernandez C and Rajendran L, Unprecedented homotopy perturbation method for solving nonlinear equations in the enzymatic reaction of glucose in a spherical matrix, Bioprocess and Biosystems Engineering,41(2), (2018), 281-294.

33. Rajendran L, Anitha S, Reply to "Comments on analytical solution of amperometric enzymatic reaction sbasedon Homotopy perturbation method, " by Ji-Huan He, Lu-Feng Mo Electrochimica Acta 102(2013)474 - 476.

12. Mathematical Analysis of Virotherapy Treatment of Cancer

Balaganesan P[1], [2]S.Muthuvel, [3]J.Kavitha and [4] R.Usha

[1] Department of Mathematics, AMET Deemed to be University, Chennai
[2] Department of Computer Science, AMET Deemed to be University, Chennai
[3] Department of Mathematics, DG Vaishivna College, Chennai
[4] Research Scholar,Department of Mathematics, AMET Deemed to be University, Chennai

Abstract: A virotherapy model in cancer is identified and analyzed in the paper. A mathematical model in virotherapy to treat cancer is identified in the paper. The mathematical model is introduced by Friedman. The mathematical model is constructed through nonlinear differential equations. The nonlinear differential equation in virotherapy is given by "the count of cancer cells, the count of infected cancer cells, the count of dead cells, and the count of virus cells that do not belong to tumor cells. The parameters in virotherapy include infection rate of cancer cells by viruses, proliferation rate of cancer cells, rate of removing cell loss resulting from dead cells, death rate of infected cancer cells, and count of virus cells that are not contained in cancer cells." Homotopy Perturbation Method is used to solve nonlinear differential equation in virotherapy. The numerical values in mathematical model in cancer virotherapy consist of variation in parameters values. The numerical values are utilized to identify the effect of optimal control in reducing the effect of cancer cell via numerical graphical design. The numerical graphical model clearly identified that optimal control in virotherapy can greatly reduce the effect of cancer cells.Significant agreement is generated by comparing the results from approximate analytical calculations and numerical simulations.

Keywords: Nonlinear Differential Equations, Count of Cancer Cells, Count of Infected Cancer Cells, Count of Dead Cells, The Death Rate of Infected Cancer Cells, Homotopy Perturbation Method.

1. Introduction

There will be a startling rise in the number of cancer diseases, as evident by the sheer number of new cases of cancer diagnosed, as indicated by the statistics of 17,000,000 new cases of cancer recorded in the year 2018, and the estimated 23.6 million people will be affected by cancer in the year 2030 [1, 2]. Moreover, it is suggested that by the year 2030, cancer will cause the demise of almost 20 million people every year. Thus, it is of the utmost importance that numerous branches of science and technology work tirelessly to better develop the progress of treatments for this disease. A broad class of diseases, referred to as cancers, involves recurring and uncontrolled proliferation and metastasis of cancerous cells. A type of tumor that consists of masses of tissue is referred to as a solid tumor. A type of cancer that affects the blood is called the leukemia type of cancer. There are two types of cancer: the benign type of tumor, which does not metastasize, and the malignant type of tumor, which metastasizes in a malicious manner[3]. At present, an assortment of therapeutic techniques has been adopted by oncologists to retard the development of cells forming tumors, leading to the eventual death of cancerous cells. It has been observed that the kind of cancer infection, the level at which cancer had developed at the time of diagnosis, the age of an individual undergoing cancer, as well as an assortment of therapeutic techniques, has a profound impact on the survival rate of an individual afflicted with such a disease. For example, prostate and pancreatic cancer have resulted in the highest and lowest survival rates of 99.2 percent and 6 percent respectively [3]. As mentioned earlier, some of the common treatments for cancer include surgery, chemo, radiotherapy, immunotherapy, hormonal therapy, and stem cell transplantation. At times, as described here, combination therapy for cancer becomes more important to totally destroy cancer cells and reduce or eradicate the possibility of recurrence of cancerous cells in an individual's body [4-7].

Combination therapy is typically used in order to benefit from the synergetic effect of certain cancer drugs and avoid adverse therapy-related side effects. For example, some chemotherapeutic agents can be used to make the tumor more susceptible to radiotherapy. The success rate of patients undergoing radiation therapy after chemotherapy will consequently be enhanced. Another example is the use of chemotherapy or radiation in conjunction with stem cell therapy [8]. The bone marrow cells, which make blood cells, are usually damaged by large doses of chemotherapy and radiation. After that damage, there is a transplantation of the stem cells.

Various therapeutic strategies are adopted by oncologists to retard the development of tumor formation while curing cancer. Combination therapy or the application of different therapeutic strategies at particular times is normally used to cure cancer while reducing the risk of relapse. In this book [13], various models are classified based on different therapeutic strategies used (combination therapy) or therapy (monotherapy). The different therapeutic strategies proposed are: Chemotherapy – Application of a number of medicinal products to cure cancer;Increasing white blood cells, in addition to the use of different medicinal drugs, is referred to as immunotherapy; Anti-angiogenic therapy involves the use of anti-angiogenic drugs to stop the formation of vessels in cancer and accelerate the treatment of the disease; During radiotherapy, the use of radiation is seen as a therapy to treat cancer; Hormone therapy is seen as a treatment that utilizes hormones or other drugs looking to regulate hormone production in the body to treat cancer; Unrelated treatments include stem cell therapy, radio virotherapy, gene therapy, and many other procedures that use a number of treatment agents for the management of cancer [13].

It is hard to explain the entire picture about how cancer behaves using different cells, as Most of the above mentioned therapeutic approaches have a number of complex systems/cell types. In addition, many of the above evaluations, which have previously been published, have pointed out that simple mathematical models, especially those focusing on different cells, are generally so generic that they are inappropriate, especially in showing how therapy actually affects the dynamics of cancer [9]. It is important to show how all these cells interact, especially in terms of conflict and coexistence, while simulating the dynamics of cancer using mathematics, in addition to showing how these cells grow and die [10].

Cancer is treated through various methods, and some of the methods either destroy the cancerous cells while others influence the bodies of the cancer in a way that they become resistant to the multiplication of the cancerous cells. An anti-cancer drug called virosophy uses virus particles to kill the cells. This type of virus is harmful to the cancerous cells but does not kill the normal cells due to the genetic changes. This type of virus is called the oncolytic virus, which means it causes cancer. Physical injection of the virus into the cancer. The virus once inside the cancer grows quickly and, in the process, several of the virus cells burst when the normal cell dies.

In the present work, techniques of Homotopy perturbation are employed to study the mathematical model of certain clauses of Virotherapy. It should be noted that unlike other results presented in the literature, the present research has not yet been mathematically investigated. On the other hand, the comparison between the numerical and mathematical results has not yet been performed. As there is no method to find the solution of the system of non-linear differential equations for the constructed model, an attempt is made to find the answer to the system of equations with the help of semi-analytical methods like the Homotopy Perturbation method. As per the analysis of the model, the pre-requirements for ideal control were discovered by Friedman et al1 [1]. Our results are the best to understand the simplified virotherapy model for the treatment of cancer.

2. Mathematical Formulation of Virotherapy Model

"Tumor, after ingoing a cancer cell, a virus activates and rapidly reproduces, and then lots of virus cells come out and spread to other cancer cells. Variables as the model developed by Friedman [11] et al. introduced: "x = count of cancer cells, y = count of infected cancer cells, n = count of dead cells, v = count of virus particles which are not contained in cancer cells". Virotherapy is defined by the following system of equations:

$$\frac{dx}{dt} = \alpha x(t) - \beta x(t)v(t) \quad (1)$$

$$\frac{dy}{dt} = \beta x(t)v(t) - \delta y(t) \quad (2)$$

$$\frac{dn}{dt} = \delta y(t) - \mu n(t) \quad (3)$$

$$\frac{dv}{dt} = b\delta y(t) - \gamma v(t) \quad (4)$$

The initial conditions are,

$$x(0) = a \geq 0,\ y(0) = b \geq 0, n(0) = n_0 \geq 0, v(0) = v_0 \geq 0 \quad (5)$$

Table 1. Description and parameter values of the Virotherapy model [*]

Symbol	*Description*	*Values*
α	Proliferation rate of cancer cells	0.02
β	viral transmission rate of tumor cells	7×10^{-8}
δ	Mortality rate of tumor cells with infection	1/18

μ	Elimination rate of deceased damaged cells	1/48
γ	Growth factor	2.5×10^{-2}
b	Reproduction rate of an infection at the time the tumor cell it infected died	50

3. Approximate analytical expression of Virotherapy using Homotopy Perturbation Method

HPM is used to solve non-linear Eqs. (1)-(5)

$$(1-M)\left(\frac{dx}{dt}-\alpha x(t)\right)+M\left(\frac{dx}{dt}-\alpha x(t)+\beta x(t)v(t)\right)=0 \quad (6)$$

$$(1-\mathrm{M})\left(\frac{\mathrm{dy}}{\mathrm{dt}}+\delta y(t)\right)+\mathrm{M}\left(\frac{dy}{dt}-\beta x(t)v(t)+\delta y(t)\right)=0 \quad (7)$$

$$(1-M)\left(\frac{\mathrm{dn}}{\mathrm{dt}}+\mu n(t)\right)+M\left(\frac{dn}{dt}-\delta y(t)+\mu n(t)\ \right)=0 \quad (8)$$

$$(1-M)\left(\frac{\mathrm{dv}}{\mathrm{dt}}+\gamma v(t)\right)+M\left(\frac{dv}{dt}-b\delta y(t)+\gamma v(t)\right)=0 \quad (9)$$

The solution of equation (6) - (9) is expressed in power series:

$$x=x_0+Mx_1+M^2x_2+M^3x_3+\cdots \quad (10)$$

$$y=y_0+My_1+M^2y_2+M^3y_3+\cdots \quad (11)$$

$$n=n_0+Mn_1+M^2n_2+M^3n_3+\cdots \quad (12)$$

$$v=v_0+Mv_1+M^2v_2+M^3v_3+\cdots \quad (13)$$

Equation (10)-(13) into Equation (6)-(9) and order the coefficients of the powers of M produce the following systems of differential equations:

$$M^0: \frac{dx_0}{dt}-\alpha x_0$$

$$M^1: \frac{dx_1}{dt}\pm\alpha x_1+\beta x_0v_0 \quad (14)$$

$$M^2: \frac{dx_2}{dt}\pm\alpha x_2+\beta x_1v_0+\beta x_0v_1$$

$$M^0: \frac{dy_0}{\mathrm{dt}}+\delta y_0$$

$$M^1: \frac{dy_1}{\mathrm{dt}}+\delta y_1-\beta x_0v_0 \quad (15)$$

$$M^2: \frac{dy_2}{\mathrm{dt}}+\delta y_2-\beta x_1v_0+\beta x_0v_1$$

$$M^0: \frac{d\mathrm{n}_0}{\mathrm{dt}}+\mu\mathrm{n}_0$$

$$M^1: \frac{d\mathrm{n}_1}{\mathrm{dt}}+\mu\mathrm{n}_1-\delta y_0 \quad (16)$$

$$M^2: \frac{d\mathrm{n}_2}{\mathrm{dt}}+\mu\mathrm{n}_2-\delta y_1$$

$$M^1: \frac{d\mathrm{v}_1}{\mathrm{dt}}+\gamma\mathrm{v}_1-b\delta y_0 \quad (17)$$

$$M^2: \frac{d\mathrm{v}_2}{\mathrm{dt}}+\gamma\mathrm{v}_2-b\delta y_1$$

4. Analytical Expression of Virotherapy

The analytical solution of equations (1) through (5) is solved in this part using a homotopy perturbation method, and the extended derivative of the HPM is provided below. $x(t) = 0.000008e^{(0.20t)} + 0.00000000000000000224e^{(0.175t)}$

$$y(t) = 0.000001e^{(-0.05556t)} + 0.00000000000002429e^{(0.175t)} \quad (19)$$

$$n(t) = 0.000002599e^{(-0.0209t)} - 0.000001599e^{(-0.05556t)} \quad (20)$$

$$v(t) = 0.0000001909e^{-0.0250t} - 0.00000009091e^{(-0.05556t)} \quad (21)$$

5. Numerical Results and Discussion

A comparison is made between the numerical solution and the analytical results. This comparison is shown graphically in Figures (1) - (9).

Figure 1 indicates the densities of cancer cells with regard to time, thus depicting that when the growth rate of cancer cells increases, so does their population, which increases steadily over time. Figure 2 depicts the population of cancer cells that are infected with the virus over time, thus showing that when the rate of cancer cell infection diminishes, so does the cell population. Figure 3, on the other hand, displays the population of cancer cells infected with the disease with respect to time. It is observed that with an increase in mortality rate of cancer cells suffering from the disease, there is a slight change in the number of cancer cells. Figure 4 depicts that when the value of increases, the number of count of dead cells is also increasing, which reaches the peak value at t = 13 and is gradually increasing with respect to time. Figure 5 depicts that when the removal rate debris of dead cells increases, then the number of count of dead cells decreases with respect to time. Figure 6 depicts that when the value of b is decreased, then the number of count of virus particles not in the cancer cell is increasing up to t = 7 and then starts decreasing rapidly with respect to time. Figure 7 depicts that when the value of decreases, then the number of count of virus particles not in the cancer cell is decreasing gradually with respect to time.

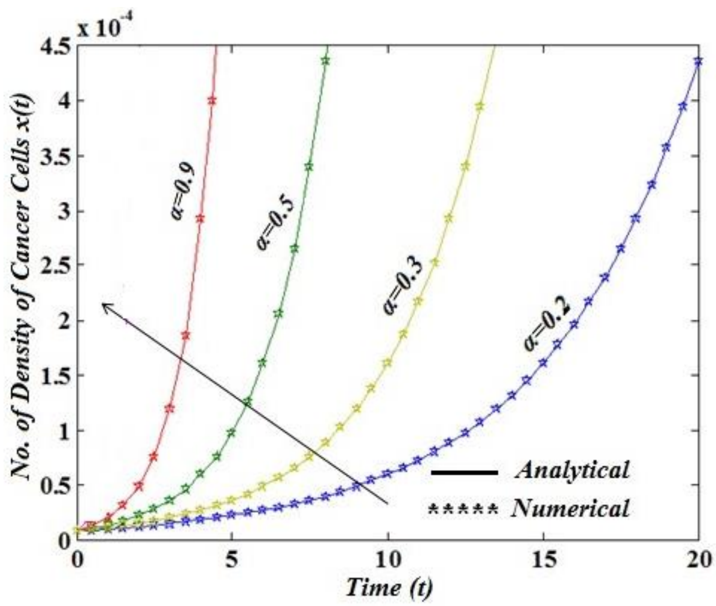

Figure 1: Variation of Number of densities of Cancer cells

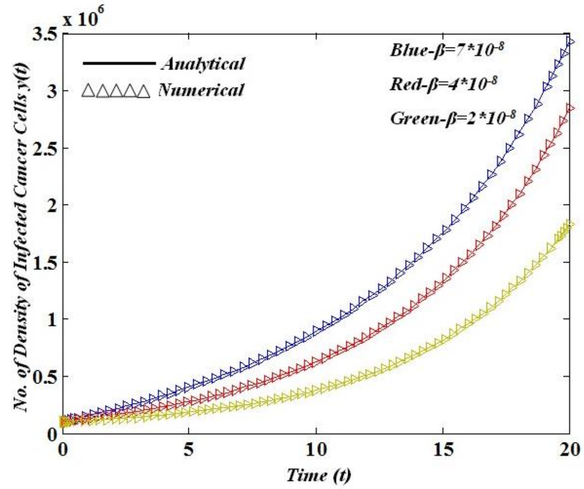

Figure 2: Variation of infected individuals birth rate and contact rate

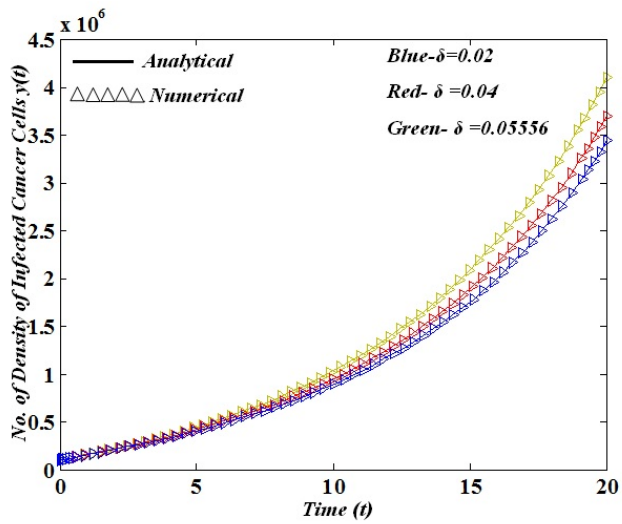

Figure 3: Variation of individuals birth rate and contact rate

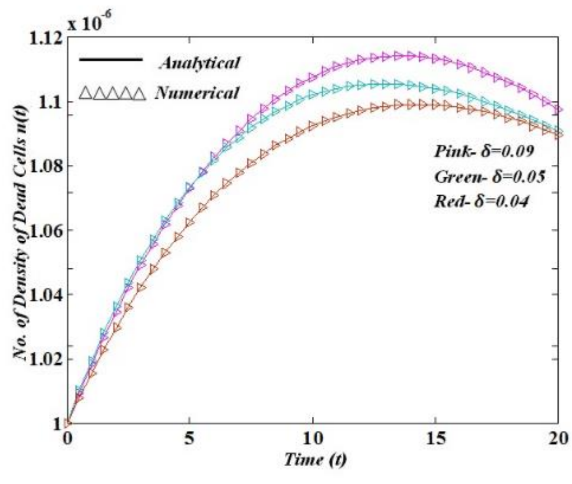

Figure 4: Count of dead cells

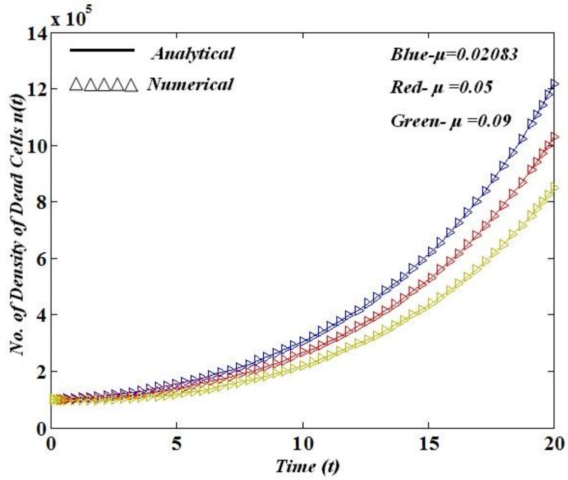

Figure 5: Comparison of dead cellscount

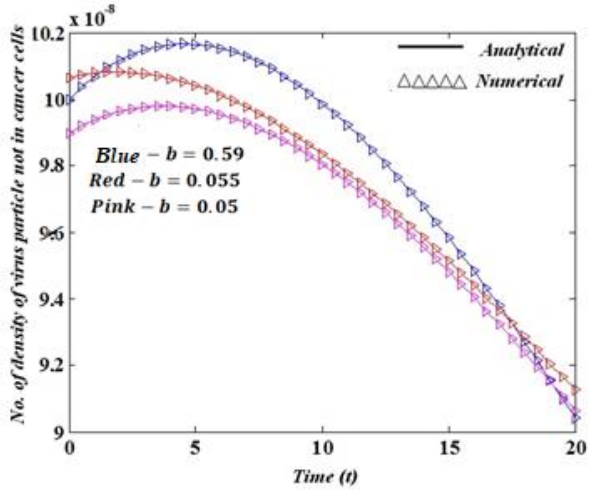

Figure 6 Comparison of count of virus particles that are not contained in cancer cellsFigure 8 shows that when the value of "b" decreases, the number of virus particles outside the cancer cells starts to reduce gradually with time.

Figure 9 illustrates the case when there is an increase in the value of then the count of the cancer cells for the infected is increasing gradually over.

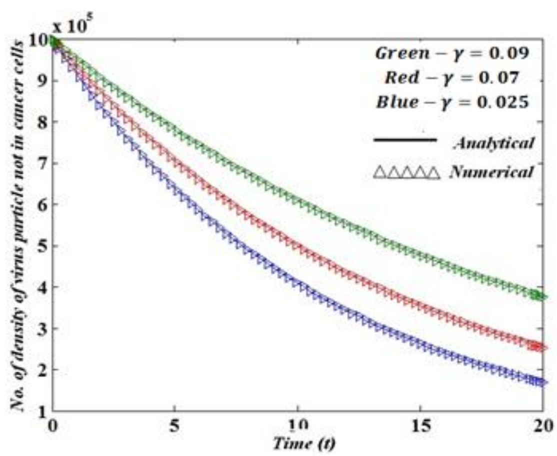

Figure 7: The count of γ virus particles not contained in cancer cells

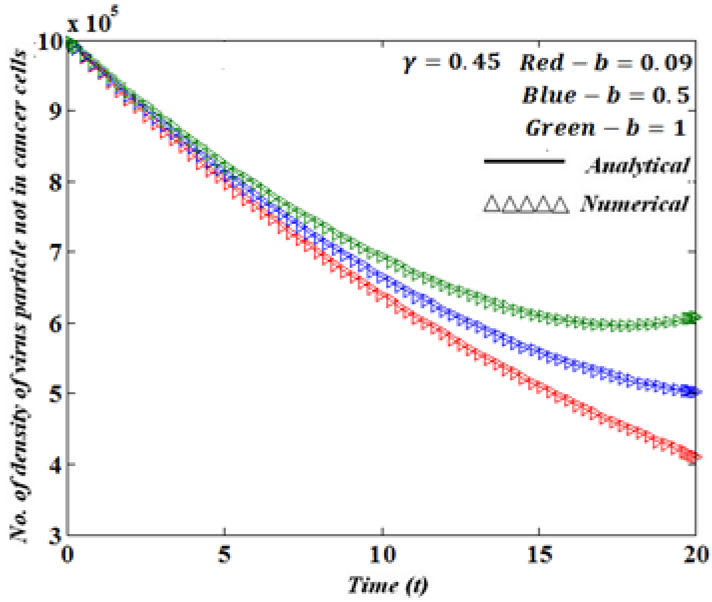

Figure 8: Thecount of γ, b virus particles not contained in cancer cells

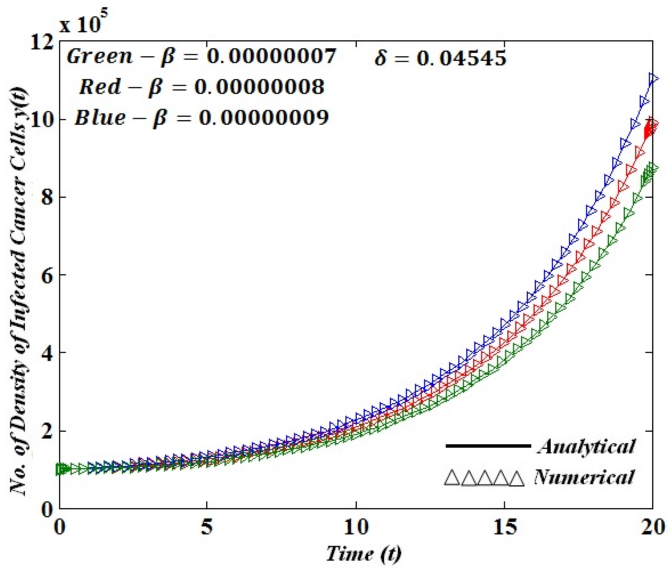

Figure 9: The count of β, γ virus particles not contained in cancer cells

5. Conclusion

The essential equation of virotherapy mathematics can be stated as: "the equation is a system of nonlinear differential equations; it contains = count of cancer cells, = count of infected cancer cells, = count of dead cells, = count of virus particles which are not contained in cancer cells". Nonlinear differential equation solutions are achieved analytically with the aid of homotopy perturbation method (HPM) technique. In this paper, solutions to the virotherapy equation were achieved analytically using the homotopy perturbation method, and this was seen to have worked well with the numerical solution. Variations in parameterization are shown in the above equation, and this is done graphically in MATLAB programming. It is also important to note that numerical solutions are achieved with the aid of MATLAB programming using "ode45 function," which has a clear consistency with the above solutions. Variation of the parameters in the graph suggest some possible values for: growth factor, the number of viral replications when the cancer cell which was infected died, rate of proliferation of cancer cells, rate of infection of viruses to cancer cells, rate of death of diseased tumor cells and rate of removal of dead cell debris. Control parameters have a big impact.

Application of this model :Includes the determination of optimum controllability of diseases by comparing the number of virus particles contained and not contained in the cancerous cell.Means to that assist us with greatly reducing the impact of the cancer cell has been discussed.

Acknowledgments: The author is very much thankful to Dr. Lilian Jasper, Principal and Management, Women's Christian College, Chennai, Tamilnadu, India.

References

1. Worldwide cancer statistics, technical report, Cancer Research, UK,https://www.cancerresearchuk.org/health-professional/cancer-statistics /worldwide-cancer
2. Cancer statistics, technical report, National Cancer Institute, https://www.cancer.gov/about cancer/understanding/statistics.
3. Cancer survival rate statistics by type of cancer. Statistics from the period between 2003 and 2009, www.cancer.gov/statistics. Accessed 31 Aug 2019.
4. Bayat Mokhtari R, Homayouni TS, Baluch N, Morgatskaya E, Kumar S, Das B, Yeger H. Combination therapy in combating cancer, Oncotarget. 2017; 38022–38043.
5. Khan K, Kerbel R. Improving immunotherapy outcomes with anti-angiogenic treatments and vice versa, Nature reviews clinical oncology. 2018; 15, 310.
6. Teles FF, Lemos JM. Cancer therapy optimization based on multiple model adaptive control,Biomed. Signal Process. Control 48. 2019; 255–264.
7. Babaei N, Salamci MU. Mixed therapy in cancer treatment for personalized drug administration using model reference adaptive control. European journal of control 50. 2019; 117–137.
8. Child JA, Morgan GJ, Davies FE, Owen RG, Bell SE, Hawkins K, Brown J. High-Dose Chemotherapy with Hematopoietic Stem-Cell Rescue for Multiple Myeloma. The new England journal of Medicine, 2003; 348.1875-1883
9. Drayson, Selby PJ. High-dose chemotherapy with hematopoietic stem-cell rescue for multiple myeloma. The new England journal of medicine. 2003; 348(19), 1875–1883.
10. Eftimie R, Bramson JL, Earn DjD, Interactions between the immune system and cancer: 33brief review of non-spatial mathematical models. Bulletin of Mathematical Biology. 2011; 73(1), 2–32.
11. Pillis LJD, Radunskaya A, A mathematical tumor model with immune resistance and drugtherapy: an optimal control approach. Computational and Mathematical Methods Medicine. 2001; 3(2), 79–100.
12. Friedman A, Tian JP, Fulci G, Chiocca EA, Wang J. Glioma virotherapy: the effects of innate immune suppression and increased viral replication capacity. Cancer Research. 2006; 66, 2314– 2319.

13. CONCENTRATION OF CONTAMINANTS IN GROUNDWATER

[1]A.Selvaraj , [2]P.Ramanathan and [3]R.Yokeshwari

Professor, Department of Mathematics, Vels Institute of Science, Technology and Advanced Studies, Chennai-600117.

[2]Department of Mechanical, AMET Deemed to be University, Chennai.

[3]Department of Mathematics, AMET Deemed to be University, Chennai.

Abstract: Groundwater pollutes by leachate is the most harming ecological effect over the whole existence of a hazardous waste landfill (HWL). To date, the percolation of bacteria and viruses through landfill leachate into the groundwater table poses a potential risk and potential hazards towards the public health and the ecosystem, remains an aesthetic concern. In this paper, we developed a mathematical model to study the mean concentration of contaminants (bacteria and viruses) by leachate, employing generalized-dispersion technique. Solute transport in porous media is discussed by means of advection - dispersion equation. The dispersion and mean concentration are obtained by Generalized-Dispersion method . Results are obtained analytically and the numerical values are computed graphically.

Keywords: Landfill, Generalized-Dispersion model, Groundwater, Contaminants, Porous medium.

1. INTRODUCTION

Groundwater contamination is a problem which affects every individual [1]. Groundwater flow and transport analysis have been an important research topic in the last three decades. Micro-organic (MO) contaminants in groundwater can have adverse effects on both the environment and on human health. They enter the natural environment as a result of various processes, their presence in groundwater is the result of current anthropogenic activity and pollution loads from the past[14]. The transport of dissolved contaminants or suspended contaminants (bacteria and virus) by flowing water is of great significance to study the relation between environmental protection and resource utilization[13].

Municipal solid waste (MSW) has become one of the main factors, which adversely influence the environment. With the MSW problems being increased, the occurrence of groundwater contamination is also increasing accordingly. Hence the study of groundwater contamination resulting from MSW landfill leachate has become a focused issue nowadays [12].

The extent of contamination depends on the nature of the contaminant and hydrogeology of the area. Most of the contaminants occur in nature as either point sources or distributed sources. Examples of point source contamination are municipal waste sites (landfill), industrial discharges, leaks and spills etc. Distributed sources occur as a result of effluent from leaking sewers and septic tanks, oil and chemical pipelines.

Landfilling has long been the major disposal method for both domestic and industrial wastes. Bacteria and virus from sewage sludges, waste water, septic tanks and other sources can be transported from groundwater to drinking water wells. During this transport, bacteria and virus can be either irreversibly or reversibly stored on surface material [5]. Valsamy and Nirmala P.Ratchagar[11] developed a mathematical model to study the unsteady transport of bacteria and virus in groundwater.

This paper deals with the study of a viscous , incompressible, contaminated fluid (bacteria and virus) flowing between two parallel plates. The particles are assumed to be spherical in shape and uniform in size. The number density of the contaminated particles is taken constant.

The main objective of this paper is to study the concentration of contaminants following the generalized dispersion model[2] .They showed that an exact solution of the unsteady convection diffusion equation valid for all time can be developed by using the series expansion originally proposed by Gill [1].The generalized dispersion theory developed can be extended to consider the dispersion phenomena for a wide variety of flows which are too complex to solve analytically [4,6,8,9].

2. MATHEMATICAL FORMULATION

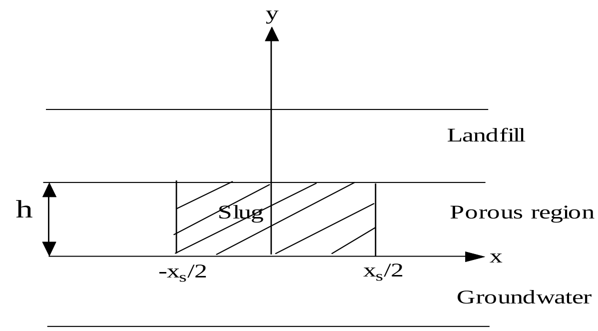

Figure1: Physical configuration

2.1 Dispersion

The concentration of contaminants(bacteria and virus) in the groundwater which diffuse in a fully developed flow, is given by

$$\frac{\partial C}{\partial t}+u\frac{\partial C}{\partial x}=D\left(\frac{\partial^2 C}{\partial x^2}+\frac{\partial^2 C}{\partial y^2}\right) \tag{1}$$

with the initial and boundary conditions,

(i) $$C(0,x,y)=\begin{cases} C_0, |x|\le \dfrac{x_s}{2} \\ 0,\ |x|>\dfrac{x_s}{2} \end{cases}$$

(ii) $$\frac{\partial C}{\partial y}(t,x,0)=\frac{\partial C}{\partial y}(t,x,h)=0$$

(iii) $$C(t,\infty,y)=\frac{\partial C}{\partial x}(t,\infty,y)=0 \tag{2}$$

where, C_0 is the concentration of the initial slug input of length x_s

where $u=\dfrac{c_0}{x}\left[\dfrac{Sinh[\sqrt{x}(y-1)]-Sinh[\sqrt{x}y]}{Sinh[\sqrt{x}]}+1\right]$

$$+\ \frac{4c_0}{\pi}\sum_{n=1}^{\infty}\frac{1}{2n+1}Sin(2n+1)\pi y\frac{(1+Gx_1)^2e^{x_1t}}{x_1(1+Gx_1)^2+SG}+\frac{(1+Gx_2)^2e^{x_1t}}{x_2(1+Gx_2)^2+SG}$$

Introducing non-dimensionless variables,

$$\theta=\frac{C}{C_0};\quad X=\frac{Dx}{h^2\bar{u}};\quad X_s=\frac{Dx_s}{h^2\bar{u}};\quad Y=\frac{y}{h};\quad \tau=\frac{Dt}{h^2};\quad u^*=\frac{u}{\bar{u}};\quad Pe=\frac{h\bar{u}}{D};$$

The equation (1) becomes,

$$\frac{\partial \theta}{\partial \tau}+U\frac{\partial \theta}{\partial X_1}=\frac{1}{Pe^2}\frac{\partial^2 \theta}{\partial X_1{}^2}+\frac{\partial^2 \theta}{\partial Y^2} \tag{3}$$

where, $\frac{1}{Pe^2}=\frac{D^2}{h^2\bar{u}^2}$ and $u^*=\frac{u}{\bar{u}}$

$$U=\frac{c_0}{Q^2 s}\left[\frac{SinhQ(y-1)-SinhQy}{SinhQ}+1\right]$$

Axial coordinate moving with the average velocity of flow is defined as $x_1=x-\bar{u}t$ which in dimensionless form is by $X_1=X-\tau,$ where, $X_1=\frac{Dx_1}{h^2\bar{u}}$

The non-dimensional initial and boundary conditions of (3) takes the form

(i) $$\theta(0,x,y)=\begin{cases}1,\left|X_1\right|\le\frac{X_s}{2}\\ 0,\ \left|X_1\right|>\frac{X_s}{2}\end{cases}$$

(ii) $$\frac{\partial \theta}{\partial y}(\tau,X_1,0)=\frac{\partial \theta}{\partial Y}(\tau,X_1,1)=0$$

(iii) $$\theta(\tau,\infty,y)=\frac{\partial \theta}{\partial X_1}(\tau,\infty,Y)=0 \tag{4}$$

Following Gill and Sankarasubramanian(1970), the solution to equation (3) can be written as a series expansion in the form

$$\theta(\tau,X_1,Y)=\theta_m(\tau,X_1)+\sum_{k=1}^{\infty}f_k(\tau,Y)\frac{\partial^k\theta_m}{\partial X_1^k} \tag{5}$$

where, θ_m is the dimensionless cross sectional average concentration, given by

$$\theta_m(\tau,X_1)=\int_0^1\theta(\tau,X_1,Y)dY \tag{6}$$

Integrating equation (21) with respect to Y in [0,1] and substituting for θ_m we get ,

$$\frac{\partial \theta_m}{\partial \tau}=\frac{1}{Pe^2}\frac{\partial^2\theta_m}{\partial X_1^2}-\frac{\partial}{\partial X_1}\int_0^1 U\theta\, dY \tag{7}$$

The generalized dispersion model with time dependent dispersion coefficient can be written as

$$\frac{\partial \theta_m}{\partial \tau}=K_1\frac{\partial \theta_m}{\partial X_1}+K_2\frac{\partial^2\theta_m}{\partial X_1^2}+K_3\frac{\partial^3\theta_m}{\partial X_1^3}+..........\,..... \tag{8}$$

Introducing equations (5) and (8) in (7) and making use of the boundary condition (ii) of (4) gives

$$K_1 \frac{\partial \theta_m}{\partial X_1} + K_2 \frac{\partial^2 \theta_m}{\partial X_1^2} + K_3 \frac{\partial^3 \theta_m}{\partial X_1^3} + ...$$

$$= \frac{1}{Pe^2} \frac{\partial^2 \theta_m}{\partial X_1^2} - \frac{\partial}{\partial X_1} \int_0^1 U \left(\theta_m(\tau, x_1) + f_1(\tau, y) \frac{\partial \theta_m}{\partial x_1} + f_2(\tau, y) \frac{\partial^2 \theta_m}{\partial x_1^2} + ... \right) dY \quad (9)$$

Comparing the coefficient of $\frac{\partial^k \theta_m}{\partial X_1^k}$ $(k = 1,2,3,......)$, we get

$$K_1 = -\int_0^1 U dY \quad (10)$$

$$K_2(\tau) = \frac{1}{Pe^2} - \int_0^1 U f_1(\tau, y) dY \quad (11)$$

$$K_3(\tau) = -\int_0^1 U f_2(\tau, y) dY, ... \quad (12)$$

Substituting equation (5) in (3)

$$\frac{\partial(\theta_m(\tau, X_1))}{\partial \tau} + f_1(\tau, y) \frac{\partial \theta_m}{\partial X_1}(\tau, X_1) + f_2(\tau, y) \frac{\partial^2 \theta_m}{\partial X_1^2}(\tau, X_1) + ...)$$

$$+ U \; \frac{\partial(\theta_m(\tau, X_1))}{\partial \tau} + f_1(\tau, y) \frac{\partial \theta_m}{\partial X_1}(\tau, X_1) + f_2(\tau, y) \frac{\partial^2 \theta_m}{\partial X_1^2}(\tau, X_1) + ...)$$

$$= \frac{1}{Pe^2} \frac{\partial^2(\theta_m(\tau, X_1))}{\partial X_1} + f_1(\tau, y) \frac{\partial \theta_m}{\partial X_1}(\tau, X_1) + f_2(\tau, y) \frac{\partial^2 \theta_m}{\partial X_1^2}(\tau, X_1) + ...)$$

$$+ \frac{\partial^2(\theta_m(\tau, X_1))}{\partial Y^2} + f_1(\tau, y) \frac{\partial \theta_m}{\partial X_1}(\tau, X_1) + f_2(\tau, y) \frac{\partial^2 \theta_m}{\partial X_1^2}(\tau, X_1) + ...) \quad (13)$$

Following Gill and Sankarasubramanian(1970) and noting

$$\frac{\partial^{k+1} \theta_m}{\partial \tau \partial X_1^k} = \sum_{i=1}^{\infty} K_i(\tau) \frac{\partial^{k+i} \theta_m}{\partial X_1^{k+i}} \qquad for\ k = 1,2,3,.......$$

we get,

$$\left[\frac{\partial f_1}{\partial \tau} - \frac{\partial^2 f_1}{\partial Y^2} + U + k_1(\tau) \right] \frac{\partial \theta_m}{\partial X_1} + \left[\frac{\partial f_2}{\partial \tau} - \frac{\partial^2 f_2}{\partial Y^2} + Uf \;\; + k_1(\tau) f_1 + k_2(\tau) - \frac{1}{Pe^2} \right] \frac{\partial^2 \theta_m}{\partial X_1^2}$$

$$+ \sum_{k=1}^{\infty} \left[\frac{\partial f_{k+2}}{\partial \tau} - \frac{\partial^2 f_{k+2}}{\partial Y^2} + U f_{k+1} + k_1(\tau) f_{k+1} + \left(k_2(\tau) - \frac{1}{Pe^2} \right) f_k + \sum_{i=3}^{k+2} k_i f_{k+2-i} \right] \frac{\partial^{k+2} \theta_m}{\partial X_1^{k+2}} = 0 \quad (14)$$

with $f_0 = 1$. Equating the coefficients of $\frac{\partial^k \theta_m}{\partial X_1^k}$ $(k = 1,2,3,.........)$ to zeros, a set of differential equations are obtained:

$$\frac{\partial f_1}{\partial \tau} = \frac{\partial^2 f_1}{\partial Y^2} - U - K_1(\tau) \tag{15}$$

$$\frac{\partial f_2}{\partial \tau} = \frac{\partial^2 f_2}{\partial Y^2} - Uf_1 - K_1(\tau) f_1 - K_2(\tau) + \frac{1}{Pe^2} \tag{16}$$

$$\frac{\partial f_{k+2}}{\partial \tau} = \frac{\partial^2 f_{k+2}}{\partial Y^2} - Uf_{k+1} - K_1(\tau) f_{k+1} - \left(K_2(\tau) - \frac{1}{Pe^2} \right) f_k - \sum_{i=3}^{k+2} K_i f_{k+2-i} \tag{17}$$

To evaluate K_i's we should know f_k's. Therefore we have to solve equation (14) subject to the initial and boundary conditions,

(i) $f_k(0.y)=0$ (18)

(ii) $\frac{\partial f_k}{\partial Y}(\tau,0)=0$ (19)

(iii) $\frac{\partial f_k}{\partial Y}(\tau,1)=0$ (20)

(iv) $\int_0^1 f_k(\tau,Y)dY = 0$, for k=1,2,3,....... (21)

From equation (10), we get K_1 as $K_1(\tau) = 0$ (22)

Equation (11) implies

$$K_2(\tau) = \frac{1}{Pe^2} - \int_0^1 Uf_1 dY$$

Let

$$f_1 = f_{10}(y) + f_{11}(\tau, y) \tag{23}$$

where, $f_{10}(y)$ corresponds to an infinitely wide slug which is independent of τ satisfies

(i) $f_{11} = -f_{10}(Y) \quad at \ \tau = 0$

(ii) $\frac{\partial f_{11}}{\partial Y} = 0 \quad at \ Y = 0$

(iii) $\frac{\partial f_{11}}{\partial Y} = 0 \quad at \ Y = 1$

(iv) $\int_0^1 f_{11} dY = 0$ (24)

Substituting (23) in (15) gives $\frac{d^2 f_{10}(Y)}{dY^2} = U(Y)$ and $\frac{\partial f_{11}}{\partial \tau} = \frac{\partial^2 f_{11}}{\partial Y^2}$ is the well-known heat conduction equation which is solved by separation of variables.

Hence the solution of f_1 is given by

$$f_1 = \frac{1}{B}\left[\frac{c_0}{xSinh\sqrt{x}}\left(\frac{Sinh\sqrt{x}y}{x}Cosh\sqrt{x}\frac{Cosh\sqrt{x}}{x}Sinh\sqrt{x} - \frac{Sinh\sqrt{x}y}{x} + \frac{y^2}{2}Sinh\sqrt{x}\right) + \right]$$

$$\frac{4c_0}{\pi^3}\sum_{n=1}^{\infty}(A)\frac{(-Sin(2n+1)\pi y)}{(2n+1)^3} - \frac{By^2}{2} + c_1 y + c_2 + \sum_{m=1}^{\infty}A_m Cos(\lambda_m Y)e^{-\lambda_m^2\tau} \tag{25}$$

where,

$$A = \frac{(1+Gx_1)^2 e^{x_1 t}}{x_1(1+Gx_1)^2 + SG} + \frac{(1+Gx_2)^2 e^{x_1 t}}{x_2(1+Gx_2)^2 + SG}$$

$$B = \frac{c_0}{xSinh\sqrt{x}}\left[\frac{2 - 2Cosh\sqrt{x} + \sqrt{x}Sinh\sqrt{x}}{\sqrt{x}} + \frac{8c_0}{\pi^2}\sum_{n=1}^{\infty}\frac{A}{(2n+1)^2}\right]$$

$$c_1 = -\frac{1}{B}\frac{c_0}{xSinh\sqrt{x}}\left(\frac{Cosh\sqrt{x} - 1}{\sqrt{x}}\right) + \frac{4c_0}{\pi^2}\sum_{n=1}^{\infty}\frac{-A}{(2n+1)^2}$$

$$c_2 = -\frac{1}{B}\frac{c_0}{xSinh\sqrt{x}}\left(\frac{1 - Cosh\sqrt{x}}{x\sqrt{x}} + \frac{1}{6}Sinh\sqrt{x}\right) + \frac{4c_0}{\pi^4}\sum_{n=1}^{\infty}\frac{-1}{(2n+1)^4} - \frac{B}{6}$$

$$+\frac{1}{B}\frac{c_0}{xSinh\sqrt{x}}\left(\frac{Cosh\sqrt{x} - 1}{x\sqrt{x}}\right) + \frac{4c_0}{\pi^4}\sum_{n=1}^{\infty}\frac{A}{(2n+1)^4}$$

$$A_m = 2\left\{\left(\frac{1}{B}\left\{\frac{c_0}{XSinh\sqrt{x}}\left(\frac{\sqrt{x}\left(Cosh^2\sqrt{x} + Sinh\sqrt{x} - Cosh\sqrt{x}\right)}{x} + Sinh\sqrt{x}\right) + \frac{4c_0}{\pi^2}\sum_{n=1}^{\infty}\frac{A}{(2n+1)^2} - b\right)\right\} + c_1$$

$$\left(\frac{-Cos(\lambda_m)}{(\lambda_m)^2}\right) - \left(\frac{1}{B}\left\{\frac{c_0}{xSinh\sqrt{x}}\left(\frac{\sqrt{x}(Cosh\sqrt{x} - 1)}{x}\right) + \frac{4c_0}{\pi^2}\sum_{n=1}^{\infty}\frac{-A}{(2n+1)^2} - B\right\} + c_1\right)$$

$$+\frac{1}{B}\left\{\frac{c_0}{xSinh\sqrt{x}}\left(\frac{-x\sqrt{x}(1 + Cosh\sqrt{x})}{x}\right) + 4c_0\sum_{n=1}^{\infty}(A)(-1)^{2n+1}\right\}\left(\frac{Cos(\lambda_m)}{(\lambda_m)^4}\right)$$

$$-\frac{1}{B}\left\{\frac{c_0}{X\sinh\sqrt{x}}\left(\frac{1 - Cosh\sqrt{x}}{x}\right) + 4c_0\sum_{n=1}^{\infty}(A)\right\}\left(\frac{1}{(\lambda_m)^4}\right) \tag{26}$$

and $\lambda_m = m\pi$.

Therefore substituting f_1 in equation (11) gives the solution of K_2.

Similarly $K_3(\tau)$, $K_4(\tau)$,... are obtained and we found that $K_i(\tau), i > 2$ are negligibly small compared to $K_2(\tau)$.

The dispersion model (8) takes the form

$$\frac{\partial\theta_m}{\partial\tau} = K_2\frac{\partial^2\theta_m}{\partial X_1^2} \tag{27}$$

3. Mean Concentration

The solution to equation (27) can be solved with the initial and boundary conditions

$$\theta_m(0, X_1) = \begin{cases} 1, |X_1| \leq \dfrac{X_s}{2} \\ 0, |X_1| > \dfrac{X_s}{2} \end{cases} \tag{28}$$

can be obtained using Fourier Transform[10] as

$$\theta_m(0, X_1) = \frac{1}{2}\left[erf\left(\frac{\frac{X_s}{2} + X_1}{2\sqrt{T}} \right) + erf\left(\frac{\frac{X_s}{2} - X_1}{2\sqrt{T}} \right) \right] \tag{29}$$

where, $T = \int_0^{\tau} K_2(y)dy \quad and \quad erf(x) = \frac{2}{\sqrt{\pi}} \int_0^{x} e^{-z^2} dz$

4. RESULTS AND DISCUSSIONS

In this paper we have studied the concentration of contaminants consisting a mixture of solid phase (bacteria and virus) and fluid phase. Results of dispersion coefficient and mean concentration are obtained analytically and the numerical values have been computed using MATHEMATICA 8.0.

Figure 2 shows that the dispersion coefficient is greatest for bacteria(G>1) when compared with virus(G<1) and the fluid (G=1).

Figure 3 shows the mean concentration θ_m with axial distance X_1 for the contaminated phase and fluid phase. It depicts the marked variation of concentration with the axial distance and the dimensionless time. The curve is bell shaped and perfectly symmetrical about the origin. Also it is apparent from the figure the mean concentration is greater for bacteria compared with fluid and virus.

Figures 4 and 5 represents the graph of mean concentration versus dimensionless time τ for contaminated phase and fluid phase outside the slug (X_s = 0.02) and (X_1=0.1) and inside the slug (X_s = 0.02) and (X_1=0.05). In general for both the cases, we observe a gradual decrease in θ_m, for increasing time τ. Also for very smaller values of τ, the concentration outside the slug and inside the slug shows a rapid decrease.

5. CONCLUSION

Groundwater contamination by pathogenic bacteria and viruses has long been recognized as a serious hazard to human health[3]. An analytical approach for analyzing two dimensional contaminant transport from a landfill has been described in detail by advection - dispersion equation. The behavior of dispersion coefficient K_2 increases with increase in time. Regarding the mean concentration, for smaller values of time τ, concentration θ_m shows a rapid decrease for both contaminated fluid phase.

6. REFERENCES

[1] Gill, W.N., A note on the solution of transient dispersion problems, Proc. Roy. Soc. London, A 298, 335-339, 1967.

[2] Gill, W.N. and Sankarasubramanian, R., Exact analysis of unsteady convective diffusion, Proc. Roy. Soc. London , A 316, 341-350, 1970.

[3] Keswick B.H and Gerba C.P, Viruses in groundwater, Environ. Sci. Technol. 14(11), 1290-1297, 1980.

[4] Mallika, K.S. and Rudraiah, N., Generalized dispersion of unsteady convective diffusion in couple stress poorly conducting fluid bounded by porous layer in the presence of an electric field, World Journal of Engineering, 8(4), 335-346, 2011.

[5] Martin Reinhard and Naomi L.Goodman, Occurence and distribution of organic chemicals in two landfills leachated plumes, Environ.Sci.Technol., 18(12), 953-961, 1984.

[6] Meena Priya, P. and Nirmala P. Ratchagar, Generalized dispersion of atmospheric aerosols on unsteady convective diffusion in couple stress fluid bounded by electrodes, Int. Journal of Applied Mathematics and Engineering Sciences, 5(1), 59-72, 2011.

[7] Mritunjay Kumar Singh, Nav Kumar Mahato and Premalatha singh, Longitudinal dispersion with time-dependent source concentration in semi-infinite aquifer. J. Earth syst.Sci. 117(6), 945-949, 2008.

[8] Nagarani, P.,Sarojamma, G. and Jayaraman, G., Exact analysis of unsteady convective diffusion in casson fluid flow in an annulus-Application to catheterized artery, Acta Mechanica, 187(1-4), 189-202, 2006.

[9] Rudraiah, N., Pal,D. and Siddheshwar, P.G., Effect of couple stress on the unsteady convective diffusion in fluid flow through a channel, BioRheology, 23(4), 349-35, 1986.

[10] Sankara Rao, Introduction to Partial Differential Equations, Prentice Hall of India, 1995.

[11] Valsamy,P. and Nirmala P.Ratchagar, Unsteady transport of bacteria and virus in groundwater, Int. Journal of Math.Sci and Engg.Appls.6,197-205, 2012.

[12] Xiaoli Liu, Enzhi Wang, Sijing Wang and Qiang Xue, The Geological society of London, IAEG, 756, 2006.

[13] Zhang Qian-fei, LAN Shou-qi, Wang Yan-ming, Xu Yong-fu, A new numerical method for groundwater flow and solute transport using velocity field, Journal of Hydrodynamics, 20(3), 356-364, 2008.

[14] Determination of micro-organic contaminants in groundwater, Korosa. A, Auersperger, P., Mali. N, Science of the Total Environment, 571(15), 1419-1431, 2016.

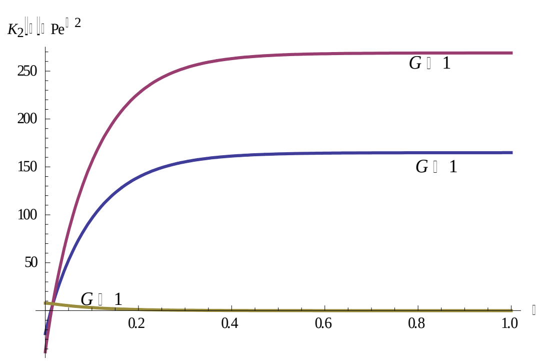

Figure 2:Dispersion coefficient varying with dimensionless time for contaminated phase and fluid phase

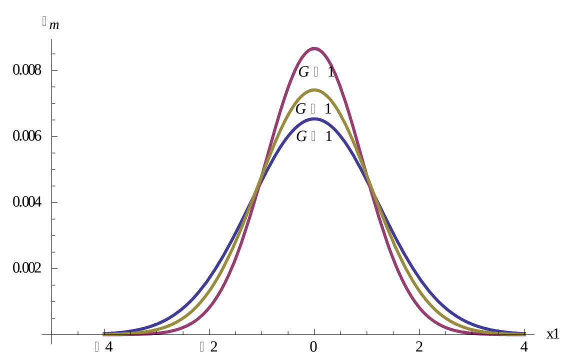

Figure 3: Mean concentration varying along axial distance at different time for fluid and Contaminated phase

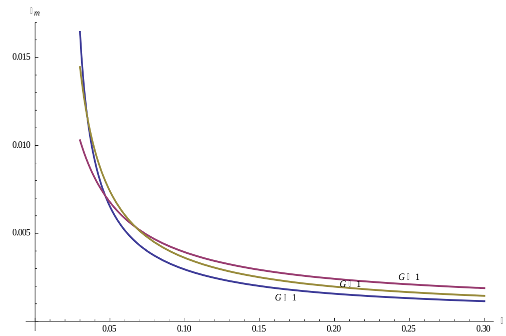

Figure 4: Mean concentration (outside the slug) varying with dimensionless time for contaminated and fluid phase

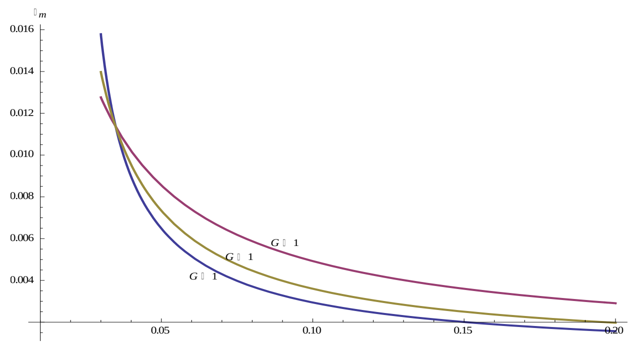

Figure 5: Mean concentration (inside the slug) varying with dimensionless time for contaminated and fluid phase

14. " Enhancing Shortage Management in Inventory Systems Using Trapezoidal Fuzzy Logic"

[1]**T. Iswarya,**
Department of Mathematics,Vels Institute of Science, Technology and Advanced Studies, Chennai
[2] **S. Senthamilselvi,**
Department of Mathematics,Vels University of Advanced Science and Technology, Chennai"
and [3]* **S.Marimuthu,** Department of Nautical Science, AMET Deemed to be Unviersity, Chennai

Abstract

In this paper, fuzzy inventory model with shortages has been considered. Trapezoidal fuzzy number with Weibull distribution is used to fuzzify the data of an inventory model. All the parameters used in the inventory model is converted to trapezoidal fuzzy numbers using function principle. We find the estimate of the total inventory cost by defuzzifing the trapezoidal fuzzy numbers using the the graded mean integration. The optimum total cost for the inventory model is found.

Keywords: Inventory · Trapezoidal fuzzy numbers · Defuzzification

1. Introduction

Inventory models are the models which is used to determine the optimum levels of the inventories which has to be maintained during the various stages of production, storing, ordering and managing the goods.

Inventory models deals with certainty and uncertainty of demand which occurs before and after the production of goods. The inventories during manufacturing can be classified as raw materials, work-in-progress and finished goods. After finishing the product, we have two costs that deals with holding the inventories. They are named as ordering costs and carrying costs.

There are two major models in the world of inventory. One is the deterministic model which deals with no uncertainty of demand and replenishment of inventories. The Probabilistic model which deal with uncertainty with demand pattern and lead time of the inventories.

Inventory models with and without Back orders are considered by Yao et al [24] in fuzzy environment. Trapezoidal number is used to fuzzify the order quantity q. With the help of centroid strategy along with the extension principle, they found the membership functions of fuzzy total cost.

*Corresponding Author

2. Preliminaries

"Definition 2.1: A Weibull distribution is defined as a random variable X is said to have a *Weibull distribution* with parameters α and β (α > 0; β > 0) if the probability density function of X is $f(x;\alpha,\beta)=\begin{cases} \frac{\alpha}{\beta\alpha} x^{\alpha\text{-}1} e^{\left(\frac{x}{\beta}\right)^{\alpha}} & x\geq 0 \\ 0 & x<0 \end{cases}$ where α is a shape parameter and β is a scale parameter."

3. Methodology

Graded Mean Integration by Chen and Hsieh [6] is used to defuzzify the fuzzy number which is based on the mean integral value with h-level. The generalised fuzzy number is described as follows.

Suppose $\widetilde{X}$ is the fuzzy number considered then $\widetilde{X}\subseteq R$. The following conditions are met by the membership function $\mu_{\widetilde{X}}$ of $\widetilde{X}$

i) $\mu_{\widetilde{X}}: R \xrightarrow{continuous} [0,1]$.

ii) $\mu_{\widetilde{X}}=0,\ -\infty<x\leq x_1$,

iii) $\mu_{\widetilde{X}}=L(x)$ is strictly increasing on $[x_1,x_2]$,

iv) $\mu_{\widetilde{X}}=w_X,\ x_2\leq x\leq x_3$,

v) $\mu_{\widetilde{X}}=R(x)$ is strictly decreasing on $[x_3,x_4]$,

vi) $\mu_{\widetilde{X}}=0,\ x_4\leq x<\infty$,

Where $0<w_X\leq 1$, *and* x_1, x_2, x_3 *and* x_4 *are real numbers.*

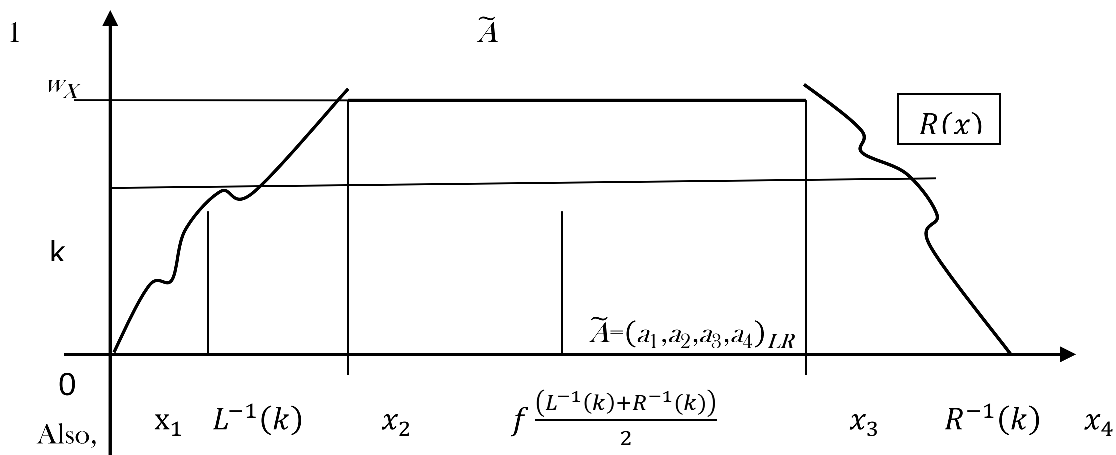

Also, ... $_1,x_2,x_3,x_4;w_X)_{LR}$
.When w_X ... $=(x_1,x_2,x_3,x_4)_{LR}$

Second, by Graded Mean Integration Representation method L^{-1} and R^{-1} are the inversed functions of L and R, respectively, and the graded mean h-level value of generalized fuzzy number $\widetilde{X}=(x_1,x_2,x_3,x_4;w_X)_{LR}$ is $\frac{h\left(L^{-1}(k)+R^{-1}(k)\right)}{2}$. Then the Graded Mean Integration Representation of $\widetilde{X}$ is $P(\widetilde{X})$ with graded w_X, where

$$P(\widetilde{X})=\int_0^{w_X}\frac{k\left(L^{-1}(k)+R^{-1}(k)\right)}{2}\,df\Big/\int_0^{w_X} f\,df \quad \text{With } 0<k\leq w_X \text{ and } 0<w_X\leq 1. \quad \text{-----(3.1)}$$

In the proposed fuzzy inventory model, we will now represent the fuzzified number as the parameter type. Let us assume that $\widetilde{Y}$ as a trapezoidal fuzzy number which is represent as $\widetilde{Y}=\left(y_1,y_2,y_3,y_4\right)$. Calculation of the Graded Mean Integration of $\widetilde{Y}$ is given by the formula (3.1) as

$$P(\widetilde{Y})=\int_0^1 k\left(\frac{y_1+y_4+\left(y_2-y_1-y_4+y_3\right)k}{2}\right)dk\Big/\int_0^1 k\,dk$$

$$P(\widetilde{Y})=\frac{y_1+2y_2+2y_3+y_4}{6} \qquad \text{------(3.2)}$$

4. Function Principle's Arithmetical Operations:

Arithmetic operations on trapezoidal fuzzy number is done using Function. The following are the arithmetical operations on fuzzy numbers done under the function principle.

Suppose $\tilde{\lambda}=(\lambda_1,\lambda_2,\lambda_3,\lambda_4)$ and $\widetilde{\Theta}=(\Theta_1,m_2,m_3,m_4)$ are the two trapezoidal fuzzy numbers. Then,

1. The addition of $\tilde{\lambda}$ and $\tilde{\Theta}$ is $\tilde{\lambda}\oplus\tilde{\Theta}=(\lambda_1+\Theta_1, \lambda_2+\Theta_2,\lambda_3+\Theta_3,\lambda_4+\Theta_4)$, where $\lambda_1,\Theta_1, \lambda_2,\Theta_2,\lambda_3,\Theta_3,\lambda_4$ *and* Θ_4 are any R.
2. The multiplication of $\tilde{\lambda}$ and $\tilde{\theta}$ is $\tilde{\lambda}\otimes\tilde{\theta}=(\phi_1,\phi_2,\phi_3,\phi_4)$, where $T=\{\lambda_1\theta_1, \lambda_1\theta_4,\lambda_4\theta_1,\lambda_4\theta_4\}$, $T_1=\{\lambda_2\theta_2, \lambda_2\theta_3,\lambda_3\theta_2,\lambda_3\theta_3\}$, $\phi_1=\min T$,

   $\phi_2=\min T_1$,$\phi_3=\max T_1$,$\phi_4=\max T_1$. If $\lambda_1,\Theta_1, \lambda_2,\Theta_2,\lambda_3,\Theta_3,\lambda_4$ *and* Θ_4 are R which are ≥ 0 , then $\tilde{\lambda}\otimes\tilde{\theta}=(\lambda_1\theta_1,\lambda_2\theta_2,\lambda_3\theta_3,\lambda_4\theta_4)$,
3. $-\tilde{\theta}=(-\theta_4,-\theta_3,-\theta_2,-\theta_1)$, then the subtraction of $\tilde{\lambda}$ and $\tilde{\theta}$ is $\tilde{\lambda}\ominus\tilde{\theta}=(\lambda_1-\theta_4,\lambda_2-\theta_3,\lambda_3-\theta_2,\lambda_4-\theta_1)$, Where $\lambda_1,\Theta_1, \lambda_2,\Theta_2,\lambda_3,\Theta_3,\lambda_4$ *and* Θ_4 are R.
4. $\frac{1}{\tilde{\theta}}=\tilde{\theta}^{-1}=\left({}^{1}/_{\theta_4},{}^{1}/_{\theta_3},{}^{1}/_{\theta_2},{}^{1}/_{\theta_1}\right)$, where$\lambda_1,\Theta_1, \lambda_2,\Theta_2,\lambda_3,\Theta_3,\lambda_4$ *and* Θ_4 R which are ≥ 0, then the quotient of $\tilde{L}$ and $\tilde{\theta}$ is $\frac{\tilde{\lambda}}{\tilde{\theta}}=\left(\frac{\lambda_1}{\theta_4},\frac{\lambda_2}{\theta_3},\frac{\lambda_3}{\theta_2},\frac{\lambda_4}{\theta_1}\right)$
5. Let α ε R. Then

   (i) $\alpha\geq 0,\alpha\otimes\tilde{\lambda}=(\alpha\lambda_1,\alpha\lambda_2,\alpha\lambda_3,\alpha\lambda_4)$

   (ii) $\alpha<0,\alpha\otimes\tilde{\lambda}=(\alpha\lambda_4,\alpha\lambda_3,\alpha\lambda_2,\alpha\lambda_1)$

5. Symbols used in the Model:

$\tilde{R}$: Fuzzy demand rate

$\tilde{Q}$: The fuzzy order quantity during a cycle of length T

$\tilde{Q}_1$: The positive inventory fuzzy level at time t, $0\leq t\leq t_1$

$\tilde{Q}_2$: The negative inventory fuzzy level at time t, $t_1\leq t\leq T$

$\widetilde{SC}$: Fuzzy shortage cost/ time unit

$\tilde{A}$: Fuzzy ordering cost / order

$\widetilde{TC}(t_1,T)$: Fuzzy total cost / time unit

$\tilde{\lambda}, \tilde{\theta}$: Fuzzy numbers

Trapezoidal Fuzzy Numbers:

$\tilde{R}=(r_1,r_2,r_3,r_4)$: Fuzzy Demand rate

$\tilde{l}=(l_1,l_2,l_3,l_4)$: Fuzzy number

$\tilde{m}=(m_1,m_2,m_3,m_4)$: Fuzzy number

$\tilde{A}=(k_1,k_2,k_3,k_4)$: Fuzzy ordering cost / order

The above are the representation of generalized fuzzy numbers in trapezoidal format.

Mathematical Formulation:

During the positive stock interval [0, t_1] and shortage interval [t_1, T], the rate of change of the inventory is given by the differential equations as follows.

$$\frac{d\widetilde{Q}_1(t)}{dt}+\theta(t)\,Q_1(t)= -\widetilde{R} \quad ..... \quad (5.1)$$

$$\frac{d\widetilde{Q}_2(t)}{dt}= -\widetilde{R} \quad ------ (5.2)$$

With the boundary conditions

$$Q_1(t)=Q_2(t)=0 \text{ at } t=t_1 \text{ and} \quad ------ (5.3)$$

$$Q_1(t)=IM \text{ and } Q_2(t)=IB \text{ at } t=T \quad -------(5.4)$$

6. Mathematical Solution for the Model

Case I: Inventory Level Without Shortage:

The inventory diminishes due to demand in the interval [0,t_1]. Therefore, level of the inventory at any time in the interval [0,t_1] is described by differential equation

From equation (5.1)

$$\frac{d\widetilde{Q}_1(t)}{dt}+\varphi(t)\,\widetilde{Q}_1(t)= -\widetilde{R} \quad -------(6.1)$$

With the boundary conditions are $Q_1(0)=IM$ and $Q_1(t_1)=0$.

From equation (5.3)

$$\widetilde{Q}_1(t)=\widetilde{R}\left[t_1-t+\alpha t^{\beta+1}+\frac{e^{\alpha t_1^{\beta+1}}}{\beta+1}-\frac{e^{\alpha t^{\beta+1}}}{\beta+1}\right] \quad -----(6.2)$$

Case II: Inventory Level with Shortage:

Differential equation is used to describe the state of inventory during [t_1, T].

From equation (5.2)

$$\frac{d\widetilde{Q}_1(t)}{dt}=-\widetilde{R}$$

$$\frac{d\widetilde{Q}_1(t)}{dt}=-(r_1,r_2,r_3,r_4)$$

$$\frac{d\widetilde{Q}_1(t)}{dt}=(r_4,r_3,r_2,r_1)$$

where $t_1<t<T$

We have the boundary conditions as $Q_2(t_1)=0$ and $Q_2(t)$ = IB

$$\widetilde{Q}_2(t) = -\widetilde{R}\,(t-t_1)$$

The solution of differential equation, from equation (5.4) is

$$Q_2(t)=\widetilde{R}(t_1-t)$$

$$Q_2(t)=(r_1,r_2,r_3,r_4)(t_1-t)$$

Therefore, for one renewal cycle the total cost has the following elements,

Holding cost:

$$\widetilde{HC}=\int_0^{t_1} H(t)\,Q_1(t)dt$$

From the equation (6.2)

$$\widetilde{HC}=\tilde{l}\tilde{R}\left[\frac{t_1^2}{2}+\frac{\alpha\beta t_1{}^{\beta+2}}{(\beta+1)(\beta+2)}\right]+\tilde{m}\tilde{R}\left[\frac{t_1^3}{6}+\frac{\alpha\beta t_1{}^{\beta+3}}{2(\beta+2)(\beta+3)}\right] \text{ -----(6.3)}$$

$$\widetilde{HC}=\left\{\begin{array}{c}(r_1l_1,r_2l_2,r_3l_3,r_4l_4)\left[\frac{t_1^2}{2}+\frac{\alpha\beta t_1{}^{\beta+2}}{(\beta+1)(\beta+2)}\right]\\ +(r_1m_1,r_2m_2,r_3m_3,r_4m_4)\left[\frac{t_1^3}{6}+\frac{\alpha\beta t_1{}^{\beta+3}}{2(\beta+2)(\beta+3)}\right]\end{array}\right\}\text{------(6.4)}$$

Shortage Cost during $[t_1, T]$:

$$\widetilde{SC}=\pi\int_{t_1}^{T}\tilde{R}(t_1-t)\,dt$$

$$\widetilde{SC}=\frac{1}{2}\,\pi\tilde{R}(T-t_1)^2 \text{ ------(6.5)}$$

$$\widetilde{SC}=\frac{1}{2}\,\pi(r_1,r_2,r_3,r_4)(T-t_1)^2 \text{ ------(6.6)}$$

Ordering Cost per order:

$$\tilde{A}=(k_1,k_2,k_3,k_4) \qquad \text{-------(6.7)}$$

Total cost function per time unit:

$$\widetilde{TC}(t_1,T)=\frac{1}{T}[\widetilde{HC}+\widetilde{SC}+\tilde{A}]$$

From equations (6.3), (6.5) and (6.7)

$$\widetilde{TC}(t_1,\ T)=\frac{1}{T}\left\{\begin{array}{c}\tilde{l}\tilde{R}\otimes\left[\frac{t_1^2}{2}+\frac{\alpha\beta t_1^{\beta+2}}{(\beta+1)(\beta+2)}\right]\oplus\tilde{m}\tilde{R}\otimes\left[\frac{t_1^3}{6}+\frac{\alpha\beta t_1{}^{\beta+3}}{2(\beta+2)(\beta+3)}\right]\\ \oplus\tilde{R}\otimes\frac{1}{2}\,\pi(T-t_1)^2\oplus\tilde{A}\end{array}\right\}$$

From equations (6.4), (6.6) and (6.8)

$$\widetilde{TC}(t_1,\ T)=\frac{1}{T}\left\{\begin{array}{c}(r_1\lambda_1,r_2\lambda_2,r_3\lambda_3,r_4\lambda_4)\left[\frac{t_1^2}{2}+\frac{\alpha\beta t_1^{\beta+2}}{(\beta+1)(\beta+2)}\right]\\ +(r_1\theta_1,r_2\theta_2,r_3\theta_3,r_4\theta_4)\left[\frac{t_1^3}{6}+\frac{\alpha\beta t_1{}^{\beta+3}}{2(\beta+2)(\beta+3)}\right]\\ +\frac{1}{2}\,\pi(r_1,r_2,r_3,r_4)(T-t_1)^2\\ +(k_1,k_2,k_3,k_4)\end{array}\right\}\text{ ------(6.8)}$$

The Necessary condition for the total cost per time unit to be minimized is

$$\frac{\partial\widetilde{TC}}{\partial t_1}=0\ and\ \frac{\partial\widetilde{TC}}{\partial T}=0$$

Given

$$\left(\frac{\partial^2\widetilde{TC}}{\partial t_1^2}\right)\left(\frac{\partial^2\widetilde{TC}}{\partial T^2}\right)-\left(\frac{\partial^2\widetilde{TC}}{\partial t_1\partial T}\right)^2>0\ and\ \left(\frac{\partial^2\widetilde{TC}}{\partial t_1^2}\right)>0$$

7. Numerical Example and Sensitivity Study

In this paper, we consider an inventory problem with variables with correct units as follows:

R=2000, λ=2.0, θ=1.5, C=10, O=50, α=0.15, β=1.5, A=50.

Let us convert the above-mentioned ordinary crisp numbers to trapezoidal fuzzy numbers using, "greater or less than Y" or "about Y".

1. "greater or less than X" = (0.92 *Y*, 0.94 *Y*, 1.02 *Y*, 1.1 *Y*), and
2. "about X" =(0.92 *Y*, *Y*, *Y*,1.02 *Y*)

Then by the above injunction, the fuzzy parameters is modified as follows:

i) Fuzzy Demand rate, R= "greater or less than 2000" R = (0)

ii) Fuzzy ordering cost, A=" about 50" = (46, 50, 50, 51)

iii) Fuzzy numbers, λ = "greater or less than 2" = (1.84, 1.88, 2.04, 2.2)

θ = "greater or less than 1.5" = (1.38, 1.41, 1.53, 1.55)

iv) α = "greater or less than 0.15" = (0.13, 0.14, 0.15, 0.16)

β = "greater or less than 1.5" = (1.3, 1.4, 1.5, 1.6)

Substituting the above values in the equations

Table: Effect of changes in limitation of the inventory problem

Parameters	%Change	T	t_1	TC
R	+40%	1.419874156	0.011670695	70.41517205
	+20%	1.421459571	0.014699532	70.33800196
	-20%	1.424000822	0.019892018	70.20544017
	-40%	1.427021837	0.026078629	70.04716039
α	+40%	1.421875009	0.015634989	70.31200099
	+20%	1.422006363	0.015861028	70.30726674
	-20%	1.422288646	0.016343423	70.29726113
	-40%	1.422440702	0.016601405	70.29196484
β	+40%	1.422858828	0.017321356	70.27687361
	+20%	1.422670438	0.017019365	70.28255366
	-20%	1.42089431	0.013621192	70.36365589
	-40%	1.418544038	0.008423917	70.50600603
λ	+40%	1.420114479	0.011907429	70.44910654
	+20%	1.420985301	0.013696952	70.37548717
	-20%	1.423751973	0.01946766	70.22971249
	-40%	1.426105064	0.024501661	70.15754767
θ	+40%	1.42212196	0.016063117	70.30295457
	+20%	1.422132987	0.016079982	70.30265333
	-20%	1.422155194	0.016113922	70.30206671

	-40%	1.422166377	0.016130998	70.30178115

Substituting the above values in the equations

$$t_1=(0.015286761,\ 0.016010255,\ 0.017695545,\ 0.01853819)$$

$$T=(1.2867336,\ 1.3582188,\ 1.5011892,\ 1.5726744)$$

Substituting the values of R, l, m, Aα, β in equation (6.8) the total cost is found as

$$\widetilde{TC}(t_1, T)=(63.268925,66.774421,73.635413,77.541909)$$

From the formula given in equation (3.1) and (3.2) and using the graded mean integration the total cost can be defuzzified. The Defuzzified Total Cost is given by TC=70.2716503

Comparing the above defuzzified value of the total cost with the crisp value of the total cost is negligible

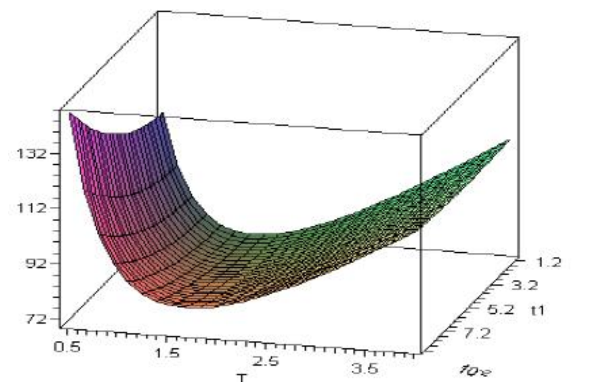

Figure-1(TC vs t_1 and T)

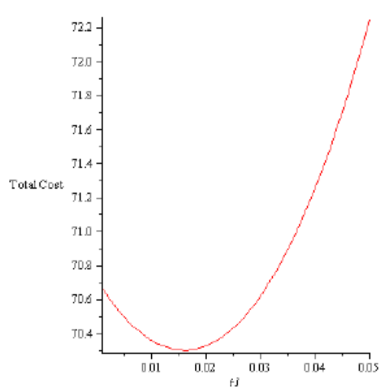

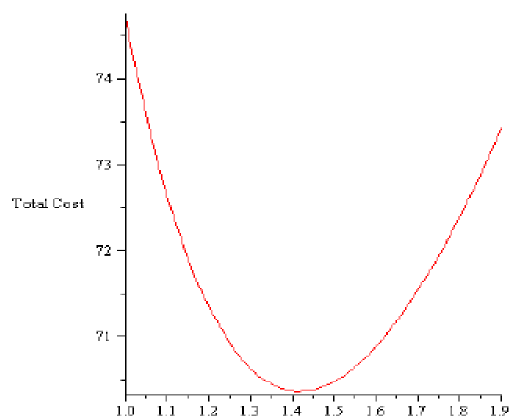

Figure-2 (TC Vs T at $t_1 = 0.01$) Figure-3 (TC Vs T at $t_1 = 0.01$) TC Vs. t_1 at T=1.42)

8. Conclusion

The above example has been defuzzified using centroid method in Graded mean Integration and relative changes have been computed. We can see that the total cost maximizes or minimizes with mere change which is considered and within our expectation level.

An analytical solution of an inventory model with holding cost and shortages under Weibull distribution is obtained. Here all the variables are considered as fuzzy. We have used Function Principle to fuzzify the inventory model and Graded Mean Integration to defuzzify the trapezoidal fuzzify numbers and solved the model. Practical problem is illustrated to support the variability of the method given above. The fuzzy inventory model is more real world and accurate than the crisp inventory model.

References

1. Abad, P.L., (1996), Optimal pricing and lot-sizing under conditions of perishability and partial backordering. Management Science, 42, 1093-1104.
2. Abad, P.L., (2001), Optimal price and order-size for a reseller under partial backlogging. Computers and Operation Research, 28, 53- 65.
3. Chang, Oct. 1, (1999), Fuzzy production inventory for fuzzy product quantity with triangular fuzzy number, Fuzzy Sets and Systems, v.107 n.1, p.37-57.
4. Chen, (1985), Fuzzy linear combination of fuzzy linear functions under extension principle and second function principle, Tamsui Oxford Journal of Management Sciences 11-31.
5. Chen, (1985), Operations on fuzzy numbers with function principle, Tamkang Journal of Management Sciences 6 13-26.
6. Chen, Hsieh, (1999), Graded mean integration representation of generalized fuzzy number, Journal of Chinese Fuzzy Systems 1-7.
7. Dubois D, Prade H (1980) Fuzzy sets and systems. Academic Press, New York
8. Ghare, P. M. and Schrader, G. F., (1983), A model for an exponentially decaying inventory. Journal of Industrial Engineering, 14, 238-243.
9. Goyal, S. K. and B. C. Giri, (2001) Recent trends in modeling of deteriorating inventory. European Journal of Operational Research, 134, 1-16.
10. Huang and Hsu, (2008) A note on a buyer-vendor EOQ model with changeable lead-time in supply chain, Journal of Information & Optimization Sciences, 29, 305–310.
11. Kuo-Chen Hung, (2009) An inventory model with generalized type demand, deterioration and backorder rates, European Journal of Operational Research, 208(3), 239-242.
12. Lee, W-C., and Wu, J-W. (2004) A Note on EOQ model for items with mixtures of exponential distribution deterioration, Shortages and time-varying demand, Quality and Quantity, 38, 457-473.
13. Liao, J.J., (2008), An EOQ model with non-instantaneous receipt and exponential deteriorating item under two–level trade credit. International Journal of Production Economics, 113,852-861
14. Mishra & L. Singh, (2011), deteriorating inventory model for time dependent demand and holding cost with partial backlogging. International Journal of Management Science and Engineering Management, X(X): 1-5
15. Mishra, V.K. and Singh, L.S., (2010), Deteriorating inventory model with time dependent demand and partial backlogging, Applied Mathematical Sciences, 4(72), 3611-3619.
16. Pareek,S., Mishra,V.K., and Rani,S., (2009), An Inventory Model for time dependent deteriorating item with salvage value and shortages, Mathematics Today, 25, 31-39.
17. Park K S (1987) Fuzzy set theoretic interpretation of economic order quantity. IEEE Transactions on Systems, Man & Cybernetics, 17: 1082-1084

18. Park, Nov./Dec. (1987), Fuzzy set theoretic interpretation of economic order quantity, IEEE Transactions on Systems, Man and Cybernetics, v.17 n.6, p.1082-1084

19. Roy, Ajanta. An inventory model for deteriorating items with price dependent demand and time varying holding cost. Advanced Modeling and Optimization, 10, 25-37

20. Skouri, K., I. Konstantaras, S. Papachristos, and I. Ganas, (2009), Inventory models with ramp type demand rate, partial backlogging and Weibull deterioration rate. European Journal of Operational Research. European Journal of Operational Research, 192, 79–92.

21. Skouri, Papachristos & Goyal, (2008), An EOQ model with trade credit period depending on the ordering quantity, Journal of Information & Optimization Sciences, 29, 947–961.

22. Syed J K, Aziz L A (2007) Fuzzy inventory models without using signed-distance method. Applied Mathematics and Information Sciences, 1(2): 203-209

23. Taha. H.A, (1997), in Operations Research, Prentice-Hall, Englewood Cliffs, NJ, USA, pp. 753-777.

24. Yao J S, Chiang J (2003) Inventory without backorder with fuzzy total cost & fuzzy storing cost defuzzified by centroid and signed-distance. European journal of operations research, 148: 401-409

25. Zimmermann H J (1991) Fuzzy set theory and its applications. 2nd Edition, Kluwer Academic Publishers, Boston/Dorgrecht/London.

Dr. P. Balaganesan is working as an Professor and Head in the Department of Mathematics, AMET Deemed to be University, Kanathur, Chennai-603112,Tamilnadu, India. He is having 30 years of extensive experience in teaching and research expertise. The author completed his doctoral studies in Mathematics in 2016 at Chennai's Hindustan Institute of Science and Technology. He has completed SET in 2018 conducted by mother Theresa University. He has published Engineering Mathematics Books. He has more than 50 research publications that have been published in various national and international journals. He is currently working in Mathematical Biology research area. He has finished three projects, two industrial, one seed money, and one consultancy. He is also a reviewer of two reputed international journals. His articles have appeared in a number of conference proceedings. He has participated in numerous symposiums, seminars, and conferences.

Dr. Renuka J. is an accomplished Assistant Professor in the Department of Mathematics at Women's Christian College (WCC), Chennai, India. She holds an M.Sc., M.Phil., and Ph.D., and has also qualified for the SET (State Eligibility Test). She is a University Rank Holder from the University of Madras in her M.Sc. degree. She has more than 20 research publications in various national and international journals. Her research interests include the mathematical analysis of infectious diseases such as malaria and cholera, as well as graph labeling.Dr. Renuka has been serving as a faculty member at WCC since 2016. Her articles have also appeared in several conference proceedings. She has actively participated in numerous symposiums, seminars, and conferences.

Dr. V. Maheswari is a dedicated and accomplished academician, currently serving as a Professor in the Department of Mathematics at Vels Institute of Science, Technology and Advanced Studies, Pallavaram, Chennai. With over 21 years of teaching experience, she has contributed effectively to both Arts and Science as well as Engineering institutions, shaping the academic growth of many students. Her area of research focuses on graph theory, especially theoretical computations on graph labeling methods and their applications. She has an impressive record of scholarly work, with 65 research articles published in reputed journals, along with 6 book chapters and 5 authored books. Dr. Maheswari has also served as a reviewer for the Journal of Discrete Mathematics and other well-recognized indexed journals, reflecting her strong research expertise and commitment to academic excellence, with her vast experience, clarity of thought, and passion for research, she brings valuable insight and integrity to the role of editor.

Dr. E. Poongothai is a dedicated and accomplished academician, currently PDF Scholar in the field of Mathematics, AMET Deemed to be University, Kanathur, Chennai-603112,Tamilnadu, India. With a strong academic background and research orientation, she has been actively involved in advanced studies and scholarly activities in the domain of Fuzzy Mathematics. Her research interests primarily focus on Fuzzy Topology, Neutrosophic Topology, and their applications in modern mathematical analysis. She has contributed to the academic community through research publications in reputed journals and participation in various national and international conferences and seminars. Dr. Poongothai is known for her clarity of thought, analytical approach, and commitment to research excellence. With her passion for mathematics and continuous pursuit of knowledge, she brings valuable insight, dedication, and academic integrity to the role of editor, ensuring quality and credibility in the publication.

ISBN 978-93-6850-545-7

HSRA PUBLICATIONS

₹ 499 /-

9 789368 505457

www.hsrapublications.com